Australian Geomechanics Volume 60 No 4 DECEMBER 2025 TAILINGS GEOTECHNICAL ENGINEERING ISSN 0818-9110

AUSTRALIAN GEOMECHANICS

JOURNAL AND NEWS OF THE AUSTRALIAN GEOMECHANICS SOCIETY ISSN 0818-9110

VOLUME 60: NO.4 DECEMBER 2025

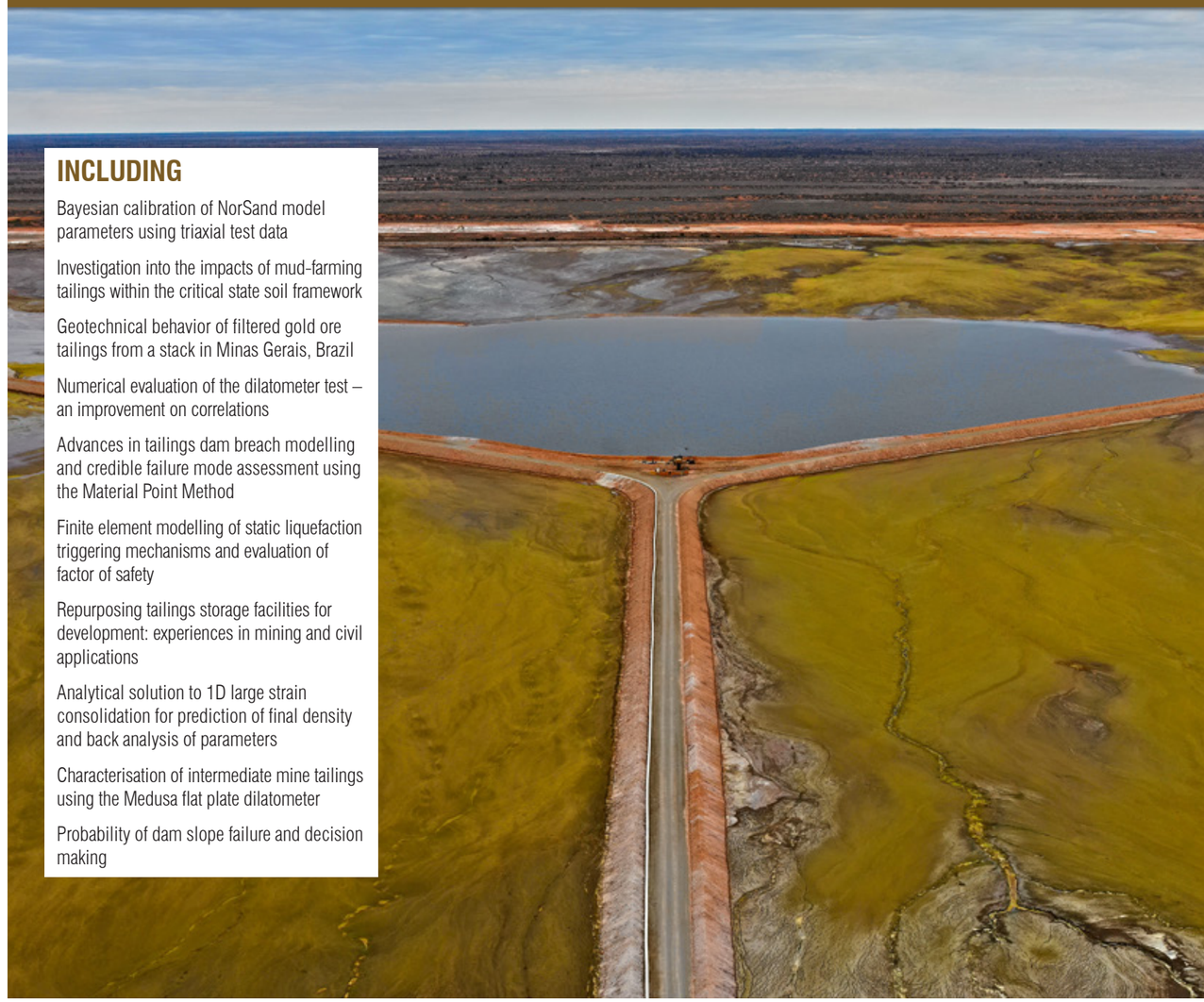

INCLUDING

AUSTRALIAN GEOMECHANICS SOCIETY

A technical society of ENGINEERS AUSTRALIA

Reducing geotechnical uncertainty

INSITU GEOTECH SERVICES

reducing geotechnical uncertainty

COMPREHENSIVE RANGE OF
IN SITU TESTING, SAMPLING
AND GEOTECHNICAL SERVICES

mick@insitu.com.au mark@insitu.com.au

0407 467 025 **0437 824 776**

bsi ISO 9001 Quality Management Systems CERTIFIED FS787470 ISO 45001 Occupational Health and Safety Management CERTIFIED OHS787471

insitu.com.au

BRISBANE | MELBOURNE | SYDNEY | HOBART | PERTH | TOWNSVILLE | PNG

Eraring Tailings Dam, New South Wales

Menard delivers innovative ground improvement solutions to the dams, tailings, and mining sectors across Australia. At the Eraring Tailings Dam, Menard mitigated undrained and seismic liquefaction risks through precision-installed Vibro Stone Columns, staged earthworks, and real-time instrumentation, achieving an increase in factor of safety above industry recommendations. The Design & Construct delivery model, combined with tailored solutions, also reduced CO_2 emissions by 84% compared to conventional alternatives.

Ground Improvement Specialist

CMC
Stone Columns
Vertical Drains
Mass Soil Mixing
Dynamic Compaction
Soil Mixing
High Energy Impact Compaction (HEIC)
Menard Vacuum™
Rapid Impact Compaction (RIC)
Slurry Walls
Jet Grouting
Dynamic Replacement
Bi-modulus Columns
Compaction Grouting
Vibrocompaction
Anchoring
Rock Grouting
Micropiling

menard

Visit menardoceania.com.au

Sydney (head office)	+61 2 9491 7100
Brisbane	+61 428 829 275
Melbourne	+61 407 926 767
Adelaide	+61 407 926 767
Perth	+61 450 402 239
Auckland (NZ)	+64 22 541 6134

At Menard, we are leaders in our industry and have a proven track record in delivering small and large ground improvement works, in this case for the tailings and dam industry. With over 25 different techniques, Menard can deliver the right solution for your project.

AUSTRALIAN GEOMECHANICS

JOURNAL AND NEWS OF THE AUSTRALIAN GEOMECHANICS SOCIETY

VOLUME 60: NO.4 DECEMBER 2025

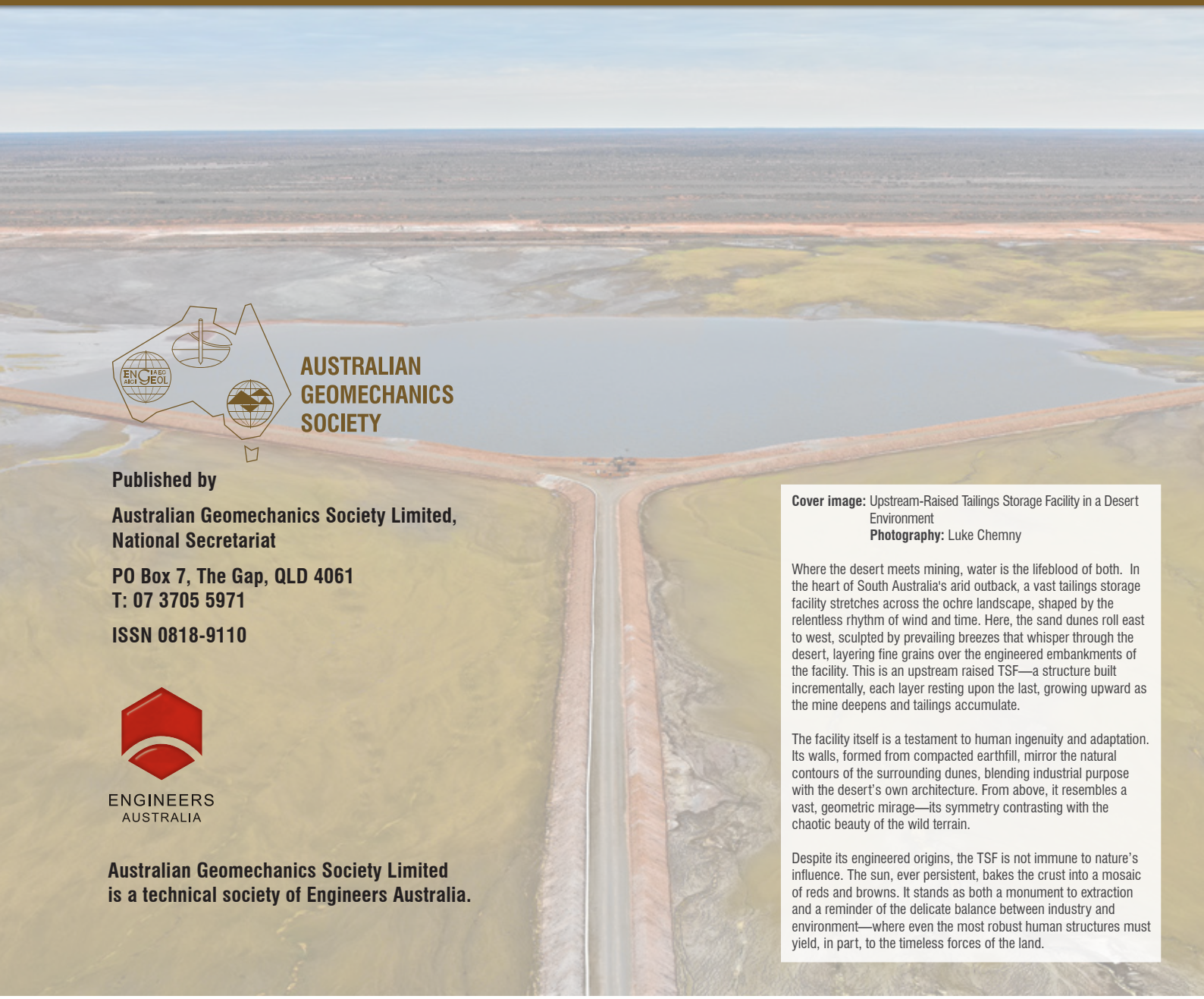

AUSTRALIAN GEOMECHANICS SOCIETY

Published by

Australian Geomechanics Society Limited,
National Secretariat

PO Box 7, The Gap, QLD 4061
T: 07 3705 5971

ISSN 0818-9110

ENGINEERS AUSTRALIA

Australian Geomechanics Society Limited is a technical society of Engineers Australia.

Cover image: Upstream-Raised Tailings Storage Facility in a Desert Environment
Photography: Luke Chemny

Where the desert meets mining, water is the lifeblood of both. In the heart of South Australia's arid outback, a vast tailings storage facility stretches across the ochre landscape, shaped by the relentless rhythm of wind and time. Here, the sand dunes roll east to west, sculpted by prevailing breezes that whisper through the desert, layering fine grains over the engineered embankments of the facility. This is an upstream raised TSF—a structure built incrementally, each layer resting upon the last, growing upward as the mine deepens and tailings accumulate.

The facility itself is a testament to human ingenuity and adaptation. Its walls, formed from compacted earthfill, mirror the natural contours of the surrounding dunes, blending industrial purpose with the desert's own architecture. From above, it resembles a vast, geometric mirage—its symmetry contrasting with the chaotic beauty of the wild terrain.

Despite its engineered origins, the TSF is not immune to nature's influence. The sun, ever persistent, bakes the crust into a mosaic of reds and browns. It stands as both a monument to extraction and a reminder of the delicate balance between industry and environment—where even the most robust human structures must yield, in part, to the timeless forces of the land.

CONTENTS

TECHNICAL PAPERS

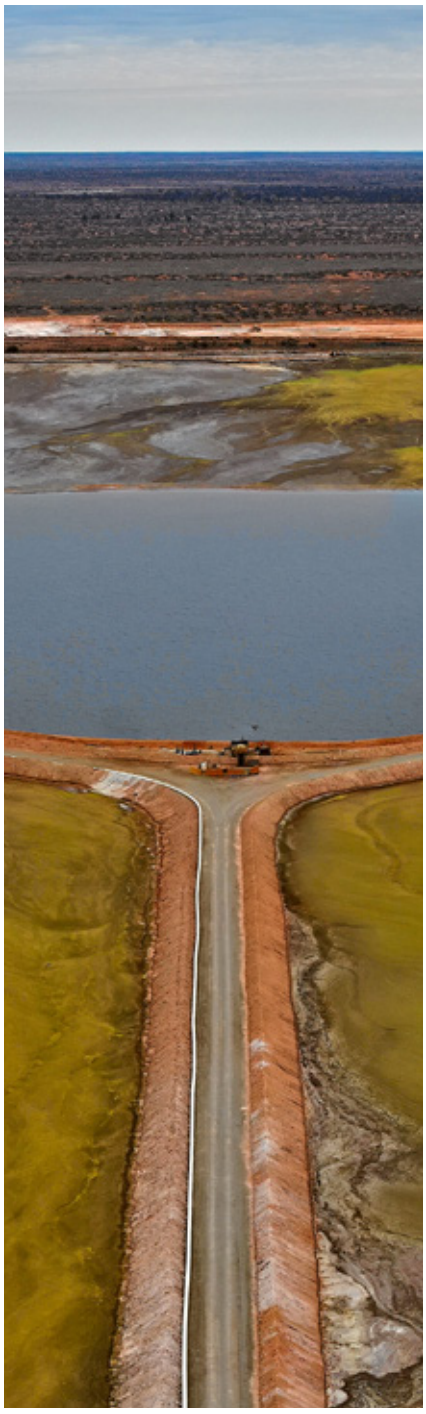

[All papers have been refereed in accordance with the full HERDC review process, unless stated otherwise]

AUSTRALIAN GEOMECHANICS SOCIETY BOARD OF DIRECTORS, NATIONAL STAKEHOLDERS GROUP, MEDIA AND ADMIN SUPPORT

TITLE	NAME	EMAIL
BOARD OF DIRECTORS		
Mr	Timothy THOMPSON *Director, Chair of Board*	chair@geomechanics.org.au
Dr	David LACEY *Director*	dlacey@fsg-geotechnics.com.au
Mr	Amir SHAHKOLAHI *Director*	amir@globalsynthetics.com.au
Ms	Joanna SYLVESTER *Director*	joanna.sylvester@ghd.com
Dr	Ali PARSA-PAJOUH *Director*	aparsa@jkgeotechnics.com.au
NATIONAL STAKEHOLDERS GROUP		
Dr	Davide GUCCIONE *Newcastle Chapter Chair*	davide.guccione@newcastle.edu.au
Prof	Cholachat RUJIKIATKAMJORN *New South Wales Chapter Chair*	cholachat.rujikiatkamjorn@uts.edu.au
Mr	Vincent BLANCHET *Queensland Chapter Chair*	vincent.blanchet@wsp.com
Ms	Lauren AMATO *South Australia & Northern Territory Chapter Chair*	lauren.amato@arup.com
Dr	Nick ROBERTS *Tasmania Chapter Chair*	nick.roberts@stategrowth.tas.gov.au
Ms	Clare BRIDGEMAN *Victoria Chapter Chair*	clare.bridgeman@douglaspartners.com.au
Dr	Andrew LIM *Western Australia Chapter Chair*	per@geomechanics.org.au
Mr	Graham SCHOLEY *ISSMGE Vice President for Australasia*	graham.scholey@wsp.com
Dr	Qianbing ZHANG *ISRM Vice President for Australasia*	qianbing.zhang@monash.edu
Mr	Anthony BOWDEN *IAEG Vice President for Australasia*	anthonyjh.bowden@gmail.com
Dr	Hugo E ACOSTA MARTINEZ *Editor, Australian Geomechanics*	editor@geomechanics.org.au
INVITED MEMBERS, COMPANY SECRETARY		
Mrs	NATALIE QUINLISK *Women in AGS Chair*	natalie.quinlisk@jacobs.com
Mr	Philip ROBINS *NZGS Chair*	chair@nzgs.org
Mr	Jon GIBBS *National Secretariat, Operations Manager*	operations@geomechanics.org.au
MEDIA AND ADMIN SUPPORT		
Ms	Sara LANESMAN *Advertisement, Australian Geomechanics*	lanesman@optusnet.com.au
Mr	James ROBINSON *Web Support*	support@geomechanics.org.au

VIEW FROM THE CHAIR

DECEMBER 2025

Like most people I generally despise feedback surveys. For 'ride-hailing' services, providing feedback is obviously built-in to the service every time we step out of a ride. And if the experience was smooth, feedback should involve one press of the screen. It's only on those occasions when the experience wasn't smooth that feedback can get more complex, and we have to decide how much we care to keep pressing the screen and typing details in. But feedback for 'ride-hailing' services can be a matter of public safety so is truthfully quite important. Less clear is the societal importance of providing feedback for every consumer transaction we make and for every online meeting we hold and for every political party we hear from on a weekly cycle, and for the learned societies where we pursue our Continuing Professional Development (CPD) hours and engage with the profession of our choice.

Beyond the CPD hours, the relevance of the Australian Geomechanics Society (AGS) to the work and livelihood of our members is often a personal choice. The choice is influenced by the use or abuse of particular technical standards that may or may not get attention at our events. It is influenced by how much state registration requirements may or may not assist the ability of some AGS members to authorise certain documents. It is influenced by the desire for greater exposure among our respective companies. And among several additional factors, it is also influenced by our stage in life and career: by young or aging families, work travel, project responsibilities, etc.

I want to thank the 238 AGS members who recently took around 6 minutes of their respective lives to provide us with feedback that will inform a new organisational strategy. Allowing for some people who didn't answer every question, the number of 238 equates to a roughly 8% sample size based on our membership of approximately 3,000. While there is an inherent bias towards engagement from those who cared enough to take 6 minutes of their lives to provide us with feedback, statistically, the internet crunched some numbers for me and I understand that for 95% confidence, 238 of 3,000 should offer a roughly 6% margin of error in the responses. So where the survey has resulted in differences of around 6% or less in the responses, I haven't lent them much significance, unless a wider trend is apparent. For the wonks among us, worth highlighting is that across gender and chapters, the responses we collected do reflect our official numbers relatively well, refer Table 1 and 2:

Table 1: Gender	2025 %	Survey %
Female	14.3	15.8

Table 2: Chapter	2025 %	Survey %
Newcastle	6.0	6.4
Queensland	24.4	25.6
South Australia/Northern Territory	4.4	8.6
Sydney/NSW	27.3	26.1
Tasmania	2.5	2.6
Victoria	22.4	21.8
Western Australia	12.9	9

Question 1: Approximately how many AGS Chapter events would you prefer to see organised each year, including Distinguished Speakers, Symposia, Workshops, etc.?

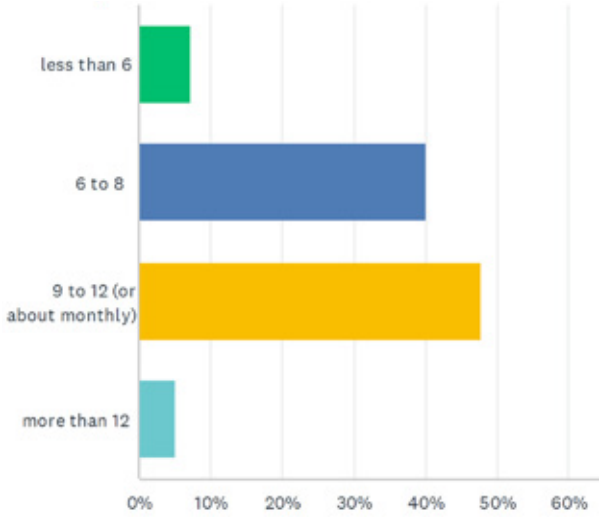

Question 2: Please rate your level of interest on a scale of 1 (lowest) to 5(highest) in the following topics for inclusion in chapter events, whether lectures, courses or workshops.

Category	Weighted Average
Ground Hazards and Risk	4.05
Soil / Rock Mechanics	3.99
Geology / Geomorphology	3.59
Foundations / Retaining Structures	3.54
Site Investigations	3.49
Legal considerations of Geomechanics practice	3.44
Applications of Artificial Intelligence to Geomechanics	3.29
Dams	3.27
Earthworks	3.12
Mining	3
Sustainability considerations of Geomechanics practice	2.88
Offshore Geotechnics	2.76

Starting with the rudimentary stuff, from Question 1 it is apparent that our members are happy for their chapters to continue delivering between 6 and 12 events per year.

Question 2 allowed the ranking of topics, listed above by the surveyed preference. 'Ground Hazards and Risk' received the highest ranking,

which isn't a major surprise. Talking about the dramatic incidents we encounter in our profession, often due to severe weather or earthquakes, does drive interest and engagement, something worth remembering when we promote geomechanics to young people. Lessons learned involving a wide range of ground hazards are generally appealing. But given the margin of error mentioned earlier, the second ranked topic of 'Soil / Rock Mechanics' appears to be just as appealing, and this may be a good reminder that we need to maintain some attention on the roots of the profession.

In the comments allowing further suggestions for topics, 'tunnelling' was most frequently mentioned. So watch-out for opportunities to collaborate with our colleagues at the Australian Tunnelling Society (an offshoot of the AGS in the early 1970s).

Question 3: In terms of overall quality including usability, content, and organisation, how do you rate the quality of the AGS Website?

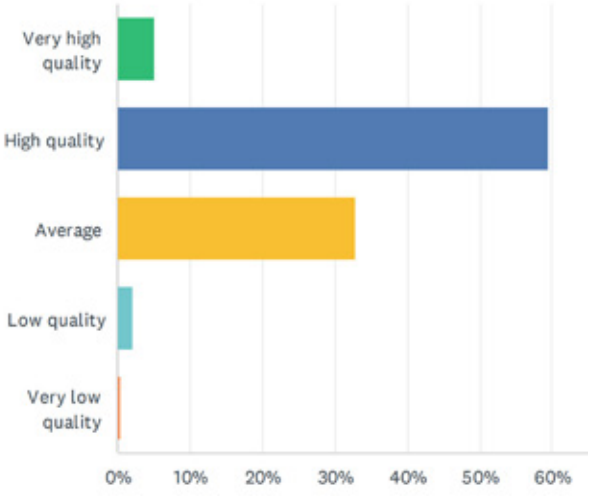

This is helpful feedback as while I think there are some aspects of the website that need to be improved, the site itself is in good shape, and is not in need of much attention under a new strategy.

Question 4:How would you describe your use of the paper version of the Australian Geomechanics Journal?

Use of Journal	Paper %	PDF %
I typically read at least one or two articles/ technical papers from every issue	60.5	27.6
I typically read at least one or two articles/ technical papers a year	21.7	25.3
Total	82.2	52.9

What stands out to me (as was the case for a survey we issued a few years back) is that people who have elected to continue receiving the paper copy of Australian Geomechanics are engaging with it more. The number of those reading at least one or two technical papers per year or more are about 30% higher for the paper version than for the online version. The quarterly journal is released online on the first day of its corresponding month and we have recently been announcing that release on Linked-In. We acknowledge that we can do more to send an email reminder, but it is apparent that behaviours are influenced. The paper copy promotes scanning and reading items of interest, whether directly sought or spontaneously encountered (including the advertisements of our sponsors). An online engagement encourages looking at the table of contents and targeting individual papers with no browsing.

And while on the topic of the journal, we received some comments about our recent decision to make it open access, free to all, members and non-members:

> *What is the point of membership if past and future journal articles are now freely available?*

We anticipated this feedback and first had discussions about it several years back in relation to the question of open access. We balanced the opportunity for more exposure for our authors and sponsors and an overall elevated profile for the journal with a fair question of what value comes from membership.

We offer CPD events, courses at reduced rates for members, and presentation videos that remain behind a membership 'pay wall'. We facilitate a community of practitioners that delivers presentations and discussions of relevance to our membership. From my attendance at two recent Engineers Australia (EA) Engineering Practice Advisory Committee (EPAC) meetings, I know we are possibly the most active Learned Society affiliated with them. I do hope that our members have some awareness of this, and that they find value in supporting us.

While we certainly don't hope for it, we acknowledge that we may lose some membership over this decision and accept that. I also want to note that we received some comments in support:

> *Applaud making the Journal open source.*

While the percentage of our membership affected by state registration requirements doesn't appear to be large in relative terms (refer Question 5), it is a persistent problem for the engineering geologists among us who lack a formal and widely recognised registration scheme in Australia. For members affiliated with the IAEG, over 40% are or are possibly affected as evident for Question 5a below.

Question 5: Has your work been negatively impacted by State Registration requirements?

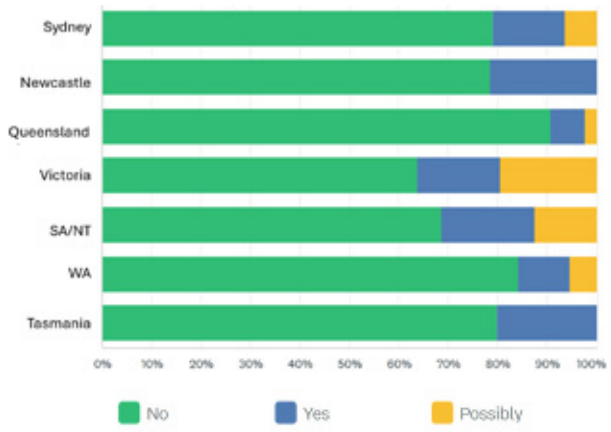

We will maintain an effort to promote the Register of Geotechnical Professionals Australia (RoGPA) scheme. Noteworthy is that while RoGPA was developed by one of my predecessors Darren Paul working with some fellow AGS members, the scheme was instigated and supported by David Cruickshanks-Boyd, EA President from 2013-2015. My fellow Board member Joanna Sylvester, our General Manager Jon Gibbs and I met with Bernadette Foley of EA on two occasions this last July. The meetings were positive, but EA is currently focussed upon the matter of attempting to unify national registration schemes across states, which happens to be the second point of interest highlighted to us most frequently in the comments received. In fact, we will be informing EA of how much many of our members are in support of their efforts. We understand that EA should be in a better position to engage further on RoGPA around January 2027. We also understand that some more work among our engineering geologists will be taking place ahead of that time to refine details relating to how RoGPA might be implemented.

Question 5a: by International Society

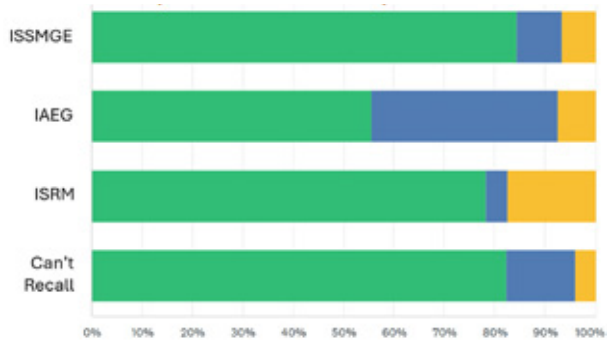

Question 6: Do you believe the AGS should be more active in advocating on behalf of our membership in areas of policy and/or planning? If yes, can you please clarify specific interests (e.g. state registration schemes, planning applications, information sharing, etc.)?

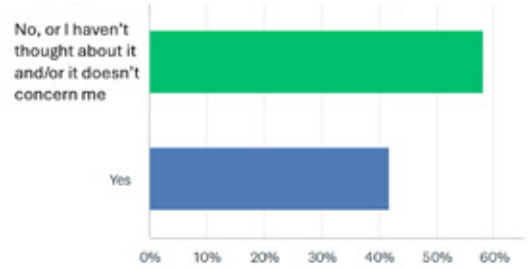

Question 6a: by Chapter

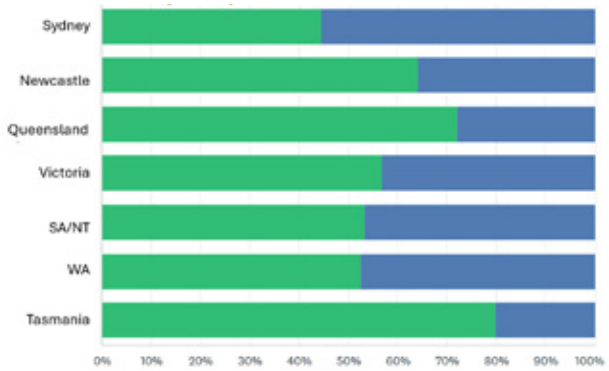

Question 6b: by International Society

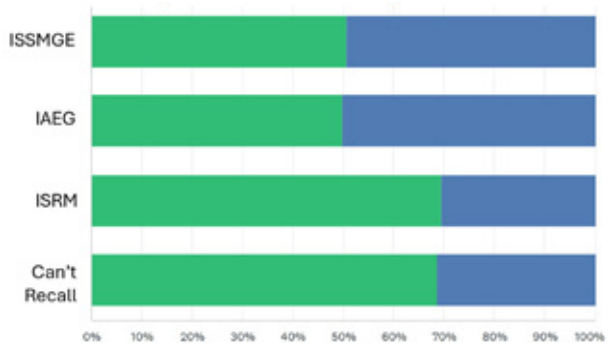

In relation to the development of a strategy for the five years ahead, the AGS leadership has had several recent discussions about the need to raise our profile beyond the normal audience, consisting of ourselves. I was very impressed by the level of engagement I observed in Auckland at the recent New Zealand Geotechnical Symposium between the NZGS and various government authorities there. Having several nationalised entities such as the New Zealand Transport Authority no doubt fosters a direct interaction that is complicated here by different state transportation agencies and others. And the 2011 earthquakes in Canterbury instigated a direct pathway between the profession and government as everyone had to navigate unchartered territory, including new meanings to be found between liquefaction and insurance policies. But the NZGS has fostered relationships and the technical guidance they have developed in recent years with the full engagement of multiple government stakeholders is laudable (not to mention their promotion of the New Zealand Geotechnical Database).

There are different appetites for advocacy from within the AGS, between the chapters and the International Society affiliations. Note an equivalent interest for advocacy from those affiliated with the ISSMGE and IAEG, even allowing for the two probably different motivations noted earlier: recognition through registration and consistency in registration across states. (As an aside, I note that 28% of survey respondents can't recall which of the three international societies they might be affiliated with. While I don't advocate for this number to be higher, I think it is a healthy reminder that some only see 'AGS'.) As I've typed in this space previously, I think EA is the most logical first partner to work more with. And if we can find the enthusiasm among our volunteers, I'm hopeful that more connections can be made.

On the topic of enthusiasm, I want to compliment the Women in AGS (WiAGS) group started by Nina Levy and now led by Natalie Quinlisk. They have drafted a 'Safe Site Guide' that we discussed at our most recent National Board and National Stakeholders Group (NSG) meeting in Sydney on 31 October. We will be refining the guide with a view to issuing early next year and the effort that has gone into it is worth replicating in more directions. From our member survey, of the roughly 15% of our membership that is female, 80% is less than 45 in age. We know that of our members under 35, over 20% are female (compared to 14% overall) and while parity doesn't have to be the objective, enthusiasm from a growing demographic among us is a thing we want to keep supporting.

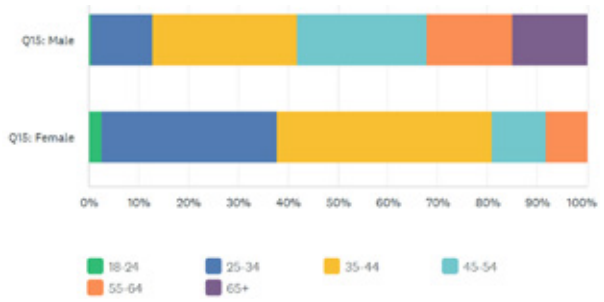

I want to provide some comments on more comments:

> *The cost for the events and workshops is far too high. It's cost prohibitive to many smaller players and their staff. This is a common gripe we have and know of many other smaller consults who feel the same way. I would assume most the presenters are volunteering their time so not sure why so high. There is plenty of experience in the membership which would be available for free to share the load for these events as required one would assume.*

Our course instructors receive a standard day-rate for their time, noting that most are taking time away from their regular day-job. They are not in fact volunteers, and fees are meant to compensate for that. The courses are also generally well-subscribed and are often less expensive than professional learning courses offered by other organisations. We will continue to review course fees in response to feedback, and do acknowledge the degree to which registration costs for anything can sometimes be more challenging for smaller organisations to absorb.

And following on from that:

> *Sounds like the only type of event AGS is interested [in] is courses that can get them more money. People know the AGS has money that is being spent on committee members to have breakfast instead of promoting the profession with local universities, offer free courses (the AGS has the resources!), engage with practitioners and bridge the gap with universities to fund research, fund charities such as Engineers Without Borders, etc*

The comment is based on several perceptions and is actually 'aspirationally' aligned with some of our recent discussions on strategy. So I include it, and to be fair, the comment also reflects a need on the part of the AGS to more effectively communicate our priorities and activities. Firstly, we will be releasing an annual report around the time of the next Annual General Meeting in April. I believe this will be the first report from the AGS in over 15 years to summarise the finances of the organisation, now a company limited by guarantee, with the intent to demonstrate more transparency and ensure on-going government compliance.

In relation to our financial commitments beyond paying our instructors, General Manager Jon Gibbs, accountant, website designer and insurances, we have two current significant investments in:

a) an update to the 2007 Landslide Risk Management Guidelines with the NZGS, and;

b) a partnership with Australian Earth Science Education to develop new educational materials for secondary schools in Australia.

We are now also reviewing a potential additional collaboration with the NZGS for their slope design guidance.

I led the organisation of the AGS Queensland Symposium in Brisbane in 2014 and 2015. I have fond memories of those events, including the time someone started washing the windows directly behind a speaker from the street outside of the Treasury Casino where we held the event. As the organiser I was the one who had to run out to the street to ask the washer to stop in the interest of maintaining the sunlight and the quiet during a presentation. From moments like that I'm very appreciative when I see chapter members – now having attended Brisbane, Sydney, and Melbourne Symposia – running around to address things (disruptions, complaints, the flow of food and coffee at breaks, etc.) that make events work, as volunteers, so that others don't have to. The monthly avocado on toast and a nice flat white in a big mug are part of the fair compensation to acknowledge the contributions that committee members make to the AGS. I would readily acknowledge that some chapter committee members are more active than others, and therefore more deserving of the avocado on toast and the nice flat white in a big mug. But varying levels of contribution sounds like most organisations, and some of the less active committee members do become more active members through familiarity and time.

While acknowledging our need to develop a strategy that will help us to better invest in our profession (and to potentially engage with universities, as rightly noted), I unapologetically endorse monthly breakfasts for our chapter committees and hope that many of our committee members stay active and engaged with time.

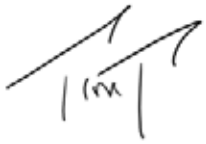

TIM THOMPSON

2025 National Chair, Australian Geomechanics Society

CHAPTER NEWS

QUEENSLAND

This report includes the Queensland Chapter news from April 2025 to October 2025. The activities included a social event and multiple technical presentations. Please visit the AGS Queensland Chapter webpage for future activity updates.

Soil and Rock Logging Course held at TMR's Northgate Core Facility, by Ian Shipway and Sally Roberts-Kelly

Friday 16 May 2025

The course which is part of National Series was fully attended by junior to intermediate geotechnical practitioners and contractors. Attendees gained valuable practical experience and tuition on describing and classifying various natural and fill materials, including rock cores from a range of geological origins. A big thanks to Transport Main Roads Queensland (TMR) for providing the venue and samples and to the presenters Ian Shipway and Sally Roberts-Kelly as well as Simon Foley for successful coordination of the Brisbane session.

Ian Shipway in action delivering lecture on soil logging to the course attendees at the Northgate Core Facility, Brisbane

Attendees watching demonstration of Point Load Index Test at the Soil and Rock Logging Course at Transport Main Roads, Brisbane.

Advancing Remote Monitoring with Satellite Technology by Dr Skevi Perdikou and Dr Andrew Lees

Wednesday 28 May 2025

Recent advances in remote monitoring with satellite technology were presented by Dr Andrew Lees and Dr Skevi Perdikou during a webinar with over 40 members attending. The presentation explores the technical foundations of satellite-based remote monitoring, focusing on key methodologies such as Interferometric Synthetic Aperture Radar (InSAR) for ground deformation detection, optical and multispectral imagery for geotechnical application.

Reimagining Unbound Road Pavement Technology: Integrating Advances in Unsaturated Soil Mechanics, Testing, Design, Construction and Performance in the Post-digital Era, E.H Davis Lecture 2021 by Professor Jayantha Kodikara

Reimagining Unbound Road Pavement Technology: Integrating Advances in Unsaturated Soil Mechanics, Testing, Design, Construction and Performance in the Post-digital Era, E.H Davis Lecture 2021 by Professor Jayantha Kodikara

Wednesday 11 June 2025

Over 40 members gathered at Rydges Fortitude Valley to hear Prof. Kodikara share insights from the SPARC Research Hub highlighting how innovations in unsaturated soil mechanics, testing, design, construction, and asset management can enhance decision making and performance across the full lifecycle of unbound road pavements. The presentation also explored future research directions, including climate resilience and sustainability, to build more adaptive and efficient infrastructure.

Prof. Jayantha Kodikara delivering a presentation on unbound pavement advances. Left to right Jared Priddle, Prof. Jayantha Kodikara and Vincent Blanchet

Insitu Testing Practical Workshop at Port of Brisbane by David Lacey and Robin Power

Thursday 12 June 2025

The AGS QLD Chapter hosted the Insitu Testing Practical Workshop,

hosted at the Port of Brisbane. Led by Dr David Lacey and Robin Power, the workshop provided early-career practitioners with hands-on experience across a broad range of insitu testing techniques. Participants engaged with geophysical methods such as Multi-channel Analysis of Surface Waves (MASW) and Ground Penetrating Radar (GPR), penetration tests including Cone Penetration Testing (CPT) with Dilatometer Test (DMT), dynamic probing systems, and bearing capacity assessments using Plate Load Tests (PLT) and Light Weight Deflectometers (LWDs).

The workshop offered a unique opportunity to observe full-scale testing and interact with experienced operators, reinforcing the importance of accurate field data in geotechnical practice. The AGS extends its appreciation to the supporters and collaborators whose contributions made this event possible: FSG Geotechnics & Foundations, Insitutek, Civil Geotechnical Consultants, Douglas Partners, Insitu Geotechnical Services, Qualtest Laboratory, QUT, WSP, and the Port of Brisbane for hosting.

Attendees and presenters stand with some of the field equipment demonstrated on the day, Port of Brisbane

International Women in Engineering Day – AGS technical breakfast

Thursday 19 June 2025

AGS QLD Chapter celebrated International Women in Engineering (+Geology) Day on Thursday, 19 June at Calile Hotel, Fortitude Valley. The morning event was sold out and attended by over 90 members. Three technical presentations were delivered by leading Women in the Ground Engineering industry.

Presentations at the morning included:

- Natalie Murphy (WSP): "Taming SEQ's Soft Soils: Probabilistic Settlement & Risk-Based Surcharge Design
- Sayteng Seah (Aurecon): "Cyclic Softening in Cohesive Soils during Earthquakes"
- Liz Elphick (PSM): "Use of RocSlope3 to Manage Bench to Multiple Bench Geotechnical Instability"

The morning was MC'd by Arsh Kaur and sponsored by Menard, CGC, Douglas Partners, BGC, ENGEO, Aurecon, FSG, SLR. The event was organised by AGS QLD Women sub-committee Arsh Kaur, Natalie Quinlisk, Hannah Down and Ramathi Gunasekera.

"IWED Event" event organisers and presenters. Left to right: Vincent Blanchet, Dr Arsh Kaur, Natalie Murphy, Liz Elphick, Sayteng Seah, Hannah Down and Ramathi Gunasekera

"The Room", attendees enjoying technical presentation with breakfast at the Calile.

Laboratory Testing Course by Richard Kelly, Ian Shipway and David Lacey

Wednesday 27 August 2025

The 2025 #AGS QLD Chapter Laboratory Testing Workshop on August 27th was a resounding success, providing valuable and hands-on experience by 22 attendees including contractors, academicians and consultants from various industries participating in.

This achievement was made possible by the collective effort of key partners. Our host ENGEO at their new laboratory facility in Yatala, QLD with Daniel Dobe and his team. Our presenters for their continuous support to the community Dr Richard Kelly, Dr David Lacey, and Ian Shipway for expertly guiding the workshop and sharing their deep industry knowledge. The event was organised and coordinated by Mohsen Sadeghi.

"The Room", attendees enjoying technical presentation with breakfast at the Calile.

Constitutive Model in Computational Geomechanics - 61 Rankine Lecture – by Professor John Carter

Wednesday 3 September 2025

The AGS Queensland Chapter hosted the 61st Rankine Lecture at Engineers Australia Auditorium in Brisbane, presented by Emeritus Professor John Carter of The University of Newcastle and was attended by over 50 members. His lecture "Constitutive Modelling in Computational Geomechanics," examined the pivotal role of constitutive models in predicting geotechnical behaviour. Professor Carter highlighted how idealisations within these models can lead to significant errors (if misunderstood or misapplied). He reviewed many constitutive models, their capabilities and limitations, and stressed the importance of aligning model attributes with the specific demands of each geotechnical problem.

The Rankine Lecture is one of the most prestigious events on the global geomechanics calendar, and its delivery in Brisbane continues to show the commitment of the AGS to bring these events to our shores. The Chapter extends its appreciation to Professor Carter for delivering this distinguished lecture, to Engineers Australia for hosting, and Clinton Chan and Jon Gibbs for organising the event.

Emeritus Professor John Carter presenting the 61st Rankine Lecture at the Hawkin Auditorium, Engineers Australia, Brisbane

Dinner with Professor John Carter Left to right: Jaime Wilson, Prof. John Carter, Prof. David Williams, Jon Gibbs, Dr. Richard Kelly, Dr. Arsh Kaur, Clinton Chan

SOUTH AUSTRALIA AND NORTHERN TERRITORY

Chapter Events

Ivy Moland, Engineering Geologist from Aurecon, delivered a presentation titled "From Field to Office," aimed at professionals interested in digital data capture in the field and its transformation into geotechnical logs. She showcased the digital transformation of geotechnical data workflows at Aurecon in Australia and New Zealand, with a detailed case study of the semi-complex New Zealand setup. The talk focused on the adoption of a new digital system that integrated field data capture with back-end data management, streamlining the conversion of raw data into geotechnical logs. Practical challenges were explored, including the setup of standardized geological descriptions, management of in-situ testing data, and verification of data across devices and platforms. Moland highlighted examples of increased efficiency that reduced the need for manual data modification, post-field data entry, and manual translation—ultimately making the process easier for both site and design staff.

Presentation by Ivy Moland (Aurecon)

Dr Matthew Duthy and Dr Peter W. Mitchell presented "Case Examples of Terra-Forming and Other Geotechnical Projects in the Adelaide Area." This presentation expanded upon a talk previously given by Dr Duthy at the SA Heritage seminar in Adelaide. Dr Duthy focused on European interactions with Adelaide's landscape and natural resources, outlining

how these interactions were initially driven by physiological and safety needs—such as access to fresh water, food, shelter, flood immunity, and transport—and later by economic development. Drawing on their combined 89 years of experience with Adelaide-based projects, the presenters outlined several geotechnical projects primarily driven by economic development. They illustrated how natural geotechnical processes, sub-surface conditions, and soil properties had been overcome or accommodated.

Presentation by Matthew Duthy (GHD)

Case histories included footing systems for building developments, with observations on load vs. deflection behaviour of spread and mat footings, and basement movements in multi-storey buildings constructed on unsaturated Adelaide clays in the CBD. The presentation also covered surface water drainage from the Adelaide plains and coastal erosion along the foreshore, discussing their impact on projects such as the Torrens Lake Weir, Torrens Outlet, Witton Bluff stabilisation, and the Barcoo Outlet. Further examples included successful infrastructure construction on the soft, compressible estuarine soils of the LeFevre Peninsula, with measured load vs. settlement behaviour of embankments. The presenters concluded with insights into the load vs. deflection responses of various pile types founded in Hindmarsh Clay, including bulbous base, CFA, precast driven, and concrete screw piles, as applied in projects like Holdfast Shores and Outer Harbor.

Presentation by Peter Mitchell (Aurecon)

Lauren Amato; SA/NT Chapter Chair

TASMANIA

Virtual technical presentation with the Victoria Chapter

One of our more recent technical talks saw a departure in presentation approach. Instead of the typical in-person presentation based in Hobart with a video link to Launceston, content was delivered fully online to the Tasmania and Victoria chapters, together.

The content – combining diverse remote monitoring techniques – presented by Drs. Andrew Lees and Skevi Perdikou of Geofem gave insights into new possibilities for characterising geohazards on both sides of Bass Strait. Future periodic co-presentations with Victoria are being considered as an option to increase interaction with Tasmania nearest AGS colleagues.

Southern Tasmania social event

AGS members from across southern Tasmania gathered for an informal catch up in Salamanca along Hobart's waterfront in August. Although social in nature, discussions inevitably shifted to diverse geomechanics topics.

Thank you to all those who turned out, despite the cool weather. It was lovely to see some fresh faces and meet prospective members. We are looking forward to similar social gatherings in Launceston and Hobart ahead of the summer holidays.

Tasmania Chapter members braving Hobart's winter cold for an overdue social catchup

Nick Roberts, Tasmania Chapter Chair

LaRGE 2026

Landslide Risk & Geo-Education

27 APRIL – 3 MAY 2026

An International Workshop of JTC1 & JTC3

QUEENSTOWN, NEW ZEALAND

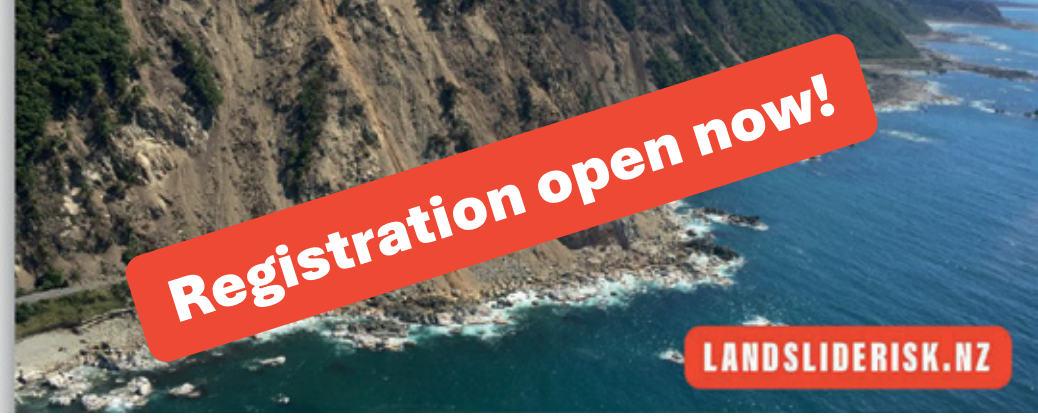

NAU MAI, HAERE MAI – WELCOME!

New Zealand invites you to a landmark internation event - the 1st International Joint Workshop of Joint Technical Committee 1 and Joint Technical Committee 3. We will share the latest research and develop best practice guidelines in the stunning city of Queenstown. Our theme *"Landslide Risk & Geo-Education"* unifies the full lifecycle of landslide risk management. It encompasses the need to educate the next generation of landslide risk managers, to understand landslide risk, and to communicate that risk to the public and decision makers so that real change is implemented. Bringing together JTC1 and JTC3 on key aspects of landslide risk – assessment, education, communication, and outreach – will drive strategic improvements in managing landslide risk. You'll hear from international experts including:

David Petley is recognised widely as a world leader in the study and management of landslides and for his popular blog on landslides which receives over 500,000 individual visits per year.

Jean Hutchinson is a Professor Emerita of Geological Engineering at Queen's University, Alberta Canada, and the Vice President of Innovative Geomechanics Inc.

Gonghui Wang is a professor at the Disaster Prevention Research Institute (DPRI), Kyoto University Japan, and serves as the head of the Research Center for Landslide Risk Cognition and Reduction at DPRI

Jo Horrocks is Chief Resilience and Research Officer at the Natural Hazards Commission, leading their science, data, and modelling to improve understanding of natural hazard risks and how to reduce them.

Reginald Hermanns is Professor at Norwegian University of Science and Technology. Research includes rock-slope stability, and the technical and societal response to landslide threats.

Lori Peek is director of the Natural Hazards Center and professor in the Department of Sociology at the University of Colorado Boulder. She has written award-winning books on the social impact of disasters.

Nicola Casagli is professor of Engineering Geology at the University of Florence, immediate past President of the International Consortium of Landslides, and President of the 6th World Landslide Forum.

Tim Davies is a former member of JTC1, convenor of the conference series on Debris-Flow Hazard Mitigation, and former Editor of Journal of Hydrology (NZ). He has held visiting fellowships at Durham University, UK and ETH-Zürich.

Ann Williams is Past Chair and Life Member of NZGS, past Vice President and Honorary Member of the IAEG and has worked internationally on landslide risk assessment and reduction.

Janusz Wasowski is the Editor-in-Chief of Engineering Geology. His research includes landslide assessment, collateral seismic hazards, and air/space-borne remote sensing.

This international workshop conference is hosted by the New Zealand Geotechnical Society and is endorsed by the member societies of the Federation of International Geo-Engineering Societies:

New Zealand Geotechnical Society

Field trips

Clyde Dam Landslide Stabilisation

Known landslides were monitored during the construction phase, and it was discovered that some 'dormant' slides in the Cromwell gorge were slowly moving downhill. Exploratory drilling for a new highway led to the discovery of a complex, high-pressure groundwater system, and this led on to an extensive drilling programme on other landslides. A strategy was developed for a fast-track stabilisation program, based primarily on the use of tunnels for both investigation and drainage.

Glenorchy Resilience Project

With a focus on education, natural hazard communication, and community resilience, this trip will visit the stunning village of Glenorchy. Directly exposed to multi-hazards from flooding, earthquakes and liquefaction, it is vulnerable to being cut off by landslides. A natural hazards adaptation strategy was developed in partnership with the local community. This tour will investigate how the strategy was developed and is being implemented with the community.

Milford Sound Cruise

Deep within Fiordland National Park lies Milford Sound, New Zealand's most stunning natural attraction. A million people a year visit Milford Sound. The nearby Alpine Fault ruptures, on average, every 330 years with a magnitude 8 earthquake, and this would likely cause a very significant rockslide. A landslide-triggered tsunami may leave no survivors, with as many as 3500 dying. This field trip will explore the decision-making process required to balance the public interest in visiting this natural wonder with the potential risk it poses.

Registration open now at landsliderisk.nz

Why attend? This landmark international event unites JTC1 and JTC3 to advance landslide risk assessment, education, communication, and outreach – creating a unique opportunity for diverse impacts, and will be attended by leading experts from around the world.

The workshop is structured around specific projects through interactive sessions. Beyond disseminating knowledge, we will generate new ideas, develop ongoing projects, and create tangible outputs including guidelines and research direction.

LaRGE2026 also delivers great training courses, keynote speeches, presentations, poster sessions, and field trips. The training courses will span landslide risk assessment, emergency response, science communication, and landslide geoeducation.

Sponsorship opportunities available now!

Why sponsor? By sponsoring, your organisation will have the opportunity to profile your ideas and solutions on the global stage as well as connect with global experts, local practitioners, government representatives and key decision makers from around the world. Your name will be associated with real deliverables that will outlive the event and drive meaningful change in New Zealand and around the world. We look forward to your participation in making LaRGE2026 a success, and to being permanently associated with the great outcomes of the workshop!

Programme – Tue 28 April to Sun 3 May 2026

Mon **New Zealand Public Holiday** - IAEG Executive meeting and reserve day for training and fieldtrips.

Tues **Field trips & exercises** - Three field trips carefully aligned with the objectives of the workshops.

Wed **Training** - Learn from industry experts in the field of landslide risk management and science communication. Offerings include land use planning for landslide risk reduction, media training, rapid building assessment, slope stability guidelines and more.

Thur **Workshop Day 1 - Susceptibility, Data & Risk.** Presentations and workshops on advanced monitoring techniques.

Fri **Workshop Day 2 - Risk to Policy.** Presentations and workshops on landslide risk assessment techniques.

Sat **Workshop Day 3 - Outreach & Education.** Presentations and workshops on geoeducation and risk communication.

Sun **Additional Field Trips & Exercises** including an informal wine-tasting landslide focused trip.

CONFERENCE CALENDAR

JANUARY 2026	
15-17	RocDyn-5 Fifth International Conference on Rock Dynamics and Applications, Singapore *https://isrm.net/conference/show/6393*
19-23	CTTU (Construction Technology in Tunnelling and Underground) and TBM DiGs (Tunnel Boring Machines in Difficult Grounds) 2026, Melbourne, Australia *https://www.monash.edu/engineering/tunnel2026*
28-30	22nd Southeast Asian Geotechnical Conference 2026 (SEAGC 2026), Manila, Philippines *https://seagc2026.pssmge.org/*
FEBRUARY 2026	
3-6	2026 Australian Earth Sciences Convention (AESC 2026), Melbourne, Australia *https://aescgsa.com.au/*
MARCH 2026	
25-28	Inaugural Pan Mediterranean Geotechnical Engineering Conference (PMGEC), Beirut, Lebanon *https://pmgec-leb.com/*
11-13	2nd International Symposium on Tailings Deposits, Hermosillo, Sonora, Mexico *https://2sisdj-hermosillo-2026.com.mx/*
25-28	Inaugural Pan Mediterranean Geotechnical Engineering Conference (PMGEC), Beirut, Lebanon *https://pmgec-leb.com/*
APRIL 2026	
16-17	8th International Conference on Geotechnics, Civil Engineering and Structures (CIGOS), Ho Chi Minh City, Vietnam *https://cigos2026.sciencesconf.org/*
27-3 May	Landslide Geo-Education and Risk (LAGER) - First International Joint Workshop of JTC1 and JTC3, Queenstown, New Zealand *https://landsliderisk.nz/* **AGS SUPPORTED**
MAY 2026	
15-21	World Tunnel Congress (WTC2026) - Connecting Communities through Underground Infrastructure, Montréal, Canada *https://www.tunnelcanada.ca/wtc2026.php*
18-20	2026 DFI-PFSF Piling & Ground Improvement Conference, Sydney, Australia *https://www.dfi-events.org/dfi-pfsf26/*
21-29	ICOLD 2026 94th Annual Meeting, Guadalajara, Mexico *https://www.icoldmexico2026.com/*
24-27	16th International Conference “Under *https://www.ucprague.com/*
JUNE 2026	
11-14	8th International Young Geotechnical Engineers Conference (8iYGEC), Graz, Austria *https://www.tugraz.at/institute/ibg/events/8iygec*
14-19	21st International Conference on Soil Mechanics and Geotechnical Engineering, Vienna, Austria *https://www.icsmge2026.org/en/*
21-24	60th US Rock Mechanics / Geomechanics Symposium, Tucson, Arizona, USA *https://armarocks.org/tucson-2026-symposium/*
21-24	12th International Conference on Bearing Capacity of Roads, Railways, and Airfields (12 BCRRA 2026), Ljubljana, Slovenia *https://bcrra.si/*
24-26	SuperPile ’26 - Piling Design and Construction Conference, New Orleans, Louisiana, USA *www.dfi.org/superpile2026*
JULY 2026	
21-24	Australian Conference on Rock Mechanics (ACRM), Melbourne, Australia *https://australiangeomechanics.org/meetings/acrm2026/* **AGS EVENT**
AUGUST 2026	
6-10	12th International Symposium on Field Monitoring in Geomechanics 2026, Indore, India *https://isfmg2026.com/*
14-16	10th International Conference on Geoscience Education (GeoSciEd X), Adelaide, Australia *https://eventstudio.eventsair.com/geoscoed-conference-2026/*
24-25	4th International Conference on Geotechnical Engineering - Resilient Geotechnics for a Sustainable Future, Colombo, Sri Lanka *https://icgecolombo2026.org/*
24-26	International Conference on Advances and Innovations in Soft Soil Engineering, Delft, Netherlands *https://www.issmge.org/events/international-conference-on-advances-and-innovations-in-soft-soil-engineering-2026*
26-28	X Latin American Congress on Rock Mechanics - an ISRM Regional Symposium, Brasilia, Brazil *https://isrm.net/conference/show/6388*

CONFERENCE CALENDAR

SEPTEMBER 2026	
7-8	3rd International Conference on Construction Resources for Environmentally Sustainable Technologies (CREST 2026), Cambridge, UK *https://engage-events.ifm.eng.cam.ac.uk/IC-CREST2026#/*
9-12	XXI Technical Dam Control International Conference, Krakow, Poland *https://tkz.is.pw.edu.pl/en/*
13-17	13 ICG – 13th International Conference on Geosynthetics - "Legacy, Evolution & Revolution in Geosynthetics", Montreal, Canada *https://www.geosyntheticssociety.org/events/13-icg-13th-international-conference-on-geosynthetics-montreal-canada/*
14-19	Eurock 2026 - Risk Management in Rock Engineering - an ISRM Regional Symposium, Skopje, North Macedonia *https://isrm.net/conference/show/6376*
16-18	Fourth International Symposium on Geotechnical Engineering for the Preservation of Monuments and Historic Sites, Athens, Greece *https://tc301-athens.com/*
OCTOBER 2026	
13-16	JTC2 Conference: 6th International Conference on Information Technology in Geo-Engineering - an ISRM Specialized Conference, Graz, Austria *https://www.icitg2026.com/*
22-25	7th International Conference on Environmental Geotechnology, Recycled Waste Materials, and Sustainable Engineering (EGRWSE-2026), Surat, India *https://www.icitg2026.com/*
26-29	Slope Stability 2026 - Slope for Safety Performance, Lima, Peru *https://www.slopestability2026.com/en*
30-6 Nov	XV IAEG World Congress, Delft, The Netherlands *https://iaeg.info/event/xv-iaeg-world-congress/*
NOVEMBER 2026	
4-6	International Conference on Performance-Based Design in Earthquake Geotechnical Engineering (PBD), Puerto Varas, Chile *https://www.pbd-v-chile.com/*
22-27	14th Asian Rock Mechanics Symposium - Rock Mechanics for the Next Generation – Innovations, Sustainability, and Resilience, Fukuoka, Japan *https://www.ec-convention.com/ARMS14/*
26-27	6th International Conference on Geotechnics for Sustainable Infrastructure Development, Hanoi, Vietnam *https://geotechn.vn/*
MARCH 2027	
17-19	7th International Conference on Grouting and Deep Mixing, Florence, Italy *https://dfi.org/events/upcoming-events/*
APRIL 2027	
12-14	International Symposium on Ground Improvement (IS-GI Lyon 2027,TC-211 Symposium), Lyon, France. *https://www.menard-group.com/isgi-lyon2027/*
23-29	World Tunnel Congress (WTC 2027), Antwerp, Belgium *https://about.ita-aites.org/future-events*
MAY 2027	
12-14	International Symposium Cone Penetration Testing CPT '27, Vancouver, British Columbia, Canada *https://www.cpt27.org/*
TBC	Geotechnics for Mountrain Infrastructure, GeoMandu 2027, Kathmandu, Nepal *https://geomandu.ngeotechs.org/*
SEPTEMBER 2027	
21-24	11th European Conference on Numerical Methods in Geotechnical Engineering (NUMGE 2027), Graz, Austria, *https://www.tugraz.at/events/numge2027/*
OCTOBER 2027	
17-23	16th ISRM International Congress on Rock Mechanics, Seoul, Korea *http://isrm2027.website.or.kr*
MARCH 2028	
26-29	18th Panamerican Conference on Soil Mechanics and Geotechnical Engineering and Geo-Congress 2028, Chicago, Illinois, USA *https://www.geocongress.org/*
JUNE 2028	
25-30	Eurock2028 - Advances in rock mechanics and rock engineering to cope with increasingly extreme conditions, Aix-en-Provence, France *https://isrm.net/conference/show/6396*
SEPTEMBER 2029	
1-5	6th International Conference on Transportation Geotechnics, Southampton, United Kingdom *https://inconference.eventsair.com/cmspreview/ictg-2029*

AGS advises that the status of events at any time should be checked using the links to the event websites.

CORPORATE MEMBERS

The Australian Geomechanics Society gratefully acknowledges the contribution made by its Corporate Members.

FIRM	ADDRESS				PHONE
5QS Consulting Group	PO Box 63	WARNERS BAY	NSW	2282	(02) 4952 1666
A. S. James Pty Ltd	15 Libbett Avenue	CLAYTON SOUTH	VIC	3169	(03) 9547 4811
AECOM Australia Pty Ltd	PO Box 1307	FORTITUDE VALLEY	QLD	4007	(07) 3553 3276
Aitken Rowe Testing Laboratories Pty Ltd	Unit 4, 2 Riedell Street	WAGGA WAGGA	NSW	2650	(02) 6939 5555
Alliance Geotechnical Pty Ltd	10 Welder Road	SEVEN HILLS	NSW	2147	1800 288 188
Anora Foundations Pty Ltd	PO Box 3282	DARRA	QLD	4076	(07) 3279 7966
Arcadis Australia Pacific Pty Ltd	Level 16/580 George Street	SYDNEY	NSW	2000	(02) 8907 9150
Arup Australia Services Pty Ltd	Level 4, 108 Wickham Street	FORTITUDE VALLEY	QLD	4006	(07) 3023 6000
ATC Williams Pty Ltd	222-225 Beach Road	MORDIALLOC	VIC	3195	(03) 8587 0985
Aurecon Australasia Pty Ltd	Level 11, 73 Miller Street	NORTH SYDNEY	NSW	2060	(02) 9465 5599
Barrason's Engineers	Shop 1, 206 Princes Hwy	PAKENHAM	VIC	3810	(03) 5940 2638
BGC Engineering Pty Ltd	Level 3, 31 Merivale St	SOUTH BRISBANE	QLD	4101	0498 814 792
Butler Partners Pty Ltd	79 Doggett Street	NEWSTEAD	QLD	4006	(07) 3852 3800
CPTS	16 Charles Place	MANLY WEST	QLD	4179	0407 375 977
Chadwick Geotechnics Pty Ltd	25 Metcalf St	DANDENONG SOUTH	VIC	3175	(03) 8796 7900
Civiltest Pty Ltd	PO Box 537	MORNINGTON	VIC	3931	(03) 5975 6644
CONETEC Pty Ltd	6 Chapman Pl	EAGLE FARM	QLD	4009	0473 923 084
Core Consultants Pty Ltd	Unit 1, 18 Lysaght St	COOLUM BEACH	QLD	4573	(07) 5475 5900
CMW Geosciences	Level 1, 60 Kingsford Smith Drive	ALBION	QLD	4010	(07) 3320 8503
Douglas Partners Pty Ltd	15 Callistemon Close	WARABROOK	NSW	2310	(02) 4960 9600
Durham Geo Slope Indicator	Unit 1/82 Reserve Street	WEMBLEY	WA	6014	(08) 9284 9090
EcoFine Material Pty Ltd	27 Rogers Way	LANDSDALE	WA	6065	(08) 9303 9297
EDG Consulting Pty Ltd	Level 1, 18 Wandoo St	FORTITUDE VALLEY	QLD	4006	0427 773 815
El Australia Pty Ltd	Suite 601, 55 Miller St	PYRMONT	NSW	2009	(02) 9516 0722
Fortify Geotech Pty Ltd	39 Sydenham Road	ALEXANDRIA	NSW	2204	(02) 9188 4033
Fugro Australia Pty Ltd	Level 1, 1060 Hay Street	WEST PERTH	WA	6005	(08) 9218 2000
GBG Group	Unit 28, 7 Salisbury Rd	CASTLE HILL	NSW	2154	(02) 9890 2122
Geobrugg Australia Pty Ltd	PO Box 2468	MALAGA	WA	6944	(08) 9249 9939
Geofabrics Australia Pty Ltd	83-93 Canterbury Road	BRAESIDE	VIC	3195	(03) 8586 9100
Geomotion (Australia) Pty Ltd	9/31-33 Chaplin Drive	LANE COVE	NSW	2066	(02) 9693 5493
Geotech Pty Ltd	174 Turner Street	PORT MELBOURNE	VIC	3207	(03) 9624 4200
Geotechnique Pty Ltd	PO Box 880	PENRITH	NSW	2751	(02) 4722 2700
Geotesta Pty Ltd	6/31-37 Howleys Road	NOTTING HILL	VIC	3168	(03) 9562 8808
GHD Pty Ltd	Locked Bag 2727	ST LEONARDS	NSW	1590	(02) 9462 4859
Global Synthetics Pty Ltd	41 Sammut St Smithfield	SMITHFIELD	NSW	2164	(02) 9725 4321
Ground Recruitment Pty Ltd	Level 28 - AMP Tower, 140 St Georges Terrace	PERTH	WA	6000	(08) 6189 4960
HAWK GEO Pty Ltd	42 Douglas Farm Road	KURRAJONG HILLS	NSW	2758	0448 086 608
HUESKER Australia Pty Ltd	23 Dacmar Rd	YAROOMBA	QLD	4573	(07) 3088 8000
Hully Foundations Pty Ltd	50-52 Francis Road	WINGFIELD	SA	5013	0439 998 469
Intrax Consulting Engineers Pty Ltd	Level 4, 469 La Trobe Street	MELBOURNE	VIC	3000	(03) 8371 0100
Ischebeck Titan (Australia) Pty Ltd	197 Queens Road	KINGSTON	QLD	4114	(07) 3208 1158
Jacobs Group (Australia) Pty Ltd	452 Flinders Street	MELBOURNE	VIC	3000	(03) 8668 3651
JC Geotechnics Pty Ltd	Suite 3A, Level 3, 1C Grand Ave	ROSEHILL	NSW	2142	(02) 8066 0665

FIRM	ADDRESS				PHONE
JK Geotechnics Pty Ltd	115 Wicks Road	MACQUARIE PARK	NSW	2113	(02) 9888 5000
KCB Australia Pty Ltd	Level 3, 150 Mary St	BRISBANE	QLD	4000	(07) 3004 0244
Keller Pty Ltd (TS)	Suite G01-02 Ground Floor, 2-4 Lyonpark Rd	MACQUARIE PARK	NSW	2113	(02) 8866 1100
Menard Oceania Pty Ltd	Level 5, 13-15 Lyon Park Road	MACQUARIE PARK	NSW	2113	(02) 9491 7100
Mott MacDonald Australia Pty Ltd	Level 17, Tower One, Collins Square, 727 Collins Street	MELBOURNE	VIC	3008	(03) 9037 7575
Norwegian Geotechnical Institute Pty Ltd	Level 7, 40 St Georges Terrace	PERTH	WA	6000	(08) 6559 6499
Pells Sullivan Meynink Pty Ltd	G3, 56 Delhi Rd	NORTH RYDE	NSW	2113	(02) 9812 5000
Piling and Concreting Australia	PO Box 1605	RUNAWAY BAY	QLD	4216	(07) 5500 5898
Probedrill Pty Ltd	9 Baling Street	COCKBURN CENTRAL	WA	6164	(08) 9417 9933
Protest Engineering	Level 3, 159 Coronation Drive	MILTON	QLD	4064	(07) 3444 6666
Red Fox Advisory Pty Ltd	Level 4, 262 Adelaide St	BRISBANE	QLD	4000	(07) 3724 9000
Scherzic Ground Investigations	PO Box 555	HOBART NORTH	TAS	7002	(03) 6273 6565
SCT Operations Pty Ltd	131a Kembla Street	WOLLONGONG	NSW	2500	(02) 4222 2777
Site Geotechnical Pty Ltd	Factory 3, 8 Cannery Court	TYABB	VIC	3913	1300 557 260
Sixense Oceania	92 Thistlethwaite Street	SOUTH MELBOURNE	VIC	3205	(03) 9510 0582
SLR Consulting Australia Pty Ltd	202 Submarine School, Sub Base Platypus	LANE COVE	NSW	2060	0402 142 942
SMEC Australia Pty. Ltd	Level 5 20 Berry Street	NORTH SYDNEY	NSW	2060	(02) 9925 5555
Statewide Geotechnical Pty Ltd	17-20 Summer Lane	RINGWOOD	VIC	3134	(03) 9879 2999
Sunwater Ltd	Unit 9, 515 St Pauls Terrace	FORTITUDE VALLEY	QLD	4006	(07) 3120 0000
SYSTRA Bamser Pty Ltd	Level 15 – Chifley Tower, 2 Chifley Square	SYDNEY	NSW	2000	(02) 8229 8154
Terrascan Pty Ltd	Unit 9, 175-179 James Ruse Drive	CAMELLIA	NSW	2142	0408 723 340
Tetra Tech Coffey Pty Ltd	Level 19, Tower B, Citadel Tower799 Pacific Highway	CHATSWOOD	NSW	2067	(02) 9406 1192
Tonkin + Taylor Pty Ltd	Level 3, 99 Coventry Street	SOUTHBANK	VIC	3006	(03) 9863 8686
Transport for NSW	Level 3, Pod H, 99 Phillip Street	PARRAMATTA	NSW	2150	(02) 8837 0246
Trilab Pty Ltd	346A Bilsen Road	GEEBUNG	QLD	4034	(07) 3265 5656
Wagstaff Piling Pty Ltd	PO Box 117	ASHGROVE	QLD	4060	(07) 3366 2555
WSP Australia Pty Ltd	Level 27, 680 George Street	SYDNEY	NSW	2000	(02) 9272 5100

ADVERTISERS

The Australian Geomechanics Society gratefully acknowledges the support from firms that advertise in *Australian Geomechanics.*

FIRM	PAGE
Black Insitu Testing	54
Broons	18
Chadwick Geotechnics	118
Datgel Pty Ltd	169
Douglas Partners	153
Durham Geo Slope Indicator P/L	Outside back cover
Engineering Training Institute Australia	38
Geobrugg Australia	154
Geofabrics Australasia	190
Geosolve	169

FIRM	PAGE
GHD Geotechnics	66
Insitu Geotechnical Services	Inside front cover
Itasca Australia Pty Ltd	81
Menard-Oceania	Inside back cover
Probedrill P/L	20
Terrascan Pty Ltd	189
Terratest Australia Pty Ltd	82
Tonkin + Taylor	100
Wagstaff Piling	170

BROONS
IMPACT ROLLERS

IMPACT ROLLERS FOR MAXIMUM COMPACTION

We add value by minimising compaction cost and risk.

The value in any project lies above the ground, but the high-risk cost can be out of sight. Broons Impact Rollers minimise the risk below ground level so you can maximise the visible return. Manufactured and tested in Australia, our square rolling dynamic compaction equipment works in every corner of the globe on some of the Earth's largest projects. Get tangible results in real time with accurate surface monitoring that paints a true picture of what's underground.

Call our engineering staff now to see how we can add value to your next project and manage the geotechnical risks.

Get in touch

1300 002 764

derek.avalle@broonsimpactrollers.com

broonsimpactrollers.com

FOREWORD TO THEMED ISSUE

TAILINGS GEOTECHNICAL ENGINEERING

Tailings geomechanics are undergoing a period of significantly increased activity and attention owing to a series of recent catastrophic failures of tailings storage facilities and the regulatory and industry response to these events. This increased attention to tailings geomechanics can be seen in increased participation in forums and conferences internationally.

This themed edition of Australian Geomechanics was planned to provide a forum to capture some of these developments from both industry and academia. The strong embrace of critical state soil mechanics (CSSM) by the tailings industry is clear from the edition, with six of the ten papers explicitly making use of and/or measuring the critical state line (CSL) of tailings in their analyses.

Of the works utilising CSSM, Contreras et al. present techniques to more rationally select parameters for the popular NorSand constitutive model, building on an increased prevalence for such rigorous parameter selection processes in the numerical modelling community. This form of calibration provides the opportunity to increase objectivity in the selection of a numerical model.

Lines and Llano-Serna carry out cone penetration testing and laboratory characterisation to examine the in situ state of mud farmed tailings, demonstrating the effects of deposition processes resulting dilative or contractive conditions. Rodrigues et al. provide a summary of a series of laboratory tests carried out on a gold tailings from Brazil, including in situ compaction data, and hydraulic conductivity and CSL results. Shen and Jefferies numerically assess the dilatometer test to enable improvement of DMT-based correlations with insight from the numerical results, with a particular emphasis on geostatic stress ratio. Llano-Serna et al. provide a summary and examples of the material point method (MPM), a numerical approach finding increased application in helping to understand tailings dam breach characteristics. Chan and Gu outlined the use of numerical modelling to assess triggering mechanisms of an upstream raised tailings storage facility (TSF), while proposing an alternative means to calculate Factor of Safety in such cases.

In other works in this themed edition, Piccolo et al. present a series of case histories on the repurposing of TSFs, important work to highlight given the need to create safely closed facilities. Swarbrick provides an analytical solution for 1D large strain consolidation for use in predicting final density, an important analysis in the calculation of storage capacity of TSFs. Naeini et al. outline the characterisation of a tailings with particular focus on use of the Medusa flat plate dilatometer, including a focus on means to obtain high quality results in intermediate soils such as tailings. Finally, Herza and Fellows-Smith examine issues around Probability of Failure (PoF) and Factor of Safety, proposing a new method to estimate slope PoF.

It is hoped that this themed edition provides a useful snapshot of developments in tailings geotechnical engineering in practice and research. Each paper published in this themed edition of Australian Geomechanics was peer reviewed in accordance with the standard practice of the Australian Geomechanics editorial board. The editors would like to thank the many authors that contributed to this themed edition as well as the reviewers who kindly donated their time and enabled the paper review process to be completely in a timely manner.

David Reid
Red Earth Engineering, Perth

Andy Fourie
The University of Western Australia, Perth

PROBEDRILL
GEOTECHNICAL SURVEY

The Leaders in Geotechnical Site Investigation

Excavator Platform CPT

CPT mounted to platform suitable for Excavator quick hitch

Ideal for hard to reach test locations

Up to 10t push

Seabed CPT

Pushing Capacity:
150kN (15 tonnes)
2.3m x 2.3m x 2.8m
(L x W x H); 5700kg
Testing Services:
CPTu; SCPTu; Ball CPT;
T-bar; DMT, Piston
Sampling (76mm dia x 3m)

Services:

- Electric Friction Cone Penetration Testing (CPT) including: 15cm (10t); 10cm (10t, 5t, 1t) cones.
- Piezocone (CPTu) and Dissipation testing
- Dilatometer (DMT) testing
- Seismic testing (SCPT & SDMT)
- Electrical Shear Vane Testing
- Dual Tube (Percussive) Soil sampler (50mm x 1000mm)
- Ball and T-bar testing
- Soil Sampling (25mm x 500mm; 35 x 1500mm)
- Water Sampling
- 50m, 32mm & 20mm Standpipe installation
- Vibrating Wire Piezometer installation (Single, Multiple; inverted)

New Services:

- Piston Sampler (60mm x 500mm)
- Multi-level VWP installation
- DGPS test location & Live data streaming
- Electronic Plate Load testing (up to 20 tonnes)

+61 8 9417 9933 · info@probedrill.com.au · www.probedrill.com.au

BAYESIAN CALIBRATION OF NORSAND MODEL PARAMETERS USING TRIAXIAL TEST DATA

Luis-Fernando Contreras [1], Humberto Rojas-Huaroto [2], Alexandra Halliday [3] and Marcelo Llano-Serna [4]
[1] SRK Consulting Australasia; [2] SRK Consulting Peru; [3] The University of Western Australia; [4] Red Earth Engineering

https://doi.org/10.56295/AGJ6041

ABSTRACT

The NorSand constitutive model is a relationship between stresses and strains that has gained attention in geotechnical engineering for tailings due to its ability to numerically represent brittle materials in a critical state framework. Current calibration practices typically rely on visual fitting that is undertaken on a test-by-test basis, to identify trends across different loading conditions imposed on a single material. This approach is often time-consuming, inaccurate, and introduces subjective bias. This study presents a Bayesian approach for calibrating the elasticity (G_{ref}, m, v) and plastic hardening (H_0, H_y) parameters of the NorSand model, utilising triaxial compression test data for a selected soil material. The approach is also extended to include the plasticity parameters N and χtc as variables for inference. The Bayesian framework integrates the NorSand model, experimental triaxial data, and predefined parameter ranges (priors) to create a posterior probability function. This posterior is then evaluated using the Markov Chain Monte Carlo (MCMC) method to estimate the most likely parameter values that best match observed soil behaviour. Additionally, this approach provides insights into parameter correlations and uncertainty, streamlining parameter estimation objectively and rationally. The methodology is demonstrated with a case study on the Fraser River sand, validated against established literature, and includes Python scripts for model implementation and Bayesian calibration.

1 INTRODUCTION

The NorSand constitutive model is widely employed in geotechnical engineering for analysing structures where accurate representation of volumetric changes is critical to structural behaviour, as in the case of monotonic loading in tailings dams. Such applications include problems involving large strains, high confinement, or excess pore pressure generation (Shuttle and Jefferies, 2010). NorSand is particularly appealing to practising engineers due to its advertised simplicity and relatively limited parameter set, many of which are directly relatable to standard laboratory tests. The model parameters are typically derived from drained and undrained triaxial test results obtained under varying initial effective stress and density conditions.

The traditional process of calibrating NorSand parameters is labour-intensive and subjective. It involves visually fitting the model on a test-by-test basis to identify trends across the dataset, which are then used to estimate the model parameters. This approach is tedious and prone to inaccuracies and biases, compromising the reliability of the calibrated parameters.

This study proposes a Bayesian framework for calibrating NorSand parameters using triaxial test data. The method identifies the parameter set that optimally fits the model to the experimental data, using a Gaussian error metric based on differences between model predictions and observed data at selected points. The NorSand model features ten soil parameters, two of which (Γ, λ) define the critical state line (CSL), three of which (G_{ref}, m, v) describe elasticity, and five of which (M_{tc}, N, X_{tc}, H_0, H_y) define plasticity. Among these, five parameters can be directly computed from the triaxial test results, leaving the elasticity (G_{ref}, m, v) and plastic hardening (H_0, H_y) parameters as the targets for calibration. However, the model can be easily adapted to include the N and χ_{tc} parameters as uncertain variables for inference. Alternatively, the NorSand model is defined by eleven soil parameters when three parameters (C_a, C_b, C_c) are used to define a curved CSL in e-ln(p') space (Li and Wang, 1998).

The Bayesian approach integrates three key components: prior information about the parameters, the NorSand model to predict soil behaviour for a given parameter set, and triaxial test data containing actual soil behaviour measurements. These elements are combined into a probabilistic function, *the posterior probability distribution* within the Bayesian framework. This posterior provides the probability of specific parameter sets and the objective of the analysis is to define the sets of parameters with higher probabilities, which correspond to the minimum differences between model predictions and observed data. The parameters are inferred by evaluating the posterior using the Markov Chain Monte Carlo (MCMC) method (Kruschke, 2015). To facilitate this process, an efficient implementation of the NorSand model in Python, utilising the forward Euler integration method, was developed.

This paper is organised as follows; Section 2 provides a concise description of the NorSand model and discusses its implementation in Python, focusing on its verification and preparation for Bayesian analysis. Section 3 introduces the

Bayesian framework, presenting the mathematical foundation for parameter inference. Section 4 applies the Bayesian methodology to the NorSand calibration problem and demonstrates the application of the proposed method using Fraser River sand (FRS) triaxial test data, highlighting the insights obtained and comparing the results with existing literature. Section 6 discusses the findings, and Section 7 presents a summary and final remarks.

2 THE NORSAND CONSTITUTIVE MODEL

2.1 MODEL DESCRIPTION

The NorSand constitutive model is a critical state soil mechanics (CSSM) framework that incorporates the influence of void ratio on soil behaviour. This makes it a valuable tool for modelling static liquefaction and other phenomena in geotechnical engineering. A key characteristic of granular soils is that their mechanical response, such as strength and deformation, is significantly affected by the pre-shearing void ratio or relative density. NorSand aims to effectively capture these variations, linking soil behaviour to the void ratio through the state parameter (Been and Jefferies, 1985).

Traditional CSSM-based models can struggle to represent the dilation behaviour of dense sands adequately and often fail to predict the contractive behaviour and potential liquefaction of loose sands. NorSand addresses these limitations by introducing the state parameter (ψ), which quantifies the difference between the soil's current void ratio (e) and its critical state void ratio (e_c). This single parameter is a comprehensive measure, linking dilation or contraction tendencies to the soil's state.

NorSand is also recognised for its relative simplicity when compared to other models able to capture contractive behaviour. NorSand is appealing to engineers due to its reliance on a relatively limited set of parameters that can be readily obtained from standard laboratory tests. The model captures a broad range of soil behaviours influenced by variations in density and confining stress. Initially developed for hydraulic fills, such as those found in tailings dams, NorSand's application has expanded to include any granular soil where behaviour is governed by contact forces and particle sliding rather than cohesive bonds (Jefferies and Been, 2015). More recently, NorSand has been widely adopted in mine tailings applications due to the oftentimes loose nature of these materials (Jefferies et al., 2019, Morgenstern et al., 2016).

The key input parameters of the NorSand model, along with typical ranges for sands, as reported in Shuttle and Jefferies (2010) are summarised in Table 1. These parameters allow the model to be calibrated to capture the elastic and plastic responses of soils under different stress conditions.

2.2 MODEL IMPLEMENTATION AND VERIFICATION

The model implementation in Python is designed to model a set of drained and undrained triaxial tests for the calibration of soil parameter values from conventional triaxial compression data, using the Bayesian framework. Consequently, the implementation does not include unload-reload loops or other less common stress paths from alternative testing conditions. The NorSand plasticity model, like other plasticity models, consists of three components: (1) a yield surface; (2) a flow rule; and (3) a hardening law (Shuttle and Jefferies, 2010). These three elements of the NorSand model are described in detail by Jefferies and Been (2015) and Cheng and Jefferies (2020), including the fundamental equations used for the Python implementation.

Version 12 of the VBA code in the Excel spreadsheet (Jefferies et al., 2015) was used as the reference for the Python implementation of the NorSand model. The method is based on imposing an increment in deviatoric plastic strain, which is followed by updating the stress relationship and determining the elastic and plastic volumetric strains using a semi explicit integration algorithm. However, this process requires a more exhaustive procedure and a greater number of conditionals in the code.

As an alternative, a more straightforward formulation based on representing strain increments using the forward Euler integration algorithm (Yin et al, 2020) was implemented to achieve the efficiency required for the Bayesian application. The method consists of assembling the constitutive elastoplastic matrix from the current stress state and estimating the new stress state considering a strain increment. This approximation introduces a minor difference when compared to the results from the Excel spreadsheet as discussed in the subsequent paragraphs, nonetheless, the procedure is sufficiently accurate for the Bayesian calibration analysis.

The Python implementation also includes the calculation of the softening term in the hardening law according to the version 18 of the VBA code, where the image critical friction ratio (M_i) is used instead of the limiting stress ratio (η_L), to simplify the formulation. In the Python implementation, the size of the strain increment determines the number of steps required for the simulation of the triaxial test and is proportional to the running time of the analysis. Various strain increment sizes were tested for the validation of the implementation, and an axial strain increment of 0.01% was found to provide optimal results.

Table 1: NorSand soil properties with typical ranges for sands (adapted from Shuttle and Jefferies, 2010)

Property	Typical Range	Remark
Critical State Line (CSL)		
Γ	0.9 – 1.4	Parameters to calculate a straight CSL in e-ln(p') space: $e_c = \Gamma - \lambda \ln(p')$
λ	0.01 – 0.07	
C_a, C_b, C_c	NA	Alternative parameters to calculate a curved CSL in e-ln(p') space: $e_c = C_a - C_b (p'/p'_{ref})^{Cb}$
Plasticity		
M_{tc}	1.2 – 1.5	Critical friction ratio, triaxial compression as reference condition
N	0.2 – 0.45	Volumetric coupling coefficient
χ_{tc}	2.5 – 4.5	State-dilatancy coefficient. Relates minimum dilatancy D_{min} to the state parameter ψ
H_0	50 – 500	Parameters to calculate the plastic hardening modulus H: $H = H_0 + H_y \cdot \psi$
H_y	NA	
Elasticity		
G_{ref} at p'_{ref}	10 – 80 MPa	Parameters to calculate the shear modulus G: $G = G_{ref} (p'/p'_{ref})^m$
m	0 – 1.0	
v	0.1 – 0.3	Poisson's ratio

The NorSand parameters and the initial state conditions used for the verification of the Python implementation against the results of the VBA code in Excel are summarised in Table 2. A comparison of results for various triaxial test conditions is presented in Figure 1. The four cases analysed include drained and undrained conditions of a dense soil and the undrained conditions of a loose soil with the additional softening index (S) set to 0 and 1. The results show very good agreement between the two implementations, accurately representing the dilative and contractive behaviours for dense and loose soils, respectively. The minor differences observed between both implementations are well within the margin of errors introduced by material variability, sampling shortcomings, testing and modelling accuracy.

Table 2: NorSand soil properties used for the verification of the Python implementation

CSL		Elasticity		Plasticity		Initial state	
Γ	1.22	G_{ref} [MPa]	20	M_{tc}	1.45	ψ_0 (dense)	-0.05
λ	0.06	m	0.49	N	0.5	ψ_0 (loose)	0.15
		v	0.15	χ_{tc}	5	p'_0 [kPa]	200
				H_0	90	R	1.0
				H_y	400		

The Python implementation of the model includes both straight and curved versions of the CSL and can simulate drained and undrained test conditions. It is incorporated within the Bayesian calibration model as a function, taking a set of input parameters and generating a data frame with the simulated triaxial tests based on the provided input information. This function is designed to be executed numerous times during the evaluation of the posterior probability distribution using the MCMC procedure and is compiled to enhance efficiency throughout the Bayesian calibration process.

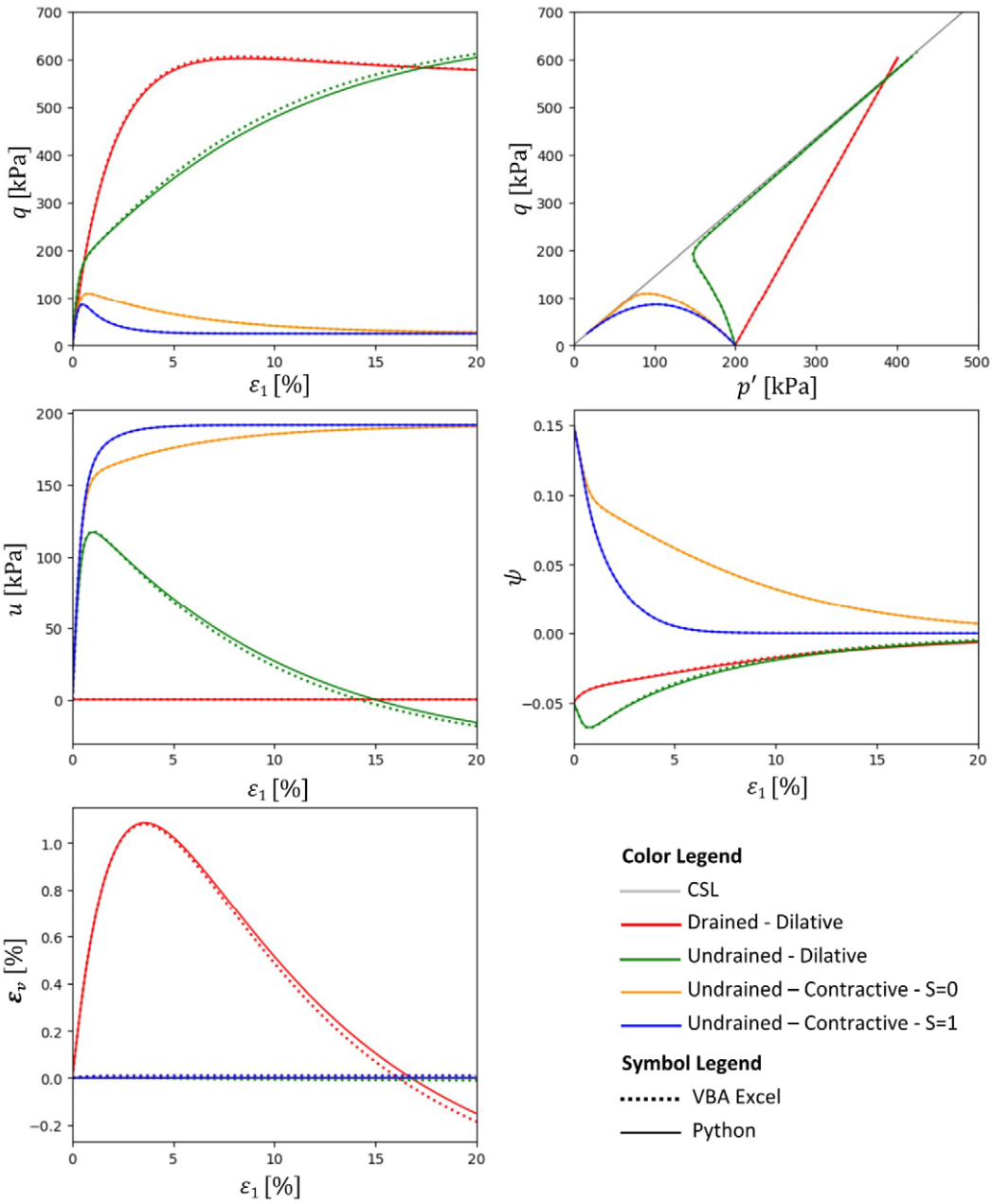

Figure 1: Comparison of results between the Python implementation of the NorSand model and the Excel/VBA code

3 THE BAYESIAN APPROACH FOR PARAMETER INFERENCE

3.1 BAYESIAN MODEL FOR PARAMETER INFERENCE

The Bayesian approach to parameter inference requires three essential components, as conceptually illustrated in Figure 2. First, a mathematical model represents the performance of the system of interest. This model incorporates predictor variables, x, and the parameters for inference, θ. Second, data — typically measurements of the system's actual performance, y_{actual} — are needed to compare against the model predictions, y_{model}. Third, prior knowledge of the parameters, such as valid ranges or credible values, must be available. These elements combine into a probabilistic function containing the uncertain parameters, θ_1 to θ_k. This function corresponds to a posterior probability distribution using Bayes' theorem and provides probability values, p, for specific parameter sets, θ. The objective of the analysis is to determine the parameter sets that maximize p, identifying the most probable values.

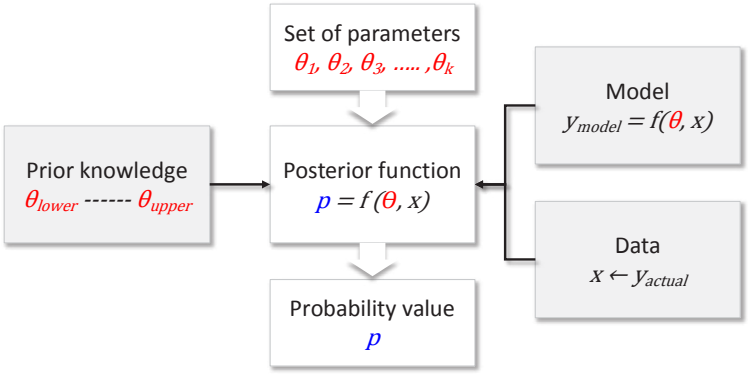

Figure 2: Conceptual representation of the Bayesian model for parameter inference

3.2 GENERIC FORMULATION OF THE BAYESIAN MODEL

Building on the framework presented by Contreras et al. (2018), the generic formulation of the Bayesian model for parameter inference in a geotechnical context is adapted here for the NorSand calibration discussed in Section 4.

A model is represented as a function *f* predicting the system response y_{model}:

$$y_{model} = f(\theta, r) \tag{1}$$

Here, θ and r are vectors of uncertain and certain model parameters, respectively. Certain parameters include predictor variables x, which define the target response variable y. If measurements of the actual system response, y_{actual}, are available, the error ϵ, representing model uncertainty, can be expressed as:

$$y_{actual} = y_{model} + \epsilon = f(\theta, r) + \epsilon \tag{2}$$

$$\epsilon = y_{actual} - f(\theta, r) \tag{3}$$

The error, ϵ, is assumed to have a normal (Gaussian) distribution around the model prediction, with standard deviation, σ. The standard deviations of the errors are also uncertain parameters that need to be inferred together with the model parameters of interest in vector, θ, and are called nuisance parameters.

The posterior probability of the uncertain parameters θ and σ given the data D can be evaluated using Bayes' theorem:

$$p(\theta, \sigma|D) = \frac{p(\theta, \sigma)p(D|\theta, \sigma)}{p(D)} \tag{4}$$

This is often expressed as (Kruschke, 2015):

$$posterior = \frac{prior \times likelihood}{evidence} \tag{5}$$

The prior $p(\theta,\sigma)$ represents initial probabilities for σ and the k uncertain parameters in θ, and is defined with uniform distributions:

$$p(\theta, \sigma) = \frac{1}{\sigma_{upper} - \sigma_{lower}} \prod_{j=1}^{k} \frac{1}{\theta_{upper\ j} - \theta_{lower\ j}} \tag{6}$$

The subscripts in this equation refer to upper and lower values defining credible ranges of the uncertain parameters. The likelihood $p(D|\theta,\sigma)$ is the probability of the data given the uncertain parameters and is defined using a normal distribution to reflect the Gaussian distribution of ϵ. The calculation is carried out for the n measurements of the system response:

$$p(D|\theta, \sigma) = \prod_{i=1}^{n} \frac{1}{\sigma\sqrt{2\pi}} e^{-\left(\frac{\epsilon^2}{2\sigma^2}\right)} \tag{7}$$

The denominator in Bayes' equation, $p(D)$, is the normalization factor computed as the integral of the numerator over the parameter space. For practical parameter inference using MCMC, this normalization term is not required. The posterior reduces to:

$$p(\theta, \sigma|D) \propto p(\theta, \sigma)\, p(D|\theta, \sigma) \tag{8}$$

Efficient sampling of this posterior distribution can be achieved using the MCMC method.

3.3 THE MARKOV CHAIN MONTE CARLO (MCMC) METHOD

MCMC is a powerful technique for sampling from probability distributions, particularly for complex, high-dimensional distributions encountered in Bayesian analysis. It generates representative samples of a distribution using a random process known as a Markov chain. While the process is random, it converges to mimic the target distribution over time.

Modern Bayesian analyses leverage open-source MCMC packages, eliminating the need for analysts to implement algorithms from scratch. Several algorithms are used to implement a MCMC process, with the Metropolis, Gibbs and Hamiltonian algorithms being among the more commonly used ones (Kruschke, 2015). In general, all the algorithms share common steps that include starting with an initial guess, evaluating a random jump, using some criterion of acceptance of the jump based on the probabilities of the two values and repeating the process of generating random jumps until enough values (samples) are defined. One advantage of this procedure is that it works even if the target function is not normalised to conform to the definition of a probability distribution.

To ensure robust results, MCMC samples must be representative of the posterior distribution, sufficiently large for accurate parameter estimation, and generated efficiently (Kruschke, 2015). Early iterations, known as the burn-in phase, are discarded to stabilize the Markov chain. Diagnostic checks, such as acceptance rate evaluations, ensure the quality of the samples.

Bayesian analyses offer rich, informative results compared to conventional parameter estimation methods. They provide insights into parameter correlations and uncertainties, enhancing both the accuracy and interpretability of geotechnical models.

4 BAYESIAN CALIBRATION OF NORSAND PARAMETERS

4.1 DESCRIPTION OF THE METHOD

The three elements — model, data and prior information — required for the implementation of the Bayesian model for parameter inference are available for the case of the NorSand model calibration. The structure of the Bayesian model for the estimation of the NorSand parameters is illustrated in Figure 3. The prior and the likelihood components are used to define the posterior function according to Bayes' rule. The NorSand model represents the model whose predictions are compared with triaxial data to define errors, which are evaluated with a normal distribution to construct the likelihood function.

The Python implementation of the NorSand model described in Section 2.2 is used as a function that takes a set of values of the input parameters and provides the predicted soil behaviour in a simulated triaxial compression test. This behaviour is represented by the response of selected variables to the changes in the axial strain (ε_1) of the simulated triaxial tests. The chosen variables for the analysis are the mean effective stress (p'), deviatoric stress (q), the volumetric response to compression represented by either the volumetric strain (ε_v) or the induced pore water pressure (u) for drained or undrained tests, respectively, and the state parameter (ψ). The uncertain NorSand parameters for inference are the elastic (G_{ref}, m, ν) and hardening (H_0, H_y) parameters. Other parameters such as the CSL (Γ, λ or C_a, C_b, C_c) and plasticity (M_{tc}, N, χ_{tc}) parameters as well as the initial soil conditions in terms of over consolidation ratio (R), state parameter (ψ_0) and mean effective stress (p'_0) are considered certain and take pre-calculated values from the data. NorSand implementations commonly available in the form of numerical simulations with specialised software or coded in VBA using an Excel spreadsheet would not be suitable for the Bayesian analysis, which requires a fast computation to perform in a reasonable time the thousands of simulations for the evaluation of the posterior function with an MCMC procedure.

The data corresponds to sets of triaxial test results covering a range of test conditions including different initial mean effective stresses and density characteristics, as well as drained and undrained stress paths during compression. The datasets include measurements of ε_1, p', q, ε_v, u and ψ where ε_1 is the predictor variable used to define the four responses (p', q, ε_v, ψ) or (p', q, u, ψ) for drained or undrained tests, respectively. The variables εv and u associated with the volumetric response to soil compression are used exclusively for the drained and undrained tests, respectively. This is to avoid the bias that the proportion of drained to undrained tests in a dataset would cause if they were used consistently for all the tests. This is because ε_v and u are zero for the undrained and drained test conditions, respectively, resulting in a perfect match between data and model predictions in this case. The quantification of errors in the four soil responses requires four standard deviations (σ_p, σ_q, $\sigma_{\varepsilon v}$, σ_ψ) that are added as uncertain variables for inference. However, since the errors in u have a different order of magnitude to the errors in ε_v, the standard deviation for errors in u is calculated as $\sigma_u = F\,\sigma_{\varepsilon v}$ and the scale factor F is an additional parameter for inference. This condition is illustrated in Figure 4 that shows how errors are measured in the Bayesian analysis.

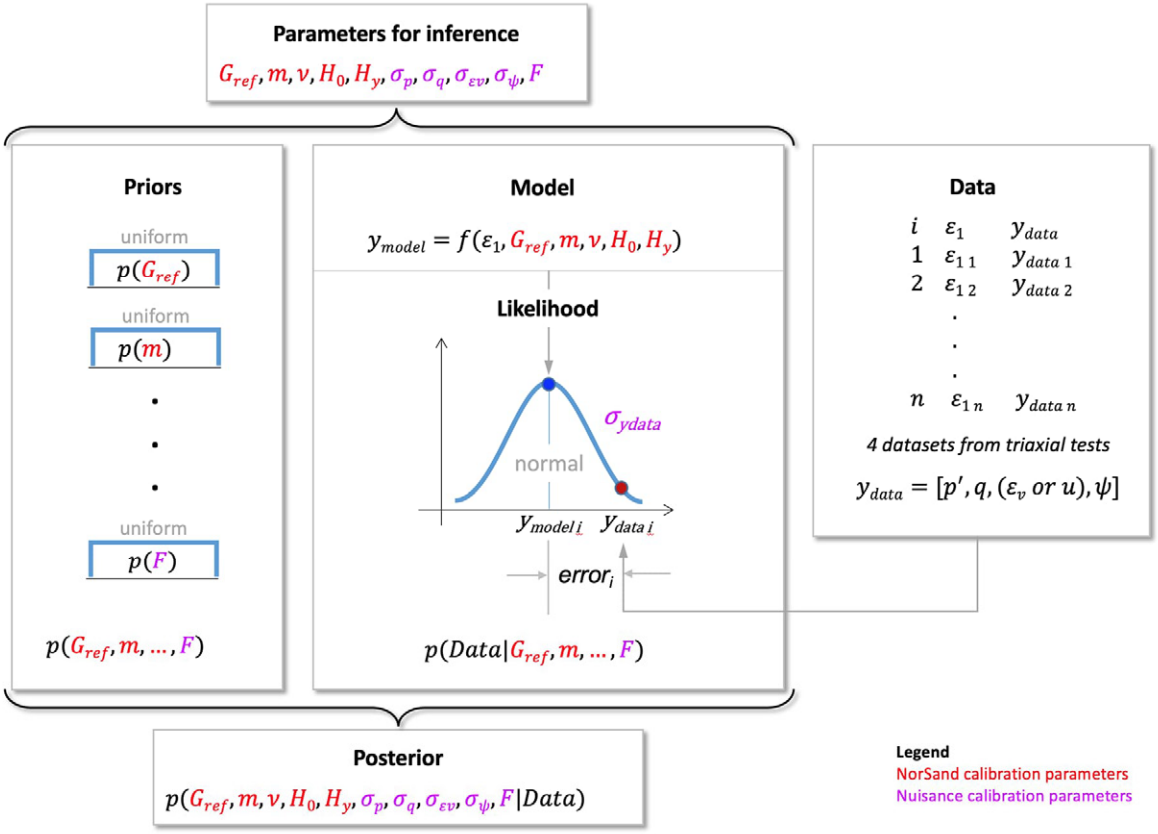

Figure 3: Conceptual basis of the Bayesian approach for the estimation of the NorSand parameters

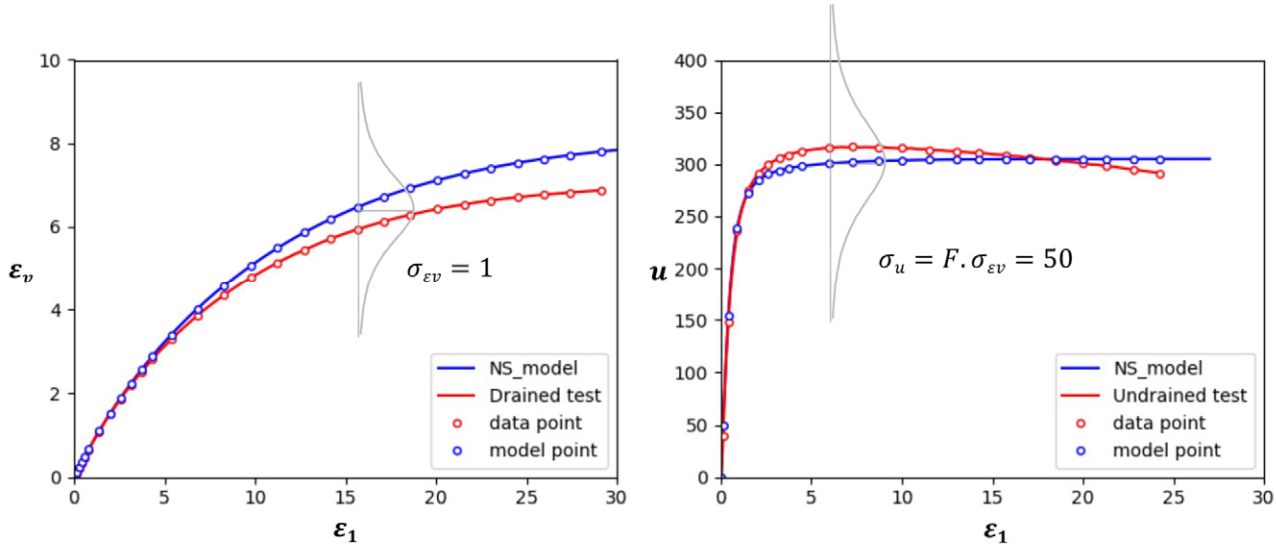

Figure 4: Measurement of errors in ε_v and u for drained and undrained tests, respectively, with a scaled normal distribution by a factor F, centred in the model prediction

The prior knowledge is represented by valid ranges of the parameters for inference, which are incorporated within the process as the bounds of uniform probability distributions indicating that, without data, any values within these bounds are a likely solution with the same probability. The NorSand Bayesian calibration model has ten parameters for inference, five soil mechanics parameters and five nuisance parameters and the ranges of these parameters must be defined before

the analysis. The priors of the parameters for inference are intended to limit their variations to plausible values without constraining the estimation within those limits.

The posterior distribution function is constructed by replacing the ten uncertain model parameters for inference (G_{ref}, m, ν, H_0, H_y, σ_p, σ_q, $\sigma_{\varepsilon v}$, σ_ψ, F) into Eqs. (6), (7) and (8). The errors are calculated for the four responses (p', q, ε_v, ψ) or (p', q, u, ψ) evaluated for drained or undrained tests, respectively, using Eq. (3) where y_{actual} are the triaxial tests data values and $f(\theta,r)$ are the respective NorSand simulation results. The posterior function is sampled with an MCMC algorithm to get the values of the parameters that minimise the errors. For this study, the 'emcee' Python package (Foreman-Mackey et al., 2013) was used. This package employs the affine-invariant ensemble sampler, which uses multiple chains running simultaneously to explore the parameter space efficiently. The quality of the MCMC result was verified ensuring that an acceptance rate between 20% and 50% was obtained as recommended for the affine-invariant sampler (Foreman-Mackey et al., 2013).

The Bayesian model for calibrating the NorSand parameters was implemented in Python and presented in a Jupyter Notebook to facilitate the understanding of the various components of the model. The code is publicly available at (https://github.com/LF-Contreras/Bayesian-calibration-NorSand-model).

4.2 EXAMPLE OF APPLICATION OF THE METHOD

4.2.1 The Fraser River sand

This study uses 12 triaxial tests (7 drained and 5 undrained) on Fraser River sand (FRS) to compare existing manual calibration results with those from the recommended procedure. These tests are a subset of the 16 tests (9 drained and 7 undrained) analysed by Jefferies and Shuttle (2011) and Jefferies et al. (2015) and is the same dataset used by Seequent (2021) in its NorSand model calibration tutorial, herein referred to as the "manual calibration".

The FRS is an alluvial deposit found extensively in the Fraser River Delta of the Lower Mainland of British Columbia, Canada (Jefferies et al, 2015). Due to its widespread presence in the densely populated and seismically active area near Vancouver, FRS has been extensively studied. Despite numerous studies in the literature, the properties of FRS remain not well defined. This is because FRS, as a natural sand with varying proportions of fines, exhibits significant geographical natural variation. Although FRS is not a tailings material, it is used in this study as a surrogate to exemplify the capabilities of the calibration procedure. The FRS was selected because numerous sources and authors use the material as a benchmark.

4.2.2 Precalculated NorSand parameters

The first step for the calibration of the NorSand parameters is to define the values of the fixed parameters that can be calculated directly from the dataset. They include the parameters defining the CSL (C_a, C_b, C_c) and the plasticity parameters (M_{tc}, N, χ_{tc}).

The stress paths of the 12 triaxial tests used for the calibration are plotted in Figure 5, indicating the start and end points of the tests. These data indicate a non-linear critical state locus in e-ln(p') space for the range of stress of the tests, therefore, the power law definition of the CSL was used as indicated in Figure 5 with p'_{ref} = 101.3 kPa, C_a = 1.01, C_b = 0.087 and C_c = 0.38. These are the same CSL parameters used by Seequent, (2021).

The critical state friction ratio, M_{tc}, the volumetric coupling parameter, N, and the parameter χ_{tc} were defined from the results of the drained dense tests according to the recommended procedure described by Jefferies and Shuttle (2011). The values obtained in this manner were very close to those used by Seequent (2021) in their calibration tutorial video and to facilitate the comparison of results, the same values (M_{tc} = 1.45, N = 0.45, χ_{tc} = 5.30) were used for the Bayesian calibration examples.

A summary of the precalculated NorSand parameters utilised for the calibration analysis is provided in Table 3. The initial conditions of the tests, which include the state parameter (ψ_0), the mean effective pressure (p'_0), and the over-consolidation ratio (R), assumed to be 1.1 for all the tests are presented in Table 4. Finally, the additional softening index (S) was set to 0, except for the undrained tests on loose samples where a value of 1 was assigned, in accordance with recommended practice.

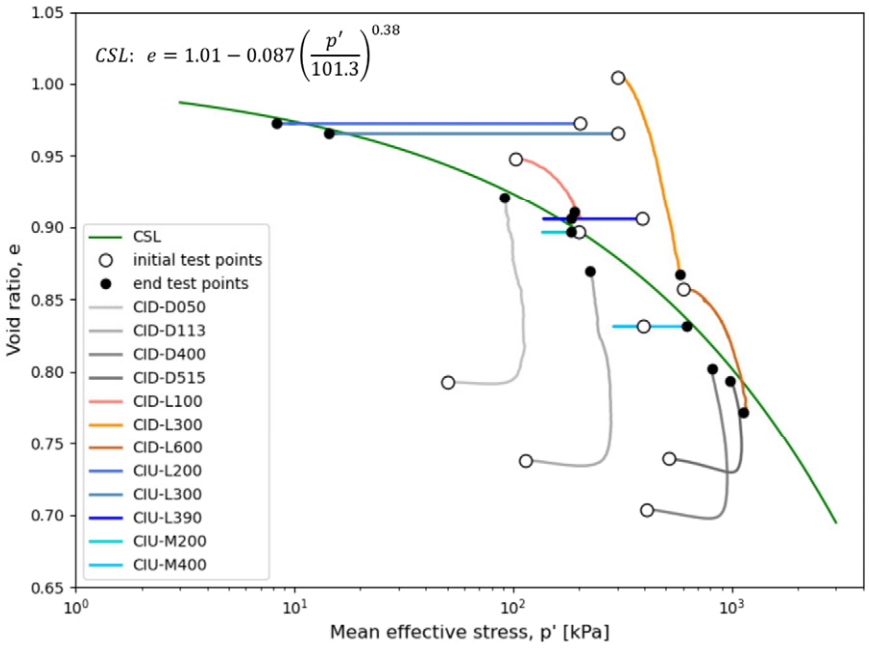

Figure 5: State paths of the twelve FRS triaxial tests used for the parameter calibration analysis

Table 3: Precalculated NorSand parameters for the dataset of triaxial tests

Property	CSL			Plasticity		
Parameter	C_a	C_b	C_c	M_{tc}	N	χ_{tc}
Value	1.010	0.087	0.380	1.45	0.45	5.30

Table 4: Initial conditions of the triaxial tests

Test ID	**CID-D050**	**CID-D113**	**CID-D400**	**CID-D515**	**CID-L100**	**CID-L300**	**CID-L600**	**CIU-L200**	**CIU-L300**	**CIU-L390**	**CIU-M200**	**CIU-M400**
Test type	Drained							Undrained				
ψ_0	-0.150	-0.181	-0.158	-0.110	0.025	0.127	0.018	0.076	0.087	0.041	-0.001	-0.033
p'_0 **[kPa]**	50	114	410	515	102	303	603	202	301	388	200	393
R	1.1	1.1	1.1	1.1	1.1	1.1	1.1	1.1	1.1	1.1	1.1	1.1

4.2.3 Priors of the uncertain parameters for inference

The uncertain parameters for inference include the elastic (G_{ref}, m, ν) and plastic hardening (H_0, H_y) parameters of the NorSand model, and the so-called nuisance parameters that include the standard deviations of the error measures (σ_p, σ_q, $\sigma_{\varepsilon v}$, σ_ψ) and the factor F to estimate σ_u from $\sigma_{\varepsilon v}$.

The uniform distributions representing the prior probability of the parameters for inference are defined with their allowable ranges of variation as indicated in Table 5. The ranges should be sufficiently broad to avoid constraining the results while ensuring consistency with the physical meaning of the parameters. The range for the standard deviation of the errors is determined based on the anticipated differences between data and predictions for each evaluated variable. For instance, the expected differences in the volumetric strains are smaller compared to the differences in mean effective or deviatoric stresses.

Table 5: Allowable ranges of variation of the uncertain parameters for inference

Parameter	G_{ref}	m	v	H_0	H_y	σ_p	σ_q	$\sigma_{\varepsilon v}$	σ_ψ	F
Upper bound	25000	0.9	0.25	150	800	100	50	1	0.1	100
Lower bound	5000	0.3	0.15	10	100	0.1	0.1	0.01	0.001	10

The initial calibration example involves the inference of five NorSand parameters, as described in Section 4.1. Additionally, a second example is provided, involving a model with seven NorSand parameters for inference. In this case, the plasticity parameters N and χ_{tc} are treated as uncertain variables for inference instead of using the precalculated fixed values. This alternative model is helpful to address the uncertainty of these parameters whose reliable estimation is often difficult due to challenges in performing high-quality testing on dense samples. This later example illustrates the flexibility of the Bayesian model for calibration and its capacity to handle numerous uncertain variables effectively.

4.2.4 Implementation of the Bayesian analysis

The methodology outlined in Section 4.2 for inferring the NorSand parameters is implemented using the Python programming language. It specifically utilizes the 'emcee' package (Foreman-Mackey et al., 2013) for evaluating the posterior function via a Markov Chain Monte Carlo (MCMC) procedure. The code is provided in a Jupyter Notebook and includes extensive comments along with the complete set of results from the calibration examples described in the paper. The programming approach prioritizes clarity of the methodology over computational efficiency.

The necessary inputs for the analysis are specified within the code and include the information from Tables 3 to 5. The triaxial tests dataset contains records of ε_1, ε_v, p', q, e, u and test names, the tests are sorted alphabetically in a csv file located in the same folder as the Jupyter Notebook. Data points for the Bayesian analysis are extracted from the raw data based on the criterion of one point per each percent of axial deformation. Consequently, a test completed with 30% axial deformation would yield 30 data points for the Bayesian analysis. These points are uniformly distributed along the length of the ε_1 raw data, ensuring that the density of data points is proportional to the number of measurements.

The posterior function is evaluated using the MCMC procedure, which is set to use 50 chains of 2,000 steps each. The initial half of the chains are discarded, resulting in 50,000 samples that define the inferred parameters. The analysis results include diagnostic plots used to assess the quality of the results, such as the trace plots of the chains and the corner plot of the inferred parameters. Additionally, the results are presented in tabular form, including the mean and the highest density interval (HDI) bounds for each parameter's distribution. Plots of q versus ε_1, q versus p', ε_v versus ε_1 and ψ versus ε_1, comparing the data with the Bayesian best fit for each test are generated. Finally, the best-defined relationships between H versus ψ_0 and G versus p'_0 with their associated HDI bounds are included in the results.

The run time of the Bayesian model is influenced by the number of chains and steps utilized for MCMC sampling and is highly sensitive to the size of the axial strain increment employed to simulate the tests using the NorSand implementation. The examples presented in this paper were executed with an axial strain increment size of 0.01% in approximately 40 minutes on a Mac computer equipped with an M1 Max processor. This was deemed an adequate condition for analysis, considering that the results exhibited only a 0.5% variation when the axial strain increment size for the NorSand simulation was halved.

4.2.5 Results of the Bayesian calibration

The complete results of the Bayesian analysis of the triaxial tests are provided along with the code in the Jupyter Notebook. The more relevant results of the NorSand calibration parameters for the FRS are shown in Figures 6 to 12. A corner plot of inferred parameters, featuring scatter plots between the five NorSand parameters sampled from the posterior distribution as well as their histograms is presented in Figure 6. The scatter plots illustrate the correlation between the inferred parameters, while the histograms define the ranges of likely values. These findings indicate a strong negative correlation between G_{ref} and m, as well as the constrained estimation of v, which is bounded by a minimum possible value of 0.15 as specified in the prior information. An extended corner plot, encompassing the ten inferred parameters including the nuisance parameters, is available and should be reviewed to ensure the adequate convergence of all parameters without constraints. A summary of the mean values of the inferred parameters is included in Figure 6. However, values within the 95% HDI of the parameter distributions indicated by the clusters of sampled values in the corner plot are considered an acceptable outcome of the calibration process.

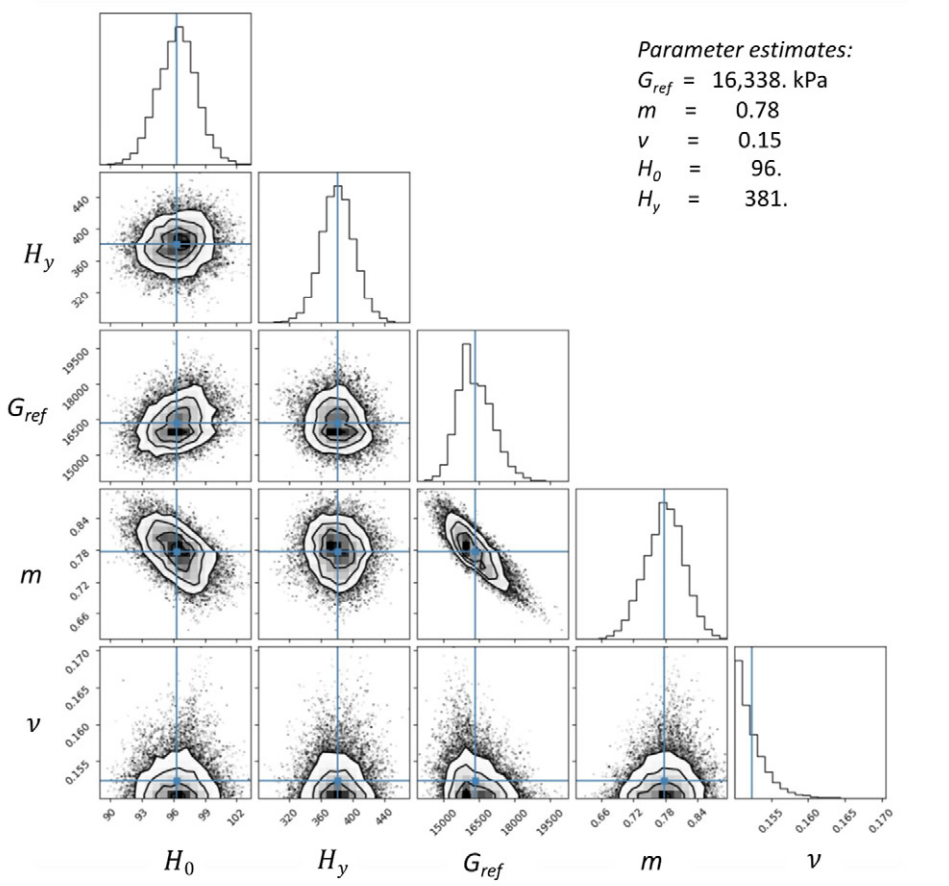

Figure 6: Corner plot of NorSand inferred parameters with the Bayesian analysis of FRS triaxial test results

The calibration defines the set of NorSand parameters that minimise the differences between the data and model predictions for the 12 triaxial tests analysed. Two examples of the FRS calibration results are illustrated in Figure 7 and 8. Figure 7 corresponds to a drained test on a dense sample (CID-D400) and Figure 8 shows the calibration result for an undrained test on a loose sample (CIU-L300). These results indicate a good match between the data and model predictions, particularly given the fact that 12 tests were fitted with the calibrated NorSand model. This random component averages out when fitting the model to several tests, enhancing the predictive accuracy of the calibrated model.

A second case of the analysis was carried out considering the plasticity parameters N and χ_{tc} as uncertain variables, raising the number of NorSand parameters for inference to seven. The results of this analysis are presented in the corner plot of Figure 9, with the mean values of the inferred parameter summarised in the same figure. The results indicate a small reduction of the parameters N and χ_{tc} in relation to the fixed precalculated values used in the five-parameter calibration case. Also, a slight increase of H_y is observed in this case, however, the values of the five parameters remain within the HDIs defined previously.

The results of the two cases of Bayesian calibration of the NorSand model with the FRS data are summarised in Table 6, showing the parameters estimated with the manual calibration described by Seequent (2021) for comparison purposes. These results show a close alignment of the calibrated elastic and plastic hardening parameters between the two cases of the Bayesian inference analysis. However, the plastic hardening parameters from the manual calibration differ from the Bayesian results and in terms of the elastic parameters a comparison cannot be done because the manual calibration does not provide a unique relationship that covers all the tests. The differences between the results of the Bayesian and manual calibrations can be appreciated in Figures 10 and 11 for the relationships between H and ψ_0 and G and p'_0, respectively. These graphs also show the bands of 95% HDI of the H and G parameters, which provide an indication of the uncertainty of these parameters. The bands are the result of the spread of the sampled values of the inferred parameters. The implications of the differences between the Bayesian and manual calibration approaches will be discussed in Section 5.

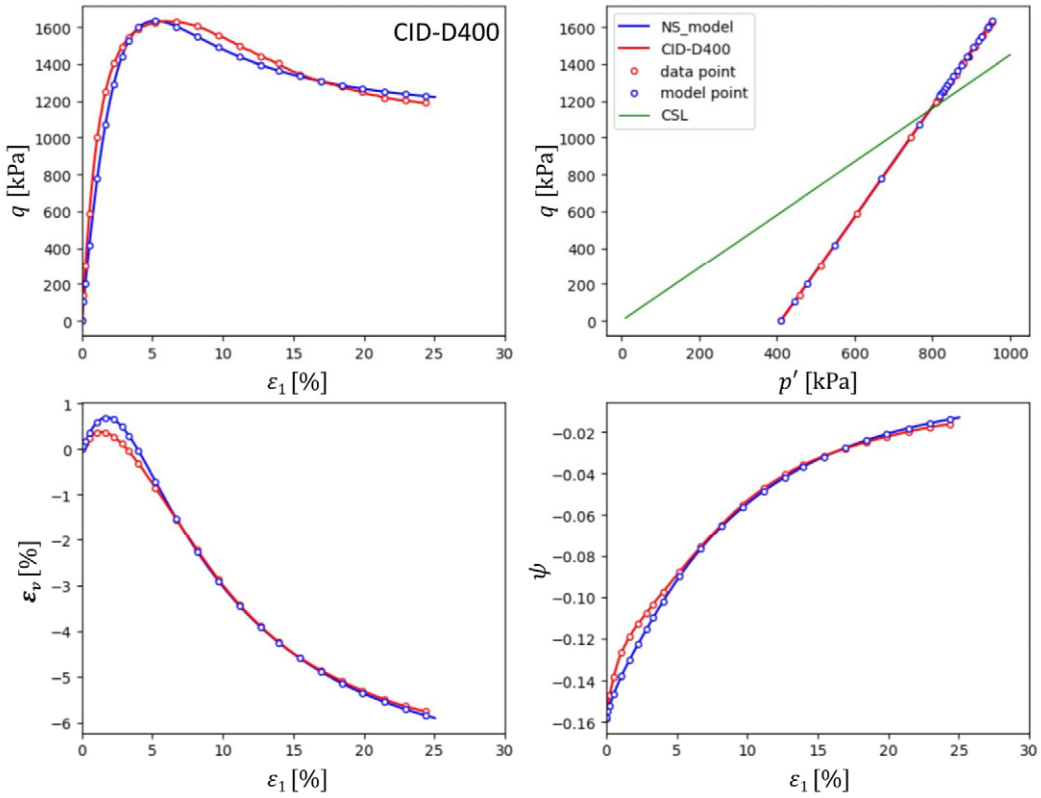

Figure 7: Example calibration of NorSand for FRS drained test on dense sample

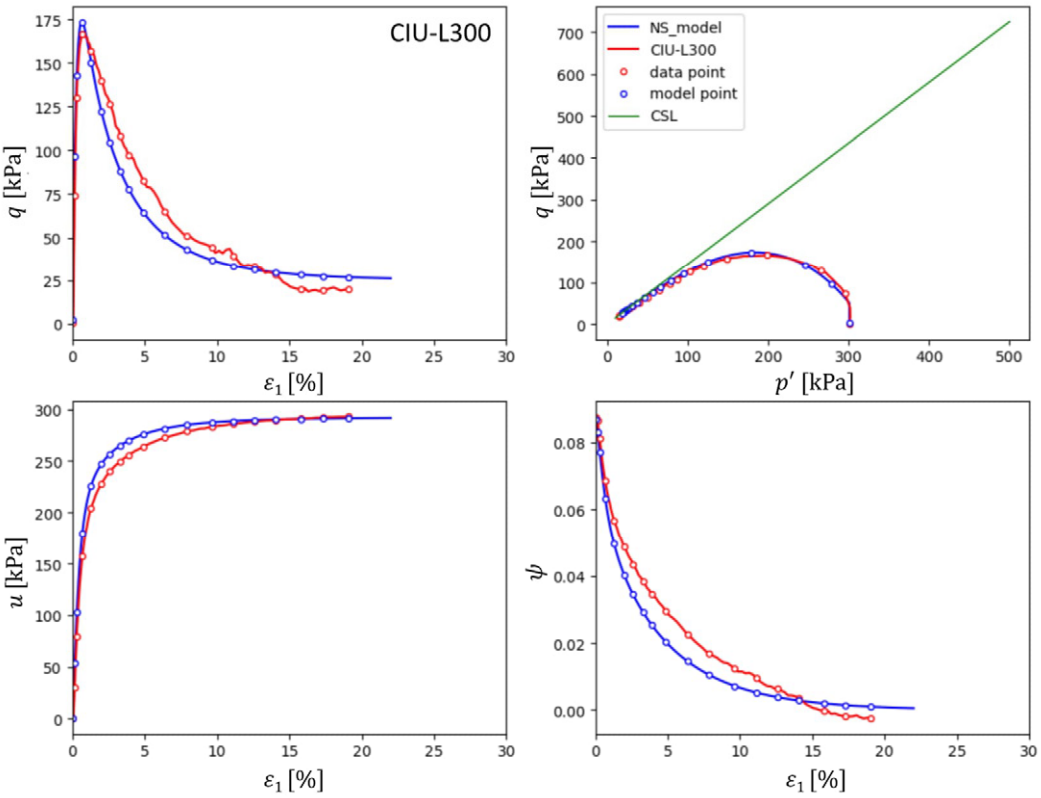

Figure 8: Example calibration of NorSand for FRS undrained test on loose sample

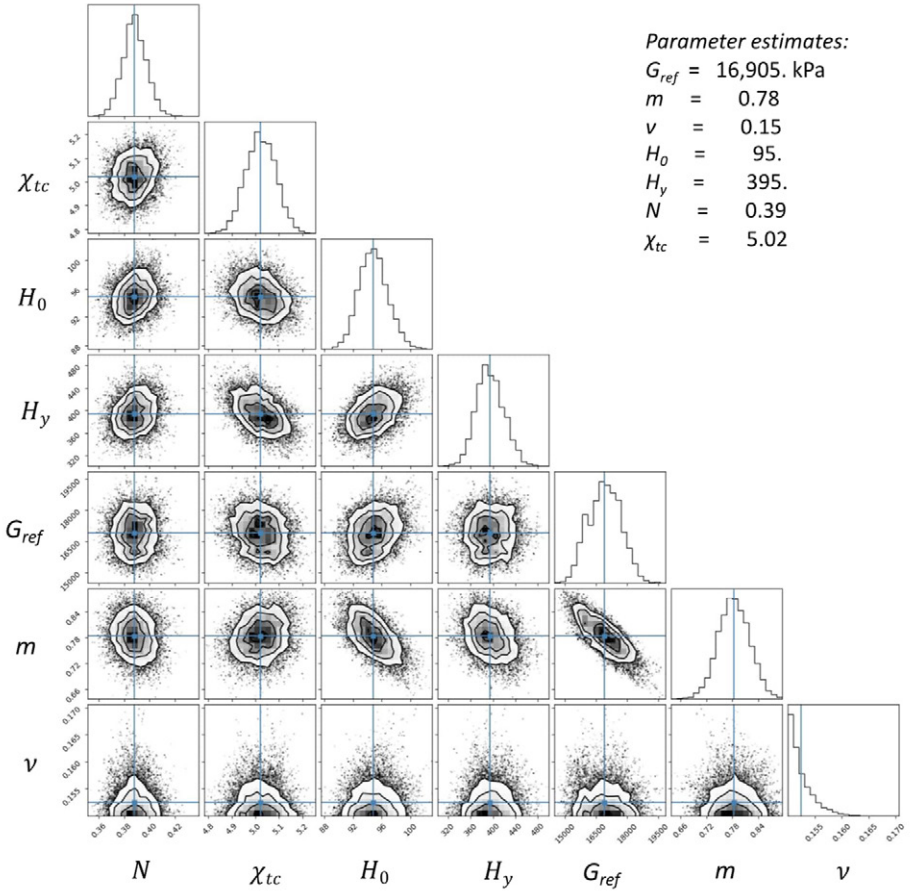

Figure 9: Corner plot of NorSand inferred parameters considering χ_{tc} and N as uncertain variables

Table 6: Comparison of results of the NorSand calibration analysis of the FRS with established results

Parameter	G_{ref}	m	ν	H_0	H_y	N	χ_{tc}
Analysis with 5 NorSand parameters for inference							
mean	**16,338**	**0.78**	**0.15**	**96**	**381**	0.51 (1)	5.24 (1)
upper bound	17,857	0.85	0.16	100	423		
lower bound	15,001	0.71	0.15	93	339		
Analysis with 7 NorSand parameters for inference							
mean	**16,905**	**0.78**	**0.15**	**95**	**395**	**0.39**	**5.02**
upper bound	18,382	0.86	0.16	99	445	0.41	5.15
lower bound	15,487	0.72	0.15	91	351	0.37	4.90
Manual calibration (Seequent, 2021)							
value	variable	0.47 (1)	0.2 (1)	61	247	0.45 (1)	5.30 (1)

Note: (1) Fix precalculated or assumed values not resulting from the calibration process.

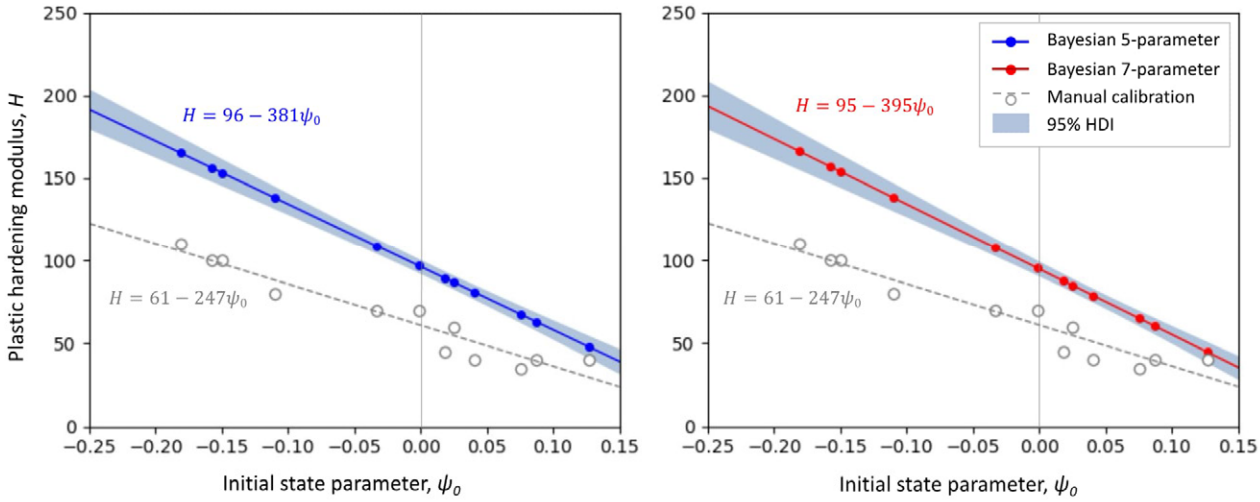

Figure 10: Plastic hardening trends defined for the FRS with the Bayesian analysis compared with the results of a manual calibration

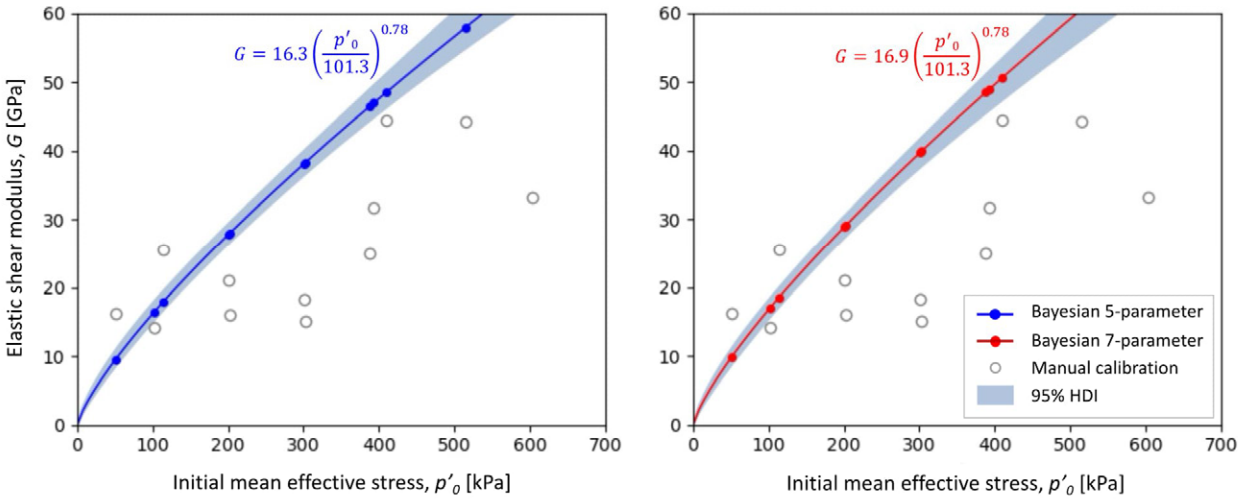

Figure 11: Elastic shear moduli trends defined for the FRS with the Bayesian analysis compared with the results of a manual calibration

The comparison between the actual and simulated state paths of the 12 triaxial tests used in the analysis for the case of the seven-parameter fitted model is shown in Figure 12. The calibrated model provides a good approximation of the FRS behaviour for the range of conditions covered with the 12 triaxial tests evaluated and can be used for geotechnical analysis. However, it is important to bear in mind the limitations of relying solely on compression triaxial data for parameter estimation. This is particularly true when applying the NorSand model in practical engineering problems such as the assessment of liquefaction triggering risk, where behaviour under other stress paths is critical.

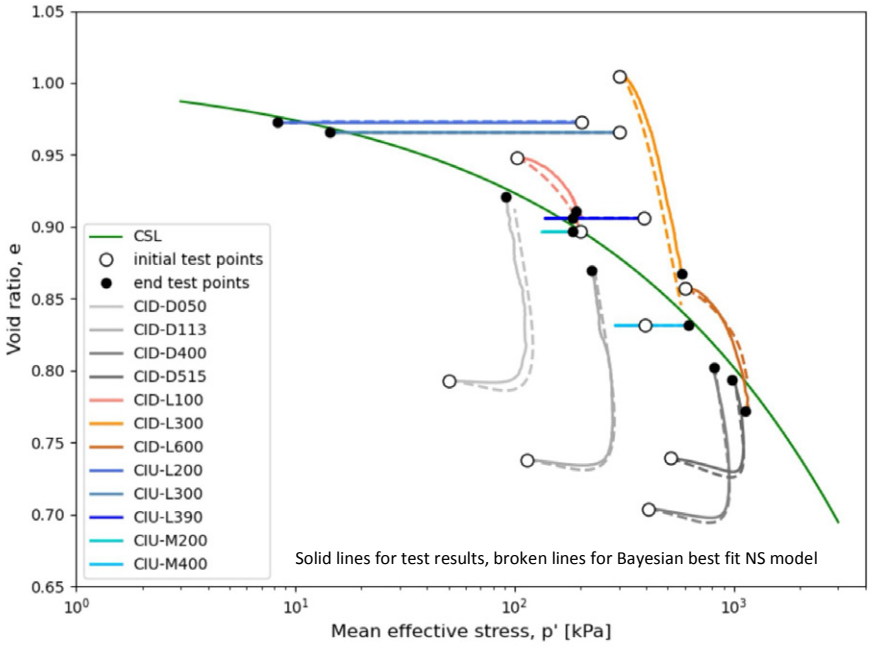

Figure 12: Comparison of the state paths of the twelve FRS triaxial tests with the fitted 7-parameter Bayesian NorSand model

5 DISCUSSION OF RESULTS

The objective of the NorSand model calibration analysis is to infer the parameters that define the trends in the variation of plastic hardening and elastic shear moduli, enabling a good fit of the model predictions to the results of the set of FRS triaxial tests used in the analysis. The relationships between H and ψ_0 and G and p'_0 are defined in the Bayesian analysis by fine-tuning parameter values to minimise the difference between observed data and model predictions. This process yields parameter uncertainty quantification derived from the probability distributions of the sampled values. In contrast, manual calibration produces a single estimate without a measure of uncertainty, based on scattered points from test-by-test visual fitting analyses.

The conventional manual calibration procedure relies on a test-by-test analysis and presents significant challenges. In this approach, multiple variables require adjustment, typically by fixing all but one variable, which is intuitively adjusted. This method is inherently time-consuming and inefficient, as it cannot consider the entire dataset simultaneously but rather evaluates each test in isolation. Consequently, it is ineffective and prone to subjectivity and bias, as the operator's intuition heavily influences the adjustment process. Additionally, this fragmented approach lacks the capability to provide measures of uncertainty for the calibrated parameters.

In contrast, the Bayesian approach offers a comprehensive and systematic method for model calibration. This approach constructs a probability function tailored to the problem at hand, incorporating the dataset, the model predictions and the bounds of the parameters investigated. By employing a Markov Chain Monte Carlo (MCMC) analysis to sample this function, the Bayesian method identifies the parameter values that maximise the function, thus minimising the differences between the model predictions and the observed data. The sampling process results allow for the quantification of uncertainty in the parameter estimates, providing a clear and objective measure of the confidence in the calibration results.

The disparity between the results from the two approaches highlights the importance of objectively measuring the goodness of fit of model predictions to data since bias can result from a subjective approach, affecting the forecasting ability of the calibrated model. The Bayesian approach provides a rational and objective measure of goodness of fit, simultaneously considering all the triaxial tests in the dataset during the inference process. Based on these considerations, it is suggested that the Bayesian results have superior predictive capabilities than the results of manual calibration. However, it is important to acknowledge that the G estimation from the manual calibration adopted in this study is not based on a single relationship between G and p'_0 and thus cannot be directly compared with the unique relationship defined in the Bayesian analysis.

6 SUMMARY AND CONCLUSIONS

The paper presents a proposed NorSand constitutive model parameter calibration method using a Bayesian framework. The NorSand model is used in geotechnical engineering for its effectiveness in capturing the influence of void ratio on soil behaviour. Traditional calibration methods are labour-intensive and subjective, often leading to inaccuracies. Furthermore, conventional approaches do not provide an alternative to understanding the calibration accuracy. This proposed Bayesian calibration approach integrates the NorSand model, triaxial data, and predefined parameter ranges to create a posterior probability function. This function is evaluated using the Markov Chain Monte Carlo (MCMC) method to estimate the most likely parameter values that minimise the difference between data values and model predictions. The methodology is demonstrated with a case study on Fraser River sand, validated against established literature, and includes Python scripts for model implementation and Bayesian calibration.

Corner plots like those presented in Figure 9 are valuable tools for sensitivity analysis. For example, a negative correlation between m and G_{ref} was observed for the Fraser River sand. These trends are not self-evident when undertaking conventional calibration processes. Neglecting such relationships could misinform sensitivity analysis or the development of fragility curves for risk assessments. Further studies using the methodologies presented herein could help the industry establish implicit correlations between key variables and credible ranges of variation with complementary probability distribution functions to inform advanced reliability-based assessments.

The Bayesian approach for calibrating the NorSand model parameters offers a more objective and rational method than traditional visual-fitting techniques. The Bayesian method provides insights into parameter correlations and uncertainties by integrating prior information, experimental data, and the NorSand model within a probabilistic framework. The case study on Fraser River sand demonstrates the effectiveness of this approach, showing that the Bayesian calibration can achieve results consistent with established literature while providing a more streamlined and accurate parameter estimation process. Implementing the NorSand model in Python and using MCMC for evaluating the posterior function further enhances the robustness and efficiency of the calibration process.

Code and data availability

The Python code and the associated data used to generate the results described in the present paper are available at (https://github.com/LF-Contreras/Bayesian-calibration-NorSand-model).

CRediT authorship contribution statement

Luis-Fernando Contreras: Conceptualization, methodology, formal analysis, investigation, software, validation, writing - original draft, writing - review and editing. **Humberto Rojas-Huaroto**: Formal analysis, investigation, software, validation, review and editing. **Alexandra Halliday**: Investigation, validation, review and editing. **Marcelo Llano-Serna**: Conceptualization, validation, review and editing.

7 REFERENCES

Been, K., and Jefferies, M.G. (1985). A state parameter for sands. *Géotechnique*, 35(2), 99–112.

Cheng, Z., and Jefferies, M. (2020). Implementation and Verification of NorSand Model in General 3D Framework. Geo-Congress 2020 GSP 318.

Contreras, L.F., Brown, E.T. and Ruest, M. (2018). Bayesian data analysis to quantify the uncertainty of intact rock strength. *Journal of Rock Mechanics and Geotechnical Engineering*, 10(1), 11-31.

Foreman-Mackey, D., Hogg, D.W., Lang, D. and Goodman, J. (2013). emcee: The MCMC Hammer. *Publications of the Astronomical Society of Pacific*, 125(925), 306–312.

Jefferies, M., and Been, K. (2015). Soil Liquefaction: A Critical State Approach, Second Edition. *CRC Press*.

Jefferies, M., Morgenstern, N.R., Van Zyl, D.J.A., and Wates, J. (2019). Report on the NTSF embankment failure, *Cadia Valley Operations for Ashurst Australia*, 1–119.

Jefferies, M.G. and Shuttle D.A. (2011). Understanding liquefaction through applied mechanics. *5th International Conference on Earthquake Geotechnical Engineering*, Santiago, Chile, January 10−13, 2011.

Jefferies, M., Shuttle, D. and Been, K. (2015). Principal stress rotation as cause of cyclic mobility. *Geotechnical Research*, 2(2), 66-96.

Kruschke, J.K. (2015). Doing Bayesian Data Analysis: A Tutorial with R, JAGS and STAN, Academic Press/ Elsevier.

Li, X.S., and Wang, Y. (1998). Linear Representation of Steady-State Line for Sand. *Journal of Geotechnical and Geoenvironmental Engineering*, 124(12), 1215–1217.

Morgenstern, N.R., Vick, S.G., Viotti, C.B., and Watts, B.D. (2016). Fundão Tailings Dam Review Panel. *Report on the immediate causes of the failure of the Fundão Dam*, 88.

Seequent, (2021). Sigma/W Material Model Series: NorSand. Webinar, March 17, 2021. Available from < https://www.seequent.com/sigma-w-material-model-series-norsand/ >

Shuttle, D. and Jefferies, M. (2010). NorSand: Description, calibration, validation and applications. *Research Gate Article* 1-31.

Yin, Z.Y., Hicher, P.Y. and Jin, Y.F. (2020). Practice of Constitutive Modelling for Saturated Soils, Tongji University Press/ Springer.

1998 EST.
PREMIER PROVIDER OF ENGINEERING TRAINING WORKSHOPS

ENGINEERING TRAINING INSTITUTE AUSTRALIA

FINE GEO5 SOFTWARE AGENTS FOR AUSTRALIA & NEW ZEALAND

Paul Uno
ETIA Director

Contact us: **(02) 9899 7447** | **info@etia.net.au** | **www.etia.net.au** Connect with us:

2025 ETIA Sponsors BarChip Inc. The Synthetic Fibre Experts · DANLEY · fine · GRANOR RUBBER & ENGINEERING INNOVATIVE EXPANSION SOLUTIONS · KATANA FOUNDATIONS · Ramset · STOTT & UNO ACCOUNTANTS • ADVISORS

INVESTIGATION INTO THE IMPACTS OF MECHANICAL IMPROVEMENT OF TAILINGS WITHIN THE CRITICAL STATE SOIL FRAMEWORK

S. H. Lines and M. Llano-Serna
Red Earth Engineering a Geosyntec Company

https://doi.org/10.56295/AGJ6042

ABSTRACT

A geotechnical investigation was undertaken in tailings and subsequently analysed within the critical state soil mechanics (CSSM) framework. The geotechnical investigation included cone penetration testing with porewater pressure measurement (CPTu) and laboratory testing. The laboratory testing was inclusive of triaxial compression testing in addition to classification and oedometer testing. The tailings samples were retrieved using the mini-block sampling (MBS) technique to minimise disturbance, though the triaxial testing included both reconstituted and testing in MBS recovered samples. The tailings material was split into four groups related to the deposition methodology used. This included mechanically improved tailings, sub-aerially deposited tailings and two types of sub-aqueous deposited tailings.

Using the triaxial test results, four critical state lines (CSLs) were defined based on fines content of 6%, 40%, 50% and 80%. Each CSL has a varying slope and intercept observing to follow a well-documented trend leading towards an Omega Point. These four CSLs were used to define a CSL region within which there is an independent CSL based on fines content, i.e., a tailings with 5% fines content have a different CSL to one of 55% based on the developed functions. The soil behaviour index (Ic) was then used to estimate the fines content of the CPTu results using three methods; Boulanger and Idriss (2014), Agaiby and Mayne (2020) and a site-specific calibration.

The CPTu results were plotted against the modelled CSL region. The results were used to predict the potential of the tailings to behave either contractive or dilative. The results of this assessment clearly demonstrate that whether the tailings material will behave in a contractive or dilative manner is related to placement strategy. Most relevantly, the assessment allowed estimation of the stress progression and at which point the dilative tailings will transition to contractive behaviour upon subsequent upstream loading. The methods used in this paper provide a robust rational framework to demonstrate the effect of various tailings management practices on design outcomes, able to be applied by practitioners for increased understanding of their tailings and hopefully leading to more informed decision making.

1 INTRODUCTION

Tailings Storage Facilities (TSF) are some of the largest man-made structures and are used to store millions of tonnes of waste materials produced by mining operations. These facilities are anticipated to only grow larger in the future as rising public demand for commodities supports the increasing mine production and associated tailings production rates (Morrison, 2021). Because of the sheer size of the facilities, the failure of a TSF is often devastating for all involved with thousands of deaths being linked to TSF failure (Hudson et al., 2024). The community, surrounding environment and company all suffer in varying degrees when a TSF failure occurs. Furthermore, TSFs are different to traditional water storage facilities (WSF) in that they are raised, often regularly, after being built, where WSFs are often built and may only be raised once or twice in their lifecycle. Raising TSFs throughout the mining process enables operations to capture economical efficiencies. The resources industry is volatile so raising a TSF for the predicted life of the mine commits what may be unnecessary capital (Williams, 2021). Raising a TSF periodically allows the procedure of an upstream raise, where the TSF is raised on top of the tailings previously deposited. An upstream raise substantially minimises costs due to the reduced requirements of earthworks. However, one of the drawbacks is that the TSF is now being raised on tailings which may exhibit reduced strengths and have the potential to behave in a contractive manner (a predisposition to volume reduction with increased pore pressure) or brittle (a predisposition to volume and strength reduction volume with increase pore pressure). The reduced strength and potential for contractive behaviour has led to larger failure rates and failure flow events occurring in upstream raised TSFs when compared to other construction methods (Halabi et al., 2022). Accurately assessing the strength and potential of tailings to behave contractively is essential to ensuring a safe and sustainable facility and is an area of ongoing research.

The risk of tailings liquefying is linked to the saturated and loose deposition methods, as tailings are typically pumped into the storage facility due to the reduced costs associated with this mode of transport in comparison to other methods such as conveyor or truck (Williams, 2021). The placement of tailings via hydraulic filling involves the tailings settling out onto the tailings beach. The results of this are that the tailings are exceptionally loose, far looser in situ than can often

be achieved in the laboratory (Reid and Fanni, 2022). Furthermore, this deposition method results in segregation of the tailings along the beach according to particle size with the coarser particles typically settling shorter distances from the spigot (Figueroa et al., 2015). An assessment of tailings behaviour based on the deposition method was undertaken within the critical state soil mechanics (CSSM) framework. A brief description of the CSSM framework will be provided, following with the site and tailings details and subsequent analysis. Both mini-block samples (MBS) and reconstituted samples were tested to determine their critical state line (CSL) with four different CSLs created based on varying fines content. To compare the laboratory results and in-situ results a site-specific fines content calibration was created. This enabled comparison of the cone penetration with porewater pressure measurement (CPTu) to the four CSLs. Lastly, the implications of the tailings deposition method will be discussed before closing on outcomes and recommendations for practitioners.

2 THEORY

When discussing the stability of a TSF it is necessary to understand the principles of liquefaction and CSSM as this influences the potential behaviour of the TSF. Liquefaction is a phenomenon in which soil loses much of its strength, generally associated with loose saturated soils, and occurs due to an increase in pore pressure reducing the effective stress state. This increase in pressure results from an undrained or partially drained condition which can be triggered by any number of mechanisms (e.g., seismic event, rapid loading, change in stress state). The case of determining a trigger has significant difficulties and recent recommendations are that for High or Extreme consequence facilities a trigger should be assumed and consequence mitigation measures prioritised when brittle material are present (ICOLD, 2023). The strength loss has the potential to reach residual strength that could be more dramatic than traditionally understood in CSSM of clay deposits. CSSM is a framework within established plasticity theory developed to deal with the behaviour of soils that exist across a range of states (i.e. void ratio or density). The critical state is the state of a soil where, were to be deformed (sheared) continuously, it would exhibit no further volume change. To assess a soils density relationship to the CSL, or the critical state, the State Parameter, ψ is used. The definition of ψ (Figure 1) is the distance between the current void ratio (i.e. density) of soil/ to the CSL void ratio. Dense soils have a negative ψ and loose soils have a positive ψ.

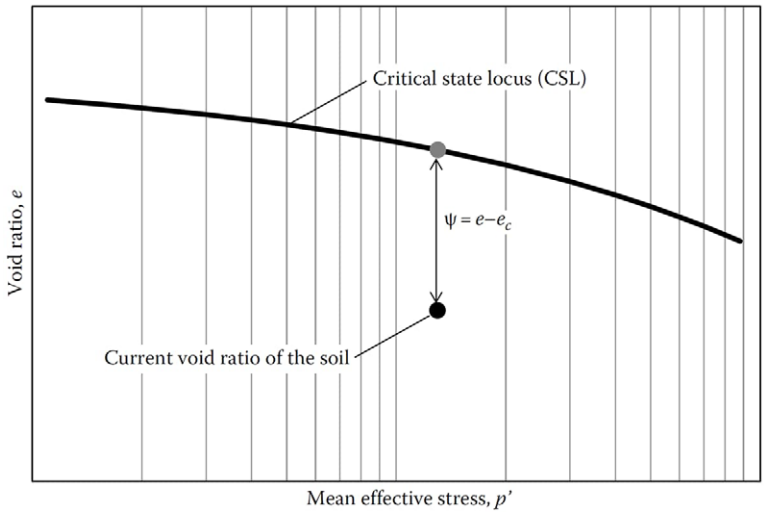

Figure 1: Definition of the state parameter for a dilative soil (Jefferies and Been, 2015)

A complication when determining a CSL is that it varies based on fines content (FC). Previous research has indicated that the CSL moves downwards to a threshold value of around 40% to 50% FC and then backwards (Papadopoulou et al., 2008; Nguyen et al., 2014). One of the aims for practitioners to determine is the in situ state of the soil and the potential for the in situ state to change based on changing conditions. This is done through in situ testing and laboratory testing of the soil. One of the more common testing procedures, and the one used throughout this case study, is the Cone Penetration Test with pore-water pressure measurement (CPTu). Laboratory testing is used to assess additional parameters of tailings, particularly when MBS can be obtained. For this case study the MBS technique was used, which has consistently shown much better-quality samples then alternative methods such as tube samples (Emdal, 2016; Amundsen et al., 2021; Lines et al., 2023). While tailings frequently comprise ground rock with or without clay minerals and have been subject to chemical processing and sometimes heated processing, indications are that they tend to follow the principles of geotechnics as applied to natural soils. This indicates that CSSM can be applied to tailings with the caveat that during mining and processing of the ore that has become tailings there may be deviances from common soil behaviour that need to be considered.

3 SITE BACKGROUND

The TSF is in Australia with the location having a tropical monsoonal climate and experiences about two metres of rainfall each year, mostly between the months of December and March. Constructed in 2018 it is a relatively young TSF having only undergone a few wall raises. It is about 1000 Ha in area and is separated into two cells, with one cell being raised each year. The design life of the TSF is approximately 25 years, with a series of 12 to 13 upstream raises anticipated, reaching a final height of about 20 m. A total of 9-10 million dry tonnes per year of tailings are deposited into the TSF.

3.1 PIEZOCONE AND CLASSIFICATION TEST RESULTS

During the start-up phase of the TSF the entirety of the TSF was not available for deposition due to mining operations within one of the cells. This resulted in suboptimal drying time after each deposition cycle. Moreover, the tailings were deposited sub-aqueously due to the accumulation of supernatant water on the operating cell. Following this start-up phase as more of the TSF became available for deposition, the tailings were deposited sub-aerially. In 2022 there was a decision to begin mechanical improvement of the tailings to increase densities near the embankment. Subsequent geotechnical investigations have led to the classification of the tailings into four distinct groups based on the CPTu profile and geotechnical parameters with each group relating to the deposition processes, this includes:

1. Mechanically improved sub-aerially deposited tailings referred to as DTAL
2. Sub-aerially deposited tailings without mechanical improvement referred to as TAL.
3. Sub-aqueously deposited tailings referred to as STAL.
4. Sensitive sub-aqueously deposited tailings referred to as SSTAL.

Two example CPTu profiles displaying the cone tip resistance and pore pressure with depth are shown in Figure 2. Of the tailings, the DTAL tailings has the highest cone tip resistance typically > 5 MPa and while the strength is a good indicator, the DTAL can be cross-referenced with the timing and location of mechanical improvement. The TAL tailings have a much lower cone tip resistance at around 2 MPa and the STAL and SSTAL tailings display < 1 MPa with the sensitive having consistently minimal cone tip resistance as low as 0.2 MPa. The dynamic pore pressure was greatest in the SSTAL, but was typically present in the other tailings, though there were instances of negative pore pressure and zero pore pressure at the surface. The second example shows an occasion where the DTAL is not at the surface but interbedded, mechanical improvement is not a continuous activity and it is often ceased for periods of time, such as during significant weather events. Sensitivity refers to the ratio of peak to residual undrained strengths. The SSTAL had a sensitivity of up to 8 when calculated with the in-situ vane shear testing (VST) results, combined with increased presence within the corresponding CCS region using the Robertson (2016) SBTn chart, resulted in designation of the ‘sensitive’ to differentiate that layer. Based on the CPTu profiles it can already be seen that the deposition technique has a significant impact on the outcome of the tailings strength.

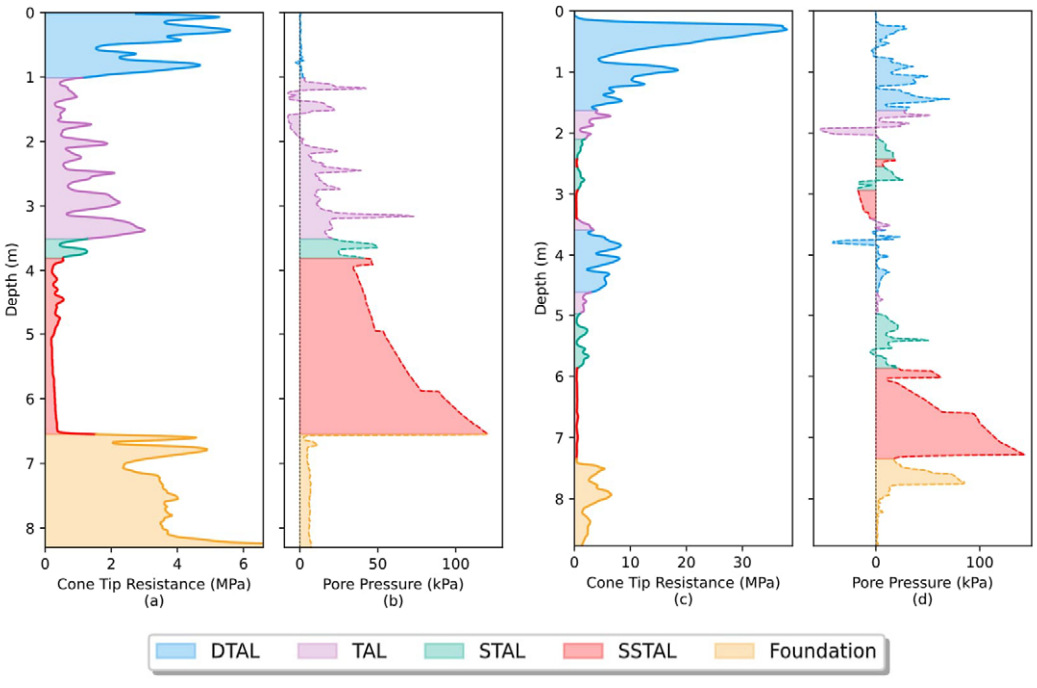

Figure 2: Example CPTu profiles displaying cone tip resistance of tailings and pore pressure. (a) and (b) form the first example and (c) and (d) form the second example

Figure 3 and Figure 4 display the particle size distribution (PSD) and the Atterberg Limits (AL) of the various tailings categories. The main takeaway from this information is that the sensitive sub-aqueous (SSTAL) tailings display an increased fines content over the other tailings categories. The high water volume on the TSF surface during deposition is the mechanism that results in the increased amount of fines present since when the tailings stream enters the supernatant pond the coarse fraction settles out rapidly leaving the fines to flow on towards the decant point. This is a well-known phenomenon in the industry.

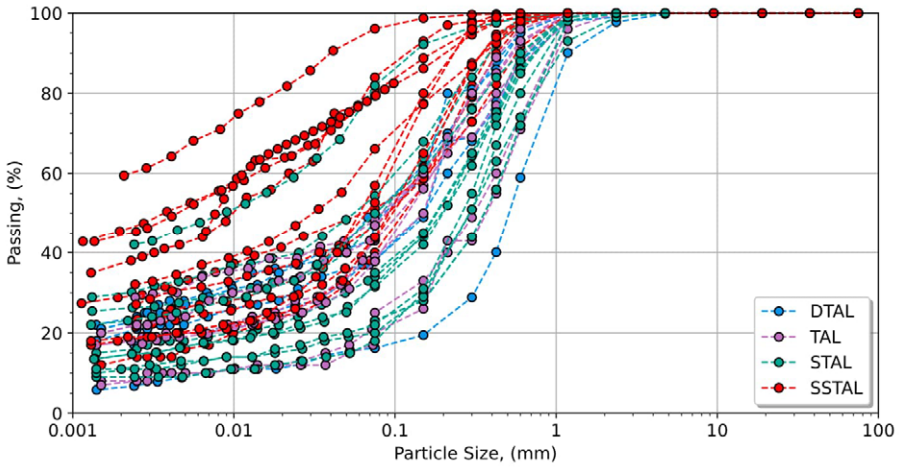

Figure 3: Particle Size Distribution (PSD) based on tailings category

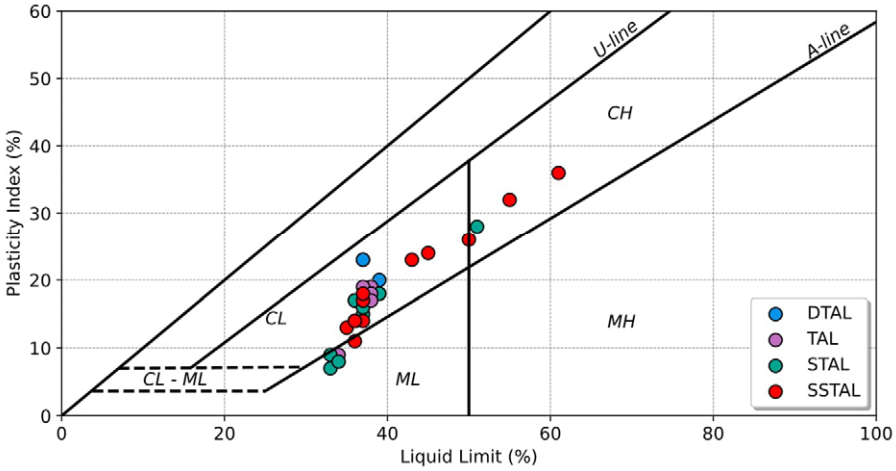

Figure 4: Atterberg Limits (AL) based on tailings category

4 RESULTS

4.1 CPTU INTERPRETATION

The tailings were initially assessed based on the framework provided by Robertson (2016) to determine the potential for contractive and dilative behaviour through the simplified CPT-based results. The results are shown in Figure 5. The darker the shaded hexagon in the figures, the more frequent that value occurs, hence the darker regions of hexagons are where the majority of values plot. The hexbin plot was chosen due to the sheer number of data, 23,376 datapoints from all 56 CPTu's. The mechanically improved tailings are primarily in the sand-like dilative zone, the sub-aerial tailings are primarily within the sand-like contractive zone with data also presenting in the sand-like dilative and transitional dilative zones. The sensitive sub-aqueous plots further within the contractive zones and lastly the sensitive sub-aqueous plots well within the clay-like contractive and sensitive clay-like contractive zones displaying the highest likelihood for contractive behaviour based on the Roberston (2016) SBTn chart.

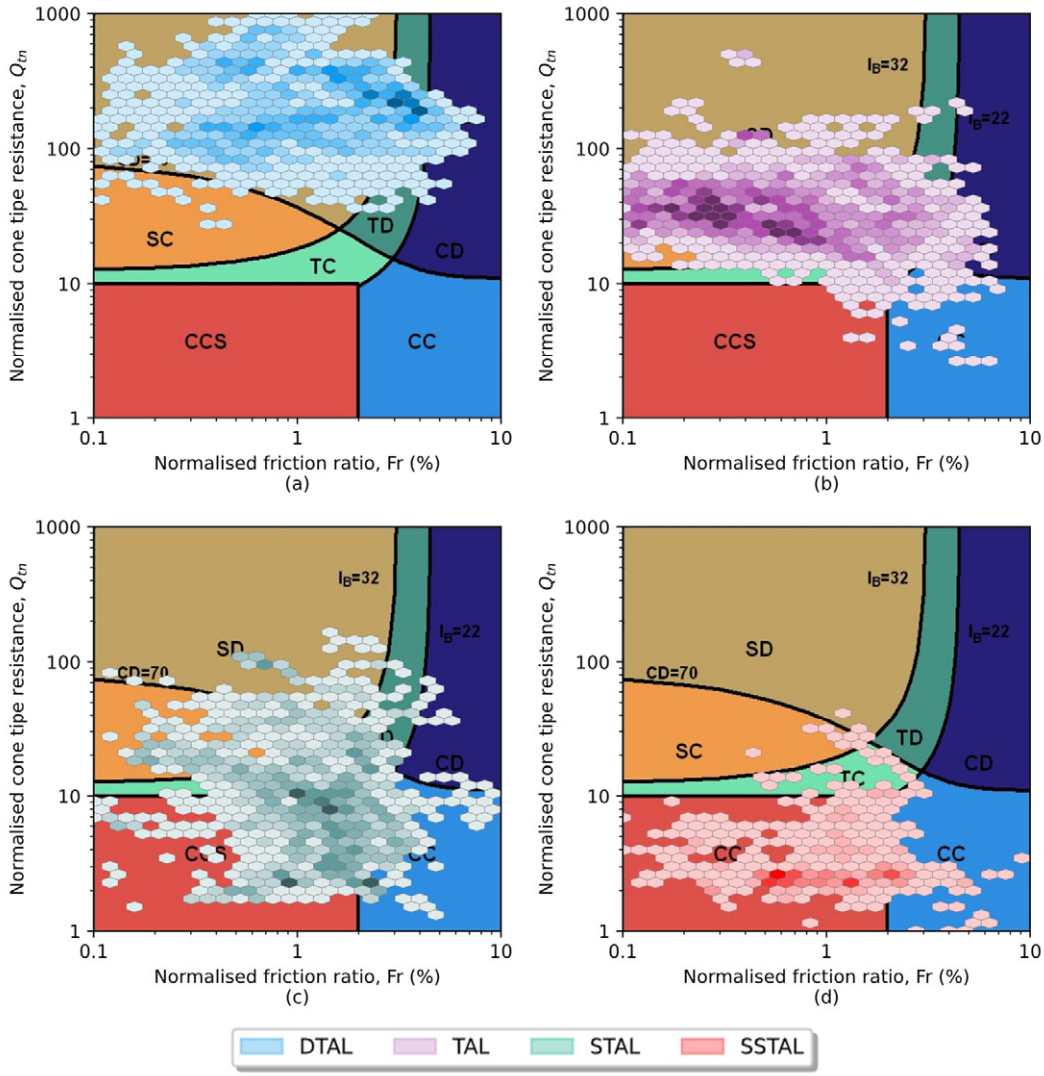

Figure 5: SBTn Chart (Robertson 2016) for various tailings material; (a) Mechanically improved (DTAL) tailings (b) Sub-aerial (TAL) tailings (c) Sub-aqueous (STAL) tailings and (d) Sensitive sub-aqueous (SSTAL) tailings

The Schneider plot (Schneider, 2008), shown Figure 6, has the added advantage of taking into consideration pore pressure. The mechanically improved (DTAL) tailings display clear dilative behaviour and as the material trends from sub-aerial (TAL) to sub-aqueous (STAL) and finally sensitive sub-aqueous (SSTAL) tailings the material becomes increasingly contractive.

The Schnieder plot can be used to assess the drainage of the CPTu during penetration (Schneider, 2008). However, caution should be applied in interpretation of these results as shear wave velocity (V_s) testing indicated the presence of microstructure, defined using a modified normalised small-strain rigidity index (K^*_G) > 330 as per Robertson (2016). Taking that into consideration, the mechanically improved (DTAL) tailings is within the drained sands region, which would be indicative of drained penetration, whereas the remaining tailings plot predominately within the transitional region. In addition to this there have been a total of 16 successful dissipation tests performed within the tailings, the t_{50} from these had a range from 90 – 1081, with a median of 439. Therefore, the dissipation tests would indicate that the penetration is essentially undrained (DeJong and Randolph, 2012).

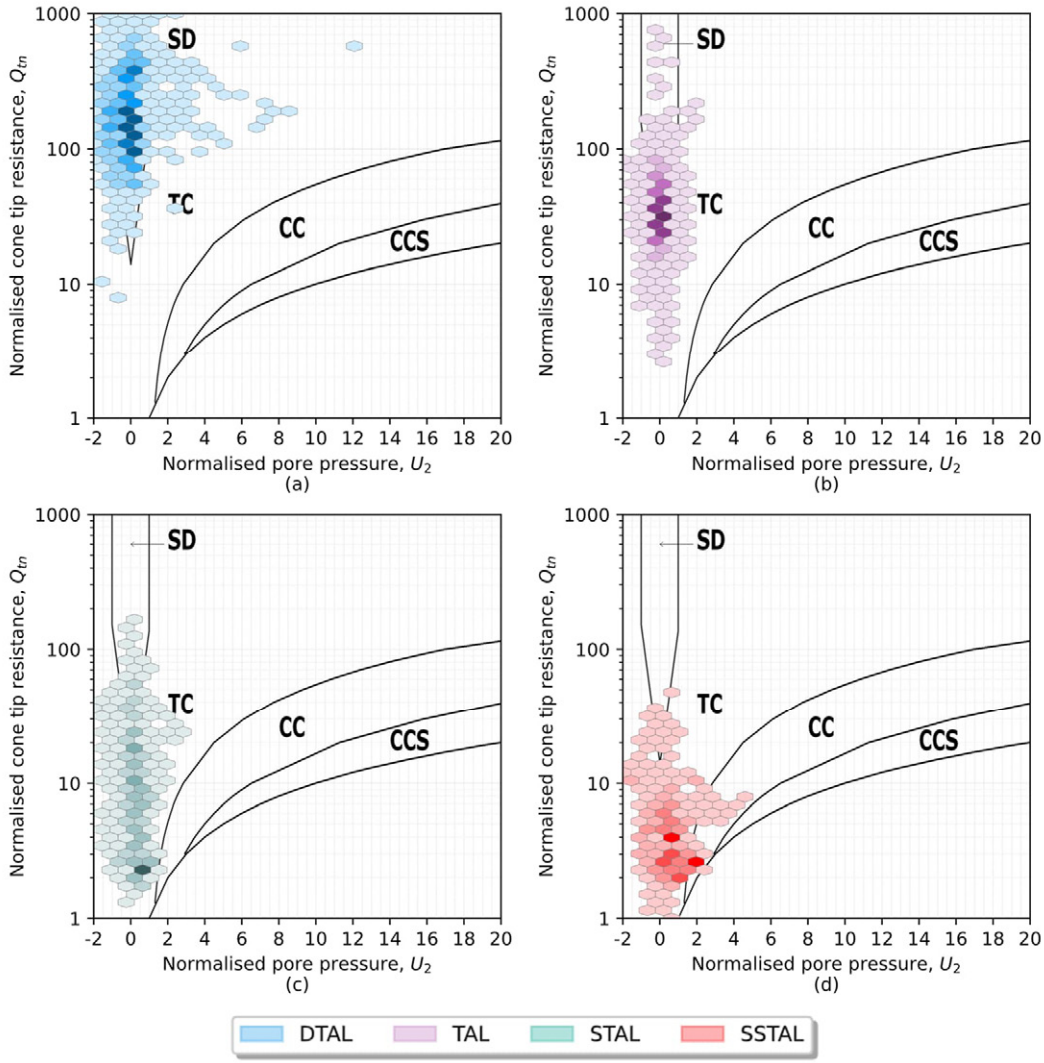

Figure 6: Schneider chart (Schneider 2008) for various tailings material; (a) Mechanically improved (DTAL) tailings (b) Sub-aerial (TAL) tailings (c) Sub-aqueous (STAL) tailings and (d) Sensitive sub-aqueous (SSTAL) tailings

4.2 CRITICAL STRESS FRICTION RATIO

Figure 7 and Figure 8 show the triaxial results displaying the deviatory stress against the mean effective stress. Figure 7 has the triaxial results categorised by tailings deposition method, while Figure 8 has the triaxial results categorised by fines content. As the CSL varies with fines content this second categorisation is useful for grouping the various CSLs derived from the triaxial results. The triaxial results also need to be considered in the context of the sample type. For the remoulded testing a more precise fines content could be targeted, whereas for the MBS the fines content has been approximated based on the PSD testing on the associated sample. However, the use of undisturbed testing does introduce some uncertainty regarding the fines content as the PSD test was conducted on a different part of the MBS as to the triaxial test. This uncertainty is considered minor in the scheme of things.

The critical state friction ratio, M, which is equal to the ratio of deviator stress to effective stress at the critical state, can be calculated from the triaxial test results. As such it is designated Mtc. Using triaxial compression as a reference case (M_{tc}) varies based depending on both deposition method and fines content. Here M_{tc} is obtained using the End of Test method commonly employed within the industry. While Bishop's Method (1971) or the Stress-Dilatancy Method is generally recommended (Ghafghazi and Shuttle, 2006) the lack of dense testing meant the End of Test method was more suitable. The trend of varying M_{tc} (and CSL) is well documented for fines content (Wood and Maeda, 2008). Interrogation of the results based on the tailings deposition method reveals that sensitive sub-aqueous and sub-aqueous tailings produces the lowest M_{tc} value ranging from 1.28 – 1.45 with the sub-aerial and mechanically improved tailings displaying a range of M_{tc} values from 1.53 – 1.64. This represents a difference of M_{tc} related to deposition method of between 7 – 12%.

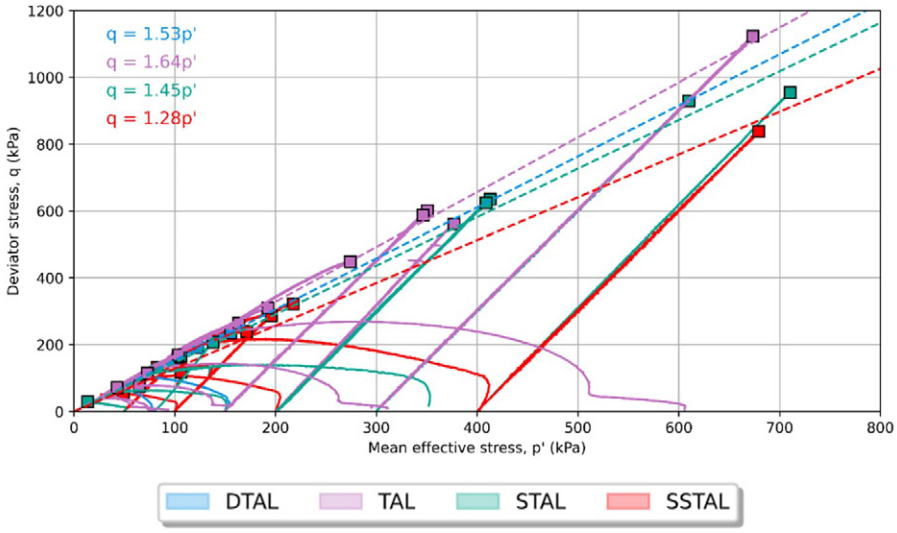

Figure 7: Triaxial test results showing deviator stress versus mean effective stress based on deposition method

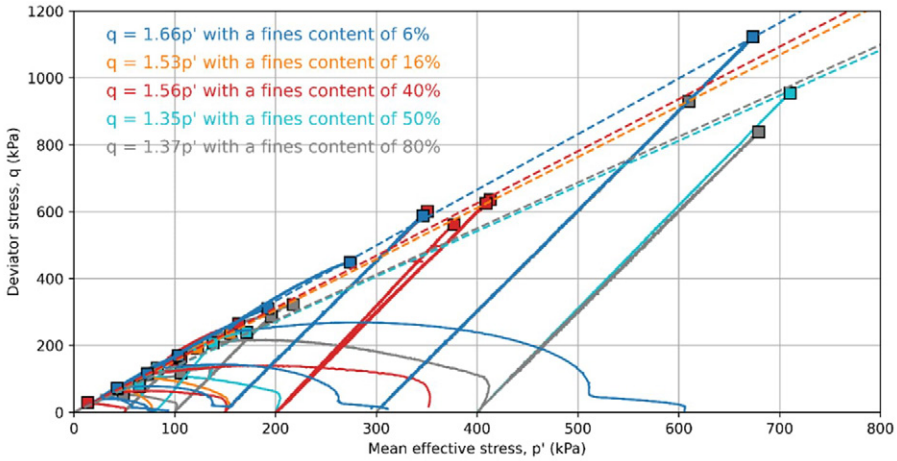

Figure 8: Triaxial test results showing deviator stress versus mean effective stress based on the fines content

Using the triaxial results categorised with fines content a correlation can be developed for M_{tc} based on the fines content, this relationship for the tailings material is shown in Figure 9. A decreasing trend of M_{tc} as fines content increases is shown with the slope being -0.0038. The decreasing trend is to be expected as the larger fines content tailings material was associated with the sub-aqueous deposition (and hence lower densities).

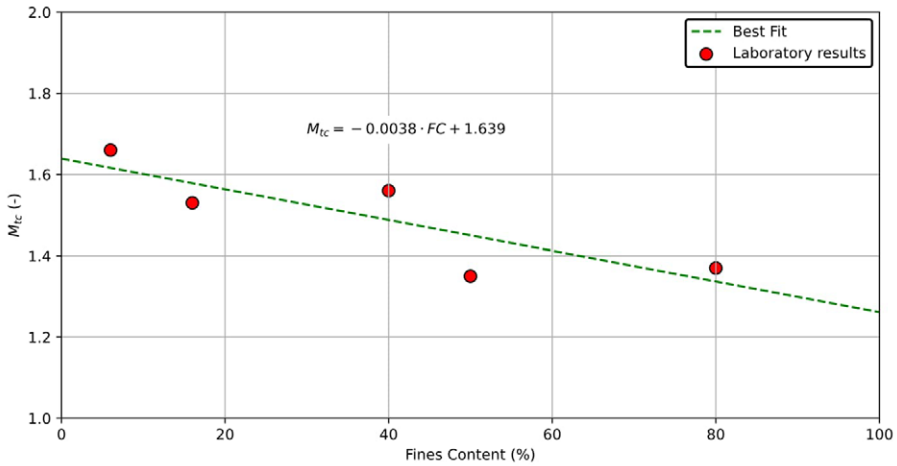

Figure 9: Critical State Friction Ratio (M_{tc}) versus Fines Content using laboratory results

4.3 CRITICAL STATE ANALYSIS

Using the triaxial test results, four CSLs in the compressibility plot were derived based on varying fines content (Figure 10). Several of the triaxial tests did not have end of test freezing implemented, these tests were not used to determine the CSLs as recommended by Reid et al. (2021). The CSLs encompass the tailings material with a fines content ranging from 6 – 80%. Using the four CSLs a region can be defined (Figure 11) where the CSL for an associated fines content between 6 – 80% can be anticipated to fall within this region. For a low fines content, the y-intercept (Γ, gamma) is 1.276 for 6% fines content. As the fines content increases Γ begins to decrease. At 40% fines content Γ is 1.007. With further increases in fines content Γ begins to increase rising to 1.058 for 50% fines content and reaching 1.195 at 80% fines content. Examining the four CSLs it can clearly be seen that the tailings material with the largest Γ has the largest slope (λ, lambda) and the tailings material with the smallest Γ has the smallest λ. This relationship suggests that the CSLs will converge at higher stress levels, which has previously been called the omega (Ω) point (Wood and Maeda, 2008) and hypothesized that it may occur with related soils. Computing the Ω-point for the CSLs produces a point at approximately p' = 8103 kPa and e = 0.38 for fines content 6%, 40% and 80%. The CSL for 50% does not fit neatly into this Ω-point location. However, obtaining a triaxial test to confirm the Ω-point would require an apparatus that goes up to 8MPa and be purely theoretical since the tailings will never experience loads near that value. Thus, this paragraph merely serves as an entertaining digression.

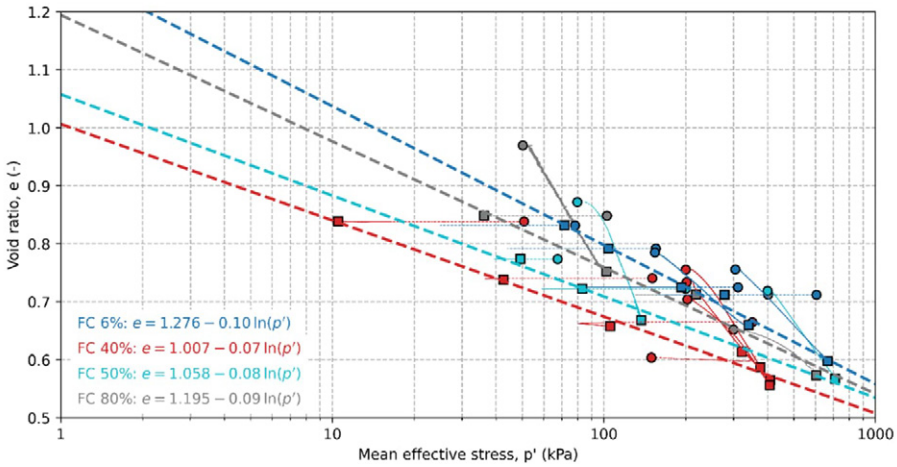

Figure 10: Critical state lines derived from the triaxial test results categorised by fines content

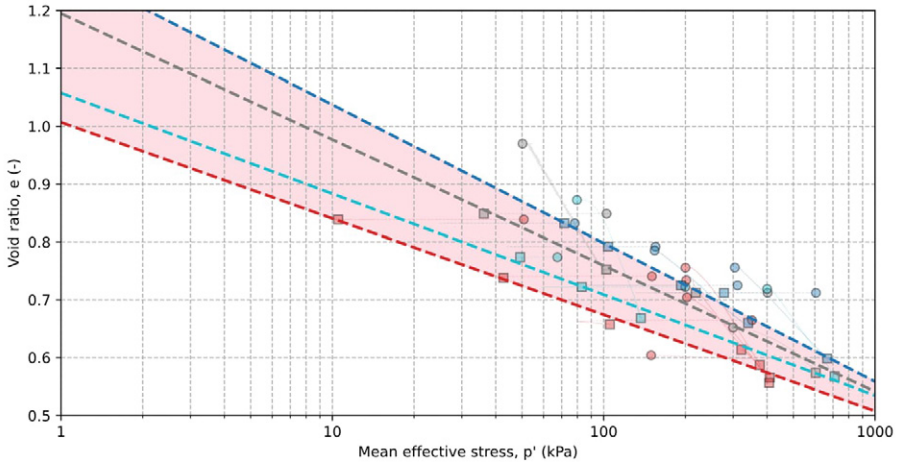

Figure 11: Critical state region defined between 6% fines content (Γ = 1.28) and 40% fines content (Γ = 1.01)

4.4 RELATING IN-SITU RESULTS TO THE CRITICAL STATE REGION

To relate the CPTu data to the CSL region, a site-specific calibration can be produced using the Soil Behaviour Type (Ic) determined from a CPTu and the laboratory PSD results from samples taken in proximity to that CPTu. The results for this form a site-specific calibration and are shown in Figure 12. Two other commonly adopted methods are shown as well, Boulanger and Idriss (2014) and Agaiby and Mayne (2020). The site-specific equation is shown in Equation (1).

$$FC = 13.83 \cdot \left(I_c{}^{1.47}\right) \quad (1)$$

The site-specific correlation is flatter than the more commonly used correlations, which indicates a wider range of potential behaviour resulting from a change in fines content than those soils that were used to develop these correlations. The advantage of a site-specific correlation as opposed to the more general correlation is that it will consider local characteristics such as grain properties, mineralogy and stress history, which all play a role in the potential behaviour of a soil. Agaiby and Mayne (2020) explored 53 well-documented geotechnical sites which would be anticipated to capture a wide range of behaviour types and that correlation more closely aligns with the site-specific correlation developed.

A limitation of creating a CSL region based on four CSLs is that there are only four discrete lines that are than extrapolated to cover an infinite number of potential CSLs. While multiple CSLs is an excellent step in the right direction, a material specific correlation can be developed relating fines content to both Γ and λ, shown in Figure 13 and Figure 14 respectively. For both functions a parabolic fit is utilised, reaching a coefficient of determination (R^2) value of 0.97 for Γ and 0.89 for λ, indicating that the data is an excellent fit for the function. This enables a more complete CSL region to be determined that can theoretically cover the entire range of fines content, shown in Figure 15. The model CSL region aligns well with the denser (dilative) side of the CSL region (lower CSL), however, the looser (contractive) side of the CSL region is considerably larger than the laboratory results indicate. There are potentially several reasons for this, such as the limitation of having a CSL at 80% fines content instead of 100% and the fact that there are limitations in preparing a loose sample in the laboratory for such high fines content.

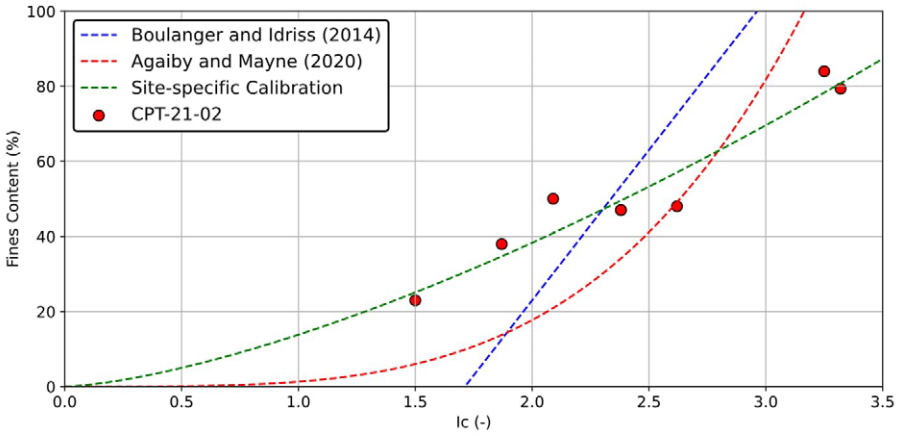

Figure 12: Site-specific fines content calibration

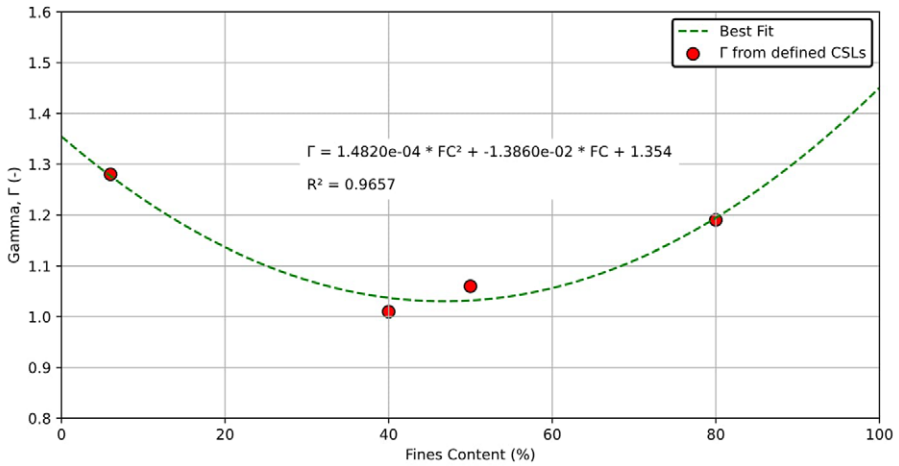

Figure 13: Gamma correlation based on the calculated result from the defined CSL

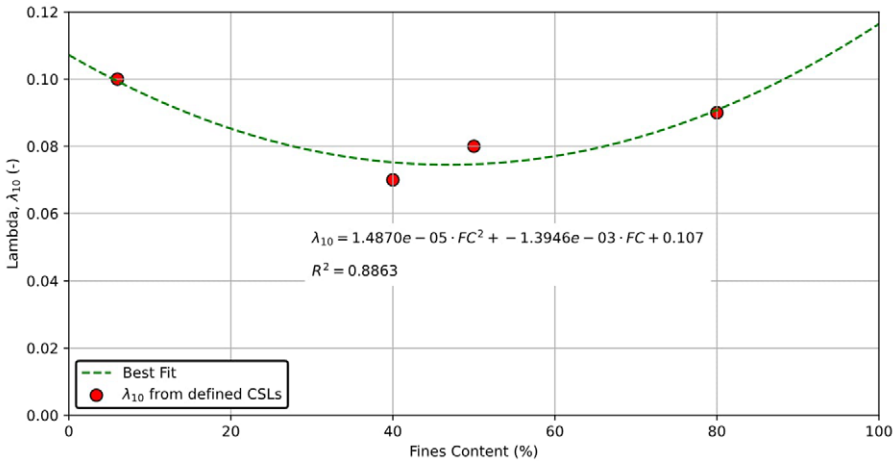

Figure 14: Lambda correlation based on the calculated result from the defined CSL

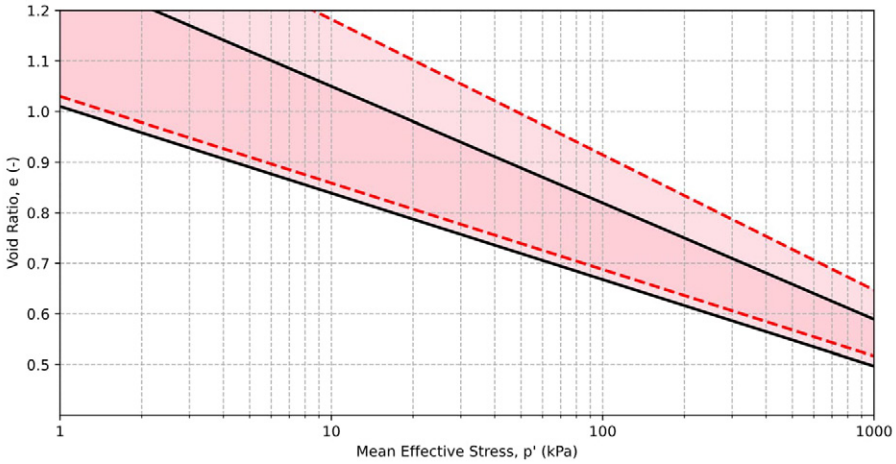

Figure 15: Laboratory region encompassed (black) CSLs function region based on four CSLs and generated (red) CSLs

With the CSL region defined and site-specific fines correlation for fines content developed, the CPTu data can now be plotted against the CSL region with each CPTu data point compared against the resultant CSL line within the CSL region. The comparison plot required the following assumptions: i) a K0 assumption of 0.6 to estimate the mean effective stress of each CPTu data point, and ii) A state parameter estimation using Jefferies and Been (2015) to determine the approximate void ratio for each CPTu datapoint. An example, the mechanically improved (DTAL) tailings is shown in Figure 16, the void ratio is approximately 0.52 when the mean effective stress is 15 kPa. For this data point the resultant CSL line points very near the lower bound of the CSL region. Data for sub-aerial (TAL) tailings is plotted in Figure 17, the mean effective stress is now approximately 38 kPa and the void ratio 0.64, the resultant CSL line has shifted upwards but is still nearer to the upper bound of the CSL region. The mean effective stress results from the CPTu's for the sub-aqueous (STAL) and sensitive sub-aqueous (SSTAL) tailings are shown in Figure 18 and Figure 19 respectively. Both STAL and SSTAL plot above the corresponding CSL, given how contractive this material has been shown, this is not surprising.

Figure 20 displays all the tailings data from the CPTu's with the CSL region shown. It is evident that a majority of the DTAL and TAL tailings can be expected to behave dilatively, with the STAL tailings moving closer to the CSL region, and the SSTAL tailings being majority within the CSL region, expected to be contractive.

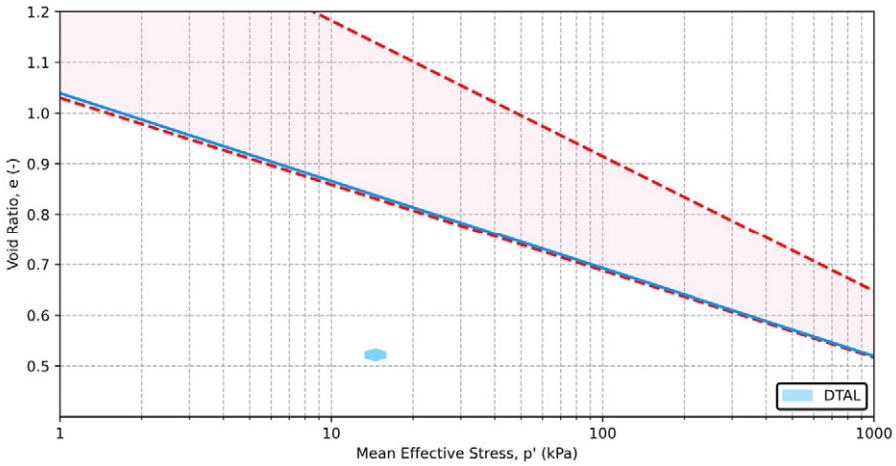

Figure 16: Modelled CSL region with example DTAL data point and corresponding CSL

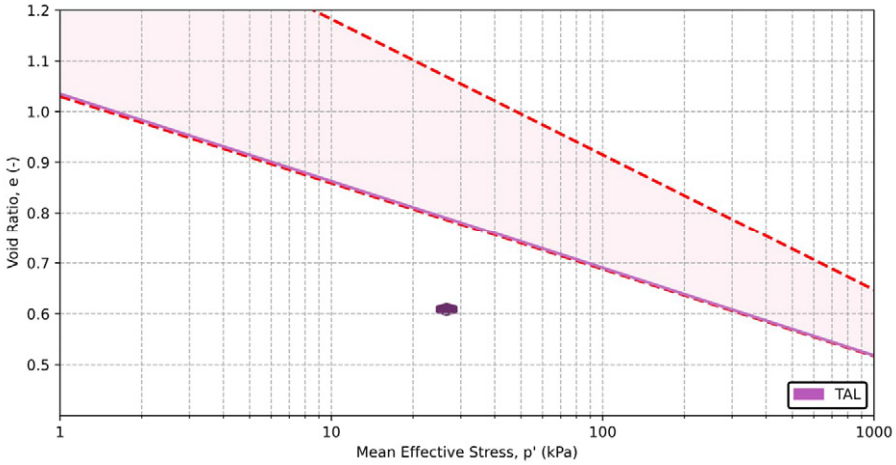

Figure 17: Modelled CSL region with example TAL data point and corresponding CSL

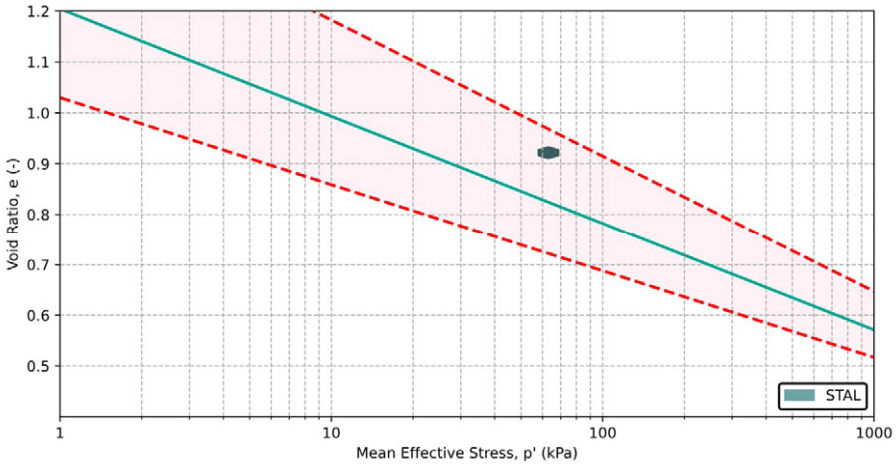

Figure 18: Modelled CSL region with example STAL data point and corresponding CSL

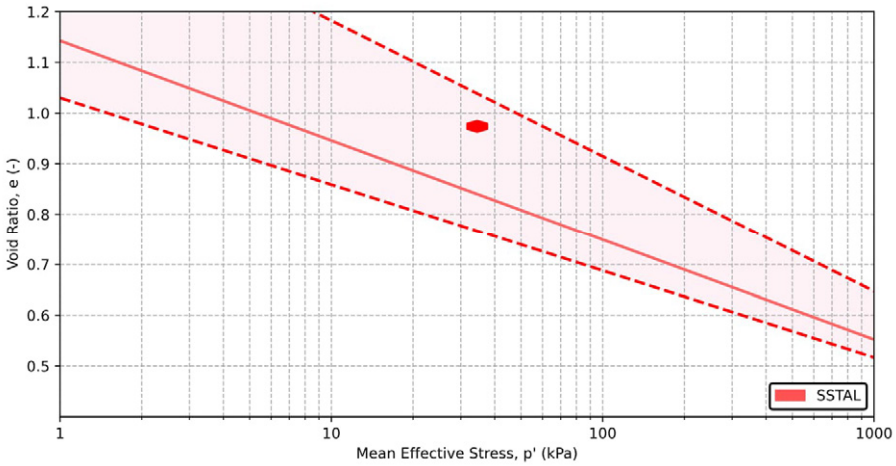

Figure 19: Modelled CSL region with example SSTAL data point and corresponding CSL

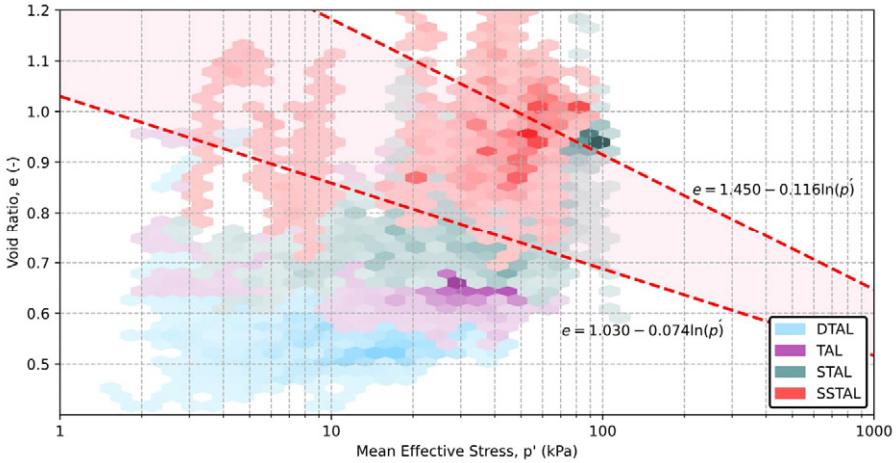

Figure 20: All CPTu results plotted over the modelled CSL region

5 DISCUSSION

The project from which these measurements were made is an upstream raised facility. As mentioned in Section 3, the TSF is a relatively young facility. This explains the low mean effective stresses of less than around 100 kPa derived from the CPTu's. The facility design philosophy considered using mechanical improvement techniques to build a structural zone, which would add resilience to the upstream raised facility. As the upstream raises continue to develop, it is expected that the mean effective stress will increase significantly causing a decrease in the void ratio. During site investigations for this TSF, MBS were retrieved, this sampling technique was utilised to minimise sample disturbance. A detailed explanation of the technique is beyond the scope of this paper but can be found in Lines et al. (2023). A total of 11 oedometer tests were performed on high quality MBSs, of which the apparent overconsolidation ratio (OCR) was calculated using the Casagrande methodology. The results indicated an apparent OCR range of 1.5 – 7.1 with a median of 2.4, indicating moderately overconsolidated tailings, most likely relating to the desiccation and microstructure present. The microstructure might be related to potential cementation well known in lateritic soils. The results suggests that some of the cementation/microstructure is regained after the tailings are deposited within the TSF and water contents are reduced via the mechanical improvement and/or crusting process. Therefore, the void ratios of the DTAL and TAL tailings are expected to follow an almost flat trend in the compressibility plot as they will follow the slope of the apparent overconsolidation line (i.e. recompression line, swelling or unloading index) on a void ratio-effective stress plot. Figure 20 is a representation of the effective stresses and void ratios estimated at the time when the CPTu surveys were conducted. With subsequent raises, the DTAL and TAL hexagon points will progressively migrate from the dilative region toward the right side of the figure and thus towards the contractive zone. An illustration of a CPTu data point of TAL and the direction and required mean effective stress increase to shift it to the CSL region is shown in Figure 21. For that specific CPTu data point an increase of approximately 120 kPa is required to relocate it from its current in situ state (dilative at the time of CPTu testing) to reach the CSL defined by its fines content. The distance between the CPTu data

(each hexagon) and its corresponding CSL can be used to understand when a specific region of tailings is transitioning from a predominately dilative state to a predominately contractive state. The classification of contractive versus dilative states is useful because it helps define the type of strength parameters required for design e.g. drained strength versus undrained strength. Figure 22 displays a histogram of all the tailings material Ψ results with the dilative/contractive boundary (Ψ = -0.05) highlighted with a dashed black vertical (CDF) line. This boundary line has historically been used by practitioners to determine what type of strength parameters are more appropriate for design. Figure 22(c) shows that approximately 80% of STAL tailings data points are contractive (seen by the crossover of the CDF line and the dilative/contractive boundary). Figure 22(d) show that approximately 95% of SSTAL tailings are contractive. Using undrained shear strength to represent the strength of STAL and SSTAL is warranted based on these results. Figure 22(a) show that approximately 99% of DTAL tailings are dilative, which indicates that effective stress parameters are adequate for this unit, this might change in the future as subsequent raises increase the mean effective stress, a combination of Figure 20 and Figure 21 could be used to predict the amount of overburden required to reach this transition phase. This information is useful for designing the slope of subsequent upstream raise batters to limit the column of tailings deposited above the structural zone and providing knowledge as to when the tailings that are currently dilative may becoming contractive in the future. Figure 22(b) shows that around 80% of the TAL material is dilative and 20% is contractive. This result means that the parameter selection of TAL is not as straightforward and should be carefully considered.

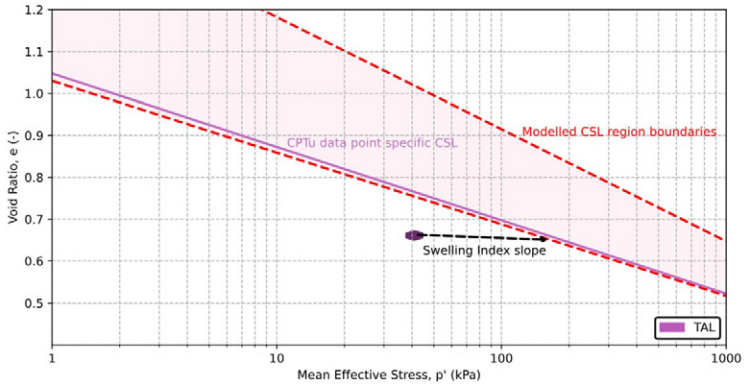

Figure 21: Illustration of TAL moving towards CSL region with increasing mean effective stress

The statistical descriptors of the state parameter estimated for each unit are summarised in Table 1. The coefficient of variation (CoV) provides insight into the relative variability of the Ψ across the different material types. A higher CoV suggests greater dispersion in the data, while a lower CoV indicates more uniformity. STAL tailings have the highest CoV (294%), meaning its Ψ values are highly variable, this CoV is larger than anticipated. In contrast, DTAL tailings have the lowest CoV (37%), suggesting that its Ψ values are relatively consistent, possibly due to the mechanical dewatering inducing a more uniform fabric. TAL and SSTAL exhibit intermediate CoV values (62% and 63%, respectively), indicating moderate variability in their state parameters. The dilative or contractive tendencies of each material can be examined using the mean ψ values, though this is a subjective threshold as a percentile may be more appropriate (i.e., a 20th percentile). However, using the mean values, DTAL (Ψ = −0.30) and TAL (Ψ = −0.10) exhibit values below the dilative/contractive threshold of ψ = -0.05, indicating dilative behaviour under shearing, with DTAL being the most dilative. STAL (Ψ = 0.03) and SSTAL (Ψ = 0.10) have mean values above the dilative/contractive threshold, meaning they are more contractive. The range of Ψ values across all the tailings types underscores their inherent variability, dependent on the deposition method, which must be carefully considered when assigning material parameters.

Table 1: Statistical summary of Ψ estimated for each tailings unit

	DTAL	TAL	STAL	SSTAL
Number of data points(n)	7,120	8,882	5,024	2,350
Minimum	-0.65	-0.40	-0.35	-0.16
Maximum	0.28	0.11	0.18	0.22
Mean	-0.30	-0.10	0.03	0.10
Std.	0.11	0.06	0.09	0.06
CoV (%)	37	62	294	63

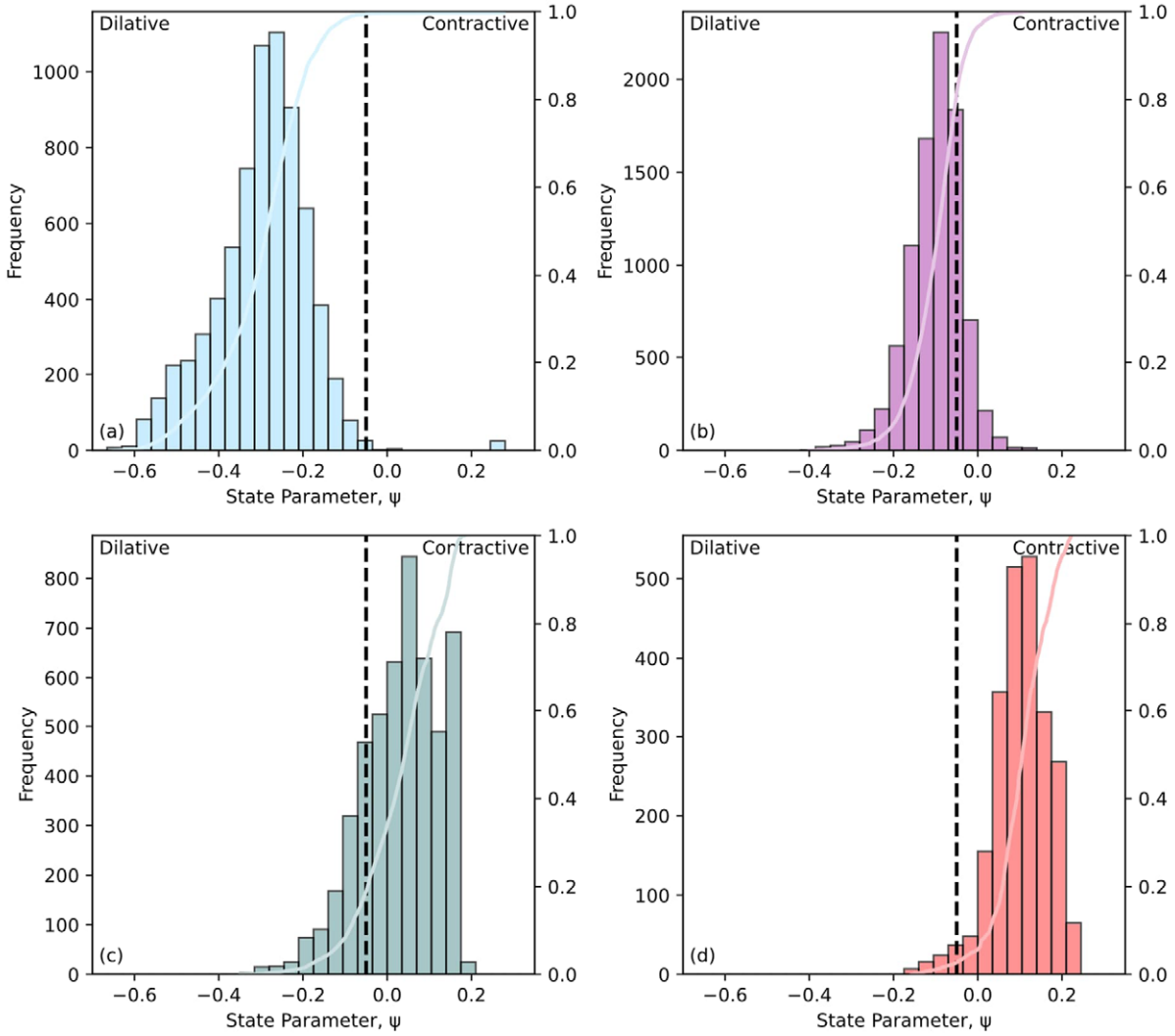

Figure 22: Histogram and CDF displaying distribution of State Parameter for each tailings category (a) DTAL (b) TAL (c) STAL and (d) SSTAL

6 SUMMARY AND CONCLUSIONS

A CPTu and laboratory investigation of tailings was undertaken on a relatively young TSF upon which mechanical improvement had recently commenced. Based upon the CPTu results and deposition methodology the tailings material was split into four groups. This included mechanically improved tailings, sub-aerially deposited tailings and two types of sub-aqueous deposited tailings. Following the site investigation a laboratory campaign was conducted with a focus on strength testing using compression triaxial. Four CSLs were developed based on fines content (5%, 40%, 50% and 80%). The CSLs displayed different slopes and intercepts, with the slopes trending towards an omega point and the intercepts varying with a decrease from 6% to 40% and then increase towards 50% and 80%. Material specific correlations for the critical state parameters M_{tc}, Ic, gamma and lambda were developed. Using the material specific correlations a CSL region generated. Using the fines correlation, the CPTu data was compared with the generated CSL region and the State Parameter estimated using Jefferies and Been (2015). On this basis the mechanically improved (DTAL) tailings were found to be 99% dilative and the sub-aerial (TAL) tailings approximately 80% dilative. Both sub-aqueously (STAL and SSTAL) tailings were found to be highly contractive, at approximately 80% for STAL and 95% for SSTAL. The variability of state parameters across tailings units shows that the deposition method and any subsequent de-watering effort such as mechanical improved has a significant impact on the potential behaviour of the tailings and whether it is dilative or contractive. Mechanical improvement of the tailings was also seen to reduce material variability which is desired from a reliability stand point. These results show the clear advantage mechanically improving can give regarding the increased strength and management of liquefactive potential. However, where mechanical improvement is not possible, sub-aerial deposition with appropriate drying times can offer a significant advantage over sub-aqueous deposition. These observations are anecdotally known by experienced tailings engineers.

The methods used in this paper provide a robust rational framework to demonstrate the effect of various tailings management practices on design outcomes. Proper deposition and pond management during operations are essential as they translate directly into strength and potential liquefaction behaviour. The plots and methods proposed here are expected to help designers use similar management strategies to plan the batters of subsequent raises based on the performance of the state parameters. For example, using the recompression index such as in Figure 21, engineers can forecast when units currently behaving as dilative can transition to contractive due to subsequent loading or upstream raises. This information is key to designing the slope of subsequent upstream batters and plan for long-term mechanical behaviour.

CRediT authorship contribution statement

Scott Lines: Writing - original draft. **Marcelo Llano-Serna**: Writing - Review and editing.

7 REFERENCES

Amundsen, H. A., Emdal, A., & Thakur, V. (2021). A new method for storage of block samples: a pilot study. *Géotechnique Letters*, 11(3), 179-186.

Bishop, A. W. (1971). Shear strength parameters for undisturbed and remoulded soil specimens. Proc. Roscoe Memorial Symp., Cambridge, 3-58.

DeJong, J.T. and Randolph, M. (2012). Influence of partial consolidation during cone penetration on estimated soil behavior type and pore pressure dissipation measurements. *J. Geotech. Geoenviron. Eng.,* 138(7): 777-788.

Emdal, A., Gylland, A., Amundsen, H. A., Kåsin, K., & Long, M. (2016). Mini-block sampler. *Canadian Geotechnical Journal*, 53(8), 1235-1245.

Figueroa, A., Santos, E., Sconagmillo, C., Valenzuela, L., & Tascon, A. (2015). Particle-Size Segregation in Tailings Sand Dams. In From Fundamentals to Applications in Geotechnics (pp. 2402-2409). IOS Press.

Ghafghazi, M., & Shuttle, D. A. (2006). Accurate determination of the critical state friction angle from triaxial tests. In Proceedings of the 59th Canadian Geotechnical Conference, Vancouver, BC, Canada (pp. 1-4).

Halabi, A. L. M., Siacara, A. T., Sakano, V. K., Pileggi, R. G., & Futai, M. M. (2022). Tailings dam failures: A historical analysis of the risk. *Journal of Failure Analysis and Prevention*, 22(2), 464-477.

Hudson-Edwards, K. A., Kemp, D., Torres-Cruz, L. A., Macklin, M. G., Brewer, P. A., Owen, J. R., & Thomas, C. J. (2024). Tailings storage facilities, failures and disaster risk. *Nature Reviews Earth & Environment*, 5(9), 612-630.

ICOLD. (2023). Tailings Dam Safety Bulletin 194. Version 1.0.

Jefferies, M., & Been, K. (2015). Soil Liquefaction: A Critical State Approach, Second Edition (2nd ed.). CRC Press. https://doi.org/10.1201/b19114

Lines, S. H., Llano-Serna, M., Rekowski, R., Ludlow, W. (2023). Identification and analysis of a complex layer within the footprint of a tailings storage facility foundation utilising mini-block sampling. Proceedings of Mine Waste and Tailings Conference, Brisbane.

Morrison, K. F. (2021). Preface to the MME Special Focus Issue on Tailings Management. *Mining, Metallurgy & Exploration*, 38(3), 1287-1288.

Nguyen, T. K., Benahmed, N., Hicher, P. Y., & Nicolas, M. (2014). The influence of fines content on the onset of instability and critical state line of silty sand. In International Workshop on Bifurcation and Degradation in Geomaterials (pp. 113-120).

Papadopoulou, A., & Tika, T. (2008). The effect of fines on critical state and liquefaction resistance characteristics of non-plastic silty sands. *Soils and foundations*, 48(5), 713-725.

Reid, D., Fourie, A., Ayala, J. L., Dickinson, S., Ochoa-Cornejo, F., Fanni, R., ... & Suazo, G. (2021). Results of a critical state line testing round robin programme. *Géotechnique*, 71(7), 616-630.

Reid, D., & Fanni, R. (2022). A comparison of intact and reconstituted samples of a silt tailings. *Géotechnique*, 72(2), 176-188.

Robertson, P. K. (2016). Cone penetration test (CPT)-based soil behaviour type (SBT) classification system—an update. *Canadian Geotechnical Journal*, 53(12), 1910-1927.

Schneider, J. A., Randolph, M. F., Mayne, P. W., & Ramsey, N. R. (2008). Analysis of factors influencing soil classification using normalized piezocone tip resistance and pore pressure parameters. *Journal of geotechnical and geoenvironmental engineering*, 134(11), 1569-1586.

Williams, D. J. (2021). Lessons from tailings dam failures—where to go from here?. *Minerals*, 11(8), 853.

Wood, D. M. & Maeda, K. (2008). Changing grading of soil: effect on critical states. *Acta Geotechnica*, 3, 3-14.

BLACK
INSITU TESTING

GEOTECHNICAL TESTING SPECIALISTS

BLACK INSITU TESTING WAS FORMED IN 2008 AS A SPECIALISED CONE PENETRATION TESTING COMPANY.

The company founders are experienced geotechnical engineers who were motivated to create Black Insitu Testing by recognising a need for high quality CPT tests to aid accurate and economic geotechnical investigations.

In addition to CPT, we provide an extensive range of other insitu testing and soil sampling services. We have 9 CPT rigs that can access a wide range of site conditions.

Detailed information on our testing services and CPT rigs is available on our website

www.blackinsitutesting.com.au

GEOTECHNICAL BEHAVIOR OF GOLD ORE TAILINGS FROM A FILTERED STACK IN MINAS GERAIS, BRAZIL

Mayara Ferreira Rodrigues[1], Márcio de Souza Soares de Almeida[1], Marcos Barreto de Mendonça[1] and Jaime Pinheiro[2]

[1]Federal University of Rio de Janeiro – UFRJ; [2]AngloGold Ashanti USA

https://doi.org/10.56295/AGJ6043

ABSTRACT

Catastrophic events related to tailings dams worldwide —notably in Brazil— have brought about the need to expand geotechnical studies on tailings disposal. Special attention should be given to mechanically compacted filtered tailings due to the significant increase in the height of such deposits, making it necessary to better understand the mechanical behavior of these structures. This paper compiles and discusses the results of field and laboratory tests on filtered gold ore tailings from an experimental embankment and a tailings stack currently operated by a mining company in Minas Gerais, Brazil. The tailings originate from the flotation stage, part of the metallurgical process of gold ore beneficiation. In-situ density tests were carried out to understand the effect of the compaction process across different layer thicknesses using various equipment types, and laboratory tests were conducted to obtain the characterization, compaction, shear strength, and hydraulic conductivity parameters of the material. Field tests demonstrated the need to restrict layer thicknesses to 30 cm and allowed for the discussion of compaction quality issues as a function of the equipment used.. Based on the index test results, the material was classified as non-plastic sandy silt. The hydraulic conductivity tests on trimmed or laboratory-compacted specimens at different void ratios indicated virtually isotropic behavior. Triaxial compression results, in which specimens reached the critical state, revealed four distinct critical state lines (CSLs), a phenomenon attributed to grain size variations observed in the samples. The results highlight the need to monitor variations in the geotechnical characteristics of tailings over the stacks service life to adjust construction processes accordingly.

1. INTRODUCTION

Among the available options, the use of filtered tailings compacted in stacks has been widely considered a viable Tailings Storage Facility (TSF) option *(Davies, 2011; Crystal et al., 2018; Ulrich, 2019; Cacciuttolo & Campomanes, 2022; Cacciuttolo and Atencio, 2023).*

Fourie et al. (2022) highlight the continuous growth of global mining activities and the reduced content of the extracted ore, resulting in increased tailings production. These conditions underscore the importance of improving the understanding of the geotechnical behavior of these materials, enabling the improvement of the disposal of filtered tailings in stacks and contributing to process efficiency, in order to create better technical basis for projects and safer structures *(Davies, 2011; Gomes et al., 2019; Furnell et al., 2022).*

As mining production continues to grow, filtered stacks have grown increasingly larger in height and volume *(Crystal et al., 2018; Fourie et al., 2022; Cacciuttolo and Atencio, 2023).* In these structures, the filtered tailings are transported by trucks or conveyors. They are then deposited and spread, homogenized using a tillage tractor until the optimum moisture content is reached, and subsequently compacted in layers of predefined thicknesses. At the end of each cycle, geotechnical quality control tests are conducted, and the process is repeated, resulting in a partially saturated structure with sufficient in-situ density and geometry, thereby eliminating the need for auxiliary containment structures *(Davies, 2011; Cacciuttolo & Campomanes, 2022).* Therefore, conducting studies on test embankments to obtain geotechnical parameters and assess the behavior of specific tailings when mechanically compacted after filtration is an essential step. Design requirements must also consider climatic challenges, regional seismicity, logistical constraints, operational scale, and availability of construction equipment *(Davies, 2011)*.

Furthermore, defining geotechnical parameters based on laboratory tests is paramount in guiding the design and operational criteria of these structures *(Davies, 2011; Crystal et al., 2018).* These experimental campaigns have continuously evolved to reduce uncertainties arising from the unique characteristics of tailings *(Fourie et al., 2022; Delgado et al., 2023).* The behavior

of tailings must be analyzed within the framework of Critical State Soil Mechanics (CSSM), as the void ratio of compacted tailings and the stress conditions to which they are subjected directly influence their shear strength *(Jefferies and Been, 2016)*. This context serves as the motivation for this study, which presents and discusses the results of an experimental campaign on filtered gold ore tailings from the flotation stage of a project in Minas Gerais State, Brazil, involving both field and laboratory tests. Field tests were conducted on an experimental embankment and a filtered tailings stack under different compaction conditions. Laboratory tests for characterization, hydraulic conductivity, and stress-strain behavior were carried out on specimens trimmed from undisturbed blocks, as well as on laboratory-compacted specimens obtained from samples collected from both structures.

2. MATERIALS AND METHODS

2.1 TAILINGS STUDIED

The tailings analyzed in this study originated from the flotation stage of the gold ore beneficiation process at an underground mine in the *Quadrilátero Ferrífero* - State of Minas Gerais, southeastern Brazil. The material was transported by truck from the filtration plant and deposited at both a tailings stack and an experimental embankment. Upon exiting the filtration plant, the tailings had a moisture content ranging from 17.4% to 24.1%.

To evaluate the behavior of the tailings under different compaction methods, data were collected from an experimental embankment with an approximate volume of 3,000 m³, constructed with 30 cm and 50 cm thick layers compacted using a track dozer, and from a tailings stack with a volume of approximately 160,000 m³, built with 30 cm thick layers compacted with a smooth drum roller without vibration.

Since the moisture content of the tailings exceeded the optimum range (12.7% to 17.4% — see section 3.2) upon leaving the filtration plant, the material was homogenized after placement using a tillage tractor to bring the material to the optimum moisture content. The layers were then leveled with a motor grader and compacted using the respective equipment.

2.2 SAMPLING AND EXPERIMENTAL CAMPAIGN

The tests were conducted in accordance with standards established by the American Society for Testing and Materials (ASTM). Field tests were performed on all layers of the experimental embankment and the filtered tailings stack to verify in situ density and moisture content. In-situ density measurements were taken on the top and bottom surfaces of all 50 cm thick layers and on selected 30 cm thick layers to evaluate variations in the degree of compaction (DC) between the two horizons. A total of 76 tests were conducted on the experimental embankment and 107 on the filtered tailings stack.

Disturbed samples from both structures were collected for laboratory characterization and compaction testing. Test specimens were then compacted in the laboratory at various void ratios to assess shear strength and hydraulic conductivity. Additionally, twelve undisturbed block samples were collected from which test specimens were trimmed for shear strength and hydraulic conductivity testing. The testing campaign is summarized in Table 1.

Table 1. Field and laboratory testing campaign.

Test	Qty.	Specifications
In-situ density	183	Hilf method
Grain size distribution: sieving and sedimentation; and particle specific gravity	29	-
Maximum and minimum void ratio	7	-
Standard Proctor compaction	59	Proctor standard energy
Falling-head permeability	24	Test specimens trimmed from undisturbed blocks or laboratory-compacted
CIU_{sat} triaxial compression	80 specimens	B Parameter ≥ 95%; p'_0 from 100 kPa to 1600 kPa. Test specimens trimmed from undisturbed blocks or laboratory compacted. Dimensions: h=110mm and D=50mm.
CID_{sat} triaxial compression	44 specimens	

Regarding the triaxial compression tests, volume variation was tracked throughout all stages, so that the void ratio at the end of shearing could be estimated with sufficient accuracy. Advanced laboratory techniques *(Jefferies & Been (2016); Viana da Fonseca et al., 2021)* such as lubricated ends, top-cap guided ram connections and the freezing method at end of shearing

were not employed in this study, as the scale of the experimental campaign and industrial requirements necessitated the use of a conventional test setup.

The behavior of the tailings was analyzed from the perspective of CSSM, by determining the Critical State Line (CSL) of the material *(Jefferies & Been, 2016)*. Only the tests that actually reached the critical state condition (i.e., a final condition marked by no further variation in shear strength, volume or pore pressure generation) were used to assess the CSL.

The critical state void ratio was obtained at the end of the specimen compaction step since the tests were carried out with volume change control throughout all phases.

3. RESULTS AND DISCUSSIONS

3.1 FIELD TESTING

3.1.1 Degree of compaction and in-situ moisture content of tailings embankments

The in-situ density test results from the experimental embankment and the filtered tailings stack are presented according to the compaction cycles and equipment used. In studies on gold ore tailings, *Zorzal et al. (2020)* suggest obtaining a degree of compaction (DC) greater than 96% to ensure dilative behavior. Although this reference may vary according to the characteristics of different tailings, this observation is considered when analyzing the degree of compaction results from the field tests.

The DC verification test results were grouped according to the compaction equipment used (track dozer and non-vibratory smooth drum roller), layer thickness (30 cm and 50 cm), number of cycles (up to three, four, five and six cycles) and in-situ test position (top and bottom of the layer) – see Figures 1 and 2. For compaction using a smooth drum roller, only the middle of the layer was tested. Each compaction cycle corresponds to two passes of the compaction equipment.

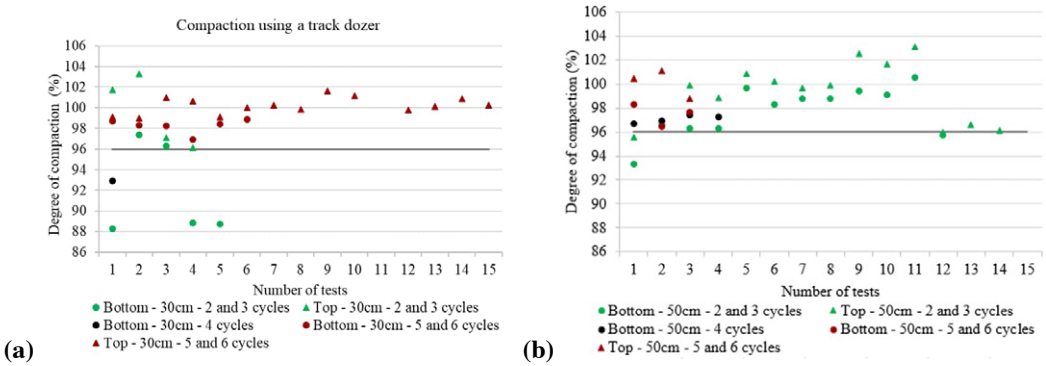

Figure 1. Degree of compaction at the top and bottom of layers compacted using a track dozer: (a) 30 cm-thick layer; (b) 50 cm-thick layer.

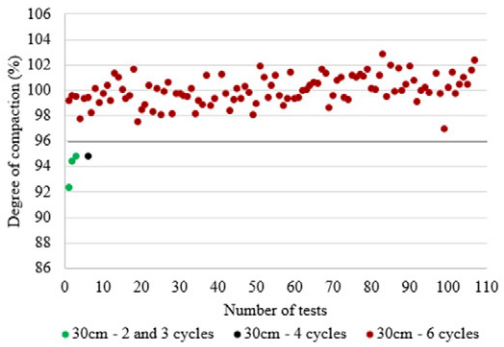

Figure 2. Degree of compaction in the middle of 30 cm-thick layers compacted using a non-vibrating smooth drum roller without vibration.

Based on the analysis of the results presented in Figures 1 and 2, the following observations were made:

- 30 cm-thick layer embankment compacted using a track dozer (Figure 1a):
  - The degree of compaction (DC) varied between the top and bottom surfaces, regardless of the number of compaction cycles applied. This variation reached up to 3% for five and six cycles and 13% for two and three cycles.
  - With two or three compaction cycles, the DC was concentrated above 95%. In contrast, with five or six cycles, it remained above 98%, at both the top and bottom surfaces, indicating a gain in DC as the number of compaction cycles increased.
  - The difference in DC between the top and bottom surfaces decreased as the number of compaction cycles increased, indicating greater homogeneity in compaction. Only one test was conducted at the base of the layer using four compaction cycles. As this test is not representative, no reliable conclusions can be drawn from this result.
- 50 cm-thick layer embankment compacted using a track dozer (Figure 1b):
  - For five and six compaction cycles, the DC of the top and bottom layers remained close to 98%. For fewer cycles, the results were more scattered, ranging from 93% to 103%.
  - The top layer results for two and three compaction cycles — higher than those obtained for five and six cycles — suggest that only the areas directly compacted by the track dozer were tested. The *USACE (1995)* notes this type of compaction heterogeneity when track dozers are used, which will be discussed later.
  - The DC varied between the top and bottom layers regardless of the number of compaction cycles, similar to the behavior observed in the 30 cm-thick layers.
  - The DC difference between the top and bottom layers was 5% for five and six cycles, and 3% for two and three cycles. With the increase in layer thickness, lower DC levels and greater scatter than those observed for the 30 cm-thick layer were expected; however, this was not observed. This result may also reflect the heterogeneity of the embankment material, as previously mentioned.
  - For four compaction cycles, an increase in DC was observed at the bottom of the layer compared to two and three cycles.
- 30 cm-thick layer embankment compacted using a non-vibrating smooth drum roller (Figure 2):
  - The use of six compaction cycles ensured an average DC close to 100%.
  - After two and three compaction cycles, the DC was lower than 95%. The lowest value observed was 92%, indicating the highest dispersion in results.
  - Four compaction cycles were insufficient to achieve DC values greater than 95%.
  - The DC tended to increase with the number of compaction cycles.

Figure 3 presents the average test results obtained under varying conditions of layer thickness, compaction equipment type, and test position, grouped according to the number of compaction cycles.

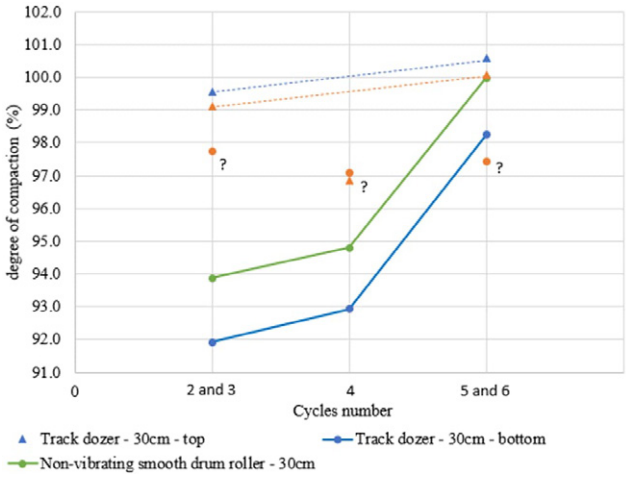

Figure 3. Average degree of compaction (DC) versus number of compaction cycles.

The analysis of the average results presented in Figure 3 led to the following conclusions:

- The DC tended to improve under all compaction conditions as the number of cycles increased.
- The dispersion of the average results decreased as the number of compaction cycles increased. For track dozer compaction on 30 cm-thick layers, the difference between top and bottom DC values was nearly 8% with two and three cycles and decreased to 3% with five and six cycles. This indicates that additional compaction cycles contributed to reduced layer heterogeneity.
- The increase in DC at the bottom of the layers was more significant when five and six compaction cycles were used.
- The use of up to four compaction cycles resulted in average DC values below 95%.
- The tests on 50 cm-thick layers exhibited behavior different from that described above. This may suggest that the tested areas were better compacted than those selected for the 30 cm-thick layer embankment, highlighting the heterogeneity of tailings compacted by track dozers. This variation may result from uneven coverage by the track dozer, as the entire surface may not have received the same number of passes. This is due to the need for precise lateral displacement of the dozer, given the gap between its tracks – a condition does not present with the smooth drum roller.

Crystal et al. (2018) and *Wilson (2021)* emphasize that adequate compaction of tailings reduces the stack's susceptibility to liquefaction, promotes dilative behavior in embankments, and requires care to avoid the formation of loose zones within the structure. In this context, based on observations of layers compacted using a track dozer, the *USACE (1995)* states that the number of compaction cycles in embankments compacted with a track dozer cannot be defined in the same way as for tamping rollers. This is due to the spacing between the equipment's tracks, which prevents the entire area corresponding to the dozer's width from being fully compacted. This operational limitation highlights the potential heterogeneity of the embankment if technical specifications and field monitoring do not ensure that the lateral displacement of the equipment adequately covers the entire surface under consistent compaction conditions.

According to *USACE (1995),* in soils with low fines content and high permeability — i.e., sandy soils — the layer thickness should be limited to 40 cm, and in materials with higher fines content, to 20 cm. *Cacciuttolo & Campamones (2022)* recommend limiting the layer thickness to 30 cm for tailings. Since the tailings under study have a sandy silt composition, the *USACE (1995)* indicates that 50 cm-thick layers are not suitable for building embankments with this type of material. This is supported by the analysis of the test results, where the DC of the 30 cm-thick layers remained above 98% for five or six compaction cycles (Figure 1a and Figure 2). *Wagner et al. (2023)* emphasize that, although there is interest in increasing layer thicknesses to improve productivity, thinner layers promote higher degrees of compaction, directly affecting the geotechnical behavior of the structure.

3.2 LABORATORY TESTING

3.2.1 Characterization and Compaction

Based on the results of geotechnical characterization and compaction tests, the tailings were classified as sandy silt according to grain size analysis, and as a low-plasticity silt (ML) according to the Unified Soil Classification System (USCS) *(ASTM D2487, 2017)*. The particle size distribution was as follows: clay content ranging from 0 to 6.5%, silt from 49% to 69.5%, and sand from 24% to 50.3%. The material was non-plastic, with specific gravity values ranging from 2.791 to 2.940 g/cm³, maximum dry density ranging from 1.679 to 1.806 g/cm³, and optimum moisture content ranging from 14.6% to 18.8%. Figure 4 shows the grain size distribution of the tailings studied, which is consistent with grain size distribution curves for gold ore tailings from various locations.

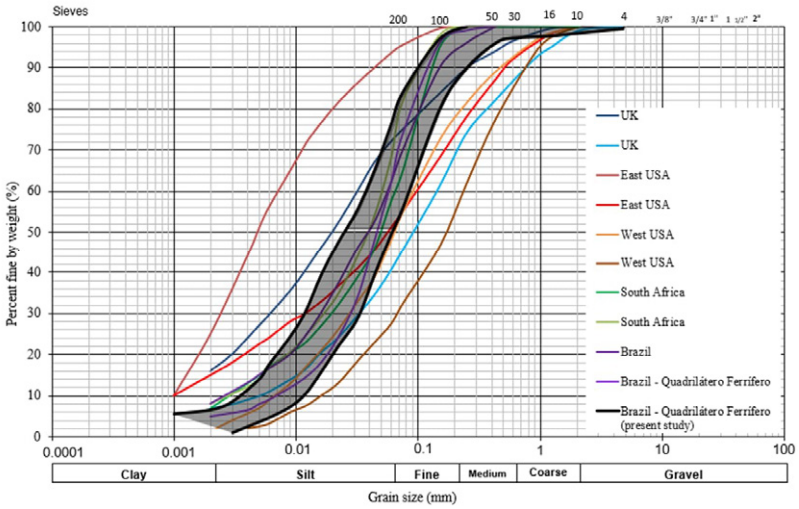

Figure 4. Comparison between the grain size distribution of the analyzed tailings and the grain size distribution curves of gold tailings presented by other authors (adapted from *Vick, 1990,* and *Bedin, 2010*).

Figure 5.a presents the Standard Proctor compaction curves obtained for each sample, as well as the average curve of all compaction tests, regardless of the dispersion among the individual curves. The dispersion of the compaction curves indicates heterogeneity among the samples. No clear correlation could be established between the variability of the compaction curves and the grain size distribution or physical properties of the tailings. Figures 5.b and 5b present the graphs showing the distribution of the obtained values of maximum dry density and optimum moisture content. The average maximum dry density of 1.763 g/cm³ and the average optimum moisture content of 16.5% are within the range reported in the literature *(Bedin, 2010; Preciado et al., 2014; Zorzal et al., 2020; Oliveira et al., 2024),* i.e., from 1.679 g/cm³ to 1.806 g/cm³.

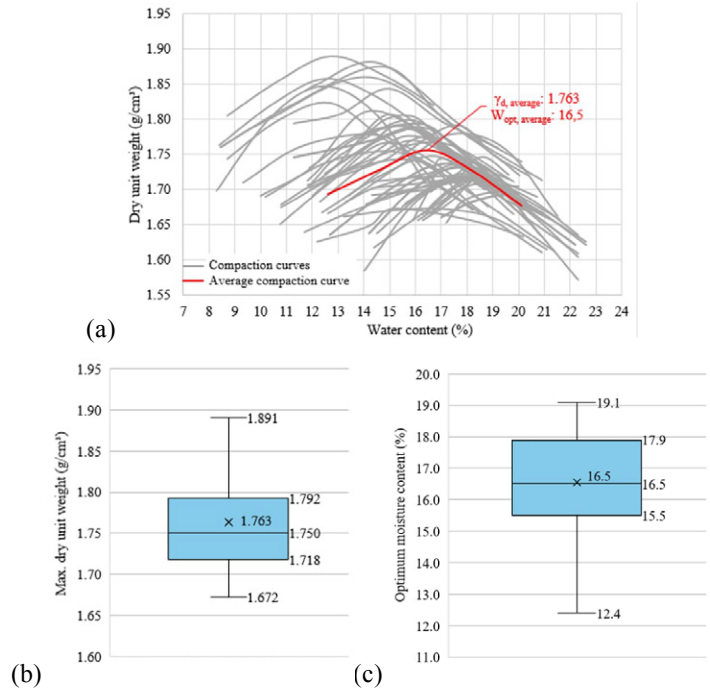

Figure 5. (a) Standard Proctor compaction curves, (b) Distribution of maximum dry density results, (c) Distribution of optimum moisture content results.

The tailings' minimum void ratio (e_{min}) ranged from 0.7 to 0.9, while the maximum void ratio (e_{max}) ranged from 1.21 to 1.40. The average values were e_{min} = 0.783 and e_{max} = 1.274, lying within the ranges observed by *Zorzal et al. (2020)* (e_{min} = 0.7 and e_{max} = 1.25) and *Oliveira et al. (2024)*, (e_{min} = 0.56 and e_{max} = 1.44), both referring to gold ore tailings in Brazil.

3.2.2 Hydraulic conductivity of the tailings

Tests were performed on specimens vertically and horizontally trimmed from undisturbed block samples collected from the experimental embankments and the tailings stack, as well as on laboratory-compacted specimens at different void ratios. The results were used to calculate the vertical (k_v) and horizontal (k_h) hydraulic conductivity of the tailings. The hydraulic conductivity ranged from 5×10^{-6} cm/s to 1.3×10^{-4} cm/s, with an average of 6.2×10^{-5} cm/s. As the void ratio decreased, there was a tendency for the hydraulic conductivity to reduce (Figure 6).

Analysis of the results from specimens trimmed in both directions (vertical and horizontal) from undisturbed samples collected in the experimental embankment and the tailings stack indicated very low anisotropy (k_h/k_v), with values between 0.6 and 1.5 — suggestion, in practical terms, that the material behaves isotropically. For this reason, anisotropy is not differentiated in the graph presented in Figure 6.

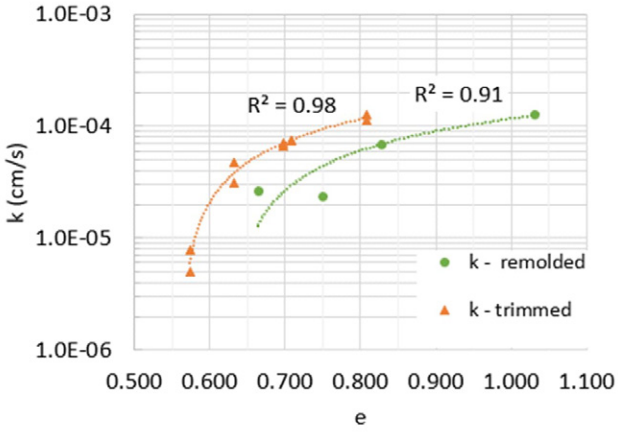

Figure 6. Hydraulic conductivity obtained.

Vick (1990) presented a study that included hydraulic conductivity tests on mine tailings with fines content greater than 30% and non-plastic or low-plasticity tailings. The results indicated hydraulic conductivity values ranging from 10^{-2} cm/s to 10^{-7} cm/s. The fines content and the non-plastic behavior of the filtered tailings analyzed in this study are consistent with the characteristics of the materials studied by *Vick (1990)* and fall within the same range of hydraulic conductivity.

The hydraulic conductivity values obtained fall within the typical range for various silt-sized mine tailings ($1x10^{-4}$ to $1x10^{-6}$ m/s), as compiled by *Dias Neto et al. (2024)*. The values found here are also close to those presented by *Qiu & Sego (2001)*— 2.7×10^{-5} to 6.7×10^{-5} cm/s — for gold tailings containing 81.3% fines (< 75 μm), classified as ML by the USCS *(ASTM D-2487, 2017)*. More recent studies on gold ore tailings from Brazil, reported by *Oliveira et al. (2024)* and *Gomes et al. (2019),* indicated hydraulic conductivity of $1.7x10^{-7}$ cm/s and $9.5x10^{-6}$ cm/s, respectively. The results obtained in this research are consistent with those reported in the literature and also reflect the typical behavior of decreasing hydraulic conductivity with decreasing void ratio as described by Carneiro et al. *(2023)*.

Carneiro et al. (2023) highlight the challenges in defining reference hydraulic conductivity values for tailings, as several factors influence their behavior. These factors directly affect hydraulic conductivity, which can vary by up to a factor of five times for the same tailings depending on the void ratio.

In accordance with current practice, permeability tests were carried out on previously saturated specimens to allow comparison with values reported in the literature. However, it is important to complement the studies by performing tests on unsaturated specimens, as filtered tailings stacks tend to remain in an unsaturated condition *(Cacciuttolo & Campomanes, 2022)*.

3.2.3 Analysis of critical state condition

From the graphical analysis of the $\eta=q/p'$ x ε_a curves, the 28 selected test specimens indicated that the critical state had been reached (Figure 7a and Figure 7b).

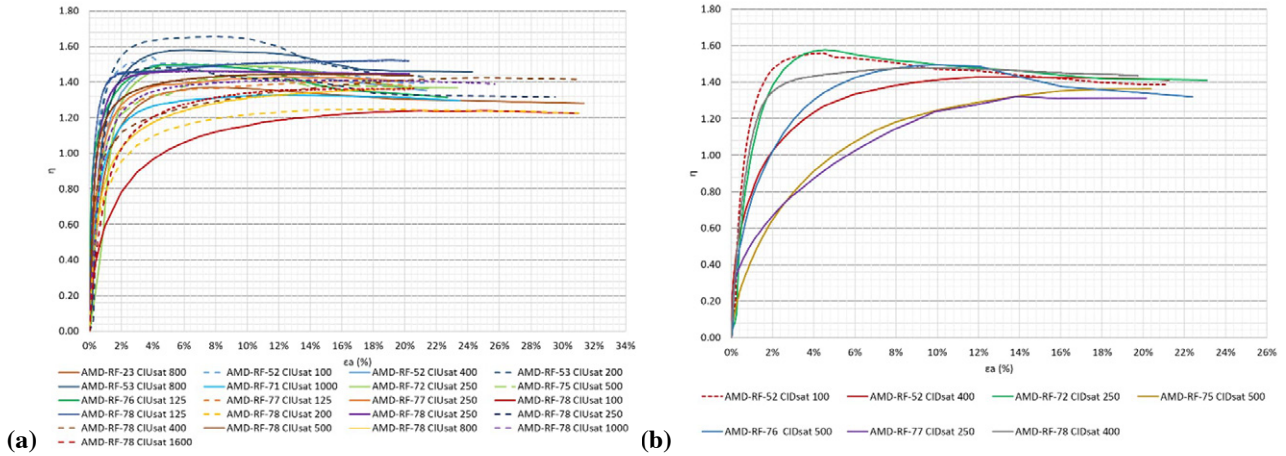

Figure 7. Plot of $\eta=q/p'$ versus ε_a. (a) CIU_{sat} tests, (b) CID_{sat} tests.

Considering the variability of the η versus ε_a curves, which may be attributed to the heterogeneity among the tested specimens, the specimens were grouped according to their grain size distribution to highlight possible changes in geomechanical behavior related to this characteristic. Four distinct groups were defined based on the similarity of their grain size distribution curves. The grain size distribution for each group, along with the corresponding average curves, is presented in Figure 8.

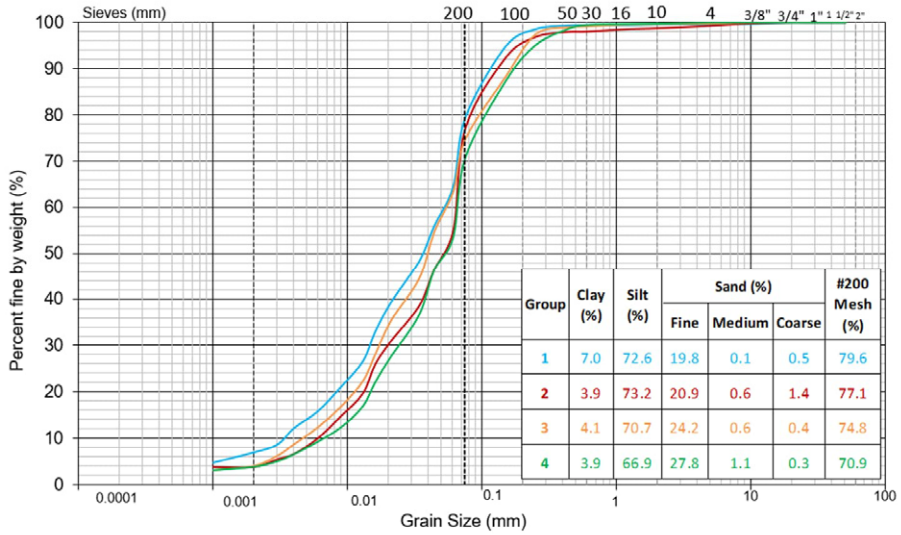

Figure 8. Average grain size distribution curves of the sample groups selected for critical state condition analysis.

For each set of tests within the same group, the Critical State Line (CSL) was plotted on the planes e x $ln\ p'$ (Figure 9a) and p' x q (Figure 9b) planes. To facilitate analysis, each CSL was drawn in the same color as the grain size distribution curve of the corresponding group. It is worth noting that the CSLs determined for the four groups differ in both position and slope, evidencing significant variation between the CSLs of tailings from the same stack and highlighting the influence of the grain

size composition on this variation. This analysis indicates that, although silt is the predominant particle size fraction of the tailings, the sand fraction may be a determining factor in the geomechanical behavior of the material.

Fourie & Papageorgiou (2001), in a study of four particle size distribution curves of gold ore tailings, addressed the difficulty of defining a unique CSL for certain tailings. In this study, four different CSLs were identified, with the material containing the highest fines content exhibiting a CSL located below the others. *Xu and Coop (2017), Li et al. (2018), Li and Coop (2018), and Coop (2015)* argue that the CSL uniqueness theory does not apply to tailings, as these materials exhibit transitional behavior, which may be related to their grain size distribution, post-compaction void ratio, and particle shape.

The findings of this study regarding the occurrence of different CSLs for the same tailings corroborate the behavior observed by the authors mentioned above. Figure 9a shows that CSL4 (in green), associated with the particle size distribution curve with the lowest fines content (Figure 8), is located above the other CSLs obtained — except for CSL1 (blue). CSL2 (in red) and CSL3 (in orange), which have higher fines content than CSL4, are positioned below all other CSLs obtained (Figure 9a), indicating the need for more compaction cycles to induce a dilatant response in the material. The CSL1 (blue) was an exception, being positioned higher despite its higher fines content, as also observed by *Carrera et al. (2011)*, suggesting a possible change in behavior with increased silt content. Grain shape and mineralogy — not evaluated in this study — may also contribute to this distinct behavior.

The observed similarity between the slopes of CLS3 and CLS4 (λ = 0.139 and 0.162, respectively), as well as the similarity between their corresponding average sand fractions, suggests that grain size distribution may influence both the M and λ values.

Despite the minor variations observed in the CSLs established in the *p' x q* plane, the variability of the CSLs in the *e x ln p'* plane is significant and appears to be associated with the grain size variations identified. This observation is consistent with the findings of *Velten et al. (2022)* in studies on gold ore tailings.

The state parameters (ψ) of the test specimens presented in Figure 9 ranged from -0.3 to 0.12, as follows: -0.07 to 0.06 (CSL1); -0.18 to 0.00 (CSL2); -0.17 to 0.12 (CSL3); and -0.3 to 0.02 (CSL4). Based on the stress path of the specimens, 23 of them exhibited dilatant behavior, while the remaining 7 exhibited contractile behavior.

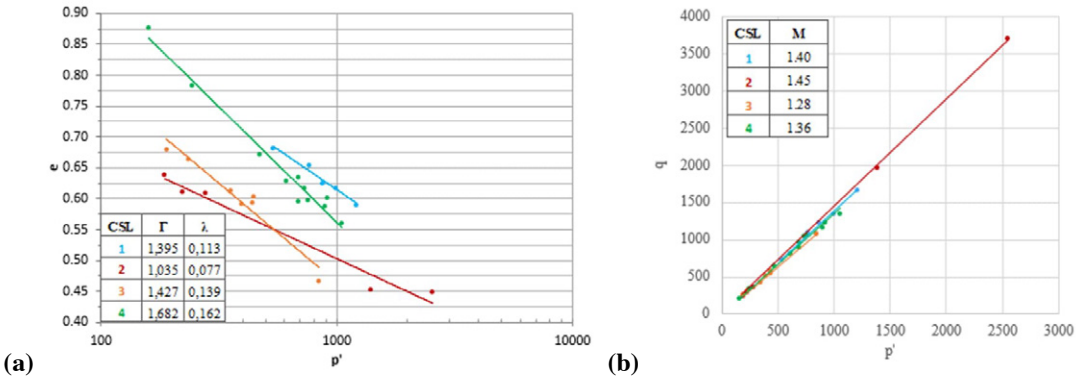

(a) **(b)**

Figure 9. CSLs obtained: (a) represented in the *e x lnp'* plane; (b) represented in the *p' x q* plane.

The critical state parameters obtained in this study are compared with those reported by other authors who analyzed gold ore tailings (see Table 3), where relatively similar results can be observed. However, the slopes of the critical state lines (λ) ranging from -0.077 to -0.162, are higher than those reported in the literature (0.05 to 0.066). Regarding the intercept parameter Γ, the results of the present study (1.035 to 1.682) fall within the range proposed by the same authors (0.80 to 2.64). The slope of the critical state line in the p'-q plane (M), which ranges from 1.28 to 1.45, is slightly higher than the results reported in other studies (1.13 to 1.39), reflecting a critical state friction angle of 31.9° to 35.7°, also higher than those observed in the referenced literature (28° to 33°). The findings of this study suggest that a minimum DC of 96% is required for the construction of the tailings stack using the material analyzed.

Table 3. Comparison of critical state parameters with values from other studies.

Author	λ	Γ	M	Φ'_{cs}
Bedin (2010)	0.045 – 0.058	2.34 – 2.64	1.33	33º
Bonin et al (2022)	0.066	0.80	1.20-1.39	-
Oliveira et al. (2024)	0.05	1.97	1.13	28º
Present study	**0.077 – 0.162**	**1.035 – 1.682**	**1.28 – 1.45**	**31.9º – 35.7º**

4. CONCLUSIONS

Laboratory and field tests were conducted to evaluate the compaction behavior, physical characterization, hydraulic conductivity, and shear strength parameters of the tailings. In addition to expanding the geotechnical database specific to filtered gold tailings, the results emphasize the significance of compaction methods in achieving desirable mechanical behavior and highlight the influence of material heterogeneity in defining geotechnical parameters.

Field test results, supported by findings in the literature, indicate that the layer thickness for these stacked tailings should be limited to 30 cm. Compaction using a smooth drum roller proved more effective in producing a homogeneous and well-compacted material. In contrast, compaction using track equipment —whether for 30 cm or 50 cm thick layers — resulted in greater variability and notable differences between the degrees of compaction at the top and bottom of the layers, indicating inefficient compaction. Achieving adequate compaction levels (DC > 96%) required a minimum of five to six compaction cycles.

Laboratory tests showed that the grain size distribution, compaction behavior, and hydraulic conductivity of the studied tailings fall within the range reported for other gold ore tailings in the literature. The critical state analysis based on the Critical State Soil Mechanics (CSSM) framework revealed significant variation in the Critical State Lines (CSLs), associated with the material's grain size composition. Except for one group, higher fines content generally corresponded to lower CSL positions, indicating a greater need for compaction to achieve dilative behavior. This variability reinforces the need for continuous (QA/QC) monitoring throughout the service life of the stacks, and for adapting compaction criteria in response to material changes and site-specific constraints, ensuring the long-term structural stability of the stacks.

.

ACKNOWLEDGEMENTS

The authors would like to thank M.Sc. Romário Stéffano Amaro da Silva for his support in the development of this paper. We also acknowledge the financial and institutional support provided by the National Council for Scientific and Technological Development (CNPq – Brazilian Agency) and the Rio de Janeiro State Research Support Foundation FAPERJ.

CRediT authorship contribution statement

Mayara Ferreira Rodrigues: Conceptualisation, Formal analysis, Writing - original draft. **Márcio de Souza Soares de Almeida:** Formal analysis, Supervision, Validation, Writing – review & editing. **Marcos Barreto de Mendonça:** Formal analysis, Supervision, Validation, Writing – review & editing. **Jaime Pinheiro:** Writing – review & editing.

REFERENCES

ASTM (2017). D2487: Standard Practice for Classification of Soils for Engineering Purposes (Unified Soil Classification System). *ASTM*. 10 p.

Bedin, J. (2010). Estudo do comportamento geomecânico de resíduos de mineração. Porto Alegre. 207 p. (*In Portuguese*)

Bonin, M., Shaigetz, M., Takch, A., & al., e. (2022). In-situ and laboratory site specific geotechnical characterization of hard rock gold mine tailings. Tailing and Mine Waste, p. 13 p.

Cacciuttolo, C., & Atencio, E. (2023). Dry stacking of filtered tailings for large-scale production rates over 100,000 metric tons per day: Envisioning the sustainable future of mine tailings storage facilities. *Minerals,* 13(11), 1445.

Cacciuttolo, C., & Campomanes, G. (2022). Practical Experience of Filtered Tailings Technology in Chile and Peru: An Environmentally Friendly Solution. (Carlito Tabelin, Ed.) Minerals, 12(7), p. 889.

Carrera, A., Coop, M., & Lancellotta, R. (2011). Influence of grading on the mechanical behavior of Stava tailings. Géotechnique, 61(11), pp. 935-946.

Carneiro, J., Marques, E., Viana da Fonseca, A. J., Ferraz, R. & Oliveira, A. (2023). Characterization of an Iron Ore Tailing Sample and the Evaluation of Its Representativeness. *Geotechnical and Geological Engineering*, 41, pp. 2833-2852 p.

Coop, M. R. (2015). Limitations of a critical state framework applied to the behaviour of natural and "transitional" soils. *6th International Symposium on Deformation Characteristics of Geomaterials*, pp. 115-155.

Crystal, C., Hore, C. & Ezama, I. (2018). Filter-Pressed Dry Stacking: Design Considerations Based on Practical Experience. *Tailings and Mine Waste*. Keystone: Colorado State University. 209-219.

Davies, M. (2011). Filtered Dry Stacked Tailings – The Fundamentals. In Tailings and Mine Waste. Vancouver. p. 9

Delgado, B., Viana da Fonseca, A. & Bittar, R. (2023). Geomechanical Behaviour of an Iron Ore Tailings under High-Stress Levels for Disposal by Dry Stacking. *Tailings and Mine Waste,* p. 10.

Dias Neto, S. L. S., Ferraz, R. L., da Silva, T. O., Marques, E. A. G., Pitanga, H. N., & Cândido, E. S. (2024). Hydraulic Characteristics of Silt-Sized Iron Ore Tailings. *Geotechnical and Geological Engineering*, 1-23.

Fourie, A. B. & Papageorgiou, G. (2001). Defining an appropriate steady state line for Merriespruit gold tailings. *Canadian Geotechnical Journal,* 38(4), pp. 695 - 706 p.

Fourie, A., Verdugo, R., Bjelkevik, A., at al. (2022). Geotechnics of mine tailings: a 2022 State of the Art. (R. a. Jaksa, Ed.) *International Conference on Soil Mechanics and Geotechnical Engineering 2022*, pp. 121-183.

Furnell, E., Bilaniuk, K., Goldbaum, M., Shoaib, M., Wani, O., Tian, X. & Bobicki, E. R. (2022). Dewatered and stacked mine tailings: a review. *Acs Es&T Engineering*, 2(5), 728-745.

Gomes, M., Filho, J., Pinheiro, J. & Crystal, C. (2019). Disposal of tailings and the mining industry perspective: a case study of the Cuiabá Mine. *Paste 2019: 22nd International Conference on Paste*. Perth: Australian Centre for Geomechanics. 219-231 p.

Jefferies, M., Been, K. (2016) Soil Liquefaction: A Critical State Approach. 2ª Ed. Taylor & Francis Group, LLC.

Li, W. &. Coop, M.R. (2018). Mechanical behaviour of Panzhihua iron tailings. *Canadian Geotechnical Journal*, 56(3), pp. 420-435 p.

Li, W., Coop, M. R., Senetakis, K. & Schnaid, F. (2018). The mechanics of a silt-sized gold tailing. *Engineering Geology*, pp. 97-108 p.

Oliveira, D., Araújo, T., & Consoli, N. (2024). Estudo do Comportamento Geomecânico de um Rejeito de Mineração de Ouro a Luz do Estado Crítico. *COBRAMSEG - Congresso Brasileiro de Mecânica dos Solos e Engenharia Geotécnica*. 8 p. (*in Portuguese*)

Preciado, H., Ale, J., Byler, B., at al. (2014). Parametric and sensitivity analysis for a proposed filtered tailings storage facility in challenging topography. *Tailings and Mine Waste* '14. 315 – 325 p.

Qiu, J. & Sego D.C. (2001). Laboratory properties of mine tailings. *Canadian Geotechnical Journal.* 38(1): 183-190.

Ulrich, B. (2019). Practical thoughts regarding filtered tailings. (A. F. AJC Paterson, Ed.) Paste 2019: Proceedings of the 22nd International Conference on Paste, Thickened and Filtered Tailings, pp. 71-79.

USACE. (1995). Engineer Manual 1110-2-1991: Construction control for earth and rock-fill dams. Washington, USA. 101 p.

Velten, R., Consoli, N., Filho, H., et al. (2022). Influence of Grading and Fabric Arising from the Initial Compaction on the Geomechanical Characterization of Compacted Copper Tailings. *Géotechnique*, 45 p.

Viana da Fonseca, A., et al. (2021). Recommended Procedures to Assess Critical State Locus from Triaxial Tests in Cohesionless Remoulded Samples. *Geotechnics*. 95 – 127 p.

Vick, S. (1990). Planning, design, and analysis of tailings dam. *BiTech, 2*. Vancouver. 369 p.

Wagner, A. C. (2023). Mechanical behavior of iron ore tailings under standard compression and extension triaxial stress paths. Journal of Rock Mechanics and Geotechnical Engineering, 15(7), pp. 1883-1894.

Wilson, G. W. (2021). The new expertise required for designing safe tailings storage facilities. *Soils and Rocks*, 1-7 p.

Xu, L., & Coop, M. R. (July de 2017). The mechanics of a saturated silty loess with a transitional mode. *Géotechnique*, 67(7), pp. 581-596 p.

Zorzal, R., Gomes, M., & Pinheiro, J. (2020). Geotechnical Tailings Characterization from Cuiabá Mine Site to Support a Dry Stacking Disposal Design for Cuiabá Dam. *Paste 2020: 23rd Internacional Conference on Paste, Thickened and Filtered Tailings*. 13 p.

Kick start your Geotechnical career with GHD

Why GHD?

Our team of over 300 ground science and engineering specialists delivers advanced solutions in geology, geotechnics, geophysics and materials testing.

At GHD, you'll work on a wide range of projects for different industries and clients, making a positive impact both locally and globally, using innovative approaches to deliver sustainable solutions. You'll be supported by experienced mentors and have opportunities to develop your career. Flexibility is part of our culture, helping you balance work and life, and explore new locations.

Your future starts here, build it with GHD.

Alistair Schofield | A GHD Associate
Geology Service Line Leader – APAC
+61 3 8687 8759 | alistair.schofield@ghd.com

Ramtin Tajeddin
Geotechnical Service Line Leader – APAC
+61 3 8687 8882 | ramtin.tajeddin@ghd.com

Discover more at ghd.com/geosciences

NUMERICAL EVALUATION OF THE DILATOMETER TEST – AN IMPROVEMENT ON CORRELATIONS

Hao Shen[1] and Michael Jefferies[2]
[1] Klohn Crippen Berger, Brisbane, Australia. [2] Consulting Engineer, Vancouver, Canada

https://doi.org/10.56295/AGJ6044

ABSTRACT

A numerical approach is used to characterize the relationship between sand state and the normalized horizontal stress index K_D/K_0 from the Marchetti dilatometer test (DMT) to gain insight on extraction of geostatic stress conditions and soil stiffness from DMT data in sands. A 3D model of the DMT was implemented in Plaxis3D using the inbuilt NorSand model to simulate the DMT test, including both the insertion and subsequent expansion. The model was validated using DMT tests in Busan Sand, conducted using a calibration chamber, which were supported by extensive triaxial testing providing the soil properties. Provided that elastic shear rigidity I_r can be determined by means of geophysical method (readily done), the present investigation suggests numerical modelling of the DMT will be useful for characterizing in situ plastic modulus (which depends on soil fabric) as well as improving the understanding of geostatic stress by avoiding empirical correlations that neglect soil properties. The methodology developed is easily applied in engineering practice.

1 INTRODUCTION

Two large tailings dams, Fundao and Briumadinho, failed from conditions of zero excess pore pressure and with no evidence of prior distress causing enormous damage and many deaths. Understanding such failures requires knowing the state of stress in the dam, since it is the proximity of that state of stress to the soil's instability locus that indicates the safety – or otherwise - of the dam. However, the Brumadinho collapse was triggered by water pressures associated with geotechnical drilling (CIMNE, 2019) and that has led to reticence (prohibition ?) of using mud rotary boreholes – which effectively precludes pressuremeter testing that would be the usual investigation method for establishing insitu stresses. The Marchetti dilatometer (DMT) – a push in test - appears a useful method in such situations.

The dilatometer test (ASTM D6635) measures soil stress and stiffness using a pushed-in-place flat-plate probe. Two pressures are measured in a DMT test, the 'lift-off' pressure ('A') for the membrane to minimally move (0.05mm) and the pressure required ('B') to displace the membrane a standard distance (1.1 mm). The pressure p_0 (at zero displacement) is linearly back-extrapolated from the measured pressures A,B (Marchetti, 2001) with the horizontal stress index (K_D) being the normalised form of the contact pressure p_0:

$$K_D = (p_0 - u_0)/\sigma'_{v0} \tag{1}$$

…where u_0 is the hydrostatic pore pressure at the depth of testing and σ'_{v0} is the in situ effective overburden stress.

The DMT displaces soil during penetration and changes (generally increasing) the adjacent horizontal stress in the ground: $K_0 \neq K_D$. It is natural to invoke a critical state approach to understand the relation between K_0 and K_D, as such an approach automatically includes "compressibility" (= the slope of the critical state locus) and dilatancy (which depends on the void ratio offset from the soil's critical state, commonly called the state parameter ψ). Thus, Jamilkowski (1988) investigated the correlation between the dilatometer amplification factor K_D/K_0 and the state parameter ψ_0 and found:

$$K_D/K_0 = k_D \exp(-m_D \psi_0) \tag{2}$$

The challenge with evaluating the DMT thus becomes determining how k_d and m_d are related to the soil's properties (e.g. λ_{10}). Two approaches have been followed: correlations developed using calibration chambers and theoretically-based models.

Calibration chambers provide large uniform samples of known void ratio and with controlled stress states (in effect a large triaxial sample) into which the DMT is pushed; several such tests provide data to obtain the best fits of the coefficients k_D and m_D. The results of published calibration chamber studies are summarized in Table 1. It can also be observed from Table 1 that different testing campaigns on both Toyoura and Ticino sands produced different coefficients for the same sand – calibration chambers involve in the order of one tonne of sand and void ratio is difficult to determine

with precision. More generally, while it has been acknowledged that both k_D and m_D are soil-specific, a wide range of values apparent in Table 1 with a gap in the literature regarding how to quantify the effect of soil properties on k_D and m_D. Given how k_D and m_D vary among different sands from the calibration chamber results in Table 1, adopting an average ("universal") fit for any soil appears to be far from accurate. Yet, utilizing physical modelling methods, such as large calibration chambers, is typically time-consuming and likely inaccessible for smaller to medium-sized projects.

Table 1 The coefficients k_D and m_D from fitting calibration chamber results for various sands

Material	$\mathbf{k_D}$	$\mathbf{m_D}$	Source
Busan sand	2.405	4.54	Choi (2008)
Ticino sand	1.32	7.33	Lawter Jr and Borden (1990)
Ticino sand	1.3	8.08	Jamilkowski (1988)
Ticino sand	1.444	8.13	Choi (2008)
Cape Fear sand	2.74	2.31	Lawter Jr and Borden (1990)
Hokksund	1.19	8.63	Lawter Jr and Borden (1990)
Toyoura sand	1.05	3.07	Lawter Jr and Borden (1990)
Toyoura sand	3.676	3.06	Choi (2008)

In terms of theoretical correlations, much of the research has focused on modelling the DMT penetration in clays (Finno, 1993; Kouretzis et al., 2015; Yu et al., 1992) as the undrained (= constant volume) situation simplifies the analysis. Penetration of the DMT in sands has not been modelled theoretically.

This opens up an opportunity for numerical modelling to support in practical engineering applications. However, numerical simulation of penetration in sands is difficult – it is large-strain, with a frictional boundary, and with rotation of principal axes. Some recent progress has been obtained for penetration of the CPT using the Discrete Element Method (Arroyo et al., 2011), the Material Point Method (Martinelli and Pisanò, 2022), and Arbitrary Lagrangian-Eulerian (Monforte et al., 2017); but convincing matches to relevant calibration chamber data remain elusive. Thus, in the case of the CPT, penetration is commonly represented as spherical-cavity expansion with subsequent correlation to calibration chamber results – a procedure that allows direct assessment of how soil properties affect the CPT response (e.g. Shuttle & Jefferies, 1998).

The approach adopted in this paper follows this 'simplify but then calibrate' approach. The simplification is to treat penetration as a lateral displacement of the soil within a 3D finite element program by the equivalent of the DMT blade. The calibration is to compare the A, B pressures computed with those measured in a calibration chamber. Necessarily, the approach needs a data set containing sufficient triaxial tests to determine soil properties and DMT calibration chamber data on that sand. Such studies are rare. The tests on Busan sand were adopted as a complete dataset for our purpose.

A further consideration is the constitutive model. A 'standard' friction-dilation model ('Non-Associated Mohr Coulomb') is inadequate as the "elastic" properties are largely dominated by plastic strains and which then require invocation of 'strain dependent modulus' – there is no simple calibration. However, the last decade or so has seen critical state models (e.g. CASM, NorSand, SaniSand) providing good to very-good matches to measured sand behaviour. As such models are based on the state parameter, so are a natural starting point to investigate equation (1). Further, these critical state models have been implemented in geotechnical modelling platforms (e.g. Plaxis, Flac, RS2 and Sigma/W). We adopted Plaxis 3D and NorSand.

2 BUSAN SAND TESTS

2.1 BUSAN SAND

Busan sand is a natural sand dredged from the South Sea of Korea, and is poorly graded angular to subangular. The data used here is that reported by Choi (2008), digitizing from the paper record (there appear to be no digital records) and also over-laying computed trends on various published figures. The sand tested had a median grain size of 315 microns and negligible silt content, but did contain significant crushed shells reflecting its marine origin. A surprisingly large e_{min} = 0.658 was measured, although its specific gravity was a near common G_s= 2.62.

2.2 TRIAXIAL TESTS AND PROPERTIES

The properties were determined using twelve drained triaxial tests spanning a range of initial void ratios and confining stress; Figure 1 shows the state-paths of these tests. Two sample reconstitution methods were used, moist tamping for the looser samples and air pluviation for the denser (denoted as M and A respectively in the test naming).

The critical state locus (CSL) was assessed from the end state of the very loose tests and further influenced by behaviour found in the slightly denser samples as illustrated on Figure 1. This CSL with λ_{10}= 0.068 is slightly more compressible that usual for 'standard' quartz laboratory sands (where λ_{10}~0.05 is more common), but that is unsurprising given the known carbonate content of Busan sand.

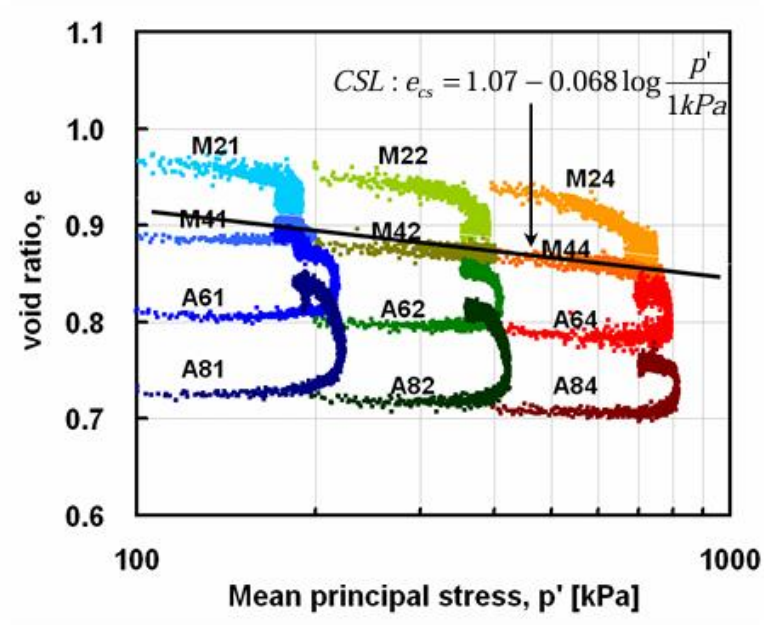

Figure 1: State paths of triaxial tests used to determine the properties of Busan sand (Choi, 2008)

The data on Busan sand as used here is taken from (Choi, 2008),. The original records were in the form of q vs e_a and e vs e_a. The void ratio trend data was fitted with the standard stress dilatancy for the triaxial test D, picking the limiting dilatancy D_{min} (the minimum because of the compression positive convention of soil mechanics) at the strain of peak strength (and which itself is presented as the stress-ratio η_{max}). The results are shown on Figure 2a, and are nicely fitted by the Taylor-Bishop 'interlocking' strength model (the trendline shown on the figure):

$$\eta_{max} = M_{tc} - (1 - N)D_{min} \quad (3)$$

…where M_{tc} is the stress ratio η in the critical state and N is Nova's (1982) volumetric coupling parameter. The meaning of these properties is illustrated on the figure and the calibrated values for Busan sand were M_{tc} =1.44 and N=0.58; both values are significantly larger than found with 'standard' laboratory quartz sands, implying that the DMT calibration will also be unusual.

The corresponding state-dilatancy behaviour shown in Figure 2b is fitted with the usual relation:

$$D_{min} = X_{tc}\, \psi_{Dmin} \quad (4)$$

…where X_{tc} = 3.6 is the state-dilatancy coefficient, and whose value is 'not unusual' for poorly graded sands. Note that the state parameter in equation (4) is the value at the occurrence of D_{min}, not the value at the start of the test; further the trend line passing through the plot origin is a theoretical requirement.

2.3 KOREAN CALIBRATION CHAMBER

The Korea University Calibration Chamber System (KUCCS) comprises a calibration chamber 1.2m diameter and 1.0m high with servo-controlled operation to consolidate soil specimens at a variety of stress paths including K_0 (zero lateral strain). Samples were prepared by an enhanced air-pluviation method to provide a uniform density of the test sample. The distinctive feature of the pluviation system was using a porous plate to minimize the effect of drop distance and to control the drop height without changing the deposition intensity.

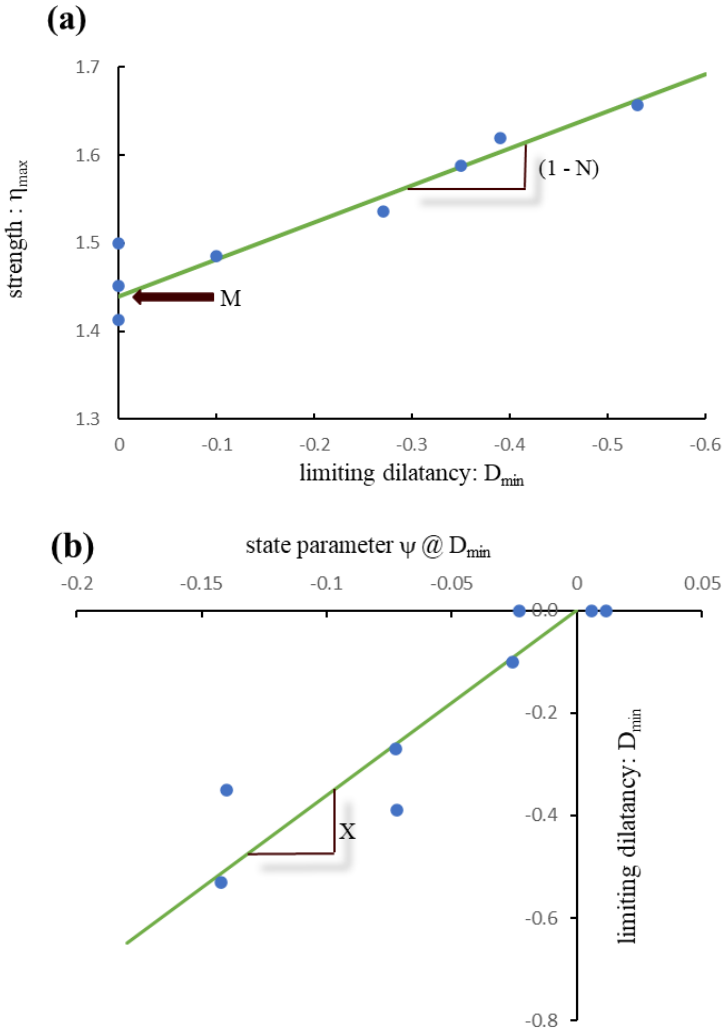

Figure 2: Properties of Busan sand in triaxial compression

2.4 ELASTICITY

The calibration chamber contained 'bender elements' for measuring the seismic shear wave velocity in the usual way. Both horizontal and vertical ray used, and G_{max} was measured during each test. We used an average of the two paths, and converted this to G_{max}. As usual, there was a strong effect of stress level and void ratio on G_{max}. We used the three-parameter elastic model:

$$G_{max} = \frac{A}{e - e_{min}} \left(\frac{\bar{p}}{1\ kPa}\right)^{n_G} \quad (5)$$

…where A is a coefficient (normally in MPa, the same units as G_{max}), n_G is an exponent on the normalized mean confining stress, and e_{min} is a third soil property that reflects the void ratio when the 'sand' transitions to 'sandstone'. All three properties were determined by simultaneous regression to minimize error between (7) and 'ground truth': Figure 3. Data was within 5% of (6), and unbiased, using the properties: A = 2.95 MPa, n_G=0.5 and e_{min} = 0.45.

2.5 DMT CALIBRATION

After applying the horizontal and vertical stress to the sample in the chamber, the DMT was pushed into the sample on the central axis. DMT tests were performed in the central depth region to avoid effects of the top and bottom boundaries of the chambers (aspects readily seen on the continuous record of a CPT that were also carried out). The DMT tests were done in the standard manner, and were performed at four vertical effective stress states and three sand densities. Both normally consolidated and over-consolidated cases were tested. The test data reduces to the expected form of horizontal stress amplification factor with ψ of equation (2), with the same trend for over-consolidated and normally consolidated samples, as illustrated on Figure 4.

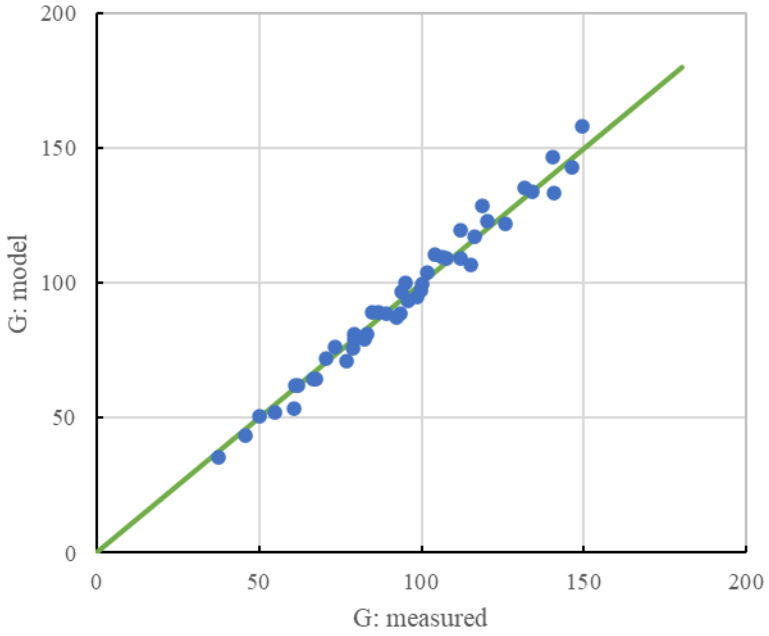

Figure 3: Comparison of elastic idealization with ground truth

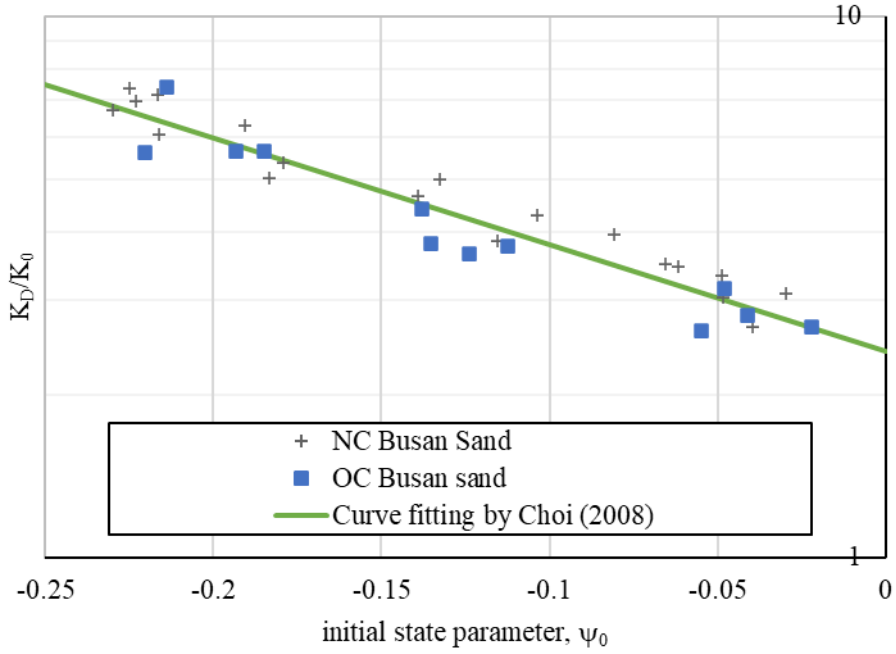

Figure 4: DMT horizontal stress amplification in Busan Sand chamber tests (Choi, 2008)

3 NUMERICAL MODEL FOR DMT

3.1 CONSTITUTIVE IDEALIZATION

Critical state theory combines soil properties – which are independent of void ratio or confining stress and in principle measurable on reconstituted samples – with 'state measures' that reflect the insitu condition of the soil and which may also show natural variability. Common state measures are the state parameter ψ (essentially controlling limiting dilatancy), over-consolidation ratio (which reflects 'structure' as well as geologic history and thus the onset of yielding), and the elastic shear modulus G_{max} (treated as a state measure because of dependence on the arrangement of soil particle contracts).

The critical state model NorSand (NS; Jefferies, 1993) was used as implemented in Plaxis3D (Bentley, 2023) and which includes the updates discussed in Shuttle & Jefferies (2016). NS includes all three state measures and the five soil properties discussed earlier: Γ, λ describe the critical state locus; M, N describe stress-dilatancy; χ describes state-dilatancy. There is one NS-specific property, the plastic hardening modulus H that describes the plastic stiffness (and which is strongly correlated to the inverse of λ). Soil properties are determined in triaxial compression and are largely familiar.

Iterative modelling is used to determine H, initially assuming a constant value for any test and then refining for the typical trend: $H = H_0 + H_\psi \psi$. Examples of the achieved calibration to four tests of different initial void ratio are shown on Figure 5; there are close fits of NS to data before peak strength, with post-peak diverging because of localization where the reported test σ–ε does not capture the sand behaviour in the localizing shear-band. The calibrated trend for H is shown on Figure 6, where the trend has been weighted to the air-pluviated samples as having the same 'fabric' as the sand placed in the calibration chamber.

The soil properties used in our simulations of the calibration chambers tests on the DMT in Busan Sand are summarized on Table 2.

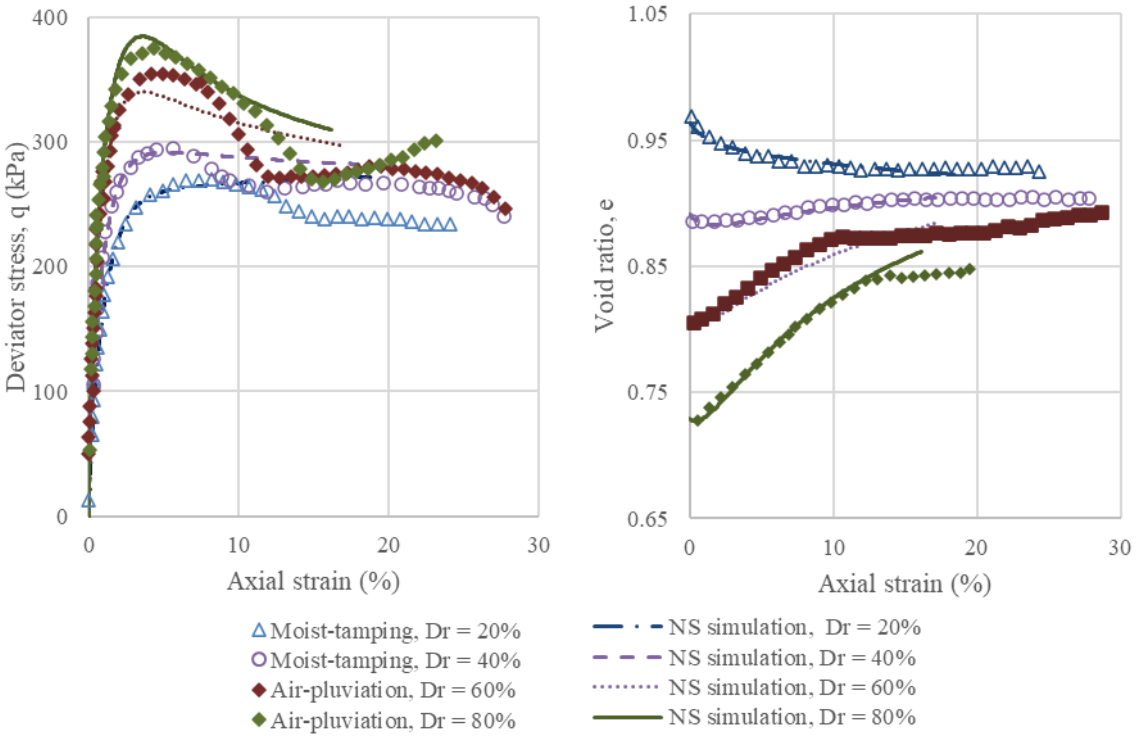

Figure 5: Achieved fits (lines) to triaxial compression data (digitized from paper record) of Busan Sand (Choi, 2008) (D_r% are initial relative densities of the sample; these tests at p_0=100 kPa)

Table 2 NorSand parameters for Busan Sand

Soil	λ_e	Γ	M_{tc}	G_{ref} (MPa)	n_G	H_ψ	H_0	N	χ_{tc}
Busan Sands	0.0295	1.07	1.44	2.95	0.5	800	90	0.55	3.6

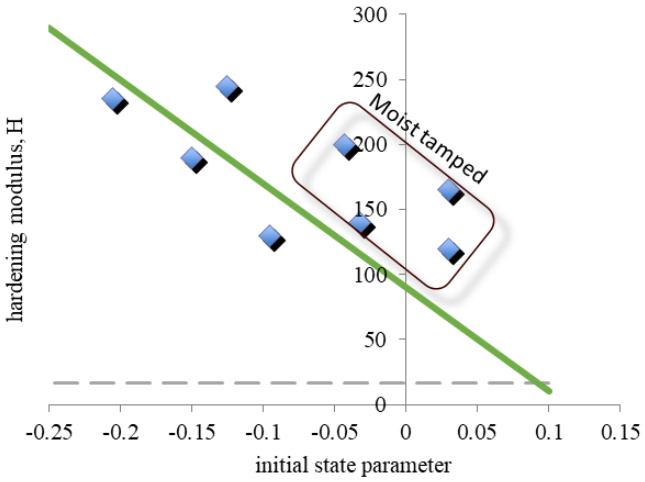

Figure 6: Calibrated trend for plastic hardening modulus

3.2 GEOMETRIC IDEALIZATION

The shape of the flat dilatometer blade (95 mm width, 15 mm thick, and the tapered section of 50 mm long) requires simulating DMT penetration as a 3D problem to accurately consider the increase in horizontal soil stresses near the membrane because of soil displacement during blade penetration; however, the symmetry of the flat blade along its midplane allows simulating only a portion equivalent to half of the flat blade's thickness, specifically aimed at displacing the central soil elements. The subsequent expansion of the DMT membrane further reinforces the requirement that the DMT test shall be treated as 3D.

3.3 INSERTION OF DMT

The insertion of the DMT was approximated by displacing the mesh horizontally such that the physical size of the DMT would then fit. This approximation does not account for the large shear strains experienced by the soil that was initially below the axis of the DMT which, as understood by a cavity-expansion analogue, would have evolved to its critical void ratio regardless of initial conditions. The approximation used does not include a layer of soil in its critical state adjacent to the DMT blade.

In terms of boundary condition, a fixed displacement along the X axis, perpendicular to the blade and just beneath the blade tip, is implemented as shown in Figure 7. This method resolves issues that would arise if a stress boundary were applied; such conditions would cause soil nodes to shift outward, disrupting symmetry boundary conditions and complicating numerical convergence. Along the Y axis adjacent to the DMT blade, a constant horizontal stress is maintained, ensuring a smooth transition of displacement rather than an abrupt jump that could distort the elements. For the rest of the displaced soil block, the bottom nodes are completely fixed, while constant stress is maintained on all other surfaces.

The mesh dimensions (2m by 2m by 1m for X, Y, and Z axes respectively, as shown in Figure 8, were optimized through trial and error to mitigate boundary effects on the analysis outcomes. The model's width along the X-axis, perpendicular to the blade, is approximately 267 times the blade's half-thickness (7.5 mm). While ensuring the model is sufficiently large is crucial to reduce boundary effects, refining the mesh near the blade's tapered section and around the membrane is equally important. This localized refinement, as shown in Figure 8, ensures that pressure measurements on the membrane are precise and helps in preventing issues with simulation convergence.

3.4 TEST IMPLEMENTATION

To model the expansion of the circumferentially fixed 60 mm diameter steel flexible membrane used in the DMT, we employed a series of 11 annuli to define the surface areas of the mesh. Displacements were prescribed based on an ideally expanding spherical cap that conforms to the 60 mm diameter membrane, varying from zero at the circumference to a maximum of 1.1 mm at the centre, as illustrated in Figure 8-b. The horizontal effective stresses on the DMT membrane area were extracted from Gauss stress points within the finite element mesh and averaged to obtain the DMT pressure measurements. This paper focuses on the contact pressure p_0, which is central to interpreting geostatic stress from the DMT.

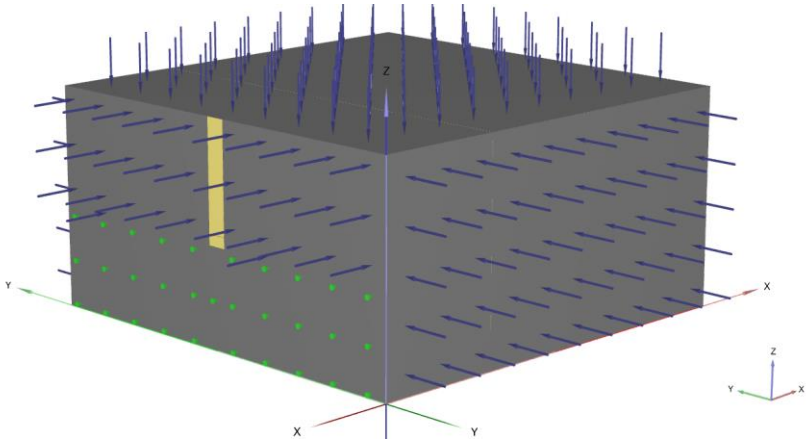

Figure 7: The deformation and stress boundary of the FEM model in Plaxis 3D

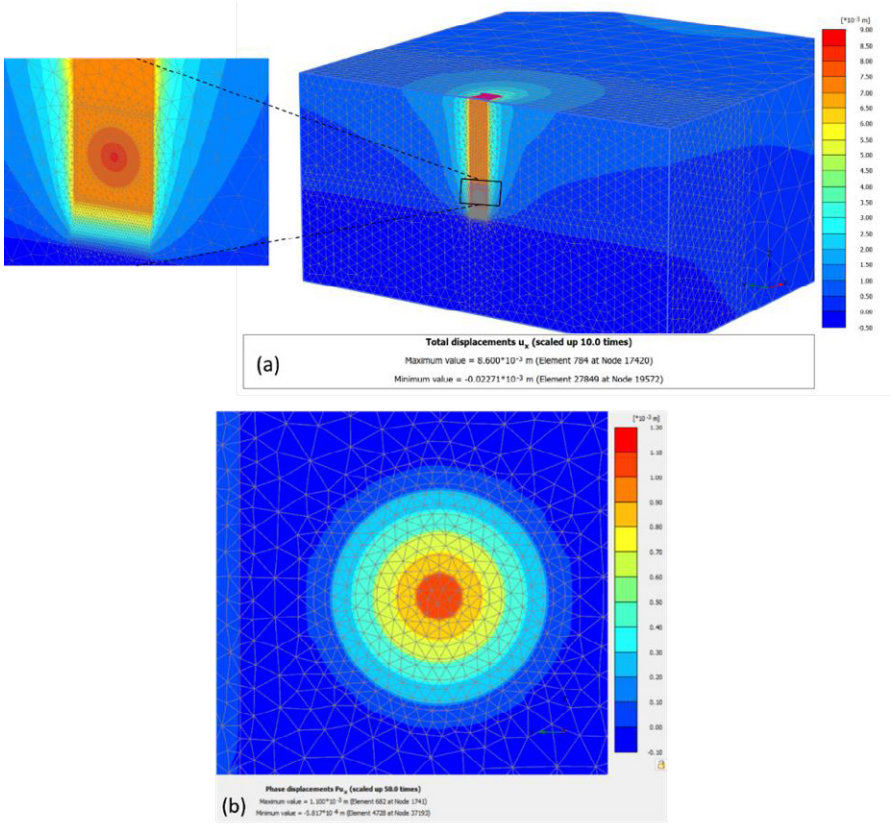

Figure 8: The FEM mesh used for analysis: (a) total horizontal displacement, (b) horizontal displacement during membrane expansion

4 VALIDATION

4.1 SIMULATIONS PROGRAMME

The DMT tests conducted in the KUCCS involved vertical loads of 50 kPa, 100 kPa, 200 kPa, and 400 kPa for normal consolidation conditions, followed by unloading at the same intervals for over-consolidation conditions. The initial void ratios of the samples were 40%, 60%, and 80% in terms of relative density, which correspond to a range of state parameters of $-0.23 < \psi_0 < -0.02$ (see Figure 4).

To cover representative ranges of void ratios tested, the simulation program included initial state parameters (ψ_0) of -0.2, -0.15, -0.1, and -0.05. As such, a total of 48 simulations were carried out in Plaxis3D (Version 2023.2.2.1059) for validation with these scenarios being summarized on Table 3. The NorSand implementation in Plaxis employs a two-parameter model for elasticity (Benteley, 2023):

$$G_{max} = G_{ref}\left(\frac{\bar{p}}{p_{ref}}\right)^{n_G} \tag{6}$$

…where G_{ref} is shear modulus in MPa at the reference at the reference pressure p_{ref} equal to 100 kPa (a convention), n_G is an exponent on the normalized mean confining stress which is the same as that in equation (5). As a result, the three-parameter elastic idealization that includes the void ratio in equation (5) was decomposed into three sets of three two-parameter elastic idealization in equation (6) to represent respective sets of void ratios. The resulting trends are illustrated in Figure 9.

Table 3: Modelling conditions of the simulation programme

G_{ref} (MPa) at = 100 kPa	n_G	OCR	K_0	σ_v	I_r = G/p
66, 83, 100	0.5	1.0	0.4	50, 100,200,400	426, 536, 602, 645, 758, 852, 913, 1072, 1205, 1291, 1515, 1826

Note: The three G_{ref} represents the sands at relative densities of 40%, 60%, and 80%, respectively.

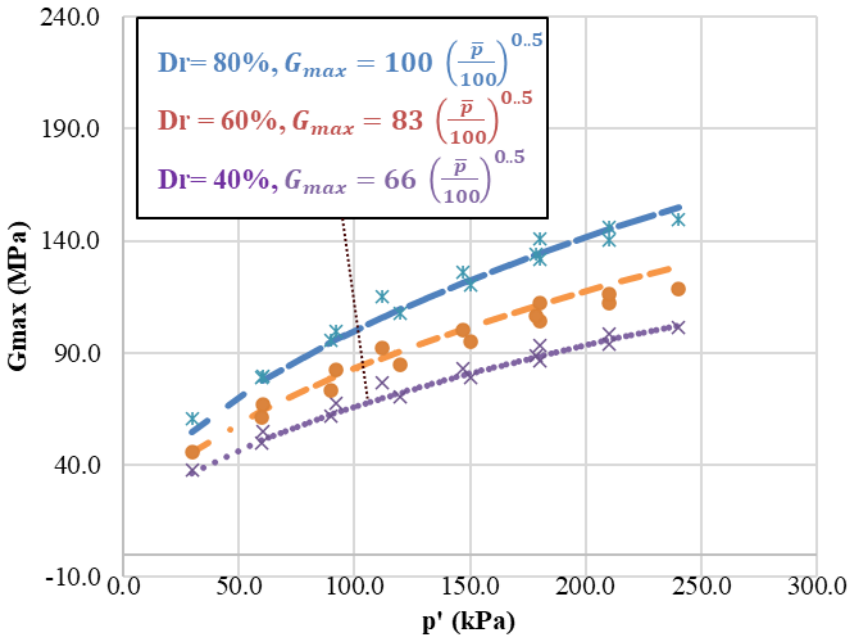

Figure 9: The two-parameter elastic idealization adopted in Plaxis 3D

4.2 SIMULATION RESULTS AND THE CORRECTIONS

Following each simulation, horizontal effective stress on the DMT membrane was extracted from Gauss stress points and averaged to obtain the contact pressure p_0. Then p_0 was normalized by means of equation (2) to obtain K_D. Figure 10 gives an example simulation showing how the contact pressure evolved during the simulated insertion of the DMT blade – a rather stiff initial response softened quickly (within 2mm) into a quasi-linear trend to p_0. During the subsequent membrane expansion, the pressure measurements become approximately linear.

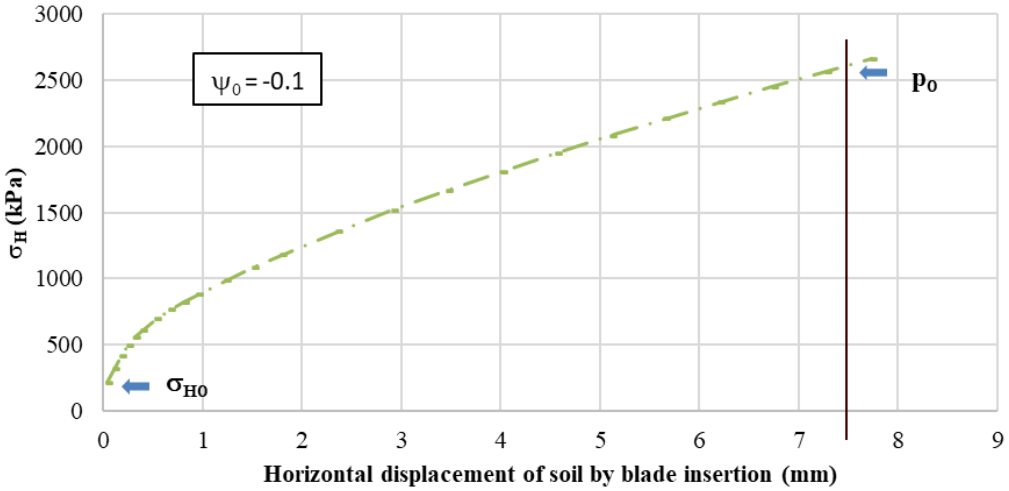

Figure 10: Example of computed evolution of contact pressure during DMT insertion

Using the soil properties presented in Table 2 and the initial states in Table 3, simulations were performed to compare with the DMT calibration chamber (CC) data from Choi (2008). While keeping the other NorSand properties constant, the DMT simulations varied only in their initial states, including initial mean effective stresses p_o, elastic shear rigidity I_r, and initial state parameter ψ_0. This allowed the creation of trend lines between the simulated normalized dilatometer horizontal index K_D/K_0 and initial state parameter ψ_0. Figure 11 presents the relationship between the fitted trend lines and the CC data.

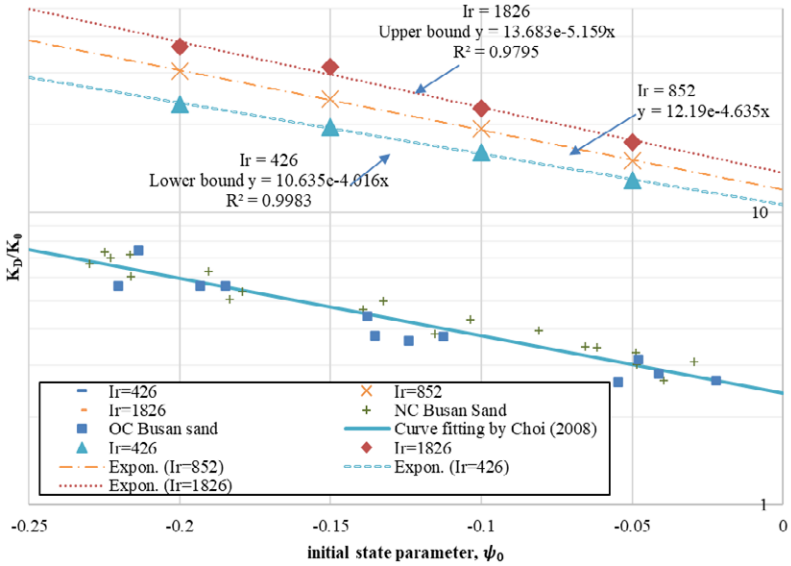

Figure 11: Comparison of numerical results for blade cavity expansion in Busan sand with data from calibration chamber test

While I_r was not considered by Choi (2008), the DMT simulations in this paper varied the trend lines according to different I_r values. The simulated K_D/K_0 results are consistently higher than the K_D/K_0 results observed in CC. This difference is not unexpected given the more stringent boundary conditions of the proposed numerical model. Similar to the universal shape function used for cavity expansion and CC normalised tip resistances in the CPT tests (Ghafghazi and Shuttle, 2008; Shuttle and Jefferies, 2016, 1998), a shape function is also necessary for the DMT tests.

The DMT shape function would compensate for aspects of the DMT sounding not captured by the numerical model. Penetration of the DMT involves friction on the blade surface similar to that measured with the CPT but we have not included that boundary condition. More seriously, the implemented model of the DMT is that for an infinitely long blade above the sensing element to simplify the geometry and avoid mesh dependency issues. In reality, as illustrated on Figure 12, the cross-section of the blade (14.3 cm^2) changes to that of the push rod (often CPT rods of 10 cm^2 cross-section) which allows soil to relax back – and, as can be observed in Figure 12 the distance of this relaxation area from the sensing element is comparable to the size of that element. The shape function is thus proposed to address these differences between the numerical blade cavity expansion and the actual blade penetration.

Figure 12: View of DMT highlighting void space in close proximity to sensor

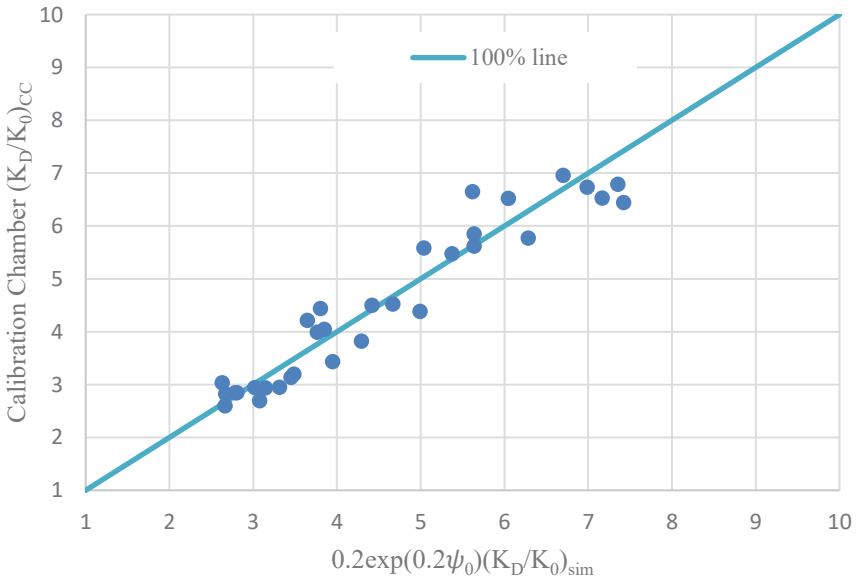

Figure 13: Simulated K_D/K_0 scaled by a shape function against K_D/K_0 in CC for Busan sands

The numerical results scale to those in the calibration chamber as:

$$(K_D/K_0)_{CC} = 0.2exp\ (0.2\psi_0)(K_D/K_0)_{sim} \tag{7}$$

…with Figure 13 comparing the simulated K_D/K_0 results, scaled by equation (7), to K_D/K_0 in CC for Busan sands. This comparison yields a Pearson correlation coefficient of 0.96 and a mean absolute error of approximately 0.29, independent of the initial state parameter (ψ_0), stress level, or elastic shear rigidity I_r.

5 USING THE PROPOSED METHODOLOGY

This study presents a numerical approach to quantify the relationship between the dilatometer amplification factor K_D/K_0 and the initial state parameter ψ_0 in sands. The method offers a framework for interpreting geostatic stress conditions and soil stiffness from DMT data. Since the proximity of the in-situ stress state to the soil's instability locus is a key indicator of tailings dam safety, the proposed approach holds significant practical importance.

However, the method has been developed based on a unique dataset —possibly the only one of its kind available in the published literature— that includes both extensive triaxial testing and calibration chamber results, which presents a limitation in terms of generalizability. In contrast, state parameter interpretation using the CPT—such as through the CPTwidget (Shuttle, D., 2019)—is more established, drawing upon a much broader and more diverse database of sands.

To apply the proposed methodology in practice, the following steps are recommended:

1. **Laboratory Testing:**
   Conduct both consolidated undrained and consolidated drained triaxial compression tests to define the critical state line, as well as to determine stress–dilatancy and state–dilatancy parameters. Accompany these with index tests including particle size distribution, specific gravity, and maximum and minimum index densities.
2. **In-situ Testing:**
   Perform DMT and CPT tests side-by-side, and obtain in-situ shear wave velocity measurements from either test as feasible.

Using the recovered state parameter from CPT data, such as that obtained via CPTwidget, the in-situ K_0 may be estimated.

Future research would benefit from additional datasets that include DMT results obtained from calibration chamber testing, alongside comprehensive laboratory testing, to further validate and refine the methodology.

6 CONCLUSION

(1) This study underscores the soil-specific nature of the relationship between K_D/K_0 and ψ_0. A gap is identified in the literature concerning the quantification of soil properties' effects on this relationship. Therefore, numerical modelling approach emerges as a viable and effective approach to bridging this gap for interpreting the DMT results across different soil types in practise, provided an appropriate soil model is used.

(2) The recent tests on the DMT in Busan Sand, conducted using a calibration chamber, offer valuable validation cases. This DMT data is supplemented by extensive triaxial testing to accurately determine the sand's properties. These tests are interpreted in the NorSand (NS) soil model, ensuring the analysis is based on well-characterized soil properties.

(3) Finite element models using Plaxis 3D, with updated Lagrangian formulation enabled, are created to simulate the DMT blade insertion process by displacing half of the flat blade's thickness and its taper tip section of the soil elements. This idealization allows for a straightforward setup of the numerical model, which can be practically repeated with different NS parameters to investigate the DMT responses. With a shape function that compensates for aspects of the DMT sounding not captured by the numerical model, the estimated K_D/K_0 to ψ_0 trends fall well within the range of results observed in normally consolidated Busan sands within the calibration chamber.

CRediT authorship contribution statement

Hao Shen: Conceptualization, Formal analysis, Writing - original draft. **Michael Jefferies**: Conceptualisation, Formal analysis, Writing – original draft, Writing - review and editing.

7 REFERENCES

Benteley, 2023. User Defined Soil Models - NorSand: An elasto-plastic model for soil behaviour with static liquefaction.

Choi, S.K., 2008. Estimation of Stress History of Sands using CPT and DMT (PhD). Korea University.

Finno, R., 1993. Analytical interpretation of dilatometer penetration through saturated cohesive soils. Geotechnique 43, 241–254. https://doi.org/10.1680/geot.1993.43.2.241

Ghafghazi, M., Shuttle, D., 2008. Interpretation of sand state from cone penetration resistance. Géotechnique 58, 623–634. https://doi.org/10.1680/geot.2008.58.8.623

Jamilkowski, M., 1988. New correlations of penetration tests for design practice. Proc ISOPT- Orlando Fla 263–296.

Jefferies, M., 1993. Nor-Sand: a simple critical state model for sand. Géotechnique 43, 91–103. https://doi.org/10.1680/geot.1993.43.1.91

Jefferies, M., Been, K., 2016. Soil Liquefaction: A Critical State Approach.

Kouretzis, G.P., Ansari, Y., Pineda, J., Kelly, R., Sheng, D., 2015. Numerical evaluation of clay disturbance during blade penetration in the flat dilatometer test. Géotechnique Lett. 5, 91–95. https://doi.org/10.1680/jgele.15.00026

Lawter Jr, R.S., Borden, R.H., 1990. Determination of Horizontal Stress in Normally Consolidated Sands by Using the Dilatometer Test: A Calibration Chamber Study. Transp. Res. Rec.

Marchetti, S., 2001. The Flat Dilatometer Test (DMT) in Soil Investigations, TC16. International Society for Soil Mechanics and Geotechnical Engineering (ISSMGE). https://doi.org/10.1007/978-3-319-73568-9_174

Marchetti, S., 1980. In situ tests by flat dilatometer. J. Geotech. Eng. Div. 106, 299–321. https://doi.org/10.1061/AJGEB6.0000934

Martinelli, M., Pisanò, F., 2022. Relating cone penetration resistance to sand state using the material point method. Géotechnique Lett. 12, 131–138. https://doi.org/10.1680/jgele.21.00145

Monforte, L., Carbonell, J.M., Arroyo, M., Gens, A., 2017. Performance of mixed formulations for the particle finite element method in soil mechanics problems. Comput. Part. Mech. 4, 269–284. https://doi.org/10.1007/s40571-016-0145-0

Shen, H., Haegeman, W., Peiffer, H., 2018. Design, Use, and Interpretation of an Instrumented Flat Dilatometer Test. Geotech. Test. J. 41, 247–262. https://doi.org/10.1520/GTJ20170090

Shuttle, D., 2019. CPTwidget: a finite element program for soil-specific calibration of the CPT.

Shuttle, D., Jefferies, M., 2016. Determining silt state from CPTu. Geotech. Res. 3, 90–118. https://doi.org/10.1680/jgere.16.00008

Shuttle, D., Jefferies, M., 1998. Dimensionless and unbiased CPT interpretation in sand. Int. J. Numer. Anal. Methods Geomech. 22, 351–391. https://doi.org/10.1002/(SICI)1096-9853(199805)22:5<351::AID-NAG921>3.0.CO;2-8

Yu, H., Carter, J., Booker, J., 1992. Analysis of the dilatometer test in undrained clay. Presented at the Predictive soil mechanics: Proceedings of the Wroth Memorial Symposium held at St Catherine's College, Oxford, 27-29 July 1992, Thomas Telford Publishing, pp. 783–795.

Notation

Subscripts

c	Critical state
0	Initial condition
1, 2 ,3	Principal directions of stress or strain
ref	Reference stress level; by convention, p_{ref} = 100 kPa
tc	Triaxial compression condition

Superscripts

e	Elastic
p	Plastic

Dimensions

F	force
L	length

Stress Variables (all stress as 'effective')

$\sigma_{1, 2, 3}$	[FL^{-2}]	Principal stresses
σ_m	[FL^{-2}]	Mean effective stress
σ_q	[FL^{-2}]	Deviatoric stress invariant
η	[-]	Dimensionless distortional stress measure h = s_q / s_m

Strain Variables

$\varepsilon_{1, 2, 3}$	[-]	Principal strains (assumed coaxial with principal stresses)
ε_v	[-]	Volumetric strain $e_v = e_1 + e_2 + e_3$
ε_q	[-]	Distortional strain measure work conjugate with s_q
D	[-]	Dilatancy, as ratio of strain rates de_v/de_q
D^p	[-]	Plastic dilatancy, as ratio of strain rates de_v^p/de_q^p

State Variables

e	[-]	Void ratio
ψ	[-]	State parameter, ψ = e - e_c

Critical State & Soil Properties

Γ	[-]	Reference void ratio on CSL, defined at p′ = 1 kPa
λ	[-]	Slope of CSL in e-ln(s_m) space for semi-log idealization
λ_{10}	[-]	Slope of CSL, but defined on base 10 logarithms (= 2.3 l)
M	[-]	Critical friction ratio, equals η_c at the critical state.
N	[-]	Nova's volumetric coupling coefficient in stress-dilatancy
χ	[-]	State dilatancy coefficient (soil property)
E, G	[FL^{-2}]	Respectively, Young's modulus and elastic shear modulus
ν	[-]	Poisson's ratio
I_r	[-]	Elastic shear rigidity
H	[-]	Plastic hardening modulus

DMT indexes

A, B	[FL^{-2}]	Respectively, the DMT measured pressures at central membrane displacements of 0.05 mm and 1.1 mm
ΔA, ΔB	[FL^{-2}]	Respectively, the DMT membrane stiffness corrections at central membrane displacements of 0.05 mm and 1.1 mm
Z_M	[FL^{-2}]	The DMT gage reading when vented to atmosphere
K_D	[-]	The DMT horizontal stress index
k_D, m_D	[-]	dimensionless coefficients in $K_D/K_0 = k_D \exp(-m_D \psi_0)$

The horizontal stress cone coefficients

a, b	[-]	dimensionless coefficients in $\sigma'_{hc}/\sigma'_{h0} = a \exp(b\psi_0)$

ITASCA Revolutionizes Mining Again!

New Simple Software for Advanced Mine-Scale Modeling

ITASCA Software

IMAT™

IMAT (ITASCA's Mining Analysis Toolbox) is an innovative software suite tailored for mining professionals, providing comprehensive numerical model pre-processing, solving, and post-processing capabilities with an intuitive point-and-click user interface — no commands or scripting needed.

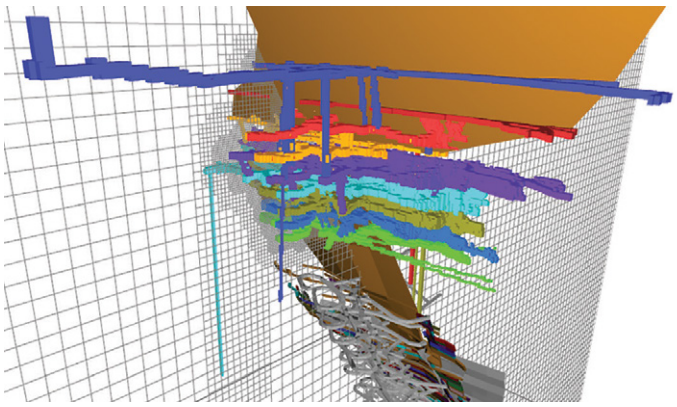

Powered by FLAC3D, IMAT simplifies the creation, meshing, and analysis of complex mining operations, offering a clear workflow that enables engineers to optimize designs, perform seismic analysis, and manage risks efficiently. IMAT includes Null, Elastic, Mohr-Coulomb, SUBI, and Hoek-Brown material models, as well as an IMASS option, for a wide variety of analyses.

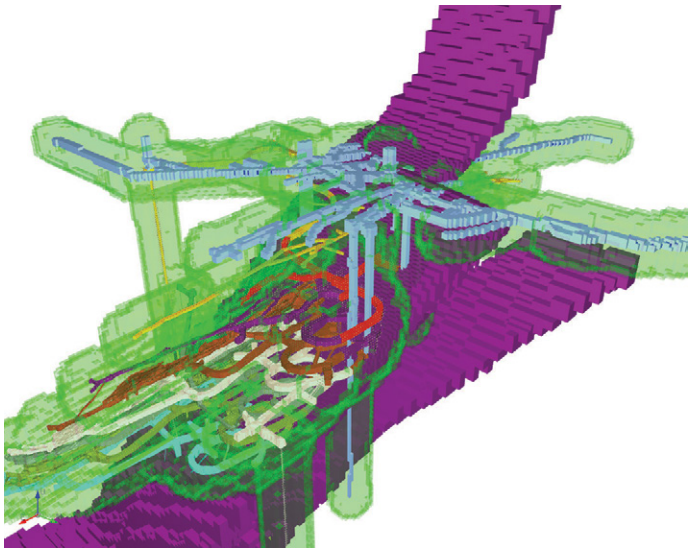

IMAT's Mining Analysis Capabilities:

- Simulate mining with timed excavation sequences.
- Predict strains, stresses, deformations, and damage around infrastructure and mine workings.
- Readily include geological structures and lithologies.
- Simplify visualization of data and results with built-in plotting and charting tools.
- Import mine seismicity data and capture synthetic seismicity for model calibration and to better understand mining-induced rock mass behavior.

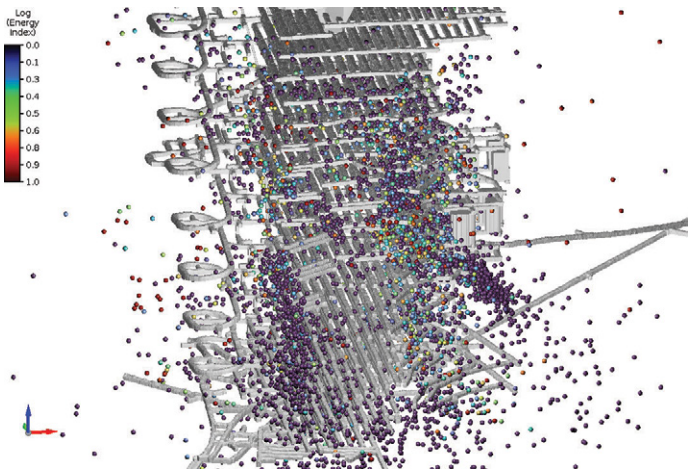

Discover More About IMAT
www.ItascaSoftware.com/IMAT

TERRATEST

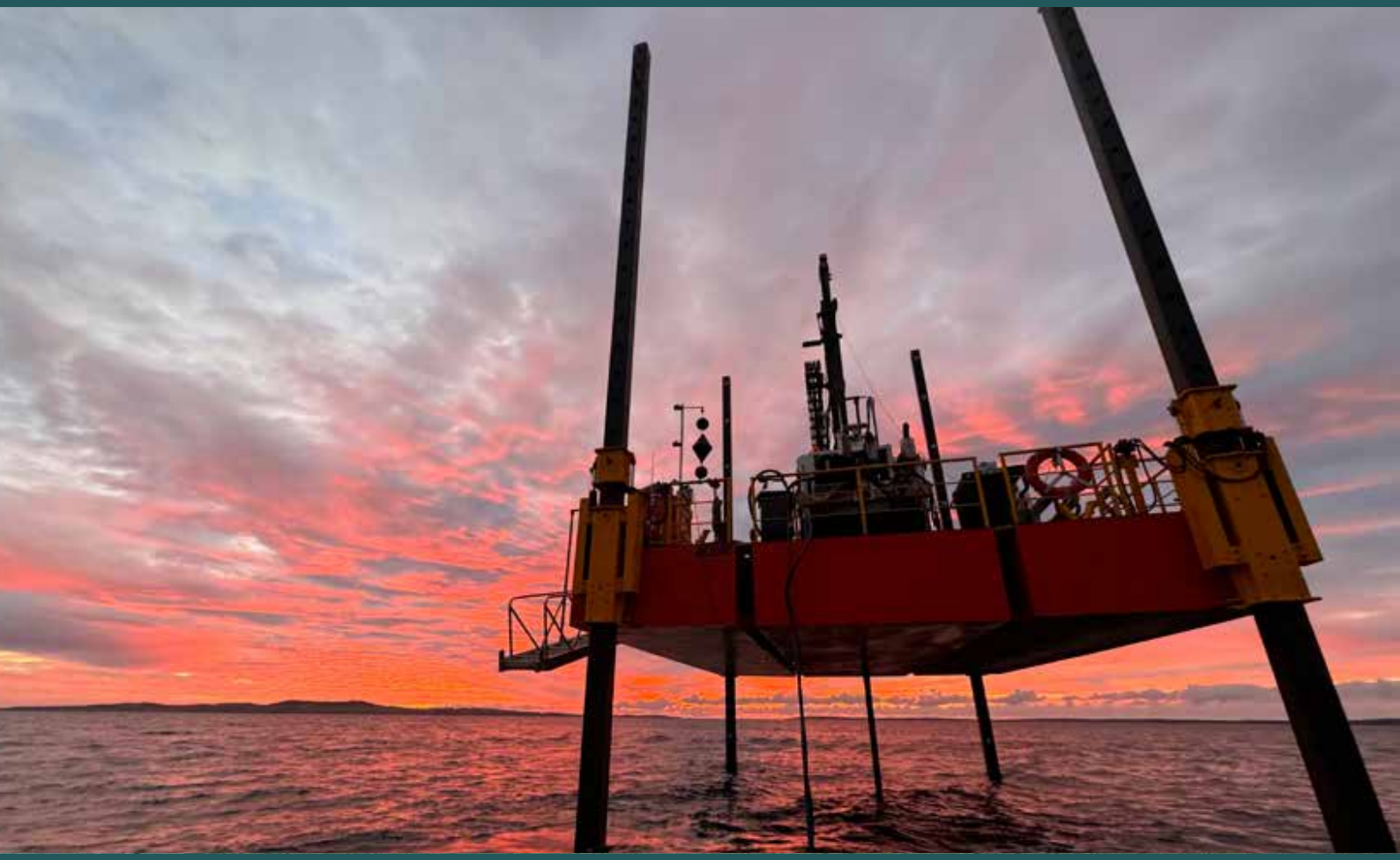

SITE INVESTIGATION DRILLERS

From the pint-sized XC to our powerful Sonic rig - from Queensland, Newcastle, Sydney, Melbourne and now Adelaide, Terratest has the tools to get the job done and the staff to ensure it's done safely.

Sydney

Simon Hamilton
E: simon@terratest.com.au
M: 0412 496 672

Newcastle

Tom Pilbro
E: tom@terratest.com.au
M: 0413 185 700

Queensland

Dave Coleman
E: dave@terratest.com.au
M: 0429 987 271

Victoria & South Australia

Simon Morris
E: smorris@terratest.com.au
M: 0429 199 445

Sonic

Simon Hamilton
E: simon@terratest.com.au
M: 0412 496 672

Environmental

Simon Hamilton
E: simon@terratest.com.au
M: 0412 496 672

terratest.com.au
1300 884 198

ADVANCES IN TAILINGS DAM BREACH MODELLING AND CREDIBLE FAILURE MODE OUTCOME IN TAILINGS DAM BREACH ASSESSMENT USING THE MATERIAL POINT METHOD

Marcelo Llano-Serna[1], Scott H Lines[1], Nicolas Pereira[1], Seyedmohammadjavad Seyedan[2], Sudheer Prabhu[1] and Mike Liu[1]

[1] Red Earth Engineering, a Geosyntec Company; [2] Geosyntec Finland

https://doi.org/10.56295/AGJ6045

ABSTRACT

Recent tailings dam failures underscore the need for better tools to understand and mitigate the potential impacts of such events. The Global Industry Standard on Tailings Management (GISTM), introduced in response to catastrophic tailings dam failures, is an aspirational standard that defines credible failure modes as technically feasible failure mechanisms. This is an excellent first step, however, GISTM does not state which methodology to assess these failure modes. A commonly employed approach that would be considered as industry standard is the Failure Modes and Effects Analysis (FMEA). The FMEA applies rigour to decision making but is still subject to subjectivity, relying on engineering judgement to inform risk. A tool that can be utilised to understand tailings dam failure further and supplement the FMEA process is the Material Point Method (MPM). A numerical method which allows for large strain, as required in breach analysis, with commonly accepted constitutive soil models and relatively limited computational power requirements in comparison to alternative large strain modelling methodologies. Six case studies utilising MPM is presented. The case studies incorporate an array of tailings facility design, location, complexity, lifecycle and regulatory environments, demonstrating how MPM can enhance understanding of the complex challenges. The benefits of utilising MPM with existing guidelines and current industry practices is highlighted, providing lessons learned and recommendations for implementation of MPM into projects. MPM is a tool that can reduce risk and promote better-informed decision-making, furthering the GISTM goal of 'zero harm to people and the environment with zero tolerance for human fatality.'

1 INTRODUCTION

Leaders in the tailings storage facility (TSF) industry recently recognised two interpretations of credible failure modes. The first is on whether the potential failure mode is possible and the second is rooted in the determination that the probability of the failure mode is considered non-negligible (Small et al., 2023). Although GISTM (2020) highlights that the term credible failure mode is not associated with a probability of an event occurring, Martens and Kupper (2024) remark that GISTM intended to emphasise that the existence of credible failure modes is not related to the facility because acknowledging a credible failure mode is not a statement of whether its probability is high or low. ANCOLD (2022) and CDA (2007) recommend conceptually connecting failure modes to unwanted consequences (e.g. the catastrophic failure of a TSF embankment) using bow-tie diagrams and assessing risk using tools such as Failure Mode and Effects Analysis (FMEA). The outcomes of these assessments are diagrams and results are qualitative and require the output of technical assessments, such as Tailings Dam Breach Assessments (TDBA), to determine the potential consequence of hypothetical failure events. CDA (2021) recommends that selected scenarios when undertaking TDBA should consider critical and credible failure mechanisms. Although the recent technical literature highlights the role of credibility in failure mode selection, the reliability of modelling credible consequences remains relatively unexplored.

This paper describes how recent advances in computational mechanics have resulted in adopting methodologies such as the Material Point Method (MPM) to improve the reliability of modelled failure modes. Background of MPM is provided, leading into four forensic studies that investigate the failure of a TSF and six industry projects ranging from a simple column collapse to a more complicated multi-plane failure surface. The extensive presentation of case studies is used to communicate the available scenarios that benefit from MPM, the core link between them is that the potential for large strain to occur is present. These scenarios are then expanded further to outline available solids content, rheological behaviour and the various methodologies that produce volume estimates. This comprehensive review of the state of MPM within the tailings industry has been designed to provide guidance in most of the relevant areas for practitioners seeking to utilise MPM within their projects.

2 MPM IN THE CONTEXT OF TDBA

The Canadian Dam Association technical bulletin on TDBAs (CDA, 2021) is one of the more recent guidelines published to inform dam safety professionals. CDA (2021) constituted a step forward, highlighting, among other key factors, the complex non-Newtonian flow behaviour exhibited by tailings. A common misconception in the industry assumes that when tailings are modelled to behave like water (Newtonian), it results in conservative consequence estimates (Llano-Serna, 2023). This assumption can be correct in certain scenarios since Newtonian behaviour results in over predicting the inundation areas (i.e., water flow will cover a larger area than mudflow). However, in other scenarios it is incorrect as the assumption of Newtonian behaviour under predicts mudflow depths, particularly near the dam toe, where mining/processing plant infrastructure is usually located. Newtonian flows can also under predict lateral spread perpendicular to the direction of the advancing plume. Larger deposition depths seen in non-Newtonian flows have the potential to flow perpendicular to the flow direction near the embankment toe. These misunderstandings can result in inadequate risk mitigation measures and mischaracterisation of risk profiles because the models used produce non-credible outcomes. Tailings, especially those contained at high solids concentration, do not behave like water (CDA, 2021).

Numerous factors and failure modes can cause tailings dam failure. One example includes tailings liquefaction, which has been demonstrated to have played a significant role in recent dam failures like Cadia in Australia or Fundão and Brumadinho in Brazil. The International Commission on Large Dams bulletin 194 (ICOLD, 2023) recommends following NASEM (2021) for guidance on state-of-practice guidelines to assess earthquake-induced soil liquefaction and its consequences. NASEM highlights the emergence of techniques such as MPM to predict liquefaction and its consequences. Additionally, the United States Society on Dams (USSD, 2022) highlighted MPM as one of the promising methods for modelling the deformation of embankment dams.

2.1 MATERIAL POINT METHOD

MPM was developed in the 1990s (Sulski et al. 1994, 1995) to address the limitations of traditional mesh-based modelling methods (e.g., Finite Element Method). MPM combines the strengths of both particle and mesh-based methods, allowing it to conduct large-strain calculations. MPM is based on continuum mechanics, and its algorithm ensures the conservation of mass and momentum in calculations. In each timestep, MPM uses a mesh to solve the equation for the conservation of momentum. The MPM algorithm saves time-dependent data in material points and resets the mesh, preventing the primary limitation of mesh-based methods. The algorithms can update stress at the beginning or end of each calculation cycle. Wallstedt and Guilkey (2008) showed that updating stress at the end is more efficient.

Explicit MPM algorithms that use simple linear functions can result in numerical errors caused by cell crossing (Sulski et al. 1994). Bardenhagen and Kober (2004) introduced the Generalized Interpolation Material Point (GIMP) to mitigate cell crossing errors and improve stability. GIMP has two main versions: uGIMP, where material point domains remain unchanged, and cpGIMP, which tracks changes within domains. Despite improvements, GIMP faces challenges to model shear deformation, tensile loading fractures, and modelling curved geometries (Sołowski et al., 2021). Sadeghirad et al. (2011) introduced the Convected Particle Domain Interpolation (CPDI) for better handling curved geometries and shear deformation. Most MPM algorithms use explicit and implicit time integration schemes (Sołowski et al., 2021), with explicit methods being much more common and it is the main focus of this work.

MPM-based tools have advantages and disadvantages that should be carefully considered. The continuum mechanics nature of MPM means that methods based on it can use common models (e.g., Mohr-Coulomb) as well as more advanced models (e.g., Nor-Sand and P2P-Sand) for capturing particle-to-particle and particle-to-fluid interactions in tailings materials. While ongoing developments of MPM are continuously improving its versatility and usability, many MPM tools are research-based and lack the robustness and support of commercial geotechnical software (i.e., FLAC or Plaxis). Most MPM tools do not incorporate the ability to replicate construction stages, making it difficult to capture instability triggers. Engineering judgment can help overcome these challenges, however it introduces subjectivity into the process.

2.1.1 Computational effort

Computational effort continues to be a key challenge for MPM. As opposed to something like the limit equilibrium method (LEM), commonly used in stability assessments. MPM is more similar to FEM or FDM methods, though potentially with slightly higher computational effort required. Over time this computational effort has decreased significantly and with more computational power being made available and the development of more powerful MPM engines this is expected to continue to decrease. Despite the extra computational effort required, the advantages of adopting MPM modelling for TDBA are significant. Being able to produce more realistic and reliable results is invaluable for assessing the potential consequences and risk of a facility. The limitations in computational effort may be mitigated with appropriate planning during the design stages and adequate modelling simplifications.

2.1.2 Software packages and tools

The modelling team has experience with the MPM engines listed in this Section. This list is not exhaustive and there are many other MPM engines available.

ANURA3D (Anura3D MPM Research Community, 2025) is the most widely known and used MPM engine. The modelling community using this tool is relatively extensive, and new users can engage the community for assistance. Anura is recommended for new MPM users due to its ease of use and low learning curve. Anura is an open-source software and available for free. Nevertheless, Anura requires a commercial pre-processing tool called GiD. The pre-processing tool brings many advantages, such as the graphic user interface (GUI), allowing modellers to define boundary condition problems without significant coding. Anura has an active community and is well documented with a manual and tutorials. The latest version of Anura has some parallelisation capabilities and Anura3D community are further improving the parallelisation of the software so it can do 3D and big 2D models in an effective and timely manner. In addition, the 2025 version of Anura3D includes stage construction ability which improves the modelling accuracy.

CB-Geo (Kumar et al., 2019) is an open-source tool for MPM simulations supporting various constitutive, multiple stress update and velocity update strategies. It is the one of the most efficient available implementations of MPM to date, supporting parallel processing and clusters computing. However, it currently only runs using Linux, it is not thoroughly documented and its development and communities are no longer active.

MPAC (Purvance and Coetzee, 2024) is the soon to be released code developed by the ITASCA Consulting Group (ITASCA) who are responsible for the widely used FLAC and PFC (Llano-Serna et al., 2024). This is a closed-sourced commercial software but will have the technical support available for users and run within the FLAC environment. So, users familiar with FLAC will have a gentler learning curve then some of the other options presented here.

MPMPUC-Rio (Fernandez, 2020) is a numerical simulator based on MPM that supports several constitutive relationships and coupled hydro-mechanical modelling. It incorporates multiprocessor memory parallelisation techniques that allow simulations of many material points, allowing for 3D models and large 2D models to be solved efficiently. However, it is closed source, command-based and lacks documentation and examples, so it is not as user-friendly. Additionally, the critical time step is limited to a fixed value that requires manual adjustment, so the efficiency of the calculation can vary greatly. The program is currently only available at the author's discretion.

Uintah-MPM (Guilkey et al., 2009) was developed at the University of Utah in 1997. Uintah provides a computational framework that includes modelling software components and libraries, including an MPM component. The MPM component of Uintah supports advanced parallelisation of processors, 2D and 3D modelling, and various constitutive models, including important geotechnical models. Uintah's open-source nature lets developers access and modify the code as needed. It also offers various time-stepping algorithms, simplifying its use. Nevertheless, the lack of a graphical interface for creating geometries makes working with the software challenging.

2.2 HISTORICAL BENCHMARKING AND FORENSIC STUDIES

Zabala (2010) simulated the failure of the Aznalcóllar dam using MPM to build the model using 15 construction stages and incorporating the brittle clay foundation characterised by means of a strain-softening Mohr-Coulomb elasto-plastic model. The model could predict the development of a localised shear band at the toe and the subsequent progressive failure with the modelled failure matching actual field observations (Figure 1). In the analysis performed no prior assumptions were made about the location, shape or depth of the failure surface.

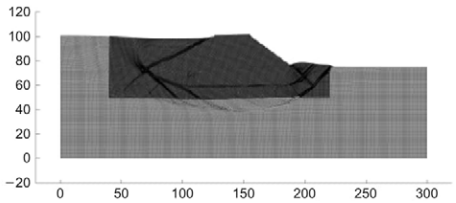

Figure 1: MPM model after tailings liquefaction, horizontal and vertical axis are expressed in metres (Zabala and Alonso, 2010)

Pierce (2021) examined the 2018 Cadia tailings dam failure, located in New South Wales, Australia. The initial and final field topography, overlaid with the MPM results is shown in Figure 2. The MPM results provide an excellent match with the final field topography, with the Pump House location from the model being within 10 m of the observed Pump House location. The model was constructed using a fully coupled hydromechanical MPM formulation for saturated materials, with the material above the water table assumed to be dry. Mohr-Coulomb was applied to the material with an undrained strength assigned for the liquefied tailings.

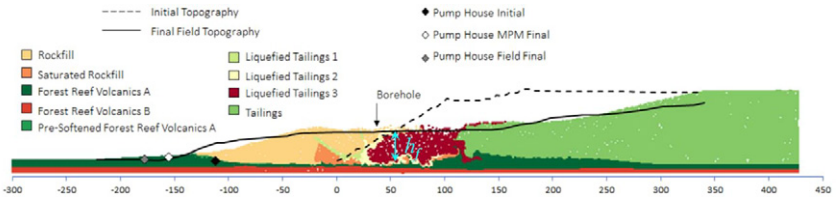

Figure 2: Cadia - MPM versus the pre and post-failure topography (modified from Pierce 2021)

An additional study utilising MPM was the Expert Panel investigation of the failure of Feijão Dam I (Robertson et al., 2019 Appendix H). This case resulted in a significant mudflow that travelled rapidly downstream with failure occurring in the space of 10 seconds and resulting in approximately 9.7 million cubic metres of tailings flowing out of the facility. MPM was able to simulate the first 15 seconds of failure with velocity ranging from 25 m/s to 30 m/s.

Talbot et al. (2024) used MPM to model the earthquake induced Lower San Fernando Dam failure. Expanding on the Chowdhury (2018) nonlinear seismic deformation analysis which was unable to capture the large deformation behaviour and post-failure equilibrium cross-section using FDM. For this case study implementation of an adhesion boundary condition was accomplished to reduce the computational cost by limiting the required area to be modelled.

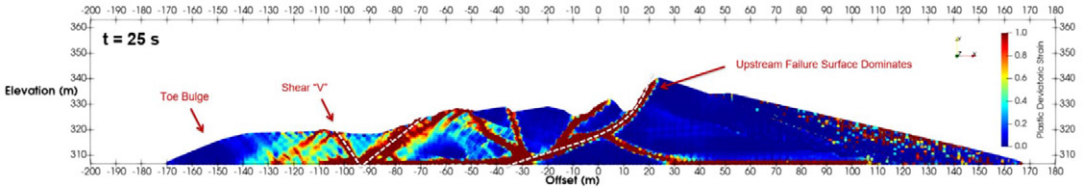

Figure 3: MPM model of Lower San Fernando Dam post-failure (Talbot et al., 2024)

3 INDUSTRY CASE SERIES

3.1 CASE SERIES SUMMARY

A significant number of projects have seen the benefits of improved TDBA studies using MPM methods. The project summary is provided in Table 1. The details described herein are the trends observed by the authors. The project summary includes upstream and downstream-built TSFs. One of the projects considers mud-farming as a dewatering strategy to build a structural zone. Another project involved an Integrated Waste Landform (IWL). Dam height ranges from 20 – 100 m. Commodities include iron ore, coal, gold, manganese, bauxite and red mud. The projects included active, inactive and closed facilities, and those undergoing closure. Most models developed were 2D, although several 3D models are shown. The number of models commissioned per year indicates an increasing trend, which shows a growing interest for this kind of numerical modelling. Multiple models have been successfully submitted to regulators in Australia and overseas. In one case, the MPM model developed was used to update internal TDBA guidelines to inform TDBA studies at the various mine sites in the client's portfolio. Clients are mostly tier-one mining companies. In one case, the TDBA was used to inform a Dam Safety Review (DSR). The MPM model developed for the DSR was instrumental in refining the Consequence Classification Assessment (CCA). A reduction in the CCA risk rating was possible due to the updated TDBA assessment using MPM techniques.

Table 1: Summary of projects for which MPM has been used to improve the outcome of TDBA

Id	Project type	Year	Number of TSFs involved in the TDBA study	Model complexity	Approximate critical cross-section height (m)	Location
1	Inactive Iron Ore Upstream TSF	2019	1	2D	86	Brazil
2	Upstream Coal TSFs	2021	3	2D	15	QLD, Australia
3	Upstream Gold TSF	2021	1	2D	20	NSW, Australia
4	Downstream Manganese TSFs, including active,	2023	5	2D	21	NT, Australia

Id	Project type	Year	Number of TSFs involved in the TDBA study	Model complexity	Approximate critical cross-section height (m)	Location
	inactive and closure construction					
5	Downstream Iron Ore TSF	2023	1	2D	25	WA, Australia
6	Upstream Mud-Farmed Bauxite TSF	2023	1	2D	10	QLD, Australia
7	Active Mining Manganese TSF	2023	1	3D	15	NT, Australia
8	IWL, Gold TSF	2023	1	2D	23	NSW, Australia
9	Closed Bauxite Upstream TSF	2023	1	3D	10	QLD, Australia
10	Inactive Coal Downstream TSF	2024	1	3D	60	QLD, Australia
11	Inactive Iron Ore Upstream TSF	2024	1	3D	86	Brazil
12	Upstream Red Mud	2024	1	2D	90	Spain
13	Downstream Red Mud Closure Construction	2024	1	2D	25	NT, Australia

3.2 CASE STUDIES

This section presents details of key case studies where MPM was used to simulate different tailings dam failure mechanisms. These case studies illustrate the versatility of MPM in capturing complex failure processes that conventional methods may oversimplify or overlook.

3.2.1 The column collapse model

The collapse of a granular column is a well-established experiment in academic publications. The experiment involves releasing a column of granular material by removing its lateral support onto a flat surface. The column fails, and some of its mass crumbles and flows onto the flat surface. In the theoretical abstraction, the instability of the material during collapse is solely driven by the column's self-weight. The research industry has historically focused on understanding how the different aspect ratios of granular columns behave upon collapse (Lube et al. 2004, 2005; Fern & Soga, 2016; Llano-Serna et al., 2016). The aspect ratio is defined as $a = h_0/d_0$, where h_0 and d_0 are the initial column dimensions (height and width, respectively) before the column collapses at $t = 0$. For example, Figure 4 shows the column collapse progression in clayey soil. Llano-Serna et al. (2016) explored aspect ratios of between 0.5 and 10 for normalised time steps of between $t = 0$ (initial conditions) and $t = 4$ (collapsed).

The authors note that the theoretical column collapse problem would better represent tailings dam collapse at very low aspect ratios. Tailings dams are some of the largest man-made structures. In the theoretical column collapse problem context, d_0, tends to infinity; a tailings dam footprint can be several hundred hectares or greater than 1,000 ha for some larger facilities. Despite this key difference between the theoretical column collapse and a real dam breach, similarities exist. A common key geometrical feature can be found between the column collapse with a low aspect ratio of a clayey material in Figure 4 and the post-failure cross-section of the Cadia dam failure in Figure 2.

The final deposited height at the intersection of the profile defined by the collapsed column and the pre-failed geometry is denoted here as h_f. The commonality of this feature is also seen in sandy column collapses, Figure 5. The numerical column collapse of a one-metre-tall loose sand column was compared against experiments. The MPM final run-out was seen to match a laboratory experiment relatively well (Fern and Soga, 2016).

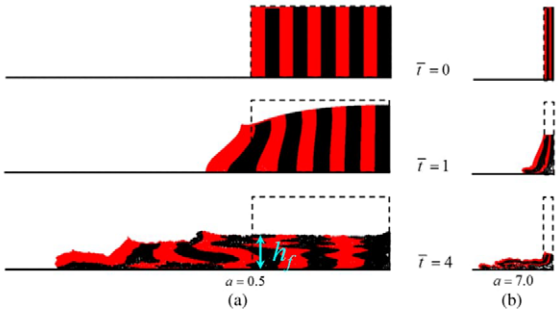

Figure 4: Example of column collapse model using MPM in clayey soil for two aspect ratios. Left: aspect ratio a=0.5, right: a=7 (modified from Llano-Serna et al. 2016)

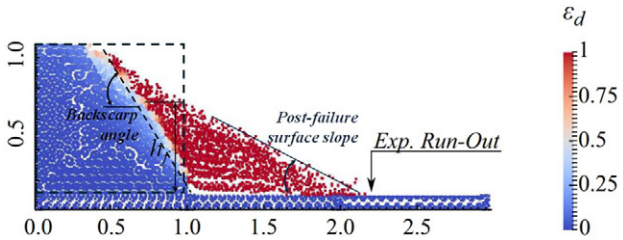

Figure 5: Example of column collapse model using MPM in loose sandy soils with an aspect ratio of one. The colourmap in the background represents the deviatoric strain, ε_d (modified from Fern and Soga, 2016)

MPM modelling allows designers to estimate the slope of downstream deposition angles, see Figure 5. A further added benefit of MPM models is that designers can estimate the interaction between the collapsing material and downstream topographic features. Conventional practices for estimating the post-failure surface slope include the theoretical semi-infinite slope method Seddon (2007) recommended and assuming a factor of safety (FS) equal to one. Adams et al. (2022) propose a method to estimate the so-called stable slope FS. The theoretical semi-infinite slope works well for homogenous deposits where the tailings properties can be assumed to be represented by one characteristic value. For facilities with interbedded tailings that cannot reasonably be considered homogenous, some consultants use the conventional Limit Equilibrium Method (LEM) to estimate the stable slope, which is done by calculating a FS of one, assuming liquefied strengths for the different types of tailings stored in the facility. The theoretical column collapse model has been applied to several TDBA summarised in Table 1. Figure 6 (Top) shows the complex layering and different types of tailings deposited due to the management strategies of a TSF built using mud-farming techniques. In this case, the column's height was approximately 30 m and its width 220 m. Figure 6 (Bottom) shows the final post-collapse geometry calculated using MPM. For this example, the run-out distance was calculated as 270 m, and the post-failure surface was 3.9°.

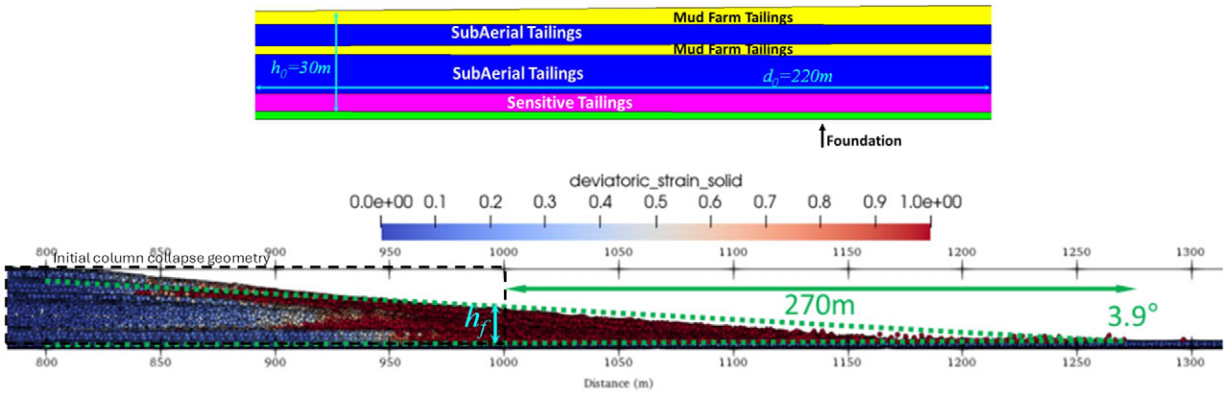

Figure 6: Column collapse modelling applied to TDBA to estimate the deposition angle. Top: initial state, Bottom: final state post-collapse

A summary of the post-failure surface angles calculated for the case studies is provided in Table 2. The results show that the post-failure surface angles vary between 2.7 - 4.2°. A comparison with literature reported by Blight and Fourie (2003) shows alignment between the results presented here and the topographic historical records of previous TSF failures. Specifically, the post-failure surface flattened to a general slope of 2 - 3°, with some portions around the failure scar being

as steep as 10 - 20° (Blight and Fourie, 2003). The close agreement between the post-failure surfaces from MPM models in Table 2 and real failures in Table 3 provides a qualitative validation that supports the credibility of the modelled outputs. Figure 5 shows that MPM also provides insights into the final back scarp angle when the magnitude of deviatoric strain is highlighted. It should be noted that none of the column collapse models summarised herein included a supernatant pond with the focus being conceptual cases 2A and 2B as defined by CDA (2021), which correspond to liquefiable and non-liquefiable tailings without a supernatant pond.

Table 2: Deposition angle calculated using MPM techniques

Id	Project	Model complexity	Post-failure surface slope
2	Upstream Coal TSFs	2D	3°-4°
6	Upstream Mud-Farmed Bauxite TSF	2D	3.9°
8	IWL, Gold TSF	2D	2.7°
11	Inactive Iron Ore Upstream TSF	3D	3.4°-4°
12	Upstream Red Mud	2D	3.9°
13	Downstream Red Mud Closure Construction	2D	4.2°

Table 3: Summary of observed post-failure surface slopes for flow failures (Blight and Fourie, 2003)

Tailings dam	Post-failure surface slope
Bafokeng	4°
Bafokeng	2°
Arcturus	3°
Saaiplas after rain	3°
Saaiplas no rain	2.3°
Saaiplas no rain	3°
Merriespruit flow slide	2°
Merriespruit failure basin	2°

In TDBA, the backscarp angle is projected through the tailings mass beginning at the base of the zone, which would become unconfined during a tailings dam breach. Adams et al. (2022) recommend that the area above the projection of the stable slope angle could liquefy and flow or slump if the lateral confinement is removed. The column collapse model provides estimates of the final backscarp angle and the post-failure surface slope that the authors interpret to be similar or equivalent to Adams' stable slope angle. CDA (2021) and Adams et al. (2022) conservatively recommend that the projection of the final back scarp angle and stable slope has its origin at the intersection between the upstream batter toe and the foundation of the TSF, see the highlighted point in Figure 7. The column collapse model results indicate that the assumption of the location of the origin of the final back scarp can be overly conservative, and the calculated mobilised volume can be greatly overestimated, especially when adopting Adams et al. (2022). This observation is validated when comparing the schematic in Figure 7 with the Cadia post-failure cross-section in Figure 2. These observations are limited to models that do not consider the presence of a supernatant pond.

CDA (2021) recommends using the final back scarp angle to draw a 3D cone of depression to estimate the volume of mobilised tailings when a kinetic model, such as an MPM model, is unavailable. Figure 8 shows the MPM modelled back scarp angle using MPM for the Cadia collapse (Pierce, 2021). The figure shows that the back scarp angle starts more than 100 m upstream from the intersection between the upstream batter toe and the foundation of the TSF. This distance is defined herein as d_b. An alternative to current practices is to refine mobilised volume estimates when a kinetic MPM model is available to estimate the final backscarp angle, d_b, the post-failure slope and h_f. The methodology applies to CDA conceptual cases 2A and 2B. Its application to conceptual cases 1A and 1B (liquefiable and non-liquefiable tailings with a supernatant pond) is possible but should be exercised carefully; such a scenario is discussed in section 3.2.4. The incorporation of measurements from a MPM column collapse model is still considered a conservative estimate because the method disregards the buttressing contribution of the embankment to the dam breach.

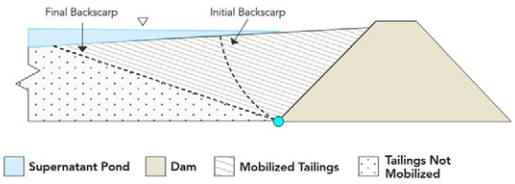

Figure 7: Schematic of the cross-section of the failure surface for a TSF (modified from CDA, 2021)

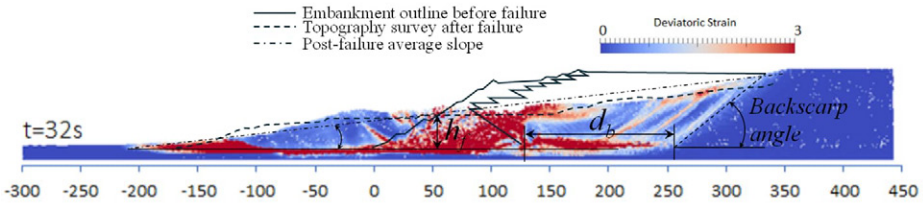

Figure 8: Geometrical features of Cadia MPM model (modified from Pierce, 2021)

3.2.2 Development of hydrographs for input in TDBA hydraulic models

CDA (2021) defines a hydrograph as a graph showing the flow rate (discharge) versus time past a specific point in a river, channel, or conduit carrying flow. The flow rate is typically expressed in cubic metres per second (m^3s^{-1}). Step 7 for undertaking TDBA following CDA involves estimating the breach outflow volumes and breach outflow hydrographs. Key parameters, such as peak flow and outflow define a hydrograph. These parameters can be analysed to assess the severity of the breach, which is influenced by factors like breach size, development time, rheological properties of the released tailings and outflow volume. Hydrographs can also support sensitivity analyses, comparing flood wave scenarios.

A key advantage of using MPM to inform TDBA is that it can be used to develop volume (discharge) vs time plots – the mobilised volume in MPM is an output, not an input variable; it is because the constitutive relationships available in MPM capture the transition between peak and residual strengths, see Zabala and Alonso (2011) and Pierce (2021). The methodology to develop a hydrograph using MPM modelling can be used in subsequent hydraulic modelling, this approach has been employed twice in the project database discussed. The application of this approach corresponds to Project three and Project 11 in Table 1. Project three is a 2D application, and Project 11 is a 3D application. Only Project three is briefly described.

For Project three the TSF was 20 m high; the critical cross section is shown in Figure 9. It comprised one starter embankment and five subsequent upstream raises. The critical failure mode assessed was static liquefaction of the tailings. The CDA conceptual case was classified as 2A. The footprint of the TSF is shaped like a pentagon; see Figure 10. For this study, it was requested by stakeholders that the failure of the entire wall, highlighted in red in Figure 10, was considered. Due to the extension of the wall in the axis perpendicular to the page, a 2D analysis was considered appropriate for developing a hydrograph.

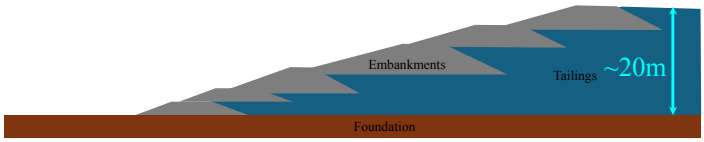

Figure 9: Critical cross-section of the embankment considered critical for TDBA scenario

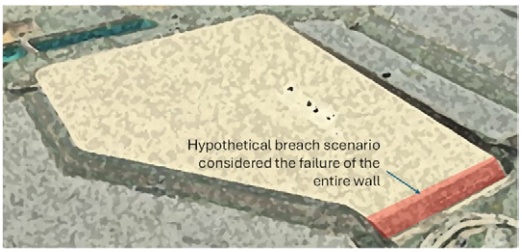

Figure 10: Panoramic view of a TSF for which TDBA was undertaken using MPM techniques, the vertical scale has been exaggerated

The MPM mesh adopted for this case study is presented in Figure 11. The MPM engine Anura was used to solve this model. Multiple conservative simplifications were considered: i) the contribution of the embankments to the collapse of the TSF was ignored, ii) a boundary condition consisting of lateral support on the upstream batters was imposed at t=0, the location of the lateral support is sketched in yellow in, iii) initial stresses were developed while the lateral support was active by imposing gravity loading in a quasi-static manner, iv) the tailings were assigned liquefied properties – a conservative 95th percentile liquefied undrained shear strength ratio (LUSSR) which resulted in a value of 0.032. An excavation boundary condition was defined at the toe of the TSF (green box in Figure 11), this boundary condition removed tailings material points that displaced beyond the TSF toe. This last boundary condition is conservative because it ignores the buttressing effect of the tailings that would otherwise deposit downstream of the failed wall. Removing the lateral support activated the TSF breach, this approach assumes a trigger. The bottom and lateral boundary conditions applied in this case study were consistent with those used in conventional geotechnical numerical modelling. It should be noted that Figure 11 shows the portion of the model near the embankment toe only. The entire model considered several hundred metres horizontally to capture the real TSF geometry.

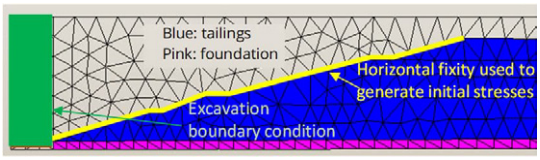

Figure 11: MPM mesh and boundary conditions required for TDBA modelling

In MPM, each material point has a mass associated with it. Building a flow rate vs time plot is ubiquitous because most MPM models are explicit in time. Figure 12 shows the plot of tailings (discharge expressed in tons per second) vs time (in seconds) obtained using MPM. The orange dots correspond to actual MPM measurements, and the red line is the moving average with a period calculated using four data points. The data was utilised to develop a series of hydrographs for subsequent inundation modelling.

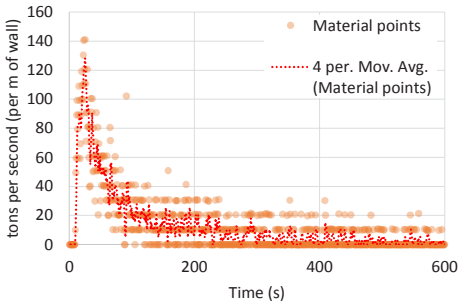

Figure 12: Calculated hydrograph using MPM

3.2.3 Cascading failure mode

A cascading failure scenario was analysed for a turkey nest TSF structure without external catchments, where the primary risk involved the potential for failure of the upstream facility to trigger overtopping of the downstream facility. The upstream facility would release a mass of tailings into the decant pond of the downstream facility, causing a significant wave. This wave could result in overtopping of the downstream dam, leading to a loss of contaminants. MPM was used in the TDBA of the upstream TSF. The application of this method corresponds to Project eight in Table 1. The upstream facility was inactive, with pumping infrastructure installed to manage rainwater run-off – a no decant pond scenario was assumed; the downstream facility was active with a decant pond. The analysis focused on quantifying the key parameters driving wave generation to assess the consequence and impact of this cascading failure. Heller et al. (2009) studied the governing parameters of landslide-generated impulse waves in reservoirs; the key parameters are presented in Figure 13.

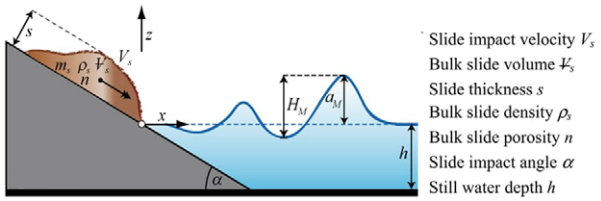

Figure 13: Sketch defining the governing parameters on impulse wave generation and the most important wave parameters (modified from Heller et al. 2009)

Inspection of Figure 13 reveals that most parameters could reasonably be estimated using topographic surveys and conventional geotechnical studies. Slide impact velocity in particular, is not usually reported in geotechnical studies. MPM was used in this case study to inform slide impact velocity.

The initial stress state was computed using FLAC. The stresses were later imported into MPMPUC-Rio. The following assumptions and simplifications were considered: i) The tailings were assigned a LUSSR of 0.07, ii) the buttressing effect of the decant pond in the downstream tailings was ignored, iii) the groundwater level in the tailings downstream was defined at 1 m below the tailings level – this assumption was needed because the MPM model did show numerical instabilities when tailings downstream were allowed to generate pore pressures near the surface. Figure 14 shows the defined regions. Figure 15 shows the final deformed dam calculated with MPM with the deviatoric strain colourmap highlighted. The final maximum horizontal displacement was expected to be approximately 2 metres. A deviatoric strain plot is useful because it reveals the location of failure surfaces when the deviatoric strain reaches unity (shown in red). Figure 16 shows the velocity vs time plot, showing that peak velocity occurs approximately ten seconds after the event is triggered and reaches maximum velocity of 1.8 m/s. The results show that after 30 seconds, the dam failure stabilised. The intensity/darkness of the orange shading inside the plot in Figure 16 indicates the number of material points for which the same velocity was recorded at each time step.

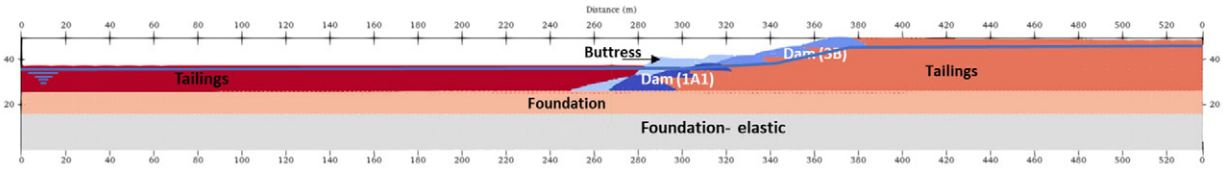

Figure 14: Cascading failure mode case study, cross section showing defined regions

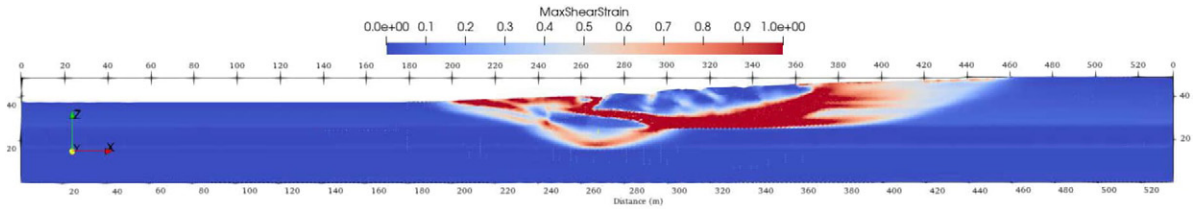

Figure 15: Final deviatoric strain colourmap with red regions indicating the position of a complex failure mechanism during a hypothetical dam breach scenario

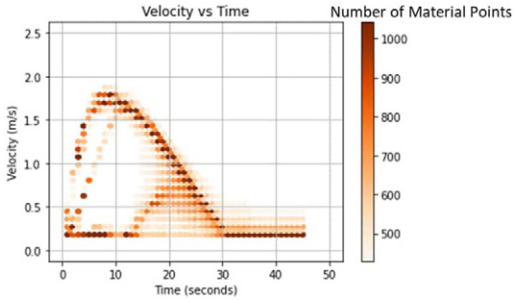

Figure 16: Velocity vs time plot during the hypothetical dam breach scenario

3.2.4 Dam breach of a dewatered/mud-farmed TSF

The following is an example of when MPM was utilised to analyse breach scenarios for an upstream TSF in Australia. A structural zone in the TSF was built using mud-farmed tailings. Anura was the MPM engine used to solve this case study. This summary corresponds to Project six in Table 1. Seyedan et al. (2024) documented a detailed description of the approach for this case study, including boundary conditions and material parameters. The mud-farmed tailings were modelled with a post-peak frictional angle of 25° and the subaerial deposited tailings with a LUSSR of 0.13.

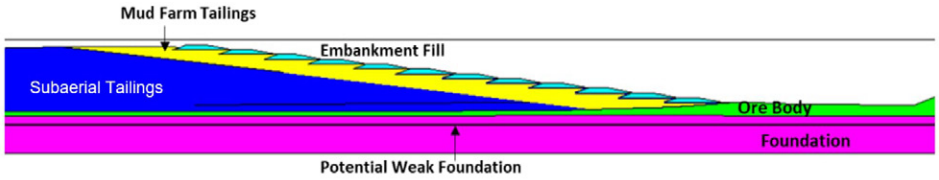

Figure 17:Typical section in the upstream mud-farmed TSF showing the structural zone in yellow and the potential weak foundation in black

A potentially weak layer was identified in the foundation. MPM was then used to investigate credible failure modes, like potential dam breaches due to foundation deterioration. The investigation applied residual material strength that could lead to dam instability. Fern and Soga (2016) demonstrated how this assumption results in conservative estimates. MPM modelling involved critical cross-sections at various stages of the TSF's lifecycle. Figure 18 displays the horizontal (X) and vertical displacement (Y) colourmap (in metres) for one of the critical cross-sections. The results indicates that the maximum horizontal displacement is 45 m, with the displacement extending approximately 60 m upstream of the TSF. The results also indicate a 10 m loss of freeboard at the crest location and shows negligible loss of freeboard at approximately 60 m upstream from the dam crest. This information was relevant for determining pond operational levels. Pond size is crucial for defining the risk profile and avoiding a release during a potential breach. This is an example of the effective use of MPM modelling in facilities with existing ponds – see CDA (2021) conceptual cases.

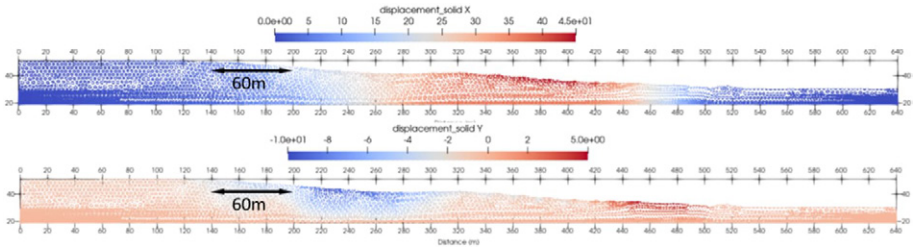

Figure 18: Horizontal and vertical displacements for the critical cross-sections in the mud-farmed TSF

3.2.5 3D MPM modelling

In certain cases, 2D models may not represent field conditions due to complex geometry, non-uniform loading conditions, etc. This section highlights two examples where 3D MPM models were used.

3D MPM modelling – Case A

An MPM model was developed as part of a risk reduction study on a TSF built using the downstream method. The dam is 60 m in height, constructed on bedrock using spoil material—a mixture of silty clay and gravel—the tailings were predominantly comprised of fine material exhibiting medium to high plasticity. The TSF was an inactive facility without a pond. This project corresponds to Project ten in Table 1. The initial stresses for this model were solved using FLAC3D and the run-out process was solved using MPMPUC-Rio. The embankment dam materials were modelled as dilative materials that would reach post-peak friction angles of between 18 - 20° during a hypothetical dam breach. Figure 19 (left) shows a panoramic view of the facility in the FLAC environment. The results from the runout analysis at the end of the simulation and after all materials had settled are shown in Figure 19 (right). The expected maximum run-out was 100 m. A key outcome was that the results predicted no loss of tailings containment should post-peak strengths develop.

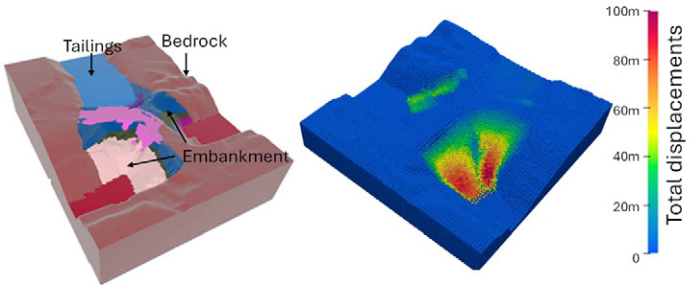

Figure 19: Left: FLAC model, right: MPM model displacements after failure

3D MPM modelling - Case B

An analysis was conducted to assess the potential impacts of a TSF failure on nearby infrastructure (i.e. road and settlement). The TSF was constructed using the upstream method, with a 8 m high starter embankment and a single raise of 2 m, for a total TSF height of 10 m. MPMPUC-Rio was the solver used. The case study is Project nine in Table 1. Following recommendations from CDA (2021), a sensitivity analysis was conducted using hypothetical dam breach scenarios, including realistic and pessimistic scenarios.

- The realistic scenario used mean strength values, representing the most likely condition.
- The pessimistic scenario assumed lower strength bound values to simulate worst-case scenario conditions.

Figure 20 shows the inundation map from the pessimistic scenario (tailings LUSSR of 0.04). In this scenario the embankments were assumed to have the same strength as tailings due to lack of geotechnical information. The TSF breach released impounded material towards the nearby settlement and reached the nearby road.

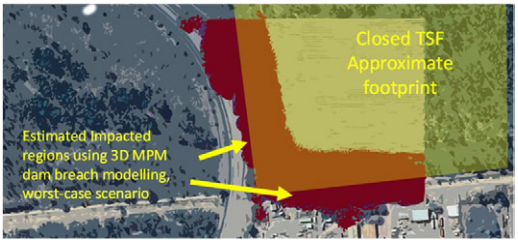

Figure 20: Inundation map of impacted regions using 3D MPM dam breach modelling for a worst-case scenario

4 DISCUSSION

MPM is an additional tool that TSF operators and design engineers can use to improve the accuracy of TDBA under certain conditions. The models presented are varied to showcase the uses of MPM, they have been included in TDBA studies for clients, including regulators in Australia and overseas. One usage that reoccurs throughout is that of emergency response planning, which benefits from the more realistic spatial and temporal results produced by MPM. The subsequent discussion includes recommendations to aid in optimising MPM modelling for the credibility of FMEAs and consequence modelling; it is supported by the results in the project database summarised in Table 1.

4.1 PARAMETERS AND MODELLING APPROACH

Hydraulic modelling or computational fluid mechanics (CFD) software like DAN3D, MADflow, FLO-2D, FLOW-3D or HEC-RAS is the most common approach to model dam breaches. The most common constitutive models in these software packages are Voellmy, Quadratic or Bingham rheology. The combination of these software packages with these constitutive relationships is a powerful tool when modelling water floods and mud floods. However, there are significant uncertainties in some of the results they can provide when modelling non-Newtonian fluid. Ghahramani et al. (2022) demonstrated one of the main uncertainties, in that irrespective of the constitutive modelling or software used, multiple sets of rheological parameters may produce very similar output results (i.e. the solution may not be unique, or there are infinite solutions). Additionally, input parameter combinations are non-transferable between models or software packages (e.g., the same viscosity and yield stress will likely produce very different outcomes when using different software packages, even when the same rheological constitutive relationship is used). Differences of several orders of magnitude in viscosity to reach the same outcome were noted by Ghahramani et al. (2022). Ghahramani et al. (2022) also reported inconsistent back-calculated viscosities when compared with independently measured rheological properties of a tailings parameter database.

MPM can be used to solve models using constitutive relationships well known by tailings practitioners, including failure criteria like Mohr-Coulomb and the elasto-plastic constitutive models Cam-Clay and Nor-Sand. Fern and Soga (2016) show how different constitutive relationships solved with the same MPM engine can provide comparable results, results which were then validated with a laboratory experiment (Figure 21). The black arrow in each figure refers to the runout distance from the laboratory experiment. These results show that MPM can provide consistency across various constitutive relationships when adopted with equivalent material parameters (see Table 4).

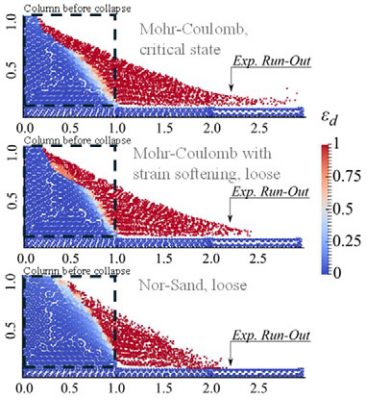

Figure 21: MPM results of simulations of a loose sand squared column of 1 m. The colourmap represents the deviatoric strain (modified from Fern and Soga, 2016)

A column collapse using two different MPM engines was modelled using Anura and MPMPUC-Rio. The material parameters for both models were kept constant to verify the transferability of parameters across different MPM implementations. The results in **Figure 22** were obtained with the same set of parameters used in different MPM engines to provide comparable results. This parameter transferability across different software packages is a feature that the most widely used software for TDBA lacks; see Ghahramani et al. (2022). The model comparison in **Figure 22** also exemplifies the evolution in computational efficiency; the mesh size is much finer in the 2020 MPMPUC-Rio than in the 2016 Anura model. A finer mesh is generally desirable because it captures more detail, such as the development of stress/strain. The capacity to develop finer meshes also translates into the capacity to solve larger models (with coarser meshes), such as those needed in TDBA studies for TSF structures.

Table 4: Summary of key strength parameters adopted by Fern and Soga (2016)

Constitutive model	Strength material parameter
Mohr-Coulomb at critical states	ϕ'=33°
Mohr-Coulomb with strain softening	ϕ'_{peak}=39° $\phi'_{residual}$=33°
Nor-Sand	M_{tc}=1.33 (ϕ'_{cv}=33°)

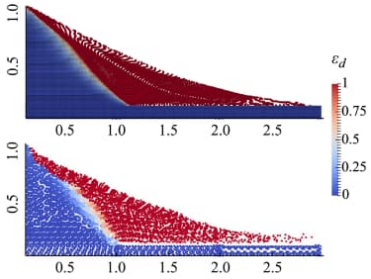

Figure 22: Comparison of the runout distances and deviatoric stress distribution for a 1 m column with an effective friction angle of 33°, top: MPMPUC-Rio, bottom: Anura3D (Soga and Fern, 2016)

4.2 SOLIDS CONTENT

CDA (2021) classifies the types of breach outflows based on the tailings solids contents: a) water flood, b) mud flood, c) mud flow, d) flows slide slumping. **Figure 23** illustrates the relationship between the concentration of solids and CDA tailings breach outflow types. The blue stars in **Figure 23** show the location within the plot of some past successful projects where MPM was used. Mud flow and Flow slide slumping (highlighted with the light blue arrows at Cv ~ 0.5) show the recommended region of tailings solids content that are capable of being modelled using MPM. It is the authors' experience that MPM modelling is most useful for emergency planning, credible failure modes and consequences involving flow slide or slumping scenarios that could lead to catastrophic damage downstream. The kind of MPM modelling presented here, derived from soil mechanics principles, could be extended to model low solids concentration

mud flows or mud floods. However, this would require rheological models to be implemented in the MPM solver (the authors note that versions of Anura and CB-Geo include Bingham rheology implementations). Solving rheology with MPM is computationally expensive, and for lower solids concentration, it is recommended to adopt the numerical techniques highlighted by CDA.

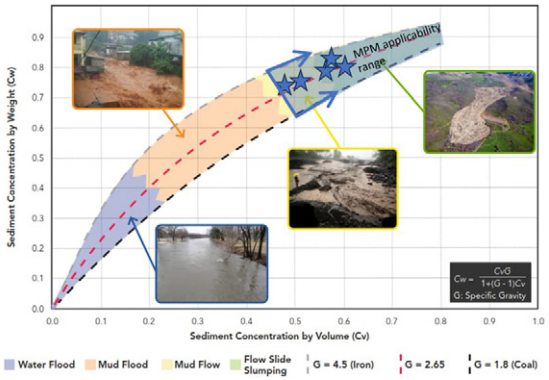

Figure 23: Flow types as a function of solids concentration, modified from CDA (2021)

4.3 RHEOLOGICAL BEHAVIOUR

Rheology describes the interrelation between stresses, strains and time-dependent behaviour. The yield stress is a key parameter measured for rheological studies to inform TDBA. Adams et al. (2018) described how the tailings transition from a slurry to a paste and then soil as the yield stress increases, developing four flowability zones. MPM modelling has been used to model tailings classified between the transition and the flowable zones. Seyedan et al. (2024) have shown examples of applying MPM models for TDBA of mud-farmed (i.e. a dewatering tailings technique that results in high solids concentrations) TSFs whereby mud-farmed tailings are classified as either not flowable or within the transition zone associated with potential slide flow or slumping scenarios. The applicability of MPM is maximised when applied to facilities with not flowable or transition tailings, as those described by Adams et al. (2018).

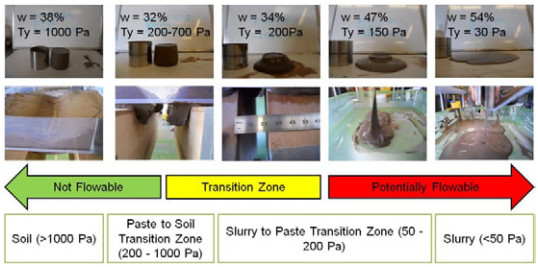

Figure 24: Tailings rheology: solids to slurry continuum (Adams et al., 2018)

4.4 TDBA CASES

CDA defined four conceptual TDBA cases (1A, 2A, 1B and 2B). The cases combine the potential for tailings runout due to flow liquefaction and the presence of a supernatant pond. Provided that tailings within a facility are within the boundaries described in Sections 4.1 and 4.2, MPM modelling for tailings dam breach estimates are applicable for cases 2A and 2B (which also encompasses a significant number of inactive and closed TSFs). MPM modelling is also appropriate for Cases 1A and 1B if tailings are characterised within the boundaries defined by solids content and rheological behaviour discussed herein, and no potential loss of pond containment can be demonstrated. For example, the results from the mud-farmed TSF shown in the study suggested that MPM could simulate the effects of a flow slide slump, provided pond containment is maintained at safe distances—typically 60 m from the dam crest for that TSF. MPM modelling may be used to estimate the release volume of solids for cases 2A and 2B, involving release of pond containment providing the releases of supernatant water and tailings are expected to occur in independent phases. MPM can inform dam breach, uncontrolled release of reservoir (URR), and rate of breach/URR for a Case 1A type of facility. The assessment to evaluate the potential loss of containment must be undertaken on a case-by-case basis with appropriate numerical modelling and assumptions. No rule of thumb can be established for complex scenarios.

4.5 VOLUME ESTIMATES

Ghahramani et al. (2024) back analysed 11 well-documented historical tailings breaches and found that for approximately 80% of the historical cases, the inundation area was the most sensitive to the total released tailings volume. Therefore, estimating the total released tailings volume is key to undertaking a TDBA. Empirical methods to estimate mobilised volume such as Rico et al. (2008), Rourke and Luppnow (2015), Concha Larrauri and Lall (2018) or Ghahramani et al. (2020) can have uncertainties of more than one order of magnitude, making its application to estimate mobilised tailings volume controversial (i.e. it can drive easily non-credible results) because mobilised volume estimates often drive the highest sensitivity to results, see Ghahramani et al. (2022, 2024).

CDA (2021) advocates the use of the cone of depression method when kinetic analysis such as MPM are not available. The results shown illustrate the potential to refine the cone of depression method by incorporating the back scarp angle, the post-failure surface slope and parameter h_f measured in column collapses. Refining the total released volume estimate with geotechnical parameters such as post-peak frictional angles or LUSSR in the true TSF geometry to estimate hydrographs.

More complex models like Nor-Sand, which can replicate the peak and liquefied strength, are alternatives suitable to improve mobilised volume estimated, but more difficult to readily implement due to the required information and budget to undertake such assessments. Fern and Soga (2016) present examples of Nor-Sand applications in the academic MPM column collapse context.

Strategies i - vii are available to practitioners looking to apply MPM to refine released tailings volume estimates. The strategies are shown and explained in order of complexity, starting with the simplest methodologies and proceeding to the most difficult. Strategies i and ii may be built up with complexity to include layering with each layer having distinct properties. These modelling strategies have seen great acceptance among stakeholders undertaking TDBA studies and have been used in the case series presented.

i) Column collapse to estimate post-failure surface slopes or backscarp angles for subsequent cone of depression volume estimates
ii) Column collapse to estimate post-failure surface slopes or backscarp angles, d_b and h_f for subsequent cone of depression volume estimates
iii) Collapse of the TSF cross-section with simplifying assumptions such as assigning the same LUSSR to tailings and embankment materials and an excavation boundary at the toe to quantify a hydrograph for subsequent hydraulic modelling for the run-out phase
iv) Collapse of the TSF cross-section with simplifying assumptions such as assigning the same LUSSR to tailings and embankment materials and modelling the run-out and deposition using MPM
v) Collapse of the TSF cross-section assigning LUSSR to tailings and residual strengths for embankment materials (this alternative has seen great acceptance between clients and engineers of record)
vi) Collapse of the TSF geometry in 3D with simplifying assumptions such as assigning the same LUSSR to tailings and embankment materials
vii) Collapse of the TSF geometry in 3D assigning LUSSR to tailings and residual strengths for embankment materials.

It is the authors view that with continuous market penetration of MPM in the tailings industry, we anticipate that models encompassing breach/failure triggering will begin to be utilised. Defined here as reproduction of a failure event that captures the transition from peak to residual/liquefied strengths due to an imposed loading condition such as seismic loading, increase in groundwater levels, lateral extrusion, creep settlement, etc. The development of hydrographs will increase as sufficient computational power becomes more readily available, enabling modelling of the run-out and tailings deposition. Specific scenarios where this may be applied include:

i) Breach/failure triggering of the TSF geometry in 3D using strain softening models such as Mohr-Coulomb with strain softening, Nor-Sand or similar, to replicate the peak to liquefied/residual state transition; see Arenas and Pereira (2024) and Saeedi et al. (2024)
ii) Breach/failure triggering of the TSF geometry in 3D using strain softening models to replicate the peak to liquefied/residual state transition and to model the potential breach width
iii) incorporation of ponding water on top of tailings to capture overtopping and embankment erosion. Some academic examples using Anura already exist; see Yang et al. (2019).

5 CONCLUSIONS

MPM as a modelling technique has been introduced and discussed as a tool for tailings practitioners in the industry to address some of the complex challenges faced when assessing risk. The development of MPM and some of available packages were highlighted. In addition to four examples of forensic studies that have employed MPM, six industry

projects (four 2D and two 3D) were briefly described, highlighting examples where MPMs usage was able to contribute to the outcomes of the project. The advantages of utilising industry standard geotechnical models within MPM are significant, while the computational effort and required expertise are the main drawbacks. Incorporating MPM into breach assessments and the various scenarios where this might be beneficial were highlighted as this aspect features heavily in most risk assessments.

Overall MPM represents a significant step towards modelling realistic scenarios that involve large strain, scenarios that we within the industry were previously not able to model efficiently. By closing the gap between modelled behaviour and actual behaviour the credibility of a failure mode can be investigated with more rigour and confidence. This interrogation of a failure mode occurring is critical for risk management of tailings facilities and feeds into FMEAs, emergency planning, category classification, breach assessments and much more. It is hoped that this paper will be beneficial to practitioners seeking to employ MPM within their projects going forward as we continue to move towards the GISTM goal of 'zero harm to people and the environment with zero tolerance for human fatality.'

CRediT authorship contribution statement

Marcelo Llano-Serna: Writing - original draft. **Scott Lines:** Writing – review and editing. **Nicolas Pereira:** Writing - original draft. **Seyedmohammadjavad Seyedan:** Writing - original draft. **Sudheer Prabhu:** Writing – review and editing. **Mike Liu:** Writing – review and editing.

6 REFERENCES

Adams, A., Brouwer, K., Robertson, P.K. and Martin, V. (2022). Evaluation of Tailings Behaviour for Dam Breaches. *Proceedings of Tailings and Mine Waste 2022*.

Arenas, A., and Pereira, N. (2024). Feijão Dam I 3D Numerical Simulation: A Comprehensive Approach, from Triggering to Dam Breach. *Proceedings of Tailings and Mine Waste 2024*.

Anura3D MPM Research Community (2025), *Anura3D Tutorial Manual version v2025*

Australian National Committee on Large Dams (ANCOLD) (2022). *Guidelines on Risk Assessment*.

Bardenhagen, S. G., & Kober, E. M. (2004). The generalized interpolation material point method. *Computer Modeling in Engineering and Sciences*, *5*(6), 477-496.

Blight, G. E., & Fourie, A. B. (2003, May). A review of catastrophic flow failures of deposits of mine waste and municipal refuse. In *International Workshop on occurrence and mechanisms of flow in natural slopes and earthfills*.

Canadian Dam Association (CDA) (2007). *Dam Safety Guidelines*

Canadian Dam Association (CDA) (2021). *Technical Bulletin: Tailings Dam Breach Analysis*

Chowdhury, K. H. (2018). Evaluation of the State of Practice Regarding Nonlinear Seismic Deformation Analyses of Embankment Dams Subject to Soil Liquefaction Based on Case Histories. University of California, Berkeley.

Concha Larrauri, P., & Lall, U. (2018). Tailings dams failures: updated statistical model for discharge volume and runout. *Environments*, *5*(2), 28.

Fern, E. J., & Soga, K. (2016). The role of constitutive models in MPM simulations of granular column collapses. *Acta Geotechnica*, *11*(3), 659-678.

Fernández, F, (2020). Modelagem numérica de problemas geotécnicos de grandes deformações mediante o método do ponto material. Pontifícia Universidade Católica de Rio de Janeiro, PUC-Rio, Rio de Janeiro, Brasil.

Global Tailings Review GTR (2020). *Global Industry Standard on Tailings Management (GISTM)*.

Ghahramani, N., Adria, D. A., Rana, N. M., Llano-Serna, M., McDougall, S., Evans, S. G., & Take, W. A. (2024). Analysis of Uncertainty and Sensitivity in Tailings Dam Breach-Runout Numerical Modelling. *Mine Water and the Environment*, *43*(1), 87-103.

Ghahramani, N., Chen, H. J., Clohan, D., Liu, S., Llano-Serna, M., Rana, N. M., ... & Take, W. A. (2022). A benchmarking study of four numerical runout models for the simulation of tailings flows. *Science of the Total Environment*, *827*, 154245.

Ghahramani, N., Mitchell, A., Rana, N. M., McDougall, S., Evans, S. G., & Take, W. A. (2020). Tailings-flow runout analysis: examining the applicability of a semi-physical area–volume relationship using a novel database. *Natural Hazards and Earth System Sciences*, *20*(12), 3425-3438.

Heller, V., Hager, W. H., & Minor, H. E. (2009). Landslide generated impulse waves in reservoirs: Basics and computation. *VAW-Mitteilungen*, *211*.

International Commission on Large Dams (ICOLD) (2022) *Bulletin 194 - Tailings Dam Safety*

Kumar, K., Salmond, J., Kularathna, S., Wilkes, C., Tjung, E., Biscontin, G., & Soga, K. (2019). Scalable and modular material point method for large scale simulations. In *2nd International Conference on the Material Point Method*. Cambridge, UK.

Llano-Serna, M. A., Farias, M. M., & Pedroso, D. M. (2016). An assessment of the material point method for modelling large scale run-out processes in landslides. *Landslides*, *13*, 1057-1066.

Llano-Serna, M. (2023). On the consequences of getting dam breach analysis wrong. *Friction. https://www.friction.news/news/on-the-consequences-of-getting-dam-breach-analysis-wrong*

Llano-Serna, M. A., Seyedan M.J., Hazard, J. (2024) A paradigm shift in geotechnical risk management: tailings dam breach analysis using material point method techniques for inactive and closed tailings storage facilities. *Australian Centre for Geomechanics.* https://acg.uwa.edu.au/2024/12/04/mine-closure-article-by-marcelo-llano-red-earth-engineering-a-geosyntec-company-mj-seyedan-geosyntec-consultants-jim-hazzard-itasca-consulting-group/

Lube, G., Huppert, H. E., Sparks, R. S. J., & Hallworth, M. A. (2004). Axisymmetric collapses of granular columns. *Journal of Fluid Mechanics*, *508*, 175-199.

Lube, G., Huppert, H. E., Sparks, R. S. J., & Freundt, A. (2005). Collapses of two-dimensional granular columns. *Physical Review E—Statistical, Nonlinear, and Soft Matter Physics*, *72*(4), 041301.

Martens, S. and Kupper, A. (2024). Credible Failure Modes: considerations for assessment and application. *Proceedings of Tailings and Mine Waste 2024*, Colorado.

National Academies of Science, Engineering and Medicine (NASEM) (2021). *State of the Art and Practice in the Assessment of Earthquake-Induced Soil Liquefaction and its Consequences*

Pierce, I. (2021). *Applying the Material Point Method to Identify Key Factors Controlling Runout of the Cadia Tailings Dam Failure of 2018* (Dissertation, Virginia Tech).

Purvance, M., & Coetzee, C. (2024). MPAC–Material Point Analysis of Continua. *Applied Numerical Modeling in Geomechanics -2024*

Robertson, P.K., de Melo, L., Williams, D.J., & Wilson, G.W. (2019). *Report of the expert panel on the technical causes of the failure of Feijão Dam I*, from http://www.b1technicalinvestigation.com/

Rico, M., Benito, G., & Diez-Herrero, A. (2008). Floods from tailings dam failures. *Journal of hazardous materials*, *154*(1-3), 79-87.

Rourke, H., & Luppnow, D. (2015). The risks of excess water on tailings facilities and its application to dam-break studies. *Tailings and Mine Waste Management for the 21st Century*, 225-230.

Saeedi, A., Martinelli, M., & Simms, P. (2024). Multi-model analyses of tailings impoundment failure and runout: part iii. *Proceedings of Tailings and Mine Waste 2024*.

Sołowski, W. T., Berzins, M., Coombs, W. M., Guilkey, J. E., Möller, M., Tran, Q. A., Adibaskoro, T., Seyedan, M., Tielen, R., & Soga, K. (2021). Material point method: overview and challenges ahead. In *Advances in Applied Mechanics*, *54*, 113-204.

Sulsky, D., Zhou, S.J. and Schreyer, H.L., 1995. Application of a particle-in-cell method to solid mechanics. *Computer physics communications*, *87*(1-2), pp.236-252.

Sulsky, D., Chen, Z. and Schreyer, H.L., 1994. A particle method for history-dependent materials. *Computer methods in applied mechanics and engineering*, *118*(1-2), pp.179-196.

Seddon, K. D. (2007, March). Post-liquefaction stability of thickened tailings beaches. In *Proceedings of the Tenth International Seminar on Paste and Thickened Tailings, Australian Centre for Geomechanics, Perth* (pp. 395-406).

Sadeghirad, A., Brannon, R. M., & Burghardt, J. (2011). A convected particle domain interpolation technique to extend applicability of the material point method for problems involving massive deformations. *International Journal for numerical methods in Engineering*, *86*(12), 1435-1456.

Seyedan, S., Arenas, A., & Llano-Serna, M. (2024). Advances in dam breach analysis appropriate for dewatered tailings storage facilities. In *Paste 2024: Proceedings of the 26th International Conference on Paste, Thickened and Filtered Tailings* (pp. 247-256). Australian Centre for Geomechanics.

Small, A., Küpper, A., Johndrow, T. and Al-Mamun, M.M. (2023). Credible Failure Modes: Summary of 2021 and 2023 Workshops. *Proceedings of Tailings and Mine Waste 2023*, Vancouver, 1245-1255.

Talbot, L. E., Given, J., Tjung, E. Y., Liang, Y., Chowdhury, K., Seed, R., & Soga, K. (2024). Modeling large-deformation features of the Lower San Fernando Dam failure with the Material Point Method. Computers and Geotechnics, 165, 105881.

United States Society on Dams (USSD) (2022). *Analysis of Seismic Deformations of Embankment Dams.*

Wallstedt, P. C., & Guilkey, J. E. (2008). An evaluation of explicit time integration schemes for use with the generalized interpolation material point method. *Journal of Computational Physics*, *227*(22), 9628-9642.

Yang, Y. S., Yang, T. T., Qiu, L. C., & Han, Y. (2019). Simulating the overtopping failure of homogeneous embankment by a Double-Point Two-Phase MPM. *Water*, *11*(8), 1636.

Zabala, F., & Alonso, E. E. (2011). Progressive failure of Aznalcóllar dam using the material point method. *Géotechnique*, *61*(9), 795-808.

FINITE ELEMENT MODELLING OF STATIC LIQUEFACTION TRIGGERING MECHANISMS AND EVALUATION OF FACTOR OF SAFETY

Jiaxi (Joshua) Chan[1], Qian Gu[2]

[1] *GHD Pty Ltd, Sydney;* [2] *GHD Pty Ltd, Perth*

https://doi.org/10.56295/AGJ6046

ABSTRACT

Static liquefaction risk is one of the major risks faced in Tailings Storage Facilities (TSFs), primarily due to the contractive and strain-softening nature of loosely deposited tailings. The safety margin against the triggering of static liquefaction is difficult to evaluate using conventional Limit Equilibrium Analysis (LEA), which considers either the peak or the residual strength (assuming liquefaction has triggered). In contrast, numerical methods such as Finite Element Method (FEM), offers deeper insight by capturing the full mobilisation process beyond failure, offering a more intuitive understanding of the available safety margin. This paper presents a case study of liquefaction triggering assessment conducted as part of the design process for a TSF.

Static liquefaction simulations in Plaxis commonly utilise static analyses with an automatic unloading approach to address strain-softening numerical issues. However, this unloading (strain-controlled) approach differs fundamentally from real-world load-controlled failure mechanisms. To more accurately capture load redistribution and failure propagation during liquefaction triggering, this study adopts dynamic analysis as a more realistic method for simulating progressive failure. This paper employs dynamic analyses to clearly visualise the disturbance thresholds associated with three triggering mechanisms: undrained surface surcharge, increase of phreatic level, and toe excavation. The stress-strain behaviour for each mechanism is examined in detail.

A new definition of Factor of Safety (FoS) is evaluated for each triggering mechanism, based on changes in both deviator stress (q) and mean effective stress (p') required to trigger failure and their equivalency around the instability ratio. This offers a dimensionless alternative (therefore less dependent on the TSF size) to the conventional threshold disturbances for assessing the adequacy of safety against liquefaction.

The analyses are based on the NorSand constitutive model developed within Critical State Soil Mechanics (CSSM), and the limitations of such analyses are also discussed.

1 INTRODUCTION

Static liquefaction has been identified as a major mechanism causing catastrophic failures of Tailings Storage Facilities (TSFs). Due to the complexity of triggering analysis for static liquefaction, the conventional approach is to conservatively assume liquefaction occurs, and then adopt the residual strength of the materials in Limit Equilibrium Analysis (LEA) against a low FoS target, such as 1.1. However, this approach overlooked the potential disturbing efforts required (the safety margin) to overcome the threshold for initiating the flow failure, potentially leading to excessive conservatism. In addition, the philosophy behind this approach is not consistent with the one widely adopted in seismic liquefaction triggering assessment, which is essentially just one of many potential triggering mechanisms. For the seismic case, the liquefied residual strength is only applied in the stability assessment if the seismic disturbance is considered sufficient to trigger failure. Despite significant uncertainties associated with the seismic triggering assessment (comparable to those in static mechanisms), ranging from uncertainties of seismic events to material behaviours, such seismic triggering assessments have been widely adopted in practice. As such, it is considered valuable to conduct static liquefaction triggering analyses despite the uncertainties and limitations that exist for such works.

Numerical analyses such as the Finite Element Method (FEM) or Finite Difference Method (FDM) with appropriate constitutive models, are capable of capturing the strain-softening process of contractive tailings and have been widely undertaken by numerous researchers and engineers (Arroyo, M. and Gens, A., 2021; Babaki and Tannant, 2024; Katebi and Li, 2024; Ortigao et al. 2024; Rivas et al. 2023; Rivarola et al., 2022; Rivarola and Tasso, 2024; Rógenes et al. 2025; Rousé, 2024; Shuttle et al., 2022; Sottile et al., 2020; Vargas-Moreno et al. 2023). Some of the most significant analyses were conducted during forensic investigations following major TSF failures (Jefferies et al., 2019; Morgenstern et al., 2016; Robertson et al., 2019), utilising software packages such as Plaxis and FLAC, along with constitutive models like NorSand and the Clay and Sand Model (CASM). FLAC, with its dynamic time-marching and artificial damping approach, is generally considered numerically more capable of handling the strain softening failure process than Plaxis, although the latter has greatly improved its capability since 2011 through the introduction of automatic unloading and arc-length

control. Plaxis features a highly user-friendly interface, which may contribute to its widespread adoption particularly among practicing geotechnical engineers, including the authors of this paper, for tasks such as static liquefaction triggering analyses (Arroyo, M. and Gens, A., 2021; Babaki and Tannant, 2024; Jefferies et al., 2019; Ortigao et al., 2024; Rivas et al., 2023; Rivarola et al., 2022; Rivarola and Tasso, 2024; Rógenes et al., 2025; Shuttle et al., 2022; Sottile et al., 2020; Vargas-Moreno et al. 2023).

Most of the Plaxis-based liquefaction triggering analyses referenced above are static simulations that rely on automatic unloading to capture strain-softening failure and post-failure behaviour. While it is numerically efficient, such an approach is essentially strain-controlled by reducing or reversing load increments to maintain equilibrium, which differs significantly from the real-world failure mechanisms that are typically load controlled (e.g. surface surcharge, phreatic level increase, etc.). This discrepancy in the simulation approach may introduce uncertainties in the load redistribution and the failure propagation, both of which are critical for identifying the triggering threshold. Rivarola and Tasso (2024) adopted the static fully-coupled analyses in order to capture the rate-dependent partial drainage during failure process. Without modelling the failure process dynamically, however, the timeframe of the failure process which affects the drainage conditions may not be simulated realistically. Considering that the progressive failure is inherently a dynamic process, the dynamic analysis approach adopted by this study is considered a more realistic method of simulating the liquefaction triggering process, which aligns with the approach published by the authors of this paper in 2020 (Gu and Chan, 2020).

To utilise triggering analyses as a design tool for the proposed TSF, a dimensionless Factor of Safety (FoS) against liquefaction triggering is considered important. While several researchers and engineers have proposed such approaches (Katebi and Li, 2024; Ortigao et al., 2024; Rógenes et al., 2025), notable inconsistencies remain in both the definitions and methodologies used to estimate FoS values. For example, Ortigao et al. (2024) used a built-in strength reduction method (c-phi') to estimate the FoS against liquefaction triggering, resulting in significantly higher values compared to those from the LEA. In the authors' view, this c-phi' reduction approach does not neither realistically simulates the triggering disturbing process nor considers the undrained conditions and is therefore unlikely to offer an appropriate estimation of FoS. Rógenes et al., (2025) suggested the use of the inverse of the ratio between η (mobilised stress ratio) andM_θ (critical state stress ratio) as a "local" FoS, which may be more indicative of the final post-failure condition than the actual triggering point of liquefaction. Using a ratio relative to the instability ratio, which has been proposed by some studies (e.g. Katebi and Li, 2024), may be analogous to adopting a peak shear strength in LEA and overlooking the progressive mobilisation of stress. In this study, a new definition for the Factor of Safety (FoS) in liquefaction triggering analysis is proposed as the stress ratio between the current stress condition and the mobilised condition at the point of triggering. This definition offers the advantage of being applicable across various triggering mechanisms, unlike some other alternative definitions, such as those based on critical height or gravity over the current values (Rógenes et al., 2025), which are not suitable for mechanisms involving toe excavation, foundation deformation, increase of phreatic condition, etc.

In this study, the NorSand constitutive model, first introduced by Jefferies (1993), was used in the analyses. The derivation of the NorSand parameters (including in-situ state parameters) was conducted through interpretation of both Cone Penetration Test (CPT) and laboratory triaxial testing, following the methodology outlined by Shuttle and Jefferies (1998). NorSand is based on fundamental concepts of the Critical State Soil Mechanics (CSSM), and it uses the state parameter (the difference between the void ratio and its critical value at the current stress) as a key controlling variable to effectively capture the strain-softening process of contractive tailings.

This study uses a TSF located at McArthur River Mine (MRM) as a case example to demonstrate the methodology of static liquefaction triggering analyses. In addition to the undrained surface surcharge triggering mechanism previously simulated by authors of this paper (Gu and Chan, 2020), triggering mechanisms of phreatic level increase and toe excavation are also presented in this study. The analyses were conducted using Plaxis 2D and incorporated the NorSand constitutive model calibrated via version 18 of Visual Basic for Applications (VBA) spreadsheet (Jefferies and Been, 2016). The embankment construction and tailings deposition stages before the liquefaction triggering were first modelled with static analyses in stages to establish realistic in-situ stress conditions. The static liquefaction triggering processes were then simulated by dynamic FEM.

2 BACKGROUND

MRM comprises two TSF cells, Cell 1 (northern) and Cell 2 (southern). The tailings slurry has been historically discharged from the embankment perimeter with the decant pond located at the centre of the cells. A typical cross-section of the TSF is presented in **Figure 1**, which comprises a starter dam and subsequent upstream raises. Two zones of tailings have been considered in the model based on the different densities interpreted from available investigation data. Although the mud farming technique has been recently implemented to improve the density of tailings above RL 10060 m, such improvement has not been considered in the model due to the lack of available data and for conservatism.

Two buttress configurations have been presented in **Figure 1**, namely the interim buttress (crest at RL 57 m) and the ultimate buttress (crest at RL 60 m), respectively. The configurations were established through LEA, with FoS of 1.6 (peak strength) and 0.9 (residual strength) for the interim buttress, and FoS of 1.9 (peak strength) and 1.1 (residual strength) for the ultimate buttress. The site has a low seismicity of 0.06 g Peak Ground Acceleration (PGA) at 1 in 10,000 Annual Exceedance Probability (AEP), and the interim buttress was found to provide sufficient stability under seismic conditions. In order to further clarify the risks of liquefaction triggering during the construction period when only the interim buttress has been completed (residual strength FoS< 1.1 target), the FEM triggering analyses were undertaken for undrained surface surcharge, phreatic level increase and toe excavations triggering mechanisms.

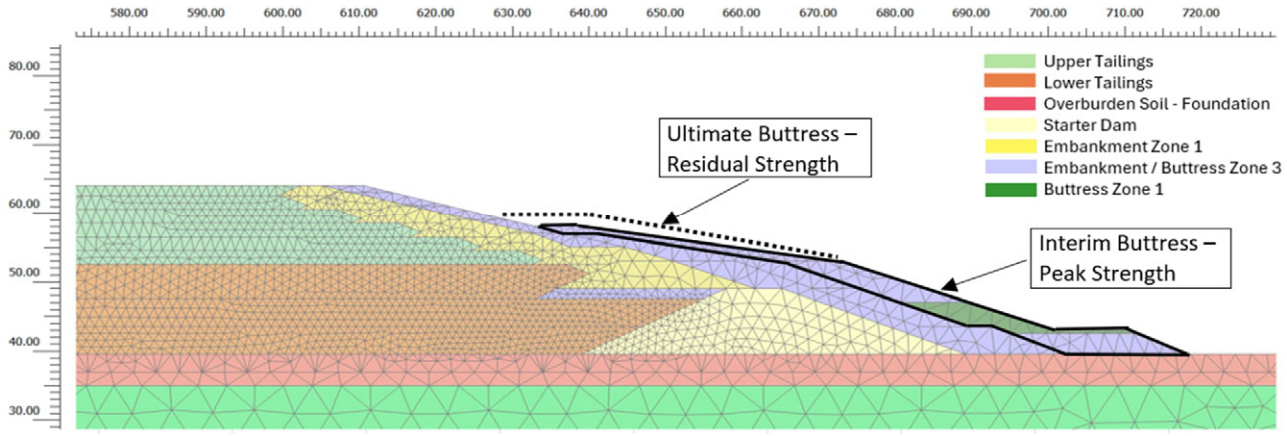

Figure 1: Typical cross section – TSF Cell 2 at MRM

3 MATERIAL PARAMETERS

3.1 TAILINGS MATERIALS

3.1.1 In-situ stress stage – Hardening Soil model

The tailings materials are generally classified as low-plasticity SILT with 70% to 85% fines, a plasticity index of 6 to 10, and a specific gravity (Gs) of 3.08 to 3.36. For the simulation stages before the liquefaction triggering process, the Hardening Soil (HS) model developed by Schanz et al. (2019) was used for the tailings materials due to its numerical stability in modelling the activation of tailing layers. The HS model parameters were selected based on the in situ and laboratory tests, as summarised in **Table 1**.

Table 1: HS soil parameters for tailings in pre-triggering stages

Material	Saturated unit weight (kN/m^3)	Effective friction angle (deg)	Effective cohesion (kPa)	$E'_{50, ref}$ (MPa)	$E'_{oed, ref}$ (MPa)	$E'_{ur, ref}$ (MPa)	Modulus dependency exponent m	Reference pressure (kPa)	K_0
Upper Tailings	23	34	0	2.5	3	9	0.6	100	0.65
Lower Tailings	23	34	0	1.5	1.5	4.5	0.6	100	0.60
Note	$E'_{50, ref}$ and $E'_{oed, ref}$ and E'_{ur} are the 50% strength Young's Modulus, Constrained Modulus and Unloading Modulus respectively, under 100 kPa reference effective confining pressure								

3.1.2 Triggering process – NorSand soil model

The Critical State Line (CSL) testing, comprising multiple undrained and drained triaxial compression tests on reconstituted samples, has been undertaken to obtain the parameters for the NorSand model (Jefferies and Been, 2016) as presented in **Table 2**. The parameters have been validated by comparing the numerically predicted undrained triaxial test results using the VBA spreadsheet (version 18) against the measured results, as shown in **Figure 2**.

It is worth noting that the G_{max} calibrated against the laboratory triaxial tests are consistently smaller (from 90% smaller in loose tests to 50% smaller for dense tests) compared to the shear wave velocity values measured from seismic CPTs. This is, however, consistent with the observations made by Shuttle and Jefferies (2016) and may be attributed to the strain rate and/or viscosity effects on the G_{max} calculated from seismic CPTs.

The in-situ State Parameters were adopted as 0.15 and 0.23 for upper and lower tailings based on the CPT results using the method recommended by Plewes et al. (1992) as shown in **Figure 3** (left). The 75th percentile of the State Parameter value was adopted. The estimated NorSand parameters have also been used in simulating 1D consolidation tests to estimate the K_0 values, which are generally within the range of values (0.5-0.7) adopted by panel reviewers for other TSF projects (Reid et al., 2021). The relationship between instability stress ratios and the state parameters was also computed from the Norsand VBA code, as shown in **Figure 3** (right).

Table 2: NorSand parameters for tailings

Material	Slope of CSL, λ_{10}	Reference void ratio Γ	Critical state q/p' ratio M_{tc}	Volumetric coupling, N	Dilatancy coefficient χ	Plastic hardening modulus H_0	Rate of change in hardening modulus H_ψ	G_{max} at 100 kPa (MPa)	Dependency exponent of G_{max}	Over-consolidation Ratio (OCR)	Softening parameter S	State parameter ψ
Upper Tailings	0.26	1.40	1.41	0.22	4.0	91	720	1.77	0.6	1.0	1.0	0.15
Lower Tailings	0.26	1.40	1.41	0.22	4.0	91	720	1.11	0.6	1.0	1.0	0.23

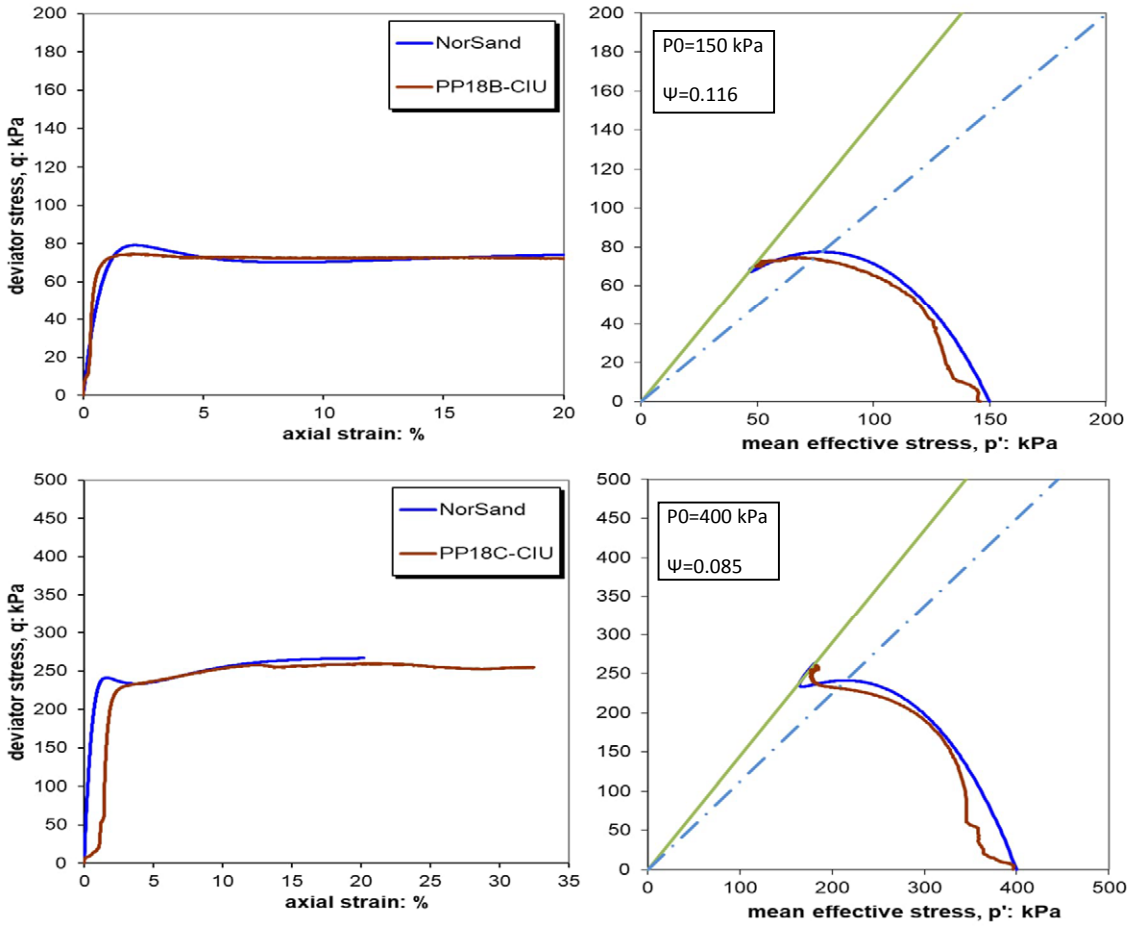

Figure 2: Undrained triaxial results from NorSand (Jefferies and Been, 2016 – version 18) against the measured data

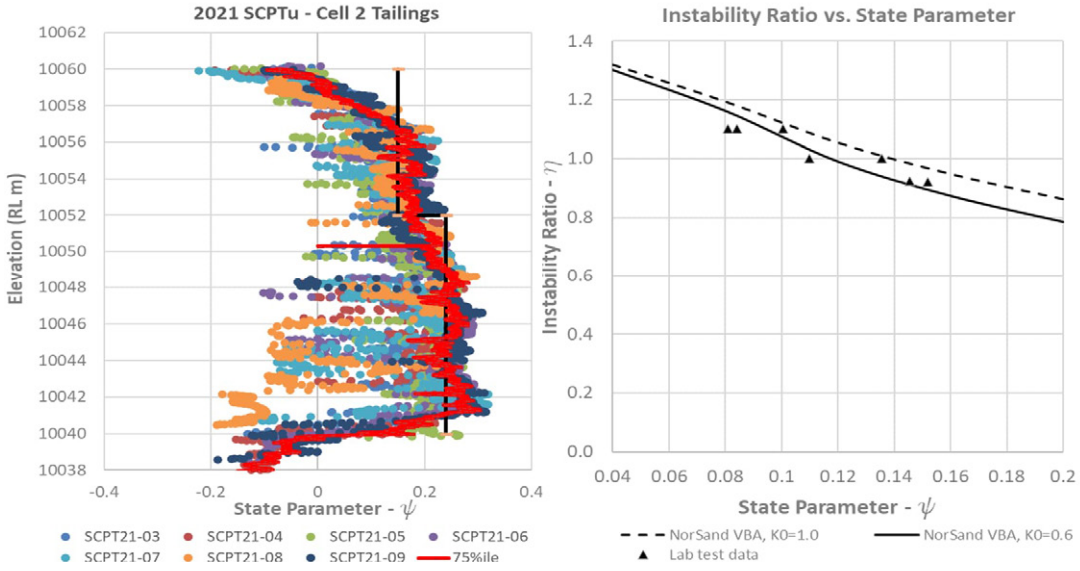

Figure 3: State parameter inferred from CPT (left) and instability ratio versus state parameters (right)

3.2 OTHER MATERIALS

The embankment and foundation materials are simulated with the Hardening Soil model (Schanz et al., 2019), for which the parameters are summarised in **Table 3**. The parameters are estimated from either geotechnical investigation information or material selection and construction specifications.

Table 3: Non-tailings material parameters

Material	Bulk unit weight (kN/m)	Effective friction angle (deg)	Effective cohesion (kPa)	$E'_{50,ref}$ (MPa)	$E'_{oed,ref}$ (MPa)	$E'_{ur,ref}$ (MPa)	Modulus dependency exponent m	Reference pressure (kPa)
Embankment / Buttress - Zone 1	20	33	0	30	30	90	0.5	100
Starter Dam	20	28	0	30	30	90	0.5	100
Embankment / Buttress – Zone 3	21	40	0	50	50	150	0.5	100
Overburden Soil – Foundation	21	28	0	20	20	60	0.5	100

3.3 DAMPING RATIO

The viscous Rayleigh Damping has been adopted to avoid eternal oscillation. A Rayleigh Damping ratio of 5% at two discrete frequencies of 0.1 Hz and 1 Hz, has been applied in all materials in the dynamic triggering analyses. The exact values of the damping ratio in the triggering analyses, however, are considered to have minor significance because the analyses are more about finding the thresholds between stable (static) and dynamic (failure) conditions, rather than accurately capturing the post-failure velocity and run-out distance, etc.

3.4 PHREATIC CONDITIONS BEFORE TRIGGERING

The pore pressure conditions of the tailings used in the FEM analysis were established by simulating the consolidation process during staged tailings deposition, as illustrated in **Figure 4**. Given that the decant pond is located over 500 meters away and the foundation is relatively permeable (10^{-6} to 10^{-8} m/s) compared to the tailings material (10^{-8} to 10^{-9} m/s), the pore pressures observed within the tailings are likely attributable mainly to consolidation effects.

Multiple suites of piezometer data and CPT dissipation test results were available within the tailings at various chainages along the embankment wall, with the representative locations shown in **Figure 4**. The maximum measurements from each suite at various chainages were superimposed in **Figure 4** for comparison. The simulated pore pressure conditions within the tailings were generally conservative relative to the piezometer measurements, and the contours were broadly consistent with the expected downward drainage behaviour.

The high pore pressure within the starter dam was caused by the high phreatic line adopted at the toe for conservatism due to the lack of piezo data here at the time of the analysis, and the historical proximity of the pond to the embankment 12 years ago at a lower elevation. The recent piezo readings have indicated negligible pore pressure at this location, confirming the conservatism. Phreatic line for the foundation was also conservatively adopted at the foundation surface level (RL 40 m).

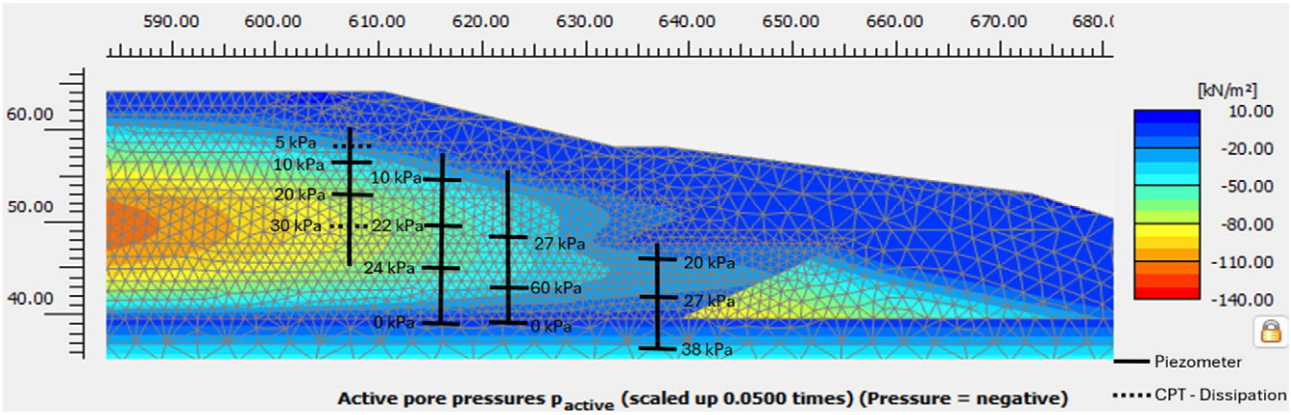

Figure 4: Pore pressure condition of tailings before the triggering process

4 TRIGGERING MECHANISM 1 – UNDRAINED SURFACE SURCHARGE

4.1 METHODOLOGY OF MODELLING

For this triggering mechanism, the procedure followed the methodology provided by the authors of this paper published in 2020 (Gu and Chan, 2020). A series of undrained surface surcharge stages, as shown in **Figure 5**, was modelled by dynamic analysis without considering the consolidation. The surcharge was increased in multiple stages and applied over the whole upper surface of the tailings. For each stage, the pressure was ramped up linearly by 10 kPa at a rate of 1 kPa per second and then held constant for 50 seconds for each stage. The duration of the constant pressure stages was selected to be adequately long to minimise any dynamic oscillations while still limiting the model run time to a manageable level.

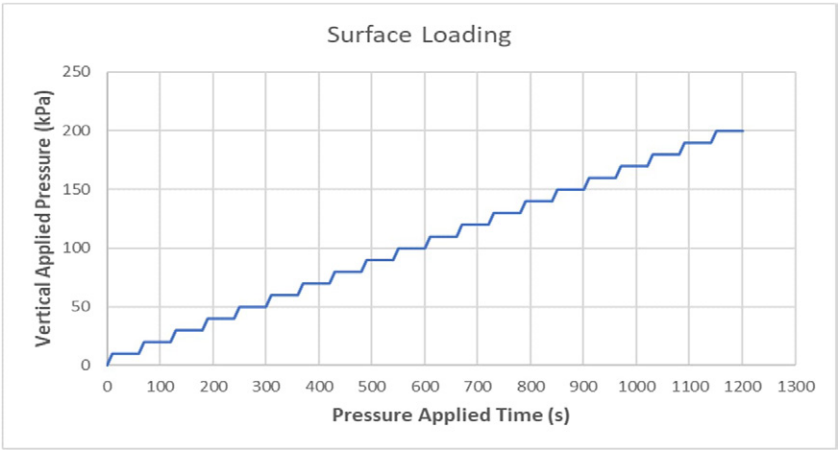

Figure 5: Time history of undrained surface disturbance pressure

To capture the failure process, multiple output points were selected along the downstream embankment surface, referenced by embankment elevation levels, to monitor the displacement. Four of these output points, which are discussed in the subsequent results, are indicated exclusively in **Figure 6**. Slip circles have also been selected along the surfaces defining the boundary of the instability zone (indicated by the concentration of shear strain) to visualise stress paths and shear resistance under different undrained surface loadings.

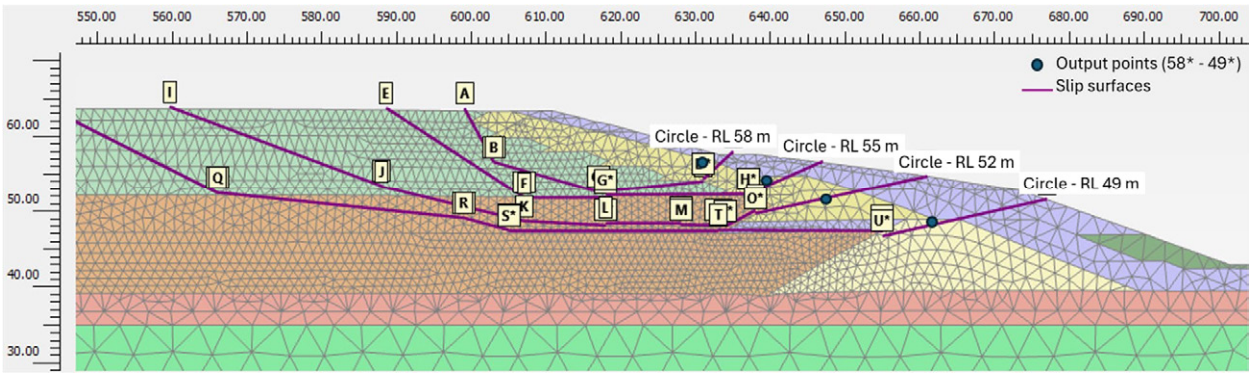

Figure 6: Cross-section with locations of slip circles and output points at different levels (RL 64 to 45 m)

4.2 THRESHOLD TRIGGERING FAILURE – UNDRAINED SURFACE SURCHARGE

Triggering of failures at different elevations can be visualised clearly by the abrupt increases of displacement and non-zero velocity under a constant stage of surface surcharge. The corresponding surface pressure that starts to cause such instability is interpreted as the threshold pressure triggering liquefaction failures. Displacement at each output point along the embankment surface is presented in **Figure 7**. The thresholds of surface surcharge versus elevation of the failure surface (exit point at embankment surface) are shown in **Figure 8**. The minimum triggering pressure is estimated to be 70 kPa for shallow slip surfaces and increases with the depth of the failure surfaces.

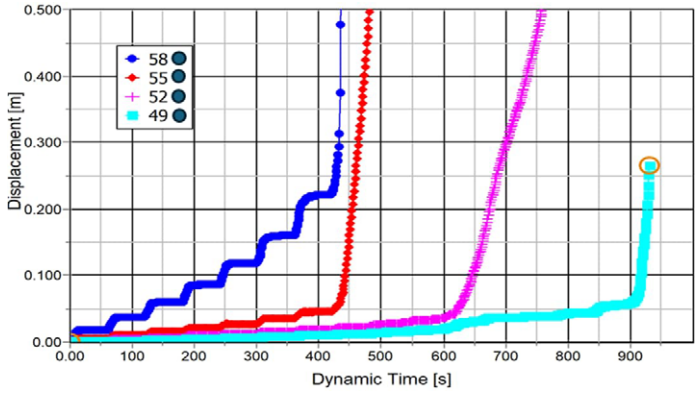

Figure 7: Displacement under different surface surcharge loads

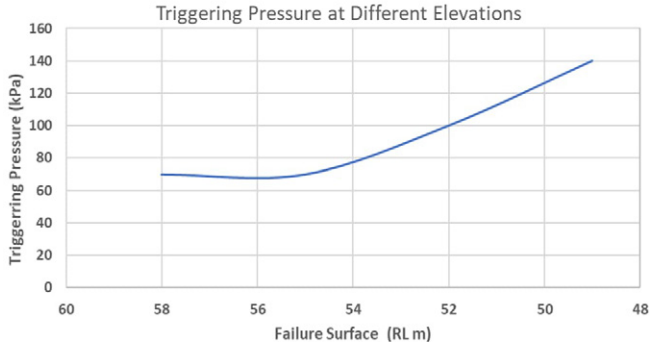

Figure 8: Threshold triggering surface surcharge vs. elevation of failure surface

4.3 STRAIN SOFTENING AND PROGRESSIVE FAILURE

To illustrate the strain softening and progressive nature of the failure caused by undrained surface surcharge, the deviator stress versus effective mean stress paths (q-p') and deviator stress (q) versus shear strain along "slip circle - RL 58 m" (location indicated in **Figure 6**) are presented in **Figure 9**. The following can be seen from the figures:

- At the completion of the drained embankment raise and tailing deposition stages, the q/p' stress ratio (η) is lower than the instability stress ratio (the ratio between peak undrained q and the corresponding p'), which is around 0.8, as expected for the embankment in a stable condition.
- Under the undrained surface loading triggering process, the mobilised q/p' stress ratio (η) increases significantly, accompanied by the consistent reduction of p' (suggesting increasing excess pore pressure), resulting in the q-p' path swerving sharply toward the Instability Line (the collapse line at the peak strength introduced and used by authors (e.g. Lade and Pradel, 1990; Ishihara, 1993; Chu and Leong, 2002; Lade and Yamamuro, 2010);
- Once the tailings are loaded beyond the instability ratio, strain softening starts, with the deviator stress (q) reducing while shear strain continues to increase, both towards the critical state condition.

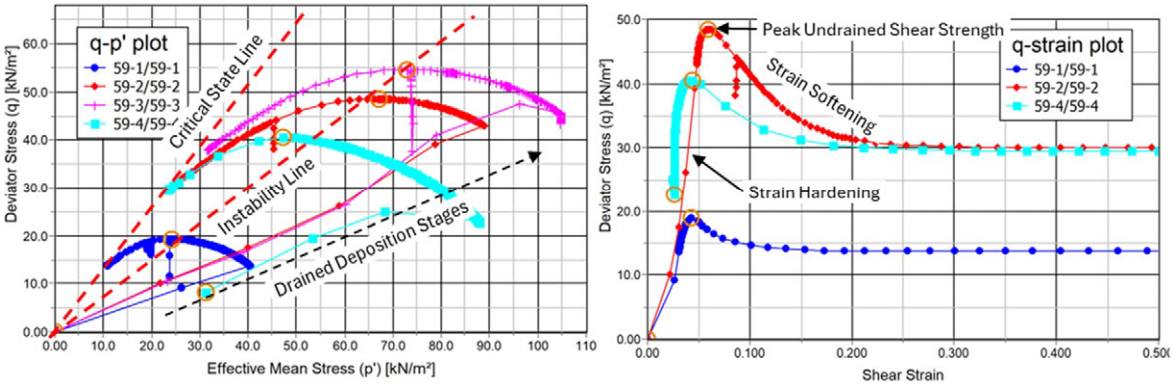

Figure 9: q-p' plot (left) and q-strain plot (right) along "circle - RL 58 m"

Figure 9 shows the development of strain-softening at the element level. The evolution of the strain-softening towards the critical state in the embankment can be visualised with the q/p' stress ratio (η) normalised against the critical state friction ratio (M), with values of 1 representing the critical state. **Figure 10** shows the development of the softening zones during the undrained triggering process using the interim buttress configuration.

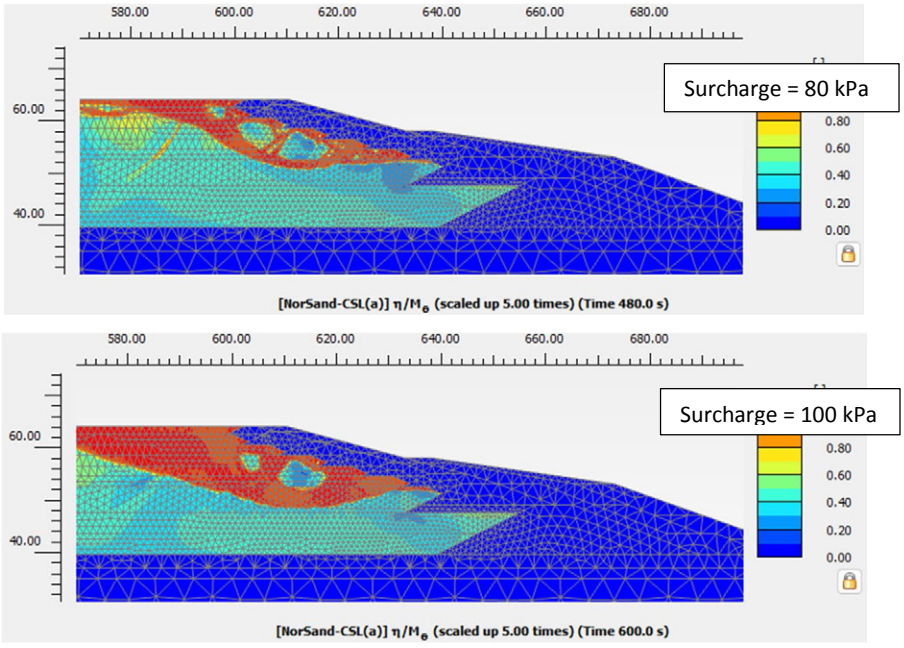

Figure 10: Evolution of softening zones within increasing surface surcharge

5 TRIGGERING MECHANISM 2 – INCREASE OF PHREATIC LEVEL

5.1 METHODOLOGY OF MODELLING

Increases in phreatic level behind the embankment, although by nature a drained process, may result in a gradual reduction of p' and shear strength towards and beyond the instability line, leading to the triggering of a brittle undrained failure. Such failures can be more abrupt compared to those induced by the surface loading described in the preceding sections, due to the lack of loading increase before failure that is usually accompanied by some precursory strain/deformation increase. This mechanism has been modelled as below.

The current NorSand model implemented in Plaxis 2D (version 2024.2) does not have the inner cap to capture the drained "unloading" contraction process and therefore cannot predict undrained liquefaction even with the stress state above the instability limits. The current study has instead adopted the Hardening Soil model during the drained phreatic level increase (which results in a stress state above the instability limit). The simulation was then switched to NorSand (so that the stress state was on the yield surface rather than inside it) to capture the undrained liquefaction failure. A Constant Shear Drained (CSD) element test was simulated in Plaxis to illustrate the above process, clearly demonstrating the capturing of liquefaction triggered as the mobilised q/p' stress ratio approached approximately 0.7 (**Figure 11**).

The insertion of **Figure 11** also shows that the dynamic analysis captured the full liquefaction process towards CSL, while the static one stopped soon after the failure started, as expected. This is one of the main reasons for adopting dynamic analyses in this study.

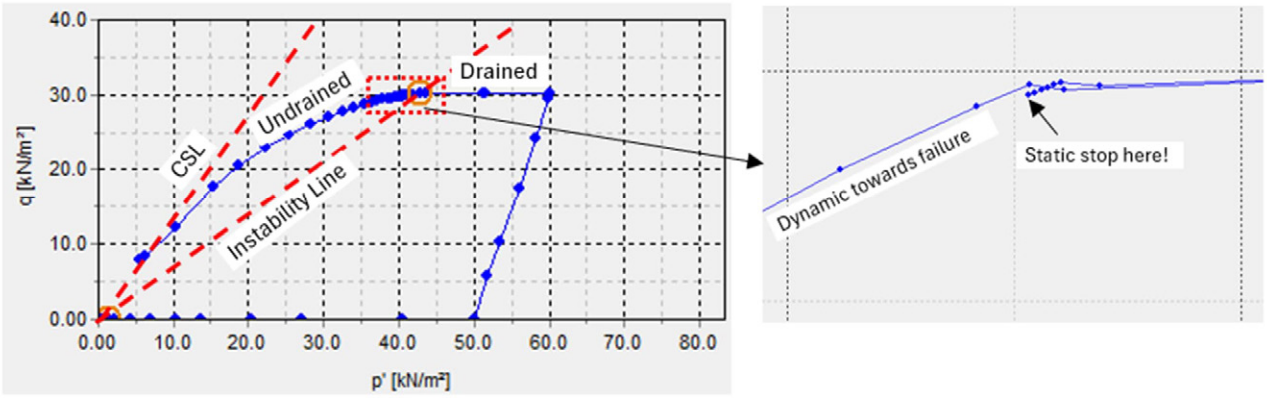

Figure 11: Element test simulated in Plaxis to illustrate unloading triggering process

In the global modelling, embankment construction and tailings deposition were the same as the static loading stages in mechanism 1. The subsequent triggering was then simulated by gradually raising the phreatic lines in multiple drained stages until it reached the upper surface of the tailings, as shown in **Figure 12**. Each raise was followed by a dynamic undrained stage using NorSand to check whether a liquefaction failure had been triggered.

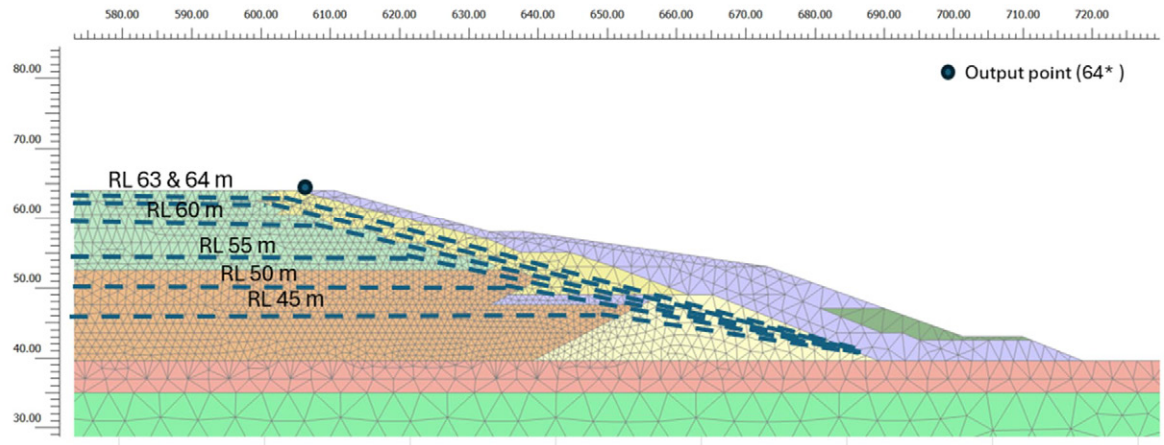

Figure 12: Increased phreatic levels to the top of TSF

5.2 THRESHOLD TRIGGERING FAILURE – PHREATIC LEVELS

The onset of liquefaction failure can be clearly visualised by the forming of a shear zone within which the displacement increases abruptly (with non-zero velocity) with the phreatic level held constant. The calculated resultant displacements from the undrained dynamic analyses corresponding to various phreatic line elevations are shown in **Figure 13**, indicating that a liquefaction failure is triggered when the phreatic level reaches RL 64 m.

The shear failure surface (indicated by the concentrated shear strain and the high stress ratio values) triggered by the phreatic level at RL 64 m is shown in **Figure 14** and **Figure 15**. Output points have been selected along the shear failure surface to capture the stress-strain behaviours prior to, during and after the triggering of the failure.

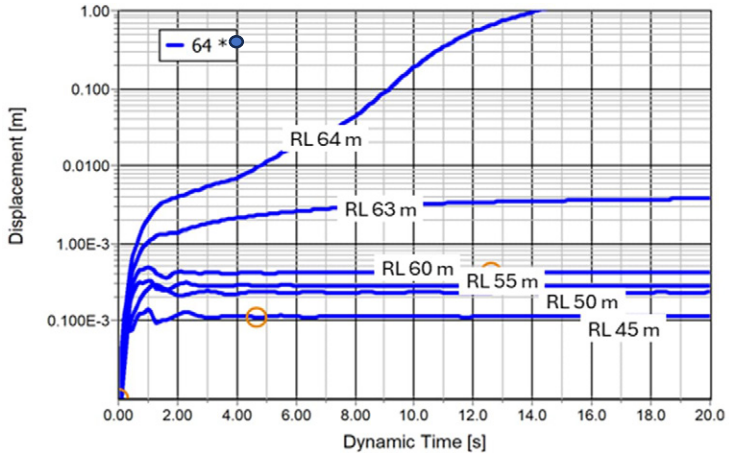

Figure 13: Dynamic displacement vs. phreatic line elevation

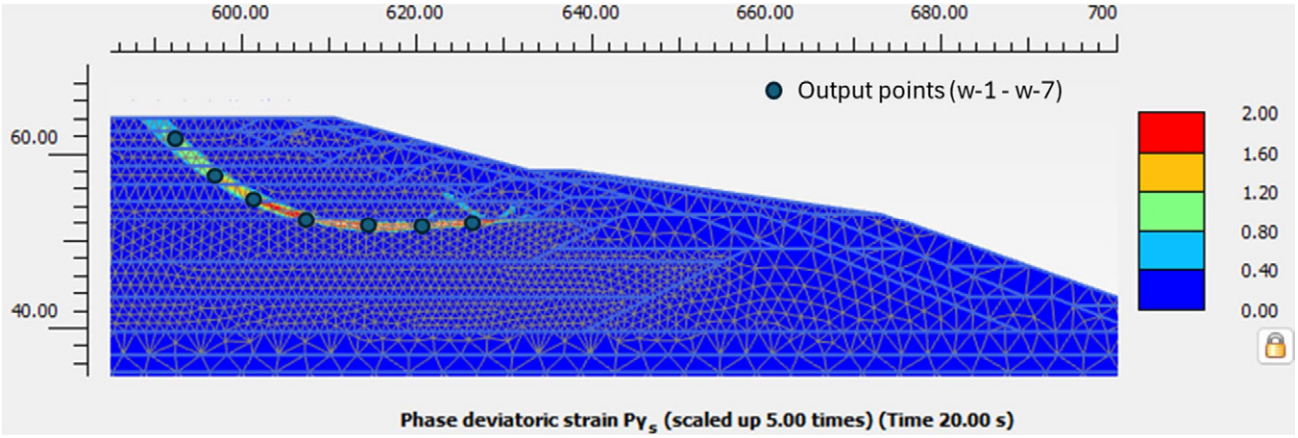

Figure 14: Concentrated shear strain defining failure surface when the phreatic line is raised to RL 64 m

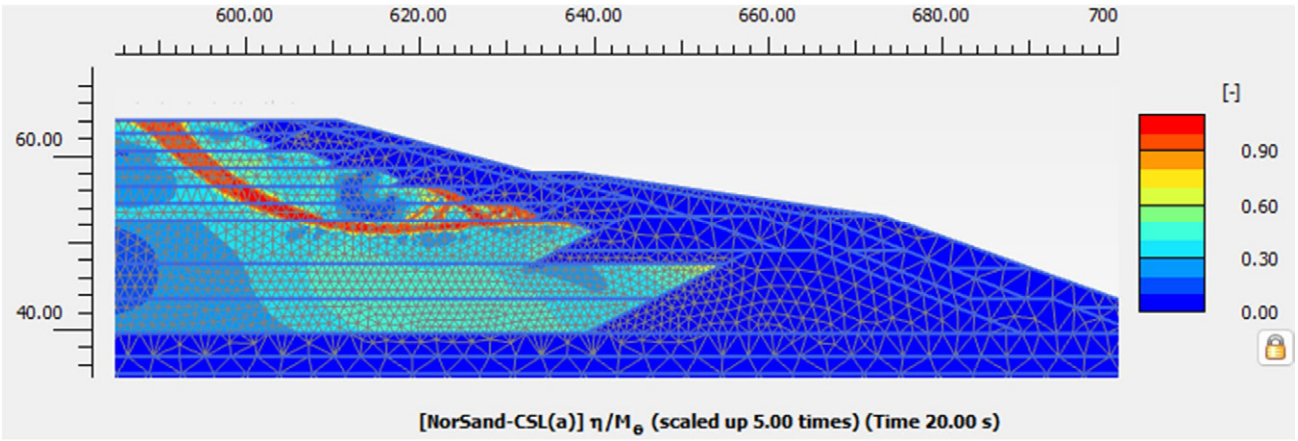

Figure 15: Stress ratio (η) against the critical state friction ratio (M) when the phreatic line is raised to RL 64 m

5.3 STRAIN SOFTENING AND PROGRESSIVE FAILURE

Similar to the surface surcharge triggering mechanism, the strain softening and progressive failure can be illustrated at the element level by examining the q-p' stress path and deviator stress (q) -strain behaviours along the failure surface, as shown in **Figure 16**. As can be seen, the increase of phreatic level results in a reduction of the mean effective stress (p'), accompanied by a mostly reduction in deviator stress q, suggesting an unloading triggering mechanism. The q versus shear strain curves show extreme brittleness of such failures, with almost no noticeable strain increase during the phreatic level rise, and instantaneous failure when the undrained dynamic mode was switched on. This failure mechanism is much more brittle compared to the undrained surface surcharge failure (**Figure 9**).

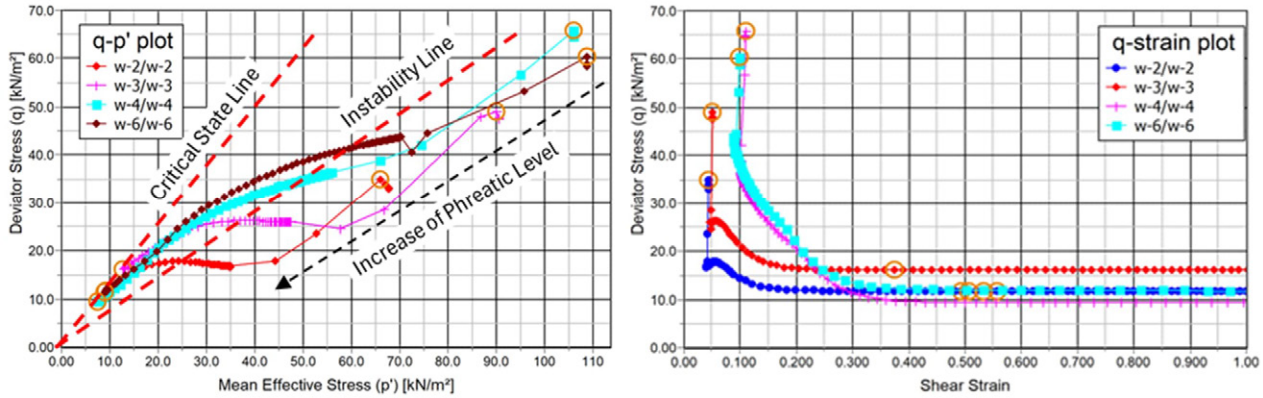

Figure 16: q-p' plot (left) and q-strain plot (right) for increased phreatic level triggering mechanism

6 TRIGGERING MECHANISM 3 – TOE EXCAVATION

7.1 METHODOLOGY OF MODELLING

Toe excavation may be required during foundation preparation works for the buttress, and the potential risk of triggering liquefaction failure by this mechanism is also evaluated using the numerical simulation. The modelling of the pre-triggering stages was the same as that discussed in previous mechanisms. The subsequent triggering was then simulated by removing the toe foundation clay layer in 1.5-meter depth intervals with an assumed batter slope of 1V:2H, as shown in **Figure 17**. A dynamic, undrained analysis stage was modelled following each stage of excavation, to check whether a failure had been triggered.

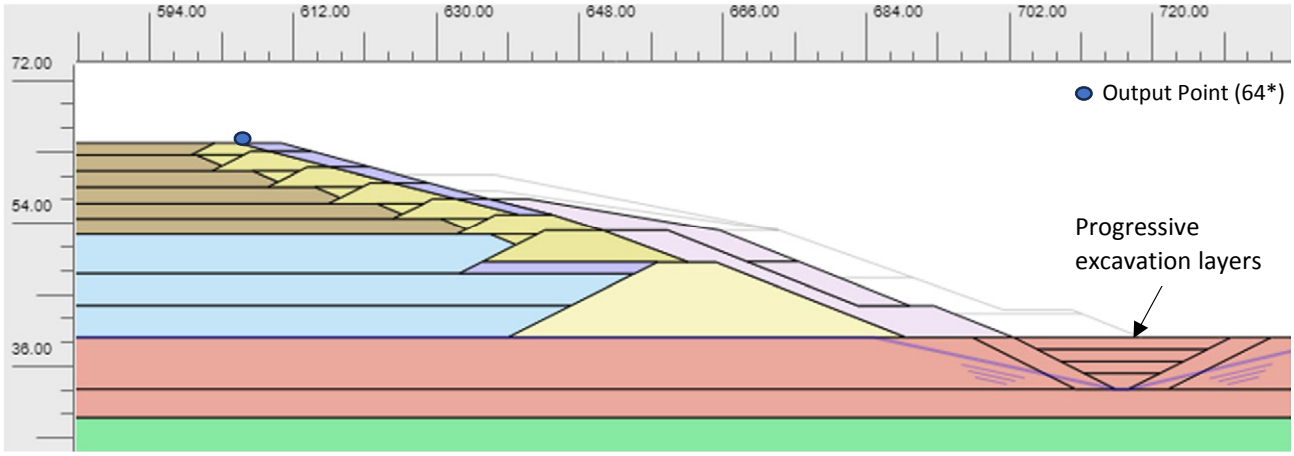

Figure 17: Toe excavation stages modelled

6.2 THRESHOLD TRIGGERING FAILURE – TOE EXCAVATION

The toe excavation mechanism in the foundation clay layer was found unable to trigger liquefaction failure due to shallow bedrock in the MRM TSF. For the purpose of illustrating the excavation triggering mechanism here, the foundation clay strength (governed by effective friction angle) has been artificially reduced from 28 degrees to 17 degrees, and the thickness increased to 10 m. As such, the results presented below are not representative of the actual conditions at MRM and potential softening behaviours of some clayey materials are also not the focus of this analysis.

The onset of liquefaction failure can be visualised by the displacement at the crest of the dam (RL 64 m) increasing abruptly (with non-zero velocity) in the dynamic analyses when the excavation depth reaches 6.5 m (**Figure 18**). The shear failure surface triggered by the toe excavation to 6.5 m is shown in **Figure 19** and **Figure 20** indicated by the concentrated shear strain and high stress ratio, respectively. A few stress points have been selected along the shear failure surface within the tailings material to illustrate the stress-strain behaviour prior to, during and after the triggering of the failure.

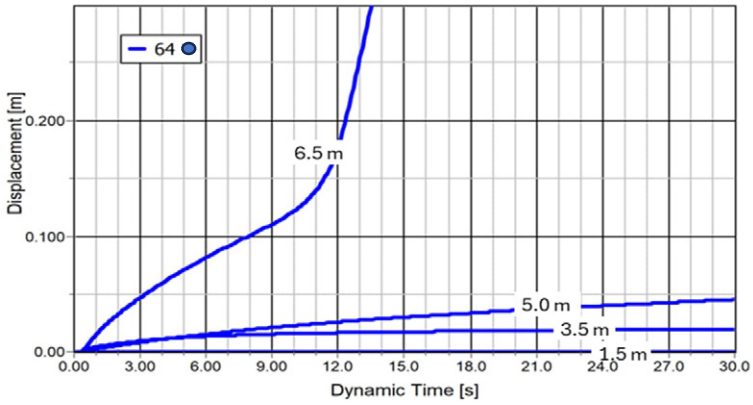

Figure 18: Dynamic displacement at crest (RL 64 m) vs. excavation depths

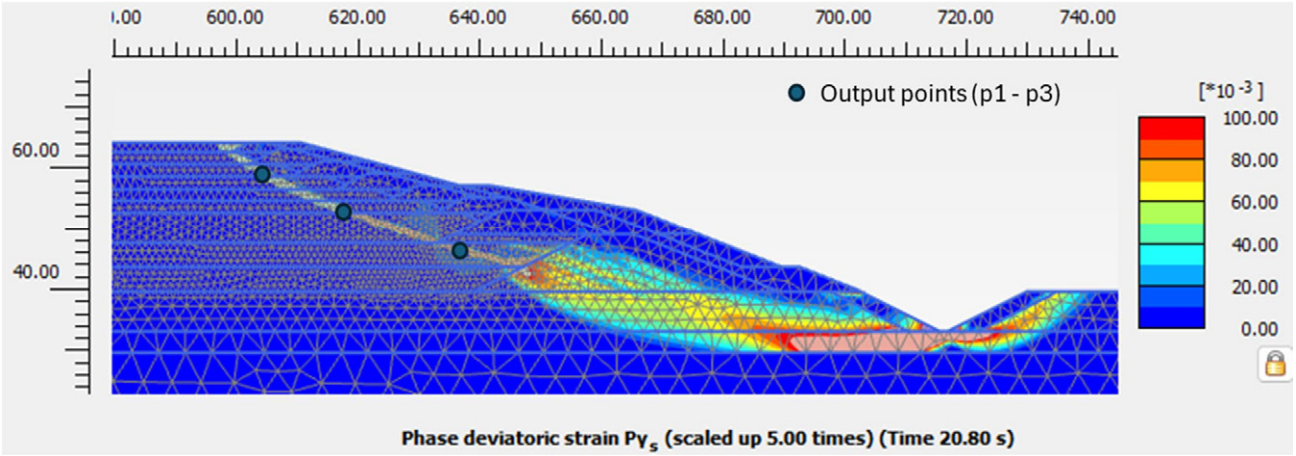

Figure 19: Concentrated shear strain defining the failure surface when the excavation depth reached 6.5 m

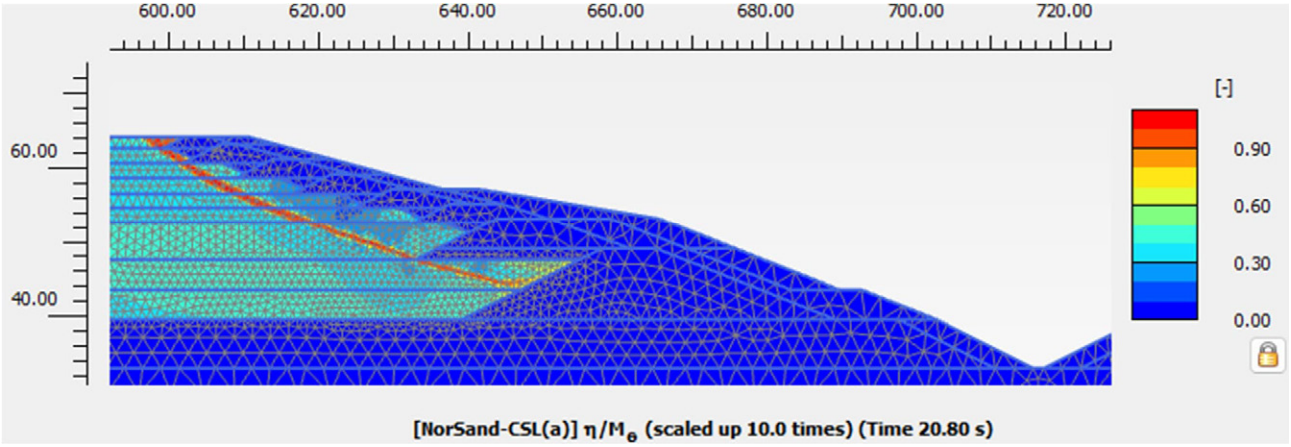

Figure 20: Stress ratio (η) against critical state friction ratio (M) when the excavation reached 6.5 m

6.3 STRAIN SOFTENING AND PROGRESSIVE FAILURE

The strain softening and progressive failure process can be illustrated at the element level by looking at the stress path and stress-strain behaviours calculated at locations along the failure surface (**Figure 21**). The toe excavation results in a slight reduction of the effective mean stress (p'), accompanied by increasing deviator stress q, pushing the q/p' stress ratio higher toward and beyond the Instability Line. Based on the pre-failure shear strain values, the toe excavation triggering seems less brittle than the phreatic level increase triggering, but more brittle than the surface surcharge one.

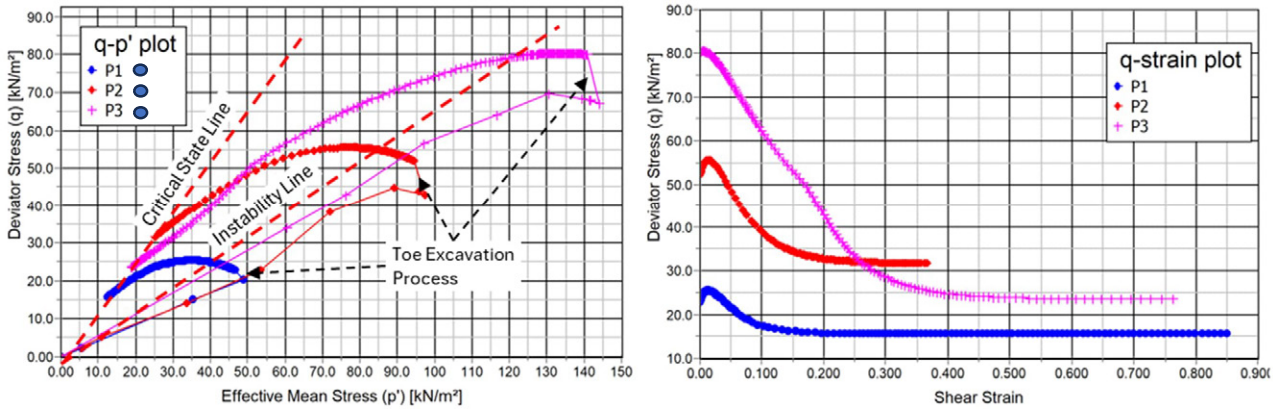

Figure 21: q-p' plot (left) and q-strain plot (right) for the excavation to 6.5 m

7 FACTOR OF SAFETY (FoS) FOR TRIGGERING

7.1 FOS VS. THRESHOLD

The preceding sections identified the threshold disturbance levels required to trigger liquefaction by different mechanisms. Although such threshold levels provide direct insight into available safety margins, one of the obvious disadvantages is their dimensional nature, expressed in units such as kilopascals for surcharge pressure, metres for the phreatic level increase and excavation depth. As a result, the same triggering disturbances do not reflect the equivalent safety margin for embankments with different scales. For example, a 5 m phreatic level increase to trigger failures implies a significantly greater safety margin for a small 5 m high embankment than for a 50 m high dam. Moreover, comparing safety levels across different mechanisms become impossible using dimensional values alone. To enable consistent evaluation of safety margins across varying TSF geometries and failure modes, a dimensionless term, such as FoS, widely adopted for LEA, needs to be defined for the FEM triggering assessment.

7.2 DEFINITION OF FOS FROM FEM TRIGGERING MODELLING PERSPECTIVE

In LEA, the FoS is simply defined as the ratio of the available resistance (strength) to the disturbing force (force) with the strength treated as a direct input parameter that remains independent to different triggering mechanisms. In contrast, for triggering assessment using FEM, the "strength" is not a direct input parameter anymore, but a result of stress-strain response controlled by the adopted effective stress parameters and the magnitude of the disturbing force imposed by different triggering mechanisms. Also, failures can be triggered not only through the loading process but also via the unloading process, where deviator stress q' reduces to trigger failure (e.g. **Figure 16**). Therefore, a new approach is proposed to estimate the FoS value for various liquefaction triggering mechanisms within FEM analyses.

The fundamental concept to derive the FoS was similar to the evaluation of safety margin to liquefaction using the instability line (e.g. Lade and Pradel, 1990; Ishihara, 1993; Chu and Leong, 2002; Lade and Yamamuro, 2010). However, unlike element-level evaluations, the FoS in this study was estimated at the average level of the slip surface. The FoS can be defined as the ratio of the available resistance (strength) to the current shear stress acting along the slip surface, as shown below.

$$FoS = \frac{R_0}{q_0} = \frac{p'_0\eta}{q_0} = \frac{p'_o\eta}{q_o} \times \frac{\frac{p'_f}{p'_f}}{\frac{q_f}{q_f}} = \frac{p'_f\eta}{q_f} \times \frac{\frac{p'_0}{p'_f}}{\frac{q_0}{q_f}} \quad \text{Eq. (1)}$$

At the failure point located on the instability line:

$$\frac{p'_f \eta}{q_f} = 1 \qquad \text{Eq. (2)}$$

The equation (1) can become:

$$FoS = \frac{p'_0}{p'_f} \cdot \frac{q_f}{q_0} \cdot \qquad \text{Eq. (3)}$$

In which:

- R_0 is resistance as defined in LEA, the deviator stress on the instability line at p'_0
- q_0 is the current deviator stress
- p'_0 is the current mean effective stress
- η is the q/p' ratio of the instability line defining the peak shear strength
- q_f is the mobilised deviator stress at the failure-triggering moment
- p'_f is the mobilised mean effective stress at the failure-triggering moment

The definitions of the above parameters are illustrated in **Figure 22** below.

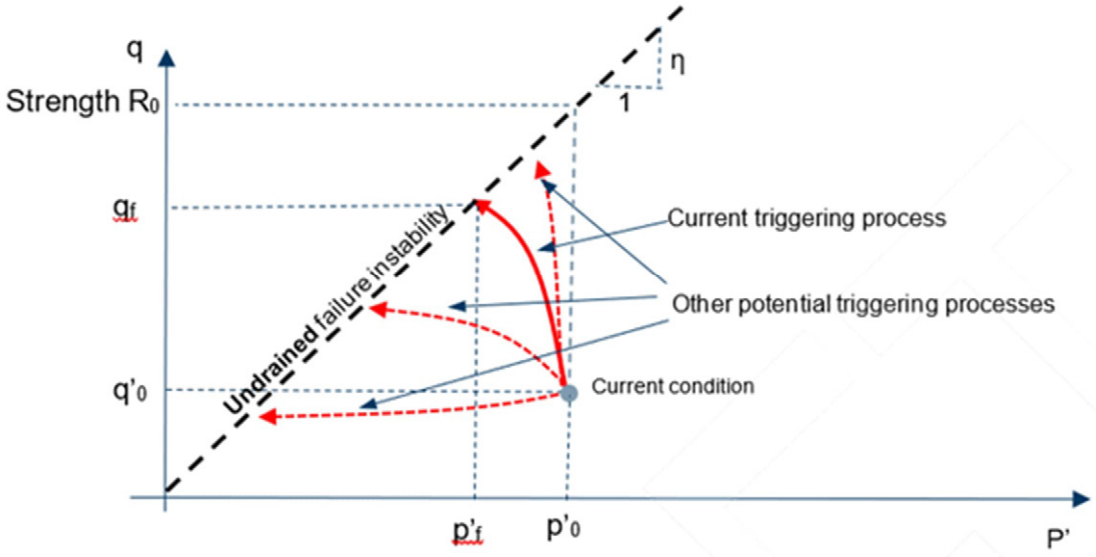

Figure 22: Schematic illustration of the meaning of parameters in Eq. (1)

Compared to the triggering analyses, the LEA defines FoS as the ratio of "shear strength" to the current shear stress without explicitly considering the change in effective stress (from p'_o to p'_f), i.e., FoS = $\frac{q_f}{q_0}$ and $\frac{p'_o}{p'_f}$=1. The "strength" (q_f) is an input parameter based on the initial effective stress (p'_o). As the LEA cannot capture shear-induced changes in effective stress p', (i.e. p'_f not computed), the effect of such changes on strength must be represented indirectly through varying strength ratios ($\frac{q_f}{p'_0}$) to reflect different stress paths. In contrast, FEM-based triggering assessment explicitly consider the evolution of effective stress p' (i.e. $\frac{p'_o}{p'_f} \neq 1$) enabling the FoS computed directly from changes of deviator stress (q) and effective mean stress (p') as outlined in Eq. (3).

When failure occurs along the whole slip surface, this definition of FoS can be applied in an average sense. The average deviator stress (q) and effective mean stress (p') can be obtained along the slip surface from the stress outputs of the FEM model. Observations indicate that the stress states of different locations at the moment of triggering failure were either above or below the instability line, which is because of the progressive nature of the failure that some points had already mobilised beyond the peak strength (crossing the instability line) while others were still undergoing hardening towards it.

7.3 FOS AGAINST STATIC LIQUEFACTION TRIGGERING MECHANISMS

Based on the above discussion and Eq. (3), FoS against surface surcharge triggering mechanisms along the embankment height are shown in **Figure 23**, together with FoS values obtained from LEA. The following can be seen from the figure:

- As expected, the FoS from triggering analyses are well within the range of the values estimated from LEA using peak and residual shear strength values.
- A general trend of FoS obtained from the triggering analysis is consistent with the LEA analysis with the lowest FoS of 1.4 obtained for slip surface daylighting the embankment elevation around RL 55 m.

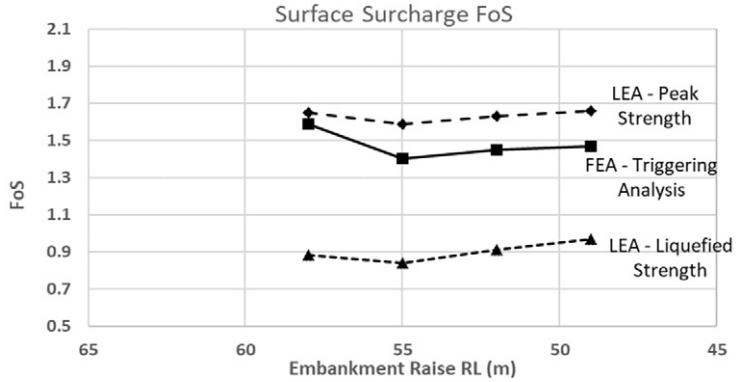

Figure 23: FoS vs embankment RL - surface surcharge mechanism

In terms of the increased phreatic level mechanism, liquefaction failure was found to be triggered when the phreatic line was elevated to RL 64 m. The corresponding slip surface daylighting at the embankment raise at RL 58 m and its FoS against triggering was calculated to be approximately **1.46**. For the same slip surface, FoS values estimated from LEM using peak strength and liquefied strength are 1.60 and 0.88, respectively. This FoS value estimated from the FEM is found to be similar to the one estimated from the surface surcharge mechanism.

As for the toe excavation mechanism, liquefaction failure was not triggered using realistic strength parameters of the in-situ foundation. In the case with the reduced strength in the foundation soils (friction angle of 17 degrees), the FoS was calculated to be approximately 1.16.

7.6 TARGET FOS FOR STATIC LIQUEFACTION TRIGGERING ANALYSES

Although not explicitly mentioned, the current minimum FoS values recommended by the Australian National Committee on Large Dams (ANCOLD) Guidelines on Tailings Dams (2019) are primarily intended for the assessments using the LEA method, and uncertainties remain regarding the applicability of the same targets to the FEM triggering analyses. To address this gap, further work is necessary from the industry to establish a standardised methodology and acceptance criteria for FEM-based triggering analyses, taking into account specific risk levels and associated uncertainties. In the interim, a target FoS of 1.5 for the triggering analyses may be considered a prudent approach for the stability of TSFs.

8 DISCUSSION AND CONCLUSION

This paper has presented the methodology and results of FEM-based triggering analyses on three potential failure mechanisms. These analyses can capture the disturbing efforts required to overcome the threshold to trigger the flow failure process, which is more realistic compared to the conventional approach assuming liquefied residual strength in LEA. Such an assumption in LEA, although conservative (if appropriate liquefied strength adopted), ignores the potential margin available against the triggering. Moreover, it is not fully consistent with the philosophy of the widely adopted seismic liquefaction triggering assessment, which evaluates the potential of triggering to inform what strength to adopt in the stability analyses.

Three static liquefaction triggering mechanisms, including the undrained surface surcharge, increase of phreatic level, and toe excavation, have been assessed in this study. For each mechanism, the required threshold levels of disturbances were identified, and corresponding dimensionless FoS values (based on a definition of q/p' ratio) have been estimated.

It shall be acknowledged, however, that significant uncertainties currently exist for the triggering analyses. One of these is whether all critical mechanisms have been adequately considered in the analyses, or whether the safety margins derived from the assessed mechanisms can reasonably serve as proxies for numerous other potential scenarios that were not explicitly investigated. One potential solutions may be to first identify critical and credible triggering mechanisms based on a comprehensive risk assessment.

As noted by Reid et al. (2021), a significant uncertainty may arise from the selection of K_0 values, which affects both the interpretation of the in-situ state parameters and the assessment of the proximity to the instability limit. Although the K_0 value in tailings is generally considered higher than the one at the normally consolidated state (~0.5) due to post-depositional disturbances (e.g. vibration due to mining activities), there remains a lack of consensus on the exact value even following in-situ testing, such as dilatometer and pressure meter tests or laboratory consolidation tests. Reid et al. (2021) also highlighted the impact of the depositional anisotropy and inclination of principal stress direction in reducing the undrained shear strength, which has not been accounted for in the current study based on the results of triaxial compression tests. Besides, the current analyses were based on strength-stress behaviour calibrated against controlled laboratory conditions, which do not fully capture complex failure mechanisms such as void redistribution, strain localisation, and intermixing during the failure processes. These limitations are common across many triggering analyses (e.g., Arroyo, M. and Gens, A., 2021; Babaki and Tannant, 2024; Katebi and Li, 2024; Ortigao et al. 2024; Rivas et al. 2023; Rivarola et al., 2022; Rivarola and Tasso, 2024; Rógenes et al. 2025; Rousé, 2024; Shuttle et al., 2022; Sottile et al., 2020; Vargas-Moreno et al. 2023). Considering these uncertainties, this study has adopted conservative assumptions for other key parameters, including pore pressure conditions and selection of state parameters.

For practical applications, all the above uncertainties condense to a question of the appropriate target FoS that shall be adopted. Establishing clear guidelines for FEM-based triggering analyses will require further industry consensus and development. In the meantime, such analyses are most likely to be applied in support of stability justification for short-term or temporary operational stages, where conservative assumptions and limited exposure durations may offer acceptable levels of risk.

Notwithstanding the aforementioned uncertainties and the need for further refinement of the analyses, the authors believe that there are intrinsic values of such triggering analyses, as demonstrated by this paper, in better understanding the risks against triggering liquefaction failures. This approach parallels the utility of more widely adopted seismic liquefaction triggering methodologies, contributing meaningfully to risk assessment and mitigation strategies.

CRediT authorship contribution statement

Jiaxi (Joshua) Chan: Formal analysis, Writing - original draft, Writing – review and editing. **Qian Gu**: Writing - original draft, Writing – review and editing.

REFERENCES

ANCOLD, 2019. Guidelines on Tailings Dam, Australian National Committee on Large Dams Incorporated, Australia.

Arroyo, M. and Gens, A., 2021. Computational analyses of Dam I failure at the Corrego de Feijao mine in Brumadinho. *Final Report for VALE SA*.

Babaki, A.P. and Tannant, D.D., 2024. Numerical evaluation of static liquefaction–induced flowslide causing the Edenville Dam failure, Michigan. *Journal of Geotechnical and Geoenvironmental Engineering*, *150*(5), p.04024034.

Bishop, A. W. (1950). Reply to discussion on "measurement of shear strength of soils" by a.w. skemptonand and a.w. bishop. Géotechnique, 2:90-108.

Chu, J. and Leong, W.K. (2002). Effect of fines on instability behaviour of loose sand. Géotechnique, 52(10), 751–755.

Drucker, D. C. (1951). A more fundamental approach to stress-strain relations. In Proceedings of the First US National Congress of Applied Mechanics, pages 487-491. ASME, ASME.

Gu and Chan (2020). Dynamic Analyses for Static Liquefaction Factor of Safety and Triggering Threshold Values in Tailings Storage Facilities Constructed by Upstream Method. 2020 ANCOLD Conference. ANCOLD.

Ishihara, K. (1993). Thirty third Rankine lecture: Liquefaction and flow failure during earthquakes. Géotechnique, 43(3), 349–415.

Jefferies, M. (1993). “Nor-sand: a simple critical state model for sand”, Géotechque 43, 91-103

Jefferies, M. and Been, K. (2016). Soil Liquefaction, a Critical State Approach. Applied geotechnics series. CRC Press.

Jefferies, M., Morgenstern, N.R., Van Zyl, D. and Wates, J., 2019. Report on NTSF embankment failure Cadia Valley operations for Ashurst Australia. *Independent Technical Review Board. Accessed May*, *1*, p.2019.

Katebi, M. and Li, S., A review of the FLAC (2D/3D) implementation of the NorSand model for static liquefaction analysis of tailings dam, 2024.

Lade, P.V. and Pradel, D. (1990). Instability and plastic flow of soils. I: Experimental Observations. Journal of Engineering Mechanics, ASCE, 116(11), 2532–2550.

Lade, P.V. and Yamamuro, J.A. (2010). Evaluation of static liquefaction potential of silty sand slopes. Canadian Geotechnical Journal, 48(2), 247–264.

Morgenstern, N.R., Vick, S.G., Viotti, C.B. and Watts, B.D., 2016. Fundão tailings dam review panel report on the immediate causes of the failure of the Fundão dam. *Cleary Gottlieb Steen & Hamilton LLP, New York*.

Ortigao, A., Sieira, A.C., Santos, F., Moraes, J. and Soares, C., 2024. Liquefaction Analysis of Four High Tailings Dams. *European Journal of Engineering and Technology Research*, *9*(3), pp.47-56.

Plewes, H.D., Davies, M.P. and Jefferies, M.G. (1992). CPT based screening procedure for evaluating liquefaction susceptibility. In Proceedings of the 45th Canadian Geotechnical Conference, Toronto, Canada.

Reid, D., Dickinson, S., Mital, U., Fanni, R. and Fourie, A., 2021. On some uncertainties related to static liquefaction triggering assessments. *Proceedings of the Institution of Civil Engineers-Geotechnical Engineering*, *175*(2), pp.181-199.

Reid D, Fanni R and Fourie A (2021) Assessing the undrained strength cross-anisotropy of three tailings types. Géotechnique Letters, https://doi.org/10.1680/jgele.21.00094.

Rivarola, L.F. and Tasso, N., 2024. Analysis of flow liquefaction triggering in tailings dams considering coupled flow-deformation. In *Proceedings of the 17th Pan-American Conference on Soil Mechanics and Geotechnical Engineering. La Serena, Chile*.

Rivarola, F.L., Tasso, N., Bernardo, K. and Sfriso, A., 2022. Numerical Aspects to Evaluate Triggering of Static Liquefaction with the HSS Model. *Mecánica Computacional*, *39*(28), pp.983-992.

Rivas, N., Sottile, M., Rivarola, F.L. and Sfriso, A., 2023. Comparing HSS and NorSand constitutive model for modeling flow liquefaction in tailings dams. In *Proc., 1st Int. Conf. on Geotechnics of Tailings and Mine Waste. London, UK: International Society for Soil Mechanics and Geotechnical Engineering (ISSMGE)*.

Robertson, P.K., L.d. Melo, D.J. Williams, and G.W. Wilson. 2019. Report of the Expert Panel on the Technical Causes of the Failure of Feijão .

Rógenes, E., Paes, I.T., Delgado, B.G., Bittar, R.J., Gomes, A.D.S., Cirone, A., Favero Neto, A.H. and Rasmussen, L.L., 2025. Assessing Static Liquefaction Triggers in Tailings Dams Using the Critical State Constitutive Models CASM and NorSand. *International Journal for Numerical and Analytical Methods in Geomechanics*, *49*(4), pp.1092-1112.

Rousé, P., Comparative analysis of P2PSand and NorSand models for static liquefaction assessment in tailings dams, 2024.

Schanz, T., Vermeer, P.A. and Bonnier, P.G. (2019). The hardening soil model: Formulation and verification. In Beyond 2000 in computational geotechnics (pp. 281-296). Routledge.

Shuttle, D.A. and Jefferies, M.G. (1998). Dimensionless and unbiased CPT interpretation in sand. International Journal of Numerical and Analytical Methods in Geomechanics, 22, 351–391.

Shuttle, D.A., and Jefferies, M.G. (2016). Determining silt state from CPTu. Geotechnical Research, 3, 90-118.

Shuttle, D., Marinelli, F., Brasile, S. and Jefferies, M., 2022. Validation of computational liquefaction for tailings: Tar Island slump. *Geotechnical Research*, *9*(1), pp.32-55.

Sottile, M.G., Cueto, I.A. and Sfriso, A.O., 2020. A simplified procedure to numerically evaluate triggering of static liquefaction in upstream-raised tailings storage facilities. *arXiv preprint arXiv:2010.11705*.

Vargas-Moreno, C.O., Guillén-Guillén, J.B., Ramírez-Chávez, R. and Preciado, H.F., 2023. Numerical Analysis for the Stress-Strain Evaluation of the Conversion of a Conventional Slurry Tailings Storage Facility to Filtered Tailings Storage Facility, Considering Different Scenarios. In *Proceedings of Tailings and Mine Waste* (pp. 29-41).

CHADWICK GEOTECHNICS

Chadwick Geotechnics is a leading supplier of testing, drilling and engineering services to the Geotechnical, Civil and Environmental disciplines across Australia and throughout the Asia Pacific region.

Key capabilities include:

Field Engineering

- Construction Engineering Services
- Logging
- Factual Investigations & Reporting
- Earthworks Supervision (including Level 1)

Laboratory

- NATA Accredited
- Construction Materials Testing
- Triaxial and Consolidation Testing
- Thermal Resistivity Testing
- Remote Laboratory Establishment

Drilling

- Sonic/Solid/Percussion/Direct Push
- Geotechnical and Environmental Systems
- NDD (Non Destructive Digging)

Instrumentation

- Supply
- Installation
- Monitoring

Think Act Be Safe

bsi. AS/NZS 4801:2001 Occupational Health and Safety Management

Engineering • Laboratory • Drilling • Instrumentation

Head Office and VIC Laboratory: Melbourne **QLD Laboratory: Sunshine Coast**

www.chadwickgeotechnics.com.au | **info@chadwickgeotechnics.com.au**

REPURPOSING TAILINGS STORAGE FACILITIES FOR DEVELOPMENT: EXPERIENCES IN MINING AND CIVIL APPLICATIONS

David Piccolo, Stephanie Salim and Jeremy C.W. Toh
PSM, Sydney

https://doi.org/10.56295/AGJ6047

ABSTRACT

Tailings being a waste product of mining and quarrying is highly compressible thus tailings dams and ponds are usually undesirable for development. However bigger picture issues such as sustainability and environmental considerations, and demand for land in urban or constrained areas, provide catalysts such that sites once thought of as undevelopable, are being considered for development. The question is, can a tailing storage facility (TSF) be used sustainably and productively after completion of mining? The aim of this paper is to show that it is not only possible, but perhaps now even desirable.

Several case studies of sustainable and productive end uses for TSFs are presented and discussed in this paper. A range of technical approaches are demonstrated in site investigations, characterisation of the tailings, and designing ground improvement works to allow reuse.

The first case history is a TSF in Western Sydney previously used as settlement ponds in a sand quarrying operation. Converting this TSF for industrial development involved ground treatment using a combination of wick drains and preload, as well as placement of engineered fill over the tailings. Another nearby TSF, is being developed as environmental wetlands which is a very different end use and thus the approach to its development is also very different. In mining, a case study is presented of construction of temporary mine infrastructure including crushing and screening plants, directly on top of an active tailings dam with ongoing settlements, a result of a geometrically highly constrained site. Some ground improvement was undertaken but because mine infrastructure has a relatively short design life and can be more tolerant to settlement, the improvement works were significantly optimised.

Collectively these case histories demonstrate a wide range of end uses for TSFs and the corresponding wide range of applicable ground improvement techniques and settlement criteria. The case histories emphasise that the geotechnical engineer needs to collaborate closely with the site owners and developers, and the designers of the future surface infrastructure, to allow TSFs to be repurposed with confidence and achieve sustainable outcomes. In particular we note the importance of all parties agreeing on practically achievable settlement criteria (as part of Landform Performance Requirements) and appropriate selection of the type of infrastructure, such that the repurposing is commensurate with the nature of the site.

1 INTRODUCTION

Tailings being a waste product of mining and quarrying is highly compressible thus tailings dams and ponds are usually undesirable for development. However bigger picture issues such as sustainability and environmental considerations, and demand for land in urban or constrained areas, provide catalysts such that sites once thought of as undevelopable, are being considered for development. The question is, can a tailing storage facility (TSF) be used sustainably and productively after completion of mining?

The aim of this paper is to show that it is not only possible, but perhaps now even desirable.

Several case studies of sustainable and productive end uses for TSFs are presented and discussed in this paper. A range of technical approaches are demonstrated in site investigations, characterisation of the tailings, and designing ground improvement works to allow reuse. The importance of appropriate Landform Performance Requirements for a given site which account for the practical limitations and capabilities of tailings, is emphasised. The role of the geotechnical engineer's job is discussed in nominating or agreeing on LPRs, and providing technical support in the form of site investigations, site characterisation, and ground improvement design to achieve the LPRs within other constraints. It is not intended to provide specific of extensive details of each case study; rather to highlight and emphasis some of the key aspects related to project success, in each case study.

2 LANDFORM PERFORMANCE REQUIREMENTS (LPRs)

Landform Performance Requirements (LPRs), as they are sometimes or often called, are simply a complete set of performance criteria to which the TSF repurposing is designed and constructed to achieve. Geotechnical LPRs can include:

- Total settlement limits.
- Differential settlement limits.
- The above, often need to have different limits and be nominated over different time frames corresponding to the design lives of various infrastructure, for example:
    - Structures.
    - Pavements.
    - Stormwater and other utilities.
- Bearing capacity and foundation stiffness for various foundation systems and retaining walls.
- Slope stability and slope face performance criteria.
- Pavement design and performance criteria.
- Other criteria usually specified for earthworks such as site classification.

Depending on the nature of the TSF, some of the LPRs may be set by regulatory requirements, for example ANCOLD (2019) Guidelines on Tailings Dams. If the TSF project involves a closure with a long required design life, criteria can become onerous and involve long return period events (flood, earthquake, etc). However repurposing of TSFs can often fall outside of ANCOLD / closure requirements.

There are many other non-geotechnical LPRs that are also applicable and need to be integrated with the geotechnical design. These can include:

- Final surface treatment considering things such as erosion, and vegetation.
- Drainage including surface run-off and infiltration.
- Environmental issues such as contamination and acid sulfate soils.

Broadly the process by which the authors usually approach the geotechnical aspects of redevelopment of a TSF involves:

1. Nominating and agreeing on appropriate LPRs with relevant parties. It is important that all parties understand that the performance of a TSF cannot be the same as the performance of a normal greenfield site. Realistic LPRs need to be agreed on and understood by all. Often this can involve various parties "meeting halfway". Should the issue of landform performance not be appropriately addressed and agreed, this can prohibit a development regardless of how good the geotechnical engineering is.
2. Investigating and characterising the TSF, to the extent required. TSFs are usually recent deposits with a varied history and without any benefits of improvement in conditions accruing from the passage of geological time, and this should be considered when planning the investigation and characterising the site.
3. Designing ground improvement works to meet the LPRs, and integrate geotechnical aspects with other disciplines.
4. Constructing the works and undertaking verification and certification that the LPRs will be achieved.

The above process is not novel or innovative, but it is important that each step is done well and in a way that recognises the variability and performance of tailings.

3 CASE STUDY 1 – INDUSTRIAL DEVELOPMENT

3.1 SITE HISTORY

The first case history relates to a TSF located in Western Sydney which was previously used as settlement ponds. The settlement ponds were created as part of the sand and gravel quarries which had operated in the 1980s. The TSF occupies an area of about 40ha and was proposed to be developed as an industrial development. Converting this TSF for industrial development involved ground treatment using a combination of wick drains and preload, as well as placement of engineered fill over the tailings.

Based on the historical photographs, key features of the settlement pond are identified and listed below:

- The quarry activities began around 1986, as seen in Figure 1(a).
- Settlement ponds are observed from 1988 and the tailings have been discharged at multiple points (at least 6), as seen in Figure 1(b).
- A delta in the settlement pond could be observed in 1991, as seen in Figure 1(c).

- Capping works started between 2001 and 2002.
- Capping works finished in between 2005 and 2006, as seen in Figure 1(d).
- Ponding water observed in some areas in 2009 and 2010.
- No major change in the site between 2010 and 2020.

3.2 CONSTRAINTS AND CRITERIA

The required structure to be place on top of the TSF includes the following:

- Bulk filling up to 7m thick.
- Industrial buildings, which includes warehouses and multi-storey office buildings.
- Retaining walls at the western boundary of TSF.

The following criteria were agreed on as part of the LPRs applying to the completed landform for the industrial development:

- Total post-construction settlements of up to 100 mm.
- Local tilts up to 1 in 300, but not associated with total settlements of more than 100 mm.
- The above, applicable over a design life of 30 years.
- Working pressure of 30kPa for the slab on ground.

Adoption of these criteria meant that is was realistic to develop the site for industrial use (warehouses and other industrial buildings, roads and other infrastructure, etc).

3.3 INVESTIGATIONS

A total of 39 Cone Penetration Tests (CPTs), including Piezo Cone Penetration Testings (CPTus), were undertaken in the tailings material to understand the character of the tailings and any buried features and to assist with the ground treatment strategies. Four historical CPTs were undertaken by other consultants and were also used to characterise the material. Of note, the CPTs were used as the basis for the site characterisation and design, and limited laboratory testing was undertaken. The CPTs provided excellent horizontal and vertical coverage ("bang for buck") without the issues that are involved laboratory testing such as sample disturbance, and number of samples required to be representative.

Dissipation testing was undertaken to understand the tailings horizontal coefficient of consolidation, C_h.

A number of test pits were also completed to understand the existing capping material and inspect the tailings material.

The CPTs, dissipation testings and test pits indicate the following:

- The CPTs indicate the presence of between 1 m and 2 m thickness of capping over the top of the tailings. Some of the areas particularly in the lower-lying north-east portion of the site may not have been capped as they were not trafficable during the investigation (too soft).
- The bedrock level is typically inferred between depths of 10m to 15m.
- The tailing thickness varies from less than 3m at the southern border of the site to 15m in the northern areas.
- The tailings properties range from a sandy silt to silt and clays, consistent with the mode and points of deposition.
- The transition from one end of the settlement pond to the other appears to be overall gradational and is related to the discharge arrangement and distance from the discharge point as expected for most conventional hydraulically deposited TSFs.

Combined with construction phase verification, the site investigation coverage proved sufficient to characterise the site and undertake the design.

3.4 CHARACTERISATION

Based on the results of the historical review and the results of the site investigation, the TSF was categorised into four settlement zones (i.e. S1 to S4) depending on the tailings characteristics and thickness of the tailings and any features (e.g. buried batters) that require special attention. Figure 2 presents the extent of each zone and Table 1 presents the adopted design parameters for each zone.

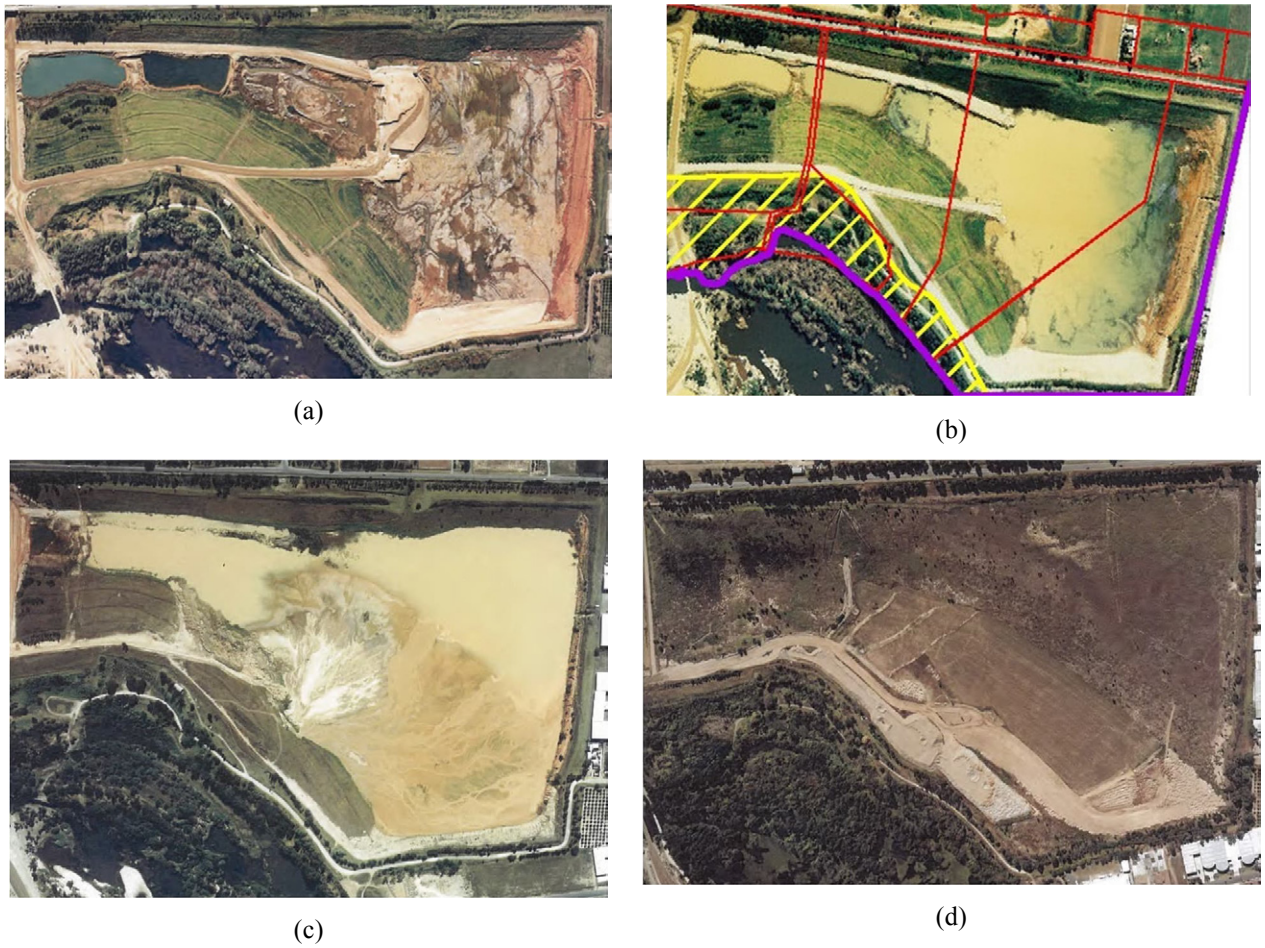

Figure 1: Historical photographs (a) quarry activities began around 1986; (b) settlement pond observed in 1988; (c) the delta formed in the settlement pond in 1991 and (d) capping works finished around 2005 and 2006 (NSW Government Spatial Services 2024)

We interpreted the characteristics of each zone as follows:

1. Area S1 is characterised by
    a. Presence of capping layer over most of the tailings, which comprises of gravelly sand and sand.
    b. Relatively thinner tailings (<4m) due to presence of underlying possible compacted fill riverbank embankment/cut batter and edge of dam.
    c. Indicative average corrected cone resistance 5 to 10MPa.
2. Area S2 is characterised by
    a. Presence of "better tailings", which typically comprises sandier materials.
    b. The tailings becoming deeper from south to north due overlying possible compacted fill and/or cut batter into bedrock.
    c. Thickness of tailings ranges from 4m to 14m.
    d. Indicative average corrected cone resistance 2MPa with peak value up to 4MPa.
    e. May contain thin layer of "poorer tailings".
3. Area S3 is characterised by
    a. Presence of "poorer tailings", which typically comprises fine-grained material.
    b. The tailings directly overlying bedrock.
    c. Thickness of tailings ranges from 10m to 14m.
    d. Indicative average corrected cone resistance 0.2 to 0.5MPa.
4. The ground conditions in area S4 were less well defined than other areas because access for investigation rigs was limited by the unsuitable surface conditions and ponding surface water. Based on the historical records, conditions in S4 were expected to be similar to area S3, however there was also the potential for conditions to be less favourable (i.e. greater magnitude of and slower settlements) due to the potential for increasingly clayey nature of tailings further from the main discharge points at the south end of the site.

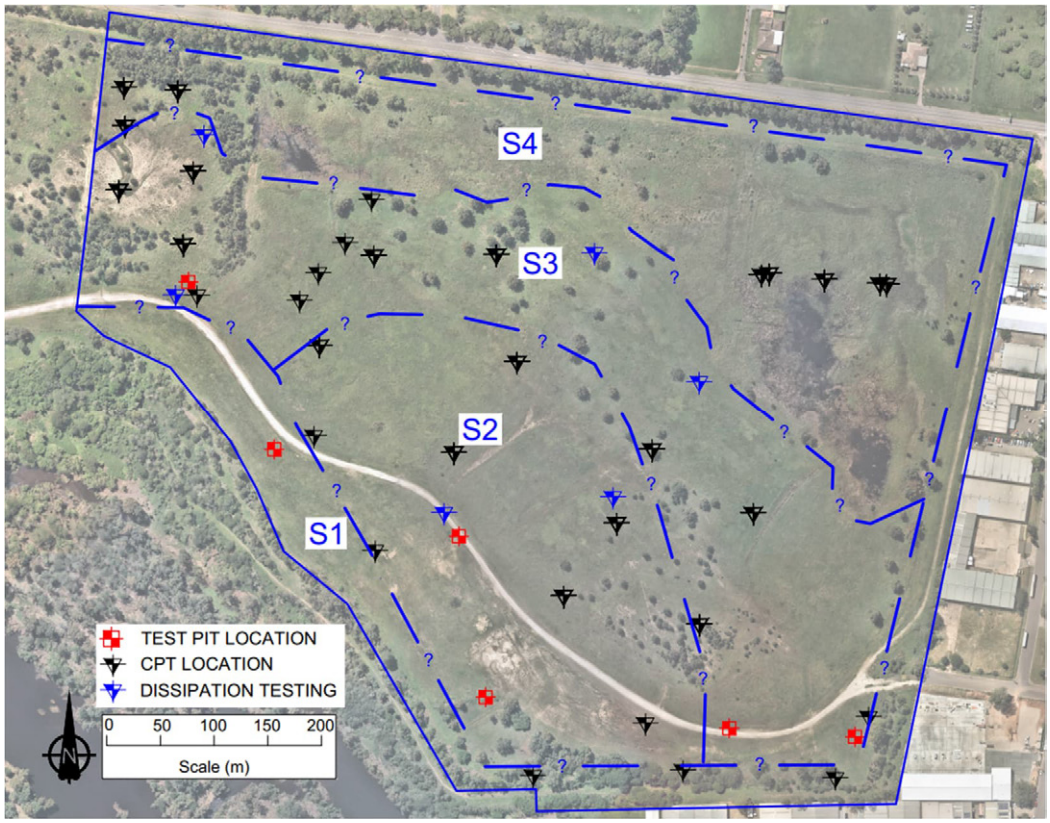

Figure 2: Plan showing the extent of four settlement zones

Table 1: Design parameters

Settlement Zone	Horizontal coefficient of consolidation, C_h (m^2/year)	Compression Ratio, C_c	Creep ratio, C_α/C_c
S1	500	"Best estimate" = 0.02 "Likely range" = 0.01 to 0.03	0.03
S2	10	"Best estimate" = 0.02 "Likely range" = 0.01 to 0.03	
S3 & S4	5	"Best estimate" = 0.02 "Likely range" = 0.01 to 0.03	

Table 2:Adopted design approach

Zone	Wick drain adopted	Permanent fill height (m)	Preload surcharge height (m)
S1	No	1 to 4	No
S2	Yes (1.5m spacing)	1 to 5	2.5m
S3 & S4	Yes (1.5m spacing)	1 to 7	3.5 to 4m

3.5 GROUND IMPROVEMENT WORKS

To achieve the required construction target timeline and the criteria listed in Section 3.2, the adopted design approach comprises a combination of the following:

- Wick drains/vertical drains. The adopted spacing is a triangular spacing of 1.5m x 1.5m connected together at the surface by horizontal drains, as indicated in Figure 3. It is noted that the adoption of horizontal drains as means of the drainage path has resulted in significant saving in cost and programme compared to utilisation of a drainage blanket as is traditionally adopted for embankment design over soft soil, but not optimal for large areas such as this site. It also eliminates the need for the wick drain to be installed through the drainage blanket which sometimes can cause negative impact on the productivity of wick drain installation e.g. when the drainage blanket is over compacted.
- Surcharge filling (preload surcharge) above the final landforms. The height of the surcharge differs for each settlement zone (e.g. S1, S2 etc.).
- The target preload period is 12 months (not including the time required for filling, and removal of surcharge). Variability in the rate of consolidation was managed by altering (increasing or decreasing) the preload period, rather than installing more wick drains.

The selection of the combination of the above is based on the tailings thickness and the design parameters, the adopted design is as presented in Table 2. The post construction secondary settlement (creep) is mainly governed by the creep rate and it determines the performance of the site over the 30-year design life. The creep rate adopted on the analyses was based on empirical data. There was a possibility that the creep rate may vary across the site, some areas might have higher creep rate than the design assumptions. he wick drains and surcharge are only adopted when the thickness of "poorer tailings" exceeds a total of 2m. Figure 4 shows a schematic diagram of the adopted design approach.

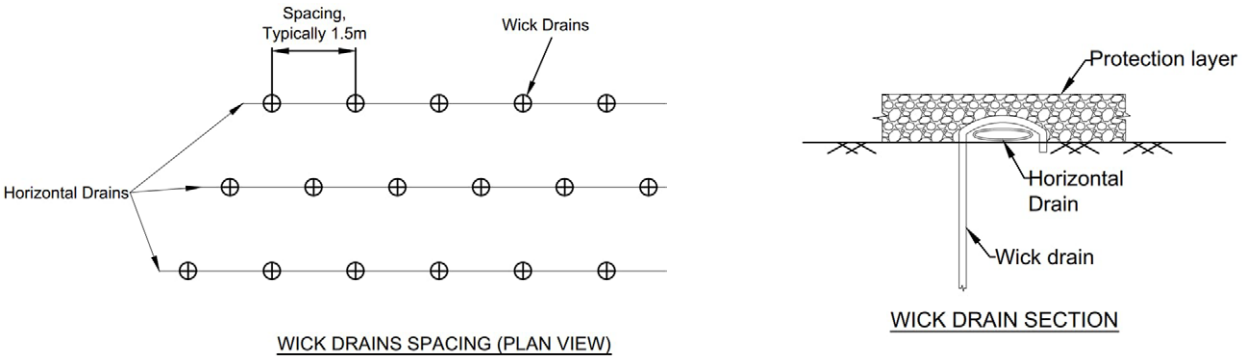

Figure 3: Typical wick drains and horizontal drain arrangement

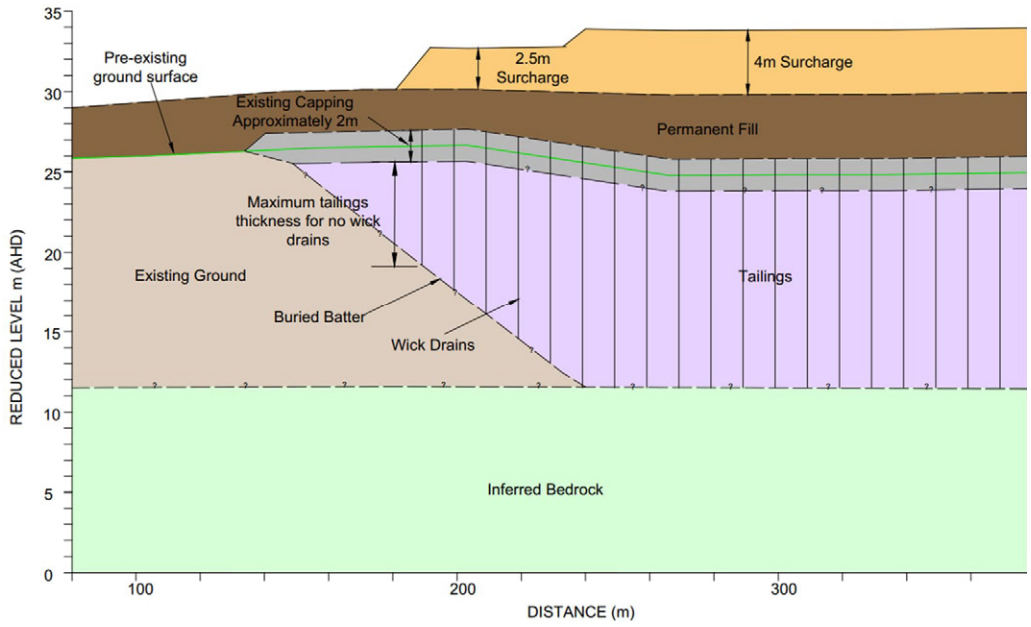

Figure 4: Schematic diagram showing the design approach

Figure 5: Aerial image at the start of the ground improvement works

3.6 DESIGN VERIFICATION

To validate the design predictions and maintain the slope stability during construction, a combination of the following instruments is adopted:

- Settlement plates.
- Surface settlement pins/markers.
- Vibrating wire piezometers.
- Wick drain penetration resistance as an indicator of tailings compressibility, refer to Salim et al. (2024).

The proposed development discussed in this section was undertaken in stages; this provided further opportunity to optimise the design of later stages by utilising the monitoring results of the early stages. The monitoring data, including the actual filling rate, was used to back-calculate the average compression ratio on each settlement plate locations.

Figure 6 presents an example of comparison between the predicted settlement during the design phase, the actual settlement based on monitoring results during the construction and the updated settlement predictions adopting the actual placement of fill (time and thickness) but still with the original design parameters. Figure 6 shows an example where the actual settlement is toward the lower end of the “likely range” of assessed settlement. Across the entire site, the back-calculated parameters were typically found to be within the range of design parameters, as presented in Table 1.

Additionally, the preload thickness was reviewed across the later stages by taking into consideration the back-analysed compression values, while maintaining the post-construction settlement criteria. This process provided an opportunity to reduce the surcharge height and preload duration where possible.

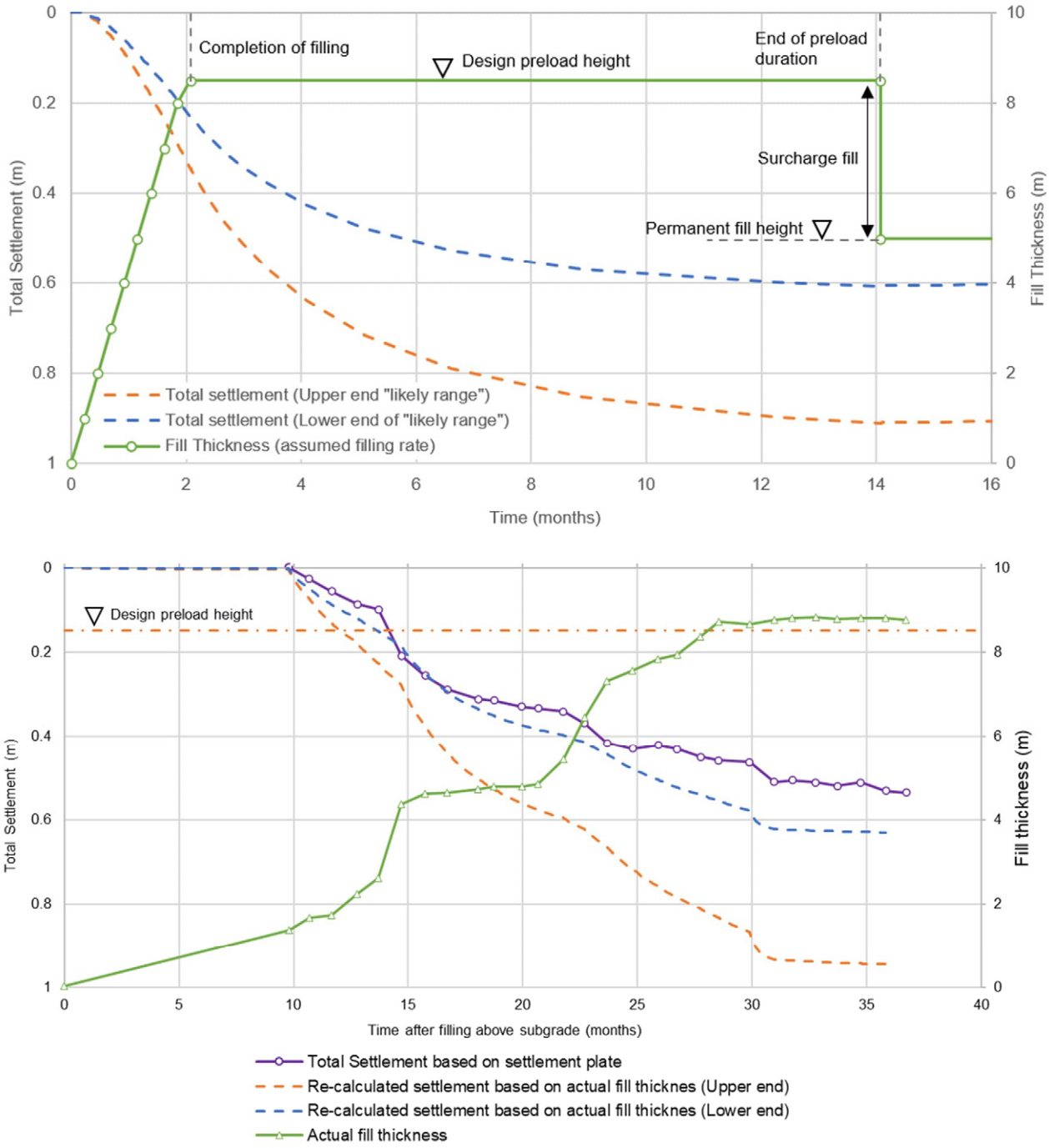

Figure 6: Comparison between (top) predicted settlement during design and (bottom) actual settlement based on monitoring results and re-calculated settlement based on the actual filling

3.7 SUMMARY

This TSF would have been unsuitable for industrial development without any ground improvements. The ground improvements at this TSF were undertaken by means of wick drains and preload to achieve the required LPRs. Selection of realistically achievable LPRs was important to ensure that the project could realistically be undertaken.

Collaboration with the contractor allows the construction to be performed in stages and thus providing an early monitoring results which gives an opportunity to optimise the design of later stages. Monitoring results were used to validate the design predictions and inform if any design changes are possible during construction (e.g. shorter preload duration, change in preload height). This was especially relevant given the large size of the site.

4 CASE STUDY 2 – ENVIRONMENTAL WETLANDS

4.1 SITE HISTORY AND PROPSOED DEVELOPMENT

Another nearby TSF, is being developed as environmental wetlands which is a very different end use and thus the approach to its development is also very different.

The proposed development comprised reshaping of the surface and construction of finger embankments to result in environmental wetland for treatment of surface water runoff from neighbouring future industrial and residential developments. The maximum embankment batter height proposed was 4.5 m.

4.2 LANDFORM PERFORMANCE REQUIREMENTS

The key to the efficient and effective redevelopment of these tailings area for use as a wetland was definition of the appropriate LPRs congruent with the proposed long term landuse.

The particularity of the proposed long term land use as a wetland was that firstly, the landform had no strict requirements on long term deformations, and secondly the landform was subject to a well established ongoing maintenance regime which included regular inspection and allowance for remediation of the embankments where poor performance resulted due to settlements, local slumping, and/or erosion. Particular emphasis was placed on maintenance in the early stages of wetland use whilst vegetation was established as part of the erosion and sediment control.

On the above basis the long term LPRs were defined as:

- Ensuring overall long term stability of the embankments infrastructure, and
- Where possible reduction of the likelihood of excessive maintenance during operation.

4.3 INVESTIGATIONS

The nature of the proposed works required access to small portions of the tailings surface, in effect only in the areas where minor excavation works or construction of finger embankments were proposed. The very soft and inundated condition of the tailings surface further constrained the ability completed intrusive investigations at the site. Further given the agreed LPRs it was deemed that a detailed understanding of the tailings conditions at depth was not required.

On the above basis a targeted investigation was undertaken which included:

- A desk top review of the tailings deposition operation.
- A site inspection
- Shallow dynamic cone penetrometer tests to test the thickness of the desiccated crust.

4.4 CHARACTERISATION

From the above the site was characterised as follows:

Site History – During the quarry operations, the area of the proposed wetlands was used as a tailings storage area. The previously excavated quarry was backfilled with tailings. Tailings comprising of silt and clay and fine sands have been deposited by subaqueous deposition over a number of years. Some areas were then capped with sandy tailings or other fill material. Subsequently some fill embankments were constructed over portions of the tailings' areas. The area had already been in use as a wetland and as such large portions of the site had been submerged by shallow ponds.

Surface and Subsurface Conditions – Based on the site observations and investigations the following conditions were assessed to be present at the Site:

- Natural soil or fill embankment.
- Sandy capping present only at some locations.
- Desiccated crust. This is the area of clay and silt tailings that have been above pond level for sufficient time to be affected by drying and thus the upper 50 - 200 mm present a higher strength than the underlying soft tailings.
- Soft tailings. These are clay and silt tailings, normally consolidated and presenting very soft to soft consistency. The desiccated crust and the soft mud are typical of a swamp area.
- Ponds. These are the areas which were submerged at the time of the inspection.

A plan showing the nominal extents of the different surface zones is presented in Figure 7. A schematic cross section of the typical site conditions is shown in Figure 8.

The natural soil and fill embankments, the areas comprising sandy tailings and the areas where a desiccated crust was present, where accessible on foot.

Figure 7: Plan image showing typical surface conditions

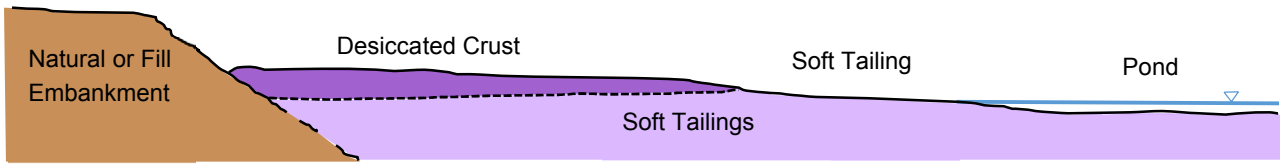

Figure 8: Cross section schematic of observed site conditions

4.5 THE BUND DESIGN

4.5.1 Zoning

Given the site conditions and the LPRs and in order to minimise the need for high quality fill, it was proposed that the bunds be constructed as a zoned embankment as shown in Figure 9.

The bund zoning consisted in a higher strength internal embankment and lower strength batters. The aim of the approach was to:

- Facilitates access for the plant during construction and for ongoing maintenance with a strong core, but also
- Allow the use of more marginal materials won from the cut works in the outer embankment.

Figure 9 presents the zoning of the different material to be used in the bunds and the basic geometry for the bunds.

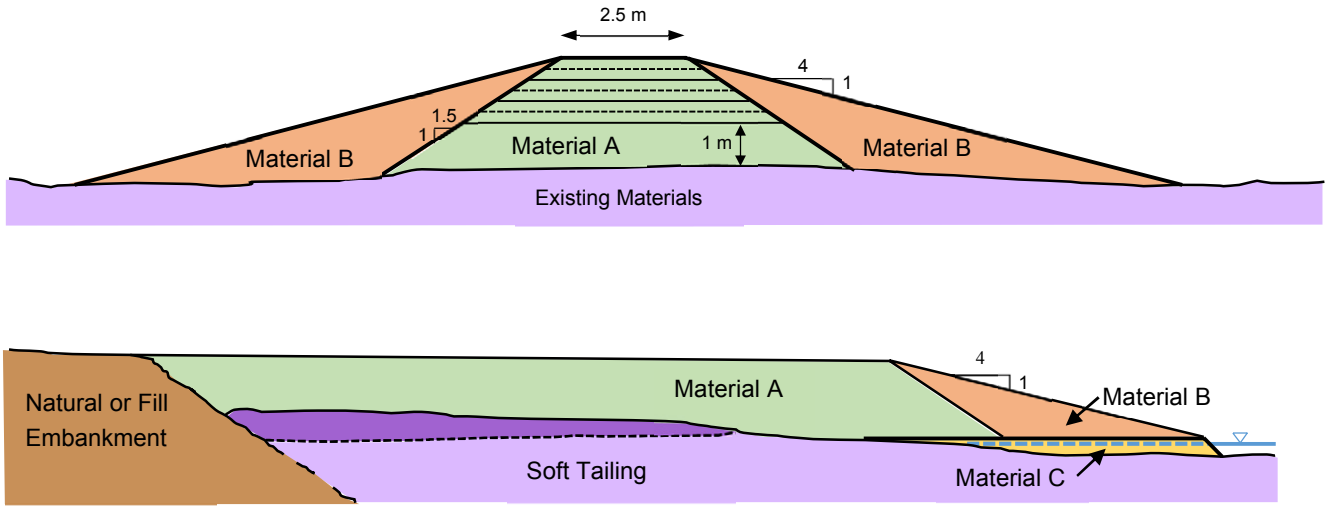

Figure 9: Material zoning in the bunds

It was proposed that the construction comprise the following steps:

- Initially a 1 m layer of imported fill or good quality site won fill (Material A) would be pushed in front of the plant to form a base for the embankment. Where ponds are present on site, a bridging layer comprising of granular imported material may have been required to form this base layer (Material C).
- Secondly, the rest of the internal embankment could then be constructed using Material A placed and compacted in layers.
- Lastly, the outer batters could be constructed with lesser quality material (Material B) placed with a lesser degree of compaction.

This approach was developed collaboratively between the contractor and the geotechnical engineer, to address both geotechnical stability and bearing capacity issues, as well as construction practicality.

4.5.2 Materials

Three (3) different materials were recommended for the embankments at the design stage. The characteristics of these materials and sources are discussed below.

- Material A (Core of the embankment): Potential sources of this material are:
  - Imported Virgin Excavated Natural Material (VENM) – Both shale, clay and sandstone are likely to be suitable materials.
  - Site won:
    - Natural or fill material from Embankments – This material could be trimmed off existing embankments within the site.
    - Capping and/or Sandy Tailings – Where capping or sandy tailings are encountered these could be reused.
- Material B (Batters):
  - Material A is suitable for use as Material B,
  - Desiccated tailings caps,
  - Soft tailings if allowed to dry, contractor should satisfy themselves that the tailings are able to dry in a timeframe suitable for the project.
  - Final surface should be protected against erosion and scour, which might include allowance for the re-vegetated surface
- Material C (Bridging layer):
  - Imported Virgin Excavated Natural Material (VENM) comprising of Sandstone fill or other rockfill sourced from site.

4.5.3 Placement requirements

Given the difficult founding conditions and the targeted performance requirements that included the need for long term maintenance, an approach to placement that allowed use of small equipment with little compactive effort was developed by the geotechnical engineer in collaboration with the contractor. The requirements adopted at design stage are listed below:

- Zone A and Zone C - Core Embankment:
  - Embankment fill shall be placed in near horizontal, laterally extensive layers of uniform material and thickness, deposited systematically across the work area. The lower layer can be up to 1.0 m thick. The maximum compacted thickness of subsequent layers shall be:
    - Either be 200 mm with tracked plant, or
    - 400 mm with proper compactor.
  - The fill shall be placed, and track rolled by at least 4 passes of an appropriately sized plant.
  - The moisture content of the fill when placed shall be assessed visually to be within 3% of optimum moisture content.
  - Temporary batters for the core embankment shall be no steeper than 1.5H:1V.
- Zone B – Batters:
  - Permanents batters shall be no steeper than 4H:1V and less than 4 m total height.
  - Material B shall be placed using suitable dozer and lightly compacted by tracking with tracked plant.
  - The moisture content of the fill when placed shall be assessed visually to be within 3% of optimum moisture content.

4.5.4 Trafficability

At design stage it was considered appropriate to pass the details of the plant selection and earthworks methodology development to the earthworks contractor who are experts in completing the works. This is because the general construction methodology including the zoning, placement, and materials had already been agreed by the geotechnical engineer. Further, safety in design requirements and any residual safety issues were clearly communicated. In order to assist the contractor completing the works some additional guidance with regards to the trafficability of the ground was provided.

The advice provided to the contractor is shown below:

- Trafficability on top of existing embankment and sandy capping should not present any issue for normal earthworks plant. The trafficability on the desiccated crust material might be achieved with wide tracks and lightweight plants, please note that the underlying subgrade is likely to be of soft to very soft consistency. Trafficability on top of wet tailings or where water is ponding is unlikely to be possible for plant. Bridging layers are likely to be required to provide a platform where small plant could work from.
- The choice of construction plant remained the responsibility of the contractor and it was recommended that the contractor visit the site prior to the start of the project in order to understand the site conditions.

4.5.5 Erosion Recommendations

It was recommended that the designer of the civil work adapt its design landscaping, erosion and scour protection requirements to account for the material zoning and compaction presented above including allowing provisions for batters to be revegetated to improve local stability and limit erosion or scour.

4.6 CONSTRUCTION EXPERIENCE

The earth bund construction used predominantly site won material with a mix of natural, existing fill and capping or reclaimed capping or sandy tailings material. Some small volume of site won river cobblestone and imported shale fill was used locally.

The initial earthwork contractor attempted to spread the material in a thick layers, pushing the material in front of the plant with a dozer to form the bund and then lightly compact the bund by trafficking (D5 dozer, 20t excavator and dump truck), see Figure 10. This approach worked relatively well in the drier and sandy parts of the tailings, but encountered issues where wet and soft clay tailings were present.

Figure 10: Earthworks moving equipment used initially

In these areas the use of relatively heavy machinery and the works starting at the end of a particularly rainy season, led to settlement of the bunds, some localised instability and formation of "mud wave", where the placement of fill material displaced the tailings underneath, with some of the tailings being displaced out in front of the advancing fill as a "mud-wave" (refer to Figure 11). This made this initial approach unfeasible for this particular design (although often "mud-waving" can be an appropriate construction technique.

Figure 11: Formation of "mud wave" and local instability during construction

This led to a revision to the plant being used on site, with smaller earth moving plant, e.g. a smaller excavator, a bobcat and a swivel tipper (see Figure 12) being selected as the earthworks plant. This increased the construction time, and allowed the tailings to consolidate and gain strength as the bund was raised. Undertaking the works during the drier season was also helpful. The method allowed the local instability, cracking and settlement that had been experienced to be remediated and the bund to be constructed generally in accordance with the specification requirements.

The final outcome (Figure 12) is a landform that is suitable to be used as a wetlands with accessible bunds which will require regular maintenance, particularly in the first few years of operations as localised settlement occurs and locally overstep batters experienced some localised slumping.

The construction highlighted the following critical factors when completing these types of capping activities:

- The earthworks contractor needs to visit the site and appreciate the site conditions and potential construction difficulties during the pricing process. Selection of appropriate equipment and scheduling of works is critical in successful implementation.
- It is important for geotechnical engineers to consider and communicate the construction risks involved especially in capping and mud-waving, and where required provide specific geotechnical advice design to cover the construction staging and methodology; particularly as necessary to meet safety in design obligations.
- The owner needs to include some flexibility in the expected delivery times and final outcome to allow responsiveness to the complex site conditions and weather effects.
- The key construction decisions are selection of plant and scheduling of works. The use of smaller plant appropriate for the site conditions and adopting slower construction timeframes allowed work in the soft tailings areas to be completed.
- Ongoing regular maintenance particularly as vegetation is established and initial settlement and strength gain occurs is an essential part of the works.

Figure 12: Revised plants with the construction of one of the bunds and some mud-waving halfway along.

4.7 SUMMARY

The purpose of an environmental wetland is well suited to a decommissioned TSF. However, unless appropriate LPRs are adopted, the design and construction may not be practical. At this site, the LPR definition was largely qualitative, ensuring that the site could be practically developed without prohibitive cost but still meeting the required end performance.

5 CASE STUDY 3 – MINE INFRASTRUCTURE

5.1 BACKGROUND

This case study is from the Ok Tedi mine in Papua New Guinea, and involves the construction of temporary mine infrastructure directly on top of an active tailings dam with ongoing primary and secondary consolidation settlements. Some ground improvement was undertaken but because mine infrastructure is temporary works, the ground improvement works were significantly optimised compared to if the infrastructure was permanent with a longer design life.

Panchalingam & Piccolo (2022) have previously presented a paper focussing on the site investigation and characterisation and this previous content is only briefly summarised herein. This paper focusses more on the site constraints and criteria, the LPRs, and the various types of designs undertaken with the corresponding ground improvement works.

5.2 CONSTRAINTS AND CRITERIA

The Ok Tedi crusher relocation project was a result of a highly geometrically constrained site within the mountainous surrounds of the Ok Tedi mine. The only location physically available for the new crusher plant was an existing active tailings dam, which also happened to be the only flat area in the vicinity, see Figure 13. Hence this was not a question of "is it feasible" rather "how can it be done". The tailings were up to 30 m deep within an infilled valley.

Required infrastructure to be constructed on top of the TSF included:

- Crushing and screening plants,
- Stockpiles and a reclamation tunnel,
- Retaining walls and slopes.
- Bulk filling up to 22 m thickness, to raise and flatten the ground level. This filling would cause significant consolidation of the tailings. Conversely in places the filling was as little as a few metres, which presented its own challenges such as achieving adequate working platforms and bearing capacity.

LPRs included:

- Design life of the infrastructure of up to 15 years.
- Achieving a raised and flat ground level to provide a platform for the infrastructure of sufficient area.
- For "primary" structures (crusher, screening plant, towers) total settlements not exceeding 50 mm. This necessitated foundations to rock including driven piles where required, although these piles were as much "ground improvement" as structural foundations, see below.
- For "secondary" structures (tunnel, conveyor, workshops, switch room) much higher settlements of up to 200 mm were permissible. This criterion was important in enabling a practical approach to the design and construction of filling and ground improvement; tighter criteria would have made the development unfeasible.

5.3 DESIGN

The design to achieve the LPRs at the site included the following (Figure 14):

- Placement of a rockfill working platform across the surface of the tailings by pushing the rockfill out onto the TSF and in doing so displacing some of the poorest surficial portions of the tailings (called as "mud-waving" approach).
- Earthworks bulk filling and construction of retaining walls and slopes to form the final landform geometry. The specification for the filling was tailored to the ROM (run of mine) material that was available. The filling needed to be sufficiently slow so as to achieve stability of the retaining walls and 2H:1V batters (which had a combined height of up to 22 m).
- Installation of driven pile foundations in specific areas (beneath where "primary" structures were located over tailings). These piles were not directly connected to the overlying structures; a rockfill load transfer platform separated the two. The benefits of this included providing more spatial coverage of the foundations, and smoothing out any differential settlements whilst keeping within the settlement limits. This design required close engagement with contractors, and the structural engineer.

This design was achievable because of the site-specific LPRs adopted, and would not have been possible otherwise.

Figure 13: Aerial photograph of the TSF where the crusher plant was to be situated

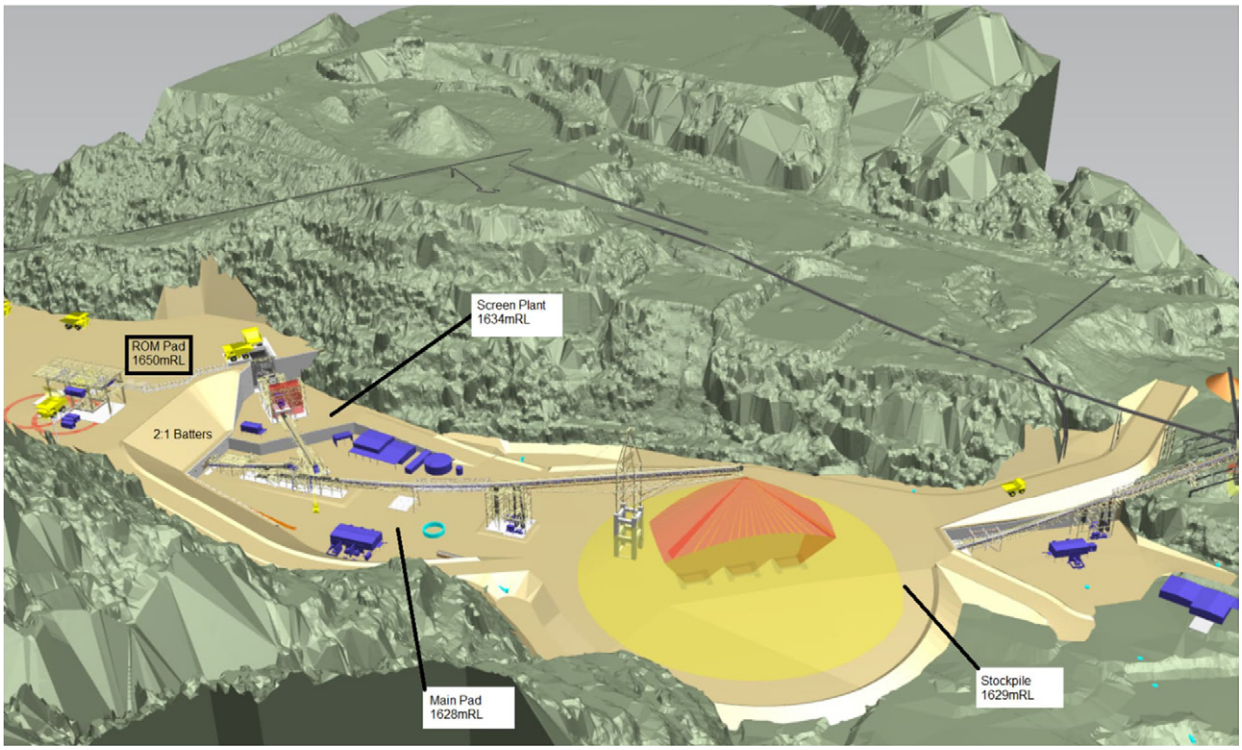

Figure 14: Overview of the TSF, with filling complete, and the new infrastructure under construction

5.4 CONSTRUCTION AND VERIFICATION

The adoption of the rockfill for mud-waving had several functions and benefits for the construction, including displacing some of the poorest quality surficial tailings, providing a limited amount of preloading to strengthen the tailings somewhat prior to construction of overlying works, and providing a working platform and confinement over top of the tailings. This mud-waving was an integral part of the design and construction, and was undertaken using a method specification with performance-based outcomes, rather than being subjected to a strict specification. "Failures" were permitted (and in fact desirable as it meant that weaker material was being displaced) during the mud-waving process provided that they did not impact safety. See Figure 15 for a photograph of the mud-waving works in progress, with the tailings displacement in front of the rockfill being obvious.

Geotechnical inspections were undertaken during construction. Monitoring included vibrating wire piezometers and settlement monitoring, see Panchalingam & Piccolo (2022) for an example of the monitoring results. The site was successfully filled and developed (Figure 16).

Figure 15: Mud-waving in progress

5.5 SUMMARY

Being a mine site, this project was focussed on operational outcomes. This meant dealing with the reality of the tailings characteristics by adopting LPRs that were not overly restrictive and allowed the use of a range of design approaches and available materials that may not otherwise have been possible, whilst still achieving the required performance over the (shorter than usual) design life.

Figure 16: Overview of the TSF, with filling complete, and the new infrastructure under construction

6 CONCLUSIONS

Collectively these case histories demonstrate a wide range of end uses for TSFs and the corresponding wide range of applicable ground improvement techniques and settlement criteria. The case histories emphasise that the geotechnical engineer needs to collaborate closely with the site owners and developers, and the designers of the future surface infrastructure, to allow TSFs to be repurposed with confidence and achieve sustainable outcomes. In particular we note the importance of all parties agreeing on practically achievable LPRs and appropriate selection of the type of infrastructure, such that the repurposing is commensurate with the nature of the site.

The case histories demonstrate that provided appropriate LPRs are agreed, TSFs can be successfully repurposed for a wide range of different developments. Geotechnical engineers, developers, and other parties are encouraged to think "outside the box" when it comes to defining LPRs, because this has a huge effect on the ability to practically and cost-effectively repurpose TSFs for sustainable end use. For example, can settlement criteria be matched to realistic expectations of landform performance and infrastructure requirements. This also applies to the design and construction, for example in the three case histories presented the initial stages of construction involved forming a capping layer or working platform by bridging or "mud-waving". This was an integral part of all three designs but method specifications and performance-based criteria were adopted rather than a typical more onerous earthworks specification. Application of a more rigorous specification to the initial filling may have precluded practical development.

CRediT authorship contribution statement

David Piccolo: Writing – original draft, Writing – review & editing. **Stephanie Salim:** Writing – review & editing. **Jeremy C.W. Toh:** Writing – original draft, Writing – review & editing.

7 REFERENCES

ANCOLD (2019) Guidelines on Tailings Dams - Planning, Design, Construction, Operation and Closure - Revision 1

Panchalingam, H. & Piccolo, D. (2022) Ok Tedi crusher replacement project: the geotechnical challenges of constructing infrastructure on top of soft tailings in remote PNG. *Australian Geomechanics* 57(1), 143-149.

Salim, S., Toh, J., & Piccolo, D. (2024) Sustainable design and construction in western Sydney: repurposing tailings dams for industrial commercial development in western Sydney. *Proc YGP*.

ANALYTICAL SOLUTION TO 1D LARGE STRAIN CONSOLIDATION FOR PREDICTION OF FINAL DENSITY

Gareth Swarbrick
PSM

https://doi.org/10.56295/AGJ6048

ABSTRACT

This paper provides closed form solutions to 1D consolidation incorporating two different forms of compressibility relationships (e vs log p and power curves), single and two-way drainage and with and without the effects of overburden. These solutions can be used in a variety of ways, such as determining final density of tailings profiles based on compressibility parameters, specific gravity and stored mass, determining the increase in tailings settlement due the placement of overburden and back analysis of tailings compressibility parameters based on the initial mass and settled height of column testing.

The paper shows the derivation of the closed form expressions for the different compressibility relationships and drainage conditions. Examples provide the applications based on publicly sourced data and data available to the authors. It can be shown that the closed form solutions closely match results derived from numerical analysis of consolidation including large strain effects. Steps to derive a final density profile are also provided with examples.

1 INTRODUCTION

Consolidation is an important consideration in tailings storage design, operation and closure. Consolidation theory provides insights into the following:

- rate of settlement (which typically reduces over time),
- amount of water released through a combination of:
    - surface expression,
    - seepage through the base or sidewalls,
- density profile which affects:
    - permeability profile (which may be interacting with connected groundwater)
    - strength profile (which is a controlling factor on the ability to support a cap),
- time to complete settlement
- overall capacity of the storage.

The reader is directed to Fourie *et al.* (2022) for a comprehensive summary of the state of art in geotechnical research in tailings including measurement and predication of consolidation.

The well-established (conventional) theory to describe rate of consolidation is that proposed by Terzaghi (1943) who assumed that the total settlement compared to the layer thickness was relatively small and rate of change could be defined by a single constant called the consolidation coefficient (Holtz and Kovacs (1981). These assumptions meant that a closed-form solution of rate of consolidation could be established. The Terzaghi approach is often termed small-strain theory reflecting these underlying assumptions. The parameter that governs total settlement due to change in stress (i.e. primary consolidation) is termed compressibility and most commonly expressed as a relationship between void ratio and vertical effective stress. This relationship is usually assumed non-linear and often taken to be log-linear.

Total settlement due to primary consolidation in soils using Terzaghi theory is usually estimated by assuming average parameters within a soil layer and using the compressibility relationship to calculate the change in void ratio based on the stress change at the centre of that layer (Holtz and Kovacs (1981). When the variation in parameters with depth is significant then the soil profile can be divided into a greater number of layers. The author is not aware of an analytical solution for the final consolidated height due to non-linear compressibility.

Tailings cover a stress range from very low stresses due to self-weight alone and therefore varying from effectively zero effective or net stress at the surface to increasing stress with depth. Tailings typically undergo a large variation in deformation as they transition from no effective stress to a final consolidated state under self-weight loading (plus overburden stress if a cap is applied). These large variations in deformation require what is termed large strain theory. Further discussion of the differences in tailings consolidation theories is provided in in Section 1.1 below.

The objective of this paper is to derive a simple, accurate solution to the final height of a column of tailings incorporating large strain effects, overburden pressure and variable drainage. The relationships developed can be used to predict behaviour without and with overburden (such as the effects of capping upon closure) and under one or two-way drainage. The relationships can also be inverted to back-calculate material properties from laboratory column settling tests and provide accurate profiles of final density and other parameters.

1.1 LARGE STRAIN FORMULATION

The most appropriate (i.e. widely accepted) theory for consolidation of tailings is the large strain formulation developed by Gibson *et al.* (1967) as opposed to the traditional small strain theory developed by Terzaghi (1943). Large strain theory incorporates the effects of the reduction in height and therefore changes in void ratio and drainage path. In addition, the large strain formulation decouples compressibility and permeability parameters. This is in contrast to the Terzaghi formulation where compressibility and permeability are combined into one single constant, the consolidation coefficient, c_v.

A good example of the difference between Terzaghi and Gibson theory was demonstrated in Carrier *et al.* (1983). The key graph from this reference is reproduced in Figure 1 where it is clear that under the same set of parameters the rate of settlement under the more appropriate large strain (i.e. Gibson) theory can be significantly faster than under the small strain (i.e. Terzaghi) theory.

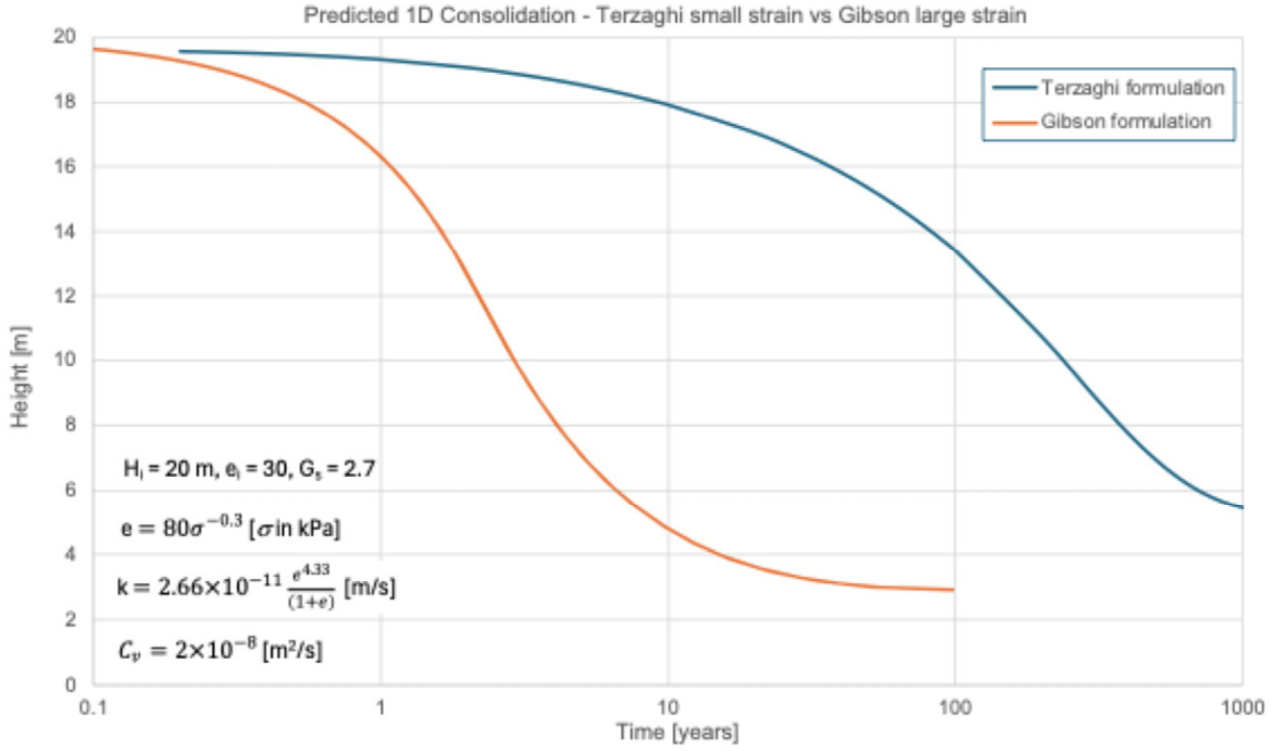

Figure 1: Comparison between small strain and large strain theory (recreated from Carrier *et al.* (1983))

The main reason that large strain theory predicts an increase in the time to consolidation is that the shortening of the draining path due to consolidation is accounted for in the theory thus properly capturing the decrease in the time to consolidate. In in small strain theory the drainage path length is assumed to remain constant.

Other key differences between consolidation analysis of tailings compared to traditional soil mechanics are:

- traditional consolidation is usually focussed on volume change driven by applied stress (e.g. foundations) whereas tailings consolidation is usually focussed on volume change driven by self-weight,
- pore pressure within tailings profiles are typically initially above hydrostatic and transition to hydrostatic or even zero if fully under-drained compared to traditional consolidation where pore pressure typically trends towards hydrostatic alone,

The solution to tailings consolidation using large strain is usually achieved using numerical integration of the non-linear differential equations that govern the theory. Numerical integration typically uses the finite difference or element method

where the profile is discretised into a series of discrete 'elements' or 'nodes'. Solutions typically require computerised code as described in Pane and Schiffman (1981), Tito (2015) and GWP (2021) to capture the changes in compressibility, permeability and drainage path.. This approach affords great flexibility in the solution of the highly non-linear large strain theory allowing incorporation of variable material properties and boundary conditions.

More discussion on the use of large strain theory can be found in Schiffman and Carrier (1990) and examples numerical solutions to the theory include Priestley (2011), Ito and Azam (2013) and Zhou *et al.* (2019).

Analytical solution to the fully consolidated state of a column of tailings (such as a single mathematical expression) has advantages. The development of such an expression is described in Section 2.

1.2 CONSOLIDATION TESTING

Irrespective of whether traditional or large strain theory is used, predicting consolidation involves estimation or measurement of compressibility and permeability. These parameters can be used to predict the final settled density profile. Test methods are designed to replicate conditions within the tailings, such as stress and pore pressure, and measure volume change in response to changes to these conditions. In some tests only stress is controlled, such as oedometers (Holtz and Kovacs (1981), while some tests allow the control of stress and pore pressure, such as Rowe cells (Rowe and Barden (1966). In some cases, tests control volume change, such as the constant rate of deformation testing (Znidarcic *et al.* (1986), Pane and Schiffman (1997). The change in response within the tailings is measured through pressure change, sample displacement and in some cases sub-sampling. There are advantages and disadvantages in all test methods and some are not well suited to capturing the highly deformable nature of tailings or mimicking low stress conditions. Testing in a conventional oedometer, for example:

- ignores self-weight affects,
- assumes homogeneous conditions within the sample,
- assumes a relatively small change in void ratio during the test (simulating the application of overburden stress),
- ignores stresses below around10 kPa,
- can exhibit errors due to seepage induced consolidation if the seepage force is higher than the applied pressure,
- usually assumes that the rate of consolidation is a constant (i.e. combing compressibility and permeability into a single c_v value however these can be differentiated),

Further discussion on the limitations of traditional oedometer testing for assessing tailings consolidation properties are provided in Ahmed *et al.* (2023).

Consequently, conventional consolidation tests are generally not suitable for determining the consolidation parameters of tailings and procedures and analyses consistent with the nonlinear consolidation theory must be used for characterisation (Fourie *et al.* (2022), Ahmed *et al.* (2023). More specialised testing, such as Rowe cells, allow compressibility and permeability to be measured independently.

Devices often termed 'slurry consolidometer' or 'slurrometer' are designed to measure low stresses and accommodate larger changes in void ratio (McBride and Baumgartner (1992), Islam *et al.* (2021), Ahmed *et al.* (2023). Slurry consolidometers are typically:

- an oedometer with an extension to facilitate a greater change in void ratio - sometimes referred to as a 'slurryometer' – for example Swarbrick (1992); or
- a purpose-built device, often mainly for research purposes such as the devices described in McBride and Baumgartner (1992), Islam *et al.* (2021)

Other more specialised testing includes derivation of consolidation properties from inverse modelling of boundary condition controlled lab testing, such as constant rate of deformation (CRD) testing (Znidarcic *et al.* (1986), Pane and Schiffman (1997) and under seepage-induced consolidation testing (SICT), see Fourie *et al.* (2022). These methods overcome some of the deficiencies of traditional testing, such as the ability to apply low stress (as in the CRD and SICT) and variation in conditions within the sample (such as CRD).

The initial void ratio generally does not affect the compressibility relationship. If the initial void ratio is relatively high samples will simply settle and not significantly affect the compressibility relationship, unless there is significant segregation. However, if the initial void ratio is relatively low due to, for example, paste thickening, or the tailings particles are highly active (highly negatively charged colloids), then the compressibility may be non-unique under low stress conditions as discussed by Imai (1981). Examples of this are described in Li *et al.* (2009) and Suthaker (1995). Under either condition it is important to test tailings based on samples at their expected void ratio upon discharge.

Simple column settling tests have some advantages over these specialist tests as they accommodate greater sample thicknesses. They also test consolidation effectively under low stress conditions similar to the upper portion of tailings in

the field, simulating non-homogeneous density, stress and pore pressure conditions. This makes them an attractive supplement to the more traditional testing described above given they can be undertaken cost effectively with inexpensive equipment. They also allow sedimentation to be studied in detail.

2 ANALYSIS OF COLUMN SETTLING BEHAVIOUR

Column settling tests are commonly used by researchers and practitioners to estimate key tailings properties, see Seddon (2021), Li and van Zyl (2024) including:

- rates of settling under varies conditions such as initial solids content, the effects of additives or different pore water chemistry,
- initially settled density at the cessation of flocculation.

Examples of column testing is provided in Fourie *et al.* (2022) and Ahmed *et al.* (2023).

Column tests can be conducted in a variety of vessels but most commonly conducted in relatively tall cylinders (typically ranging from, but not limited to, 0.5 to 2 m in height)) with diameters that are large enough to reduce drag effects to an acceptable level (typically greater than 100 mm), see) Swarbrick and Fell (1992), Seddon (2021) and Li and van Zyl (2024). Columns can either be operated as sealed at the base (one way drainage or often termed 'undrained') or with additional drainage from the base (two-way drainage or often termed 'drained'). The terms *drained* and *undrained* have been used in this paper to describe column tests with two-way drainage (drained base) and one-way drainage (sealed base) respectively.

The column test method simply requires the sample to be placed in the column in an initial, mixed state (suspension) and allowed to settle over time. The suspension progresses though several stages beginning with flocculation (aggregation of particles within the suspension), followed by settling (particles coming into contact), the process continues with consolidation (particles in contact increasing in density as excess pore pressure is squeezed out due to self-weight). This process is well presented by the conceptual diagram of Imai (1981) which is reproduced in Figure 2.

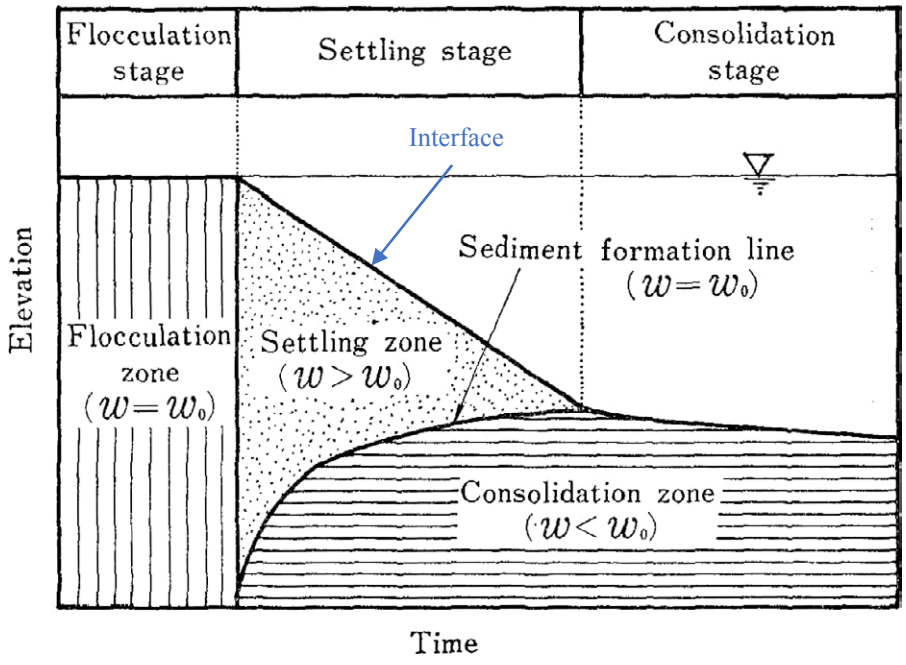

Figure 2: Conceptual diagram of a tailings suspension progressing from flocculation to consolidation (Modified from Imai, (1981): Conceptual diagram of a tailings suspension progressing from flocculation to consolidation (Imai (1981))

The height of the solid-water interface is measured over time, initially at high frequency when the change in solids height is rapid, reducing as the rate of settlement decreases following the interface line as indicated on Figure 2. Once settling is completed the sample continue to consolidate over time within the column. An example of column settling testing including how samples can be prepared and tested is provided in Yang *et al.* (2011).

An example of column settling is shown in Figure 3.

Figure 3: Simple column settling test

Once all downward vertical movement has ceased then the material in the column can be assumed to be fully settled. This represents a state to the far right of the interface line on Figure 2 when there is no further reduction in height due to self-weight. Under these conditions:

- the final average void ratio is known (assuming the initial average solids content and particle density are known),
- pore pressure can be estimated as either being hydrostatic in the case of undrained or effectively zero in the case of a drained test,
- the distribution of void ratio within the column will be related to the effective stress and the relationship between void ratio and effective stress.

These conditions can be harnessed to derive the parameters that describe the compressibility relationship between void ratio and effective stress by integrating void ratio over the length of the sample and comparing this to the average void ratio.

To undertake this integration, it is required to know the form of the void ratio and effective stress relationship as only the parameters of this relationship can be derived and not the relationship itself. The most common form is the well-known logarithmic relationship between void ratio, e, and effective stress, σ':

$$e = e_o - C_c \log(\sigma') \quad (1)$$

However, the common consensus in tailings consolidation research is that this relationship does not properly capture the relationship between e and σ' over the full range of effective stress experienced by tailings. There have been a number of alternate expressions suggested by researchers such as Krizek *et al.* (1977), Gibson *et al.* (1981), Carrier *et al.* (1983). One of the most common expressions is this simple power relationship found by Somogyi (1980), Carrier and Beckman (1984), Swarbrick (1995), Murphy (1997) and others:

$$e = A\sigma'^{b} + e_{\min} \quad (2)$$

The term e_{min} is the minimum void ratio representing a lower bound that compressibility may asymptote to and taken as zero in many cases. The value of e_{min} can be derived simply by curve fitting or based on the maximum density derived by other means, such as air drying. Examples of equations 1 and 2 are shown in Figure 4.

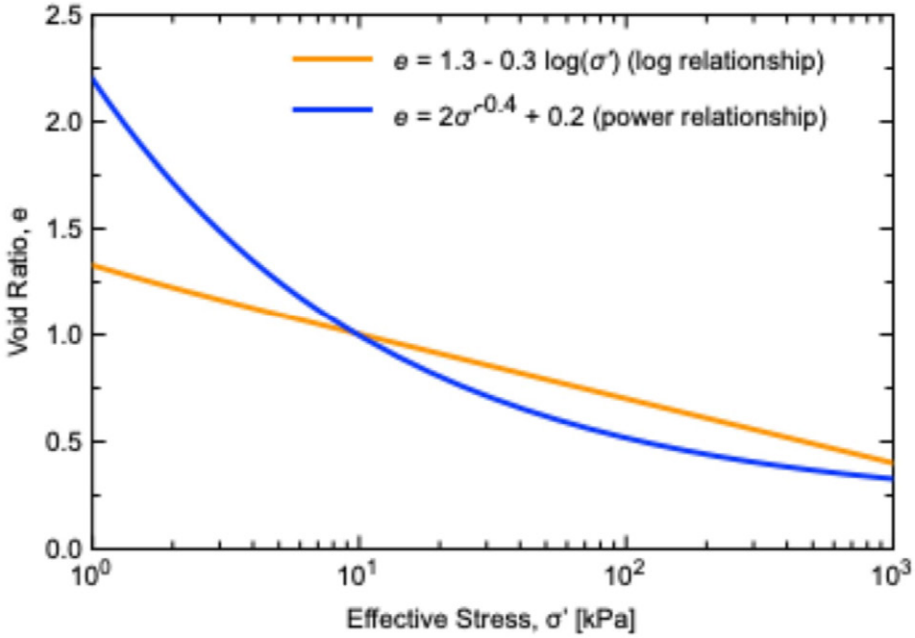

Figure 4: Examples of the logarithmic and power compressibility relationships

Other forms of the compressibility relationship are occasionally used however there is general agreement that tailings compressibility is well represented by the stated power function as discussed in Fourie *et al.* (2022).

Solutions to the derivation of the parameters of both equations (1) and (2) from column tests by integration, these being e_o, C_c, A , b and $e_{\min}$, are provided below.

It is not possible to directly integrate the conditions within a column settlement test using Cartesian coordinates, given the dependence on void ratio on effective stress and vice versa. Consequently, most solutions utilise a coordinate transform to perform the integration. The most common transform for consolidation is the use of Lagrangian or material coordinates, see Gibson *et al.* (1981), Schiffman *et al.* (1988). Material coordinates represent a reference system that is fixed to the solid skeleton and not to Cartesian coordinates thereby taking into account deformation of the soil skeleton.

Use of material coordinates allows the height of a column to be represented as an equivalent height of solid, H_s, which can be derived from the initial height, H_i, and initial void ratio, e_i, of the test:

$$H_s = \frac{H_i}{1+e_i} \tag{3}$$

Because the amount of solid is fixed, H_s is a constant with only the volume (or height for a 1D column) of fluid changing. If the void ratio is expressed in material coordinates, $e = f(\zeta)$, the final height of the tailings, H_f, can be derived from:

$$H_f = \int_o^{H_s} \left[1 + e(\zeta)\right] \partial\zeta \tag{4}$$

Firstly, it is assumed that we can express void ratio as a unique function of effective stress at the cessation of primary consolidation such that $e = f(\sigma')$, noting the potential effects of high initial solids content as discussed in Section 1.2. We can then derive an expression for effective stress as a function of the material coordinate, $\sigma' = f(\zeta)$ by combining stress due to the solid particles alone based on particle unit weight, γ_s, plus the weight of water (integrated over void ratio), less hydrostatic pore pressure (assuming a drained column) plus any addition uniform surcharge pressure, p, such as a capping material. The resulting relationship in material coordinates is:

$$\sigma'(\zeta) = \gamma_s \zeta + \gamma_w \left(\int_0^{\zeta} [e] d\zeta \right) - \gamma_w h + p \tag{5}$$

Where h is the depth below the surface. We can also express h in terms of the material coordinates:

$$h(\zeta) = \int_0^{\zeta} [1+e] \mathrm{d}\zeta \tag{6}$$

Substituting Eqn 3 into Eqn 2 results in a simple expression for effective stress under fully consolidated, hydrostatic conditions in terms of material coordinates:

$$\sigma'(\zeta) = [\gamma_s - \gamma_w]\zeta + p \tag{7}$$

Under drained conditions the expression simplifies to:

$$\sigma'(\zeta) = \gamma_s \zeta + p \tag{8}$$

This means that effective stress can be written entirely in terms of material coordinates.

$$H_f = \int_o^{H_s} [1 + e(\sigma'(\zeta))] \partial\zeta \tag{9}$$

In the case of an assumed $e(\sigma')$ relationship based on Eqn 1 this integral becomes:

$$H_f = \int_o^{H_s} \left[1 + e_o - C_c \log\left([\gamma_s - \gamma_w]\zeta + p \right)\right] \partial\zeta \tag{10}$$

In the case of an assumed $e(\sigma')$ relationship based on Eqn (2) this integral becomes:

$$H_f = \int_0^{H_s} \left[A\left([\gamma_s - \gamma_w]\} + p \right)^b + e_{\min}\right] \partial\zeta \tag{11}$$

Expanding and simplifying Eqn 10 gives this expression for a e log p relationship:

$$H_f = H_s\left(1 + \left[e_o - C_c \log\left(\frac{[\gamma_s - \gamma_w]H_s + p}{\exp(1)}\right) + \frac{C_c p}{[\gamma_s - \gamma_w]H_s} \log\left(\frac{p}{[\gamma_s - \gamma_w]H_s + p}\right)\right]\right) \tag{12}$$

While expanding and simplifying Eqn 11 gives this expression for a power relationship:

$$H_f = H_s\left(1 + e_{\min}\right) + \frac{A\left([\gamma_s - \gamma_w]H_s + p\right)^{b+1} - Ap^{b+1}}{[\gamma_s - \gamma_w](b+1)} \tag{13}$$

Equations 12 and 13 are closed-form solutions to the consolidated height and can be used in a number of applications as discussed in subsequent sections. Verification of these relationships is also provided.

If the column is drained or there is no surcharge loading, then Eqns 12 and 13 can be simplified. For example, Eqn 13 without pore pressure becomes:

$$H_f = H_s\left(1 + e_{\min}\right) + \frac{A\left([\gamma_s]H_s + p\right)^{b+1} - Ap^{b+1}}{[\gamma_s](b+1)} \tag{14}$$

Eqn 13 without surcharge loading reduces to:

$$H_f = H_s\left(1 + e_{\min}\right) + \frac{A\left([\gamma_s - \gamma_w]H_s\right)^{b+1}}{[\gamma_s - \gamma_w](b+1)} \tag{15}$$

While Eqn 13 without pore pressure or surcharge loading reduces to:

$$H_f = H_s\left(1 + e_{\min}\right) + \frac{A\left([\gamma_s]H_s\right)^{b+1}}{[\gamma_s](b+1)} \tag{16}$$

Eqn 12 can be simplified in the same manner. The average final void ratio, e_f^{avg}, is given by:

$$e_f^{\text{avg}} = \frac{H_i}{H_f} - 1 \tag{17}$$

3 VERIFICATION

The validity of equations 12 and 13 were checked in a variety of ways. If parameter constants such as C_c and b are set to zero, then void ratio becomes a constant and these equations reduce to $H_f = H_s(1 + e)$ as expected. These relationships were also checked by comparing H_f derived by numerical integration, equivalent to finite difference integration used by programs such as Pane and Schiffman (1981), Tito (2015) and GWP (2021).

3.1 VERIFICATION USING LAYER APPROXIMATION

An approximate solution to a fully consolidated tailings profile was derived using a discrete layered approach similar to that described in Holtz and Kovacs (1981). The process is as follows:

1. Divide the profile into a number of layers assuming each can be approximated by a constant void ratio.
2. Calculate the effective stress at the centroid of each layer based on the density derived from the constant void ratio, the weight of overlying layers and pore pressure based on depth (hydrostatic or none for undrained or drained, respectively).
3. Estimate the void ratio from the effective stress using Eqn 1 or 2.
4. Recalculate the void ratio and iterate over these steps until a converged solution is found.

Figure 5 shows a comparison of settled heights calculated by the approximate, layered approach described above and Eqn 12. The example is for a column of tailings initially 10 m high with an initial, uniform void ratio of 1.5. The compressibility is given by the expression $e = 1.378 - 0.321 \log(\sigma')$.

Multiple solutions are provided for the column divided up into 1 to 20 layers and with uniform surcharge loading ranging from 1 to 50 kPa. The closed-form solution given by Eqn 12 is plotted as a constant, dashed line.

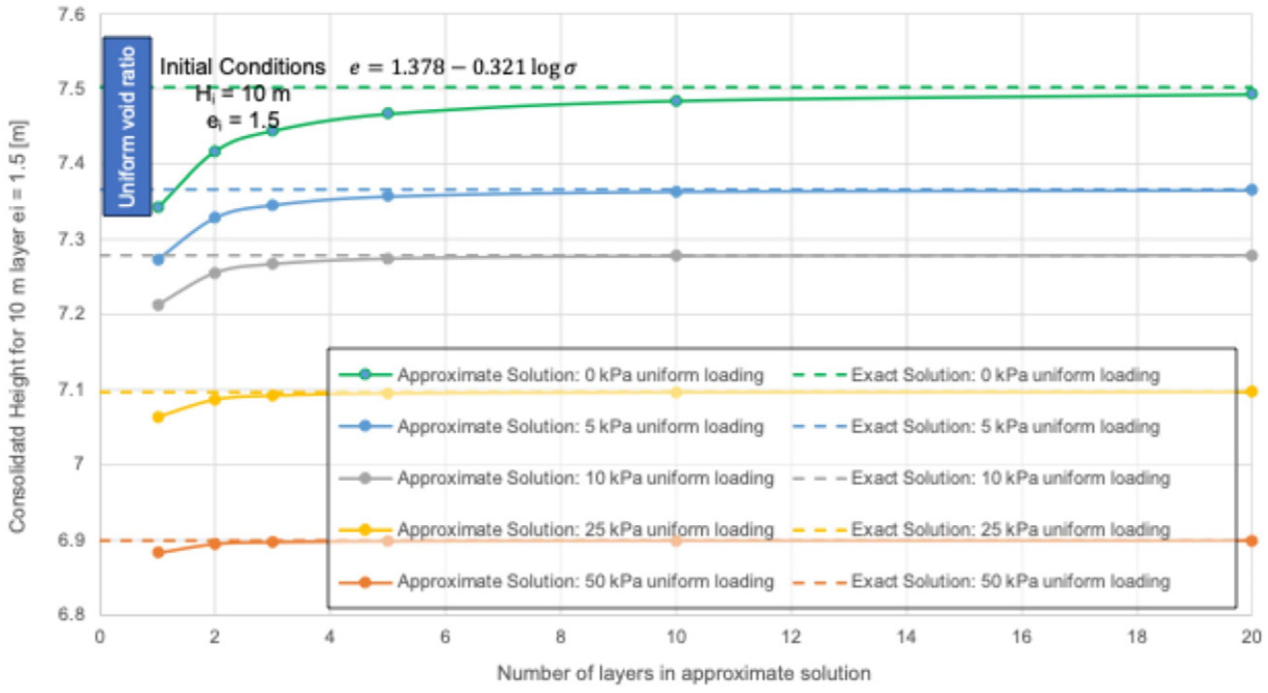

Figure 5: Comparison of the approximate solution based on a number of layers and applied surcharge load and the closed-form solution in Eqn (12)

From Figure 5 it is evident that:

- the approximate solution approaches the closed-form solution as the number of layers increases,
- the approximate solution predicts higher consolidation in all cases,
- the difference between approximate and closed-form solutions is less with increasing layers and increasing surcharge loading.

These results are aligned with expectations given that the determination of consolidated height in traditional soil mechanics assumes that compression is due to external loading (such as overburden) alone and has no self-weight

component. This means the error from using the approximate solution is generally small. Figure 5 shows that this error is always conservative because the approximate solution always over predicts the amount of settlement.

Figure 6 reinterprets the results shown in Figure 5 by plotting the height against the applied load rather than number of layers. The results show that the error reduces with increasing surcharge load and the approximate solution predicts greater consolidation in all cases.

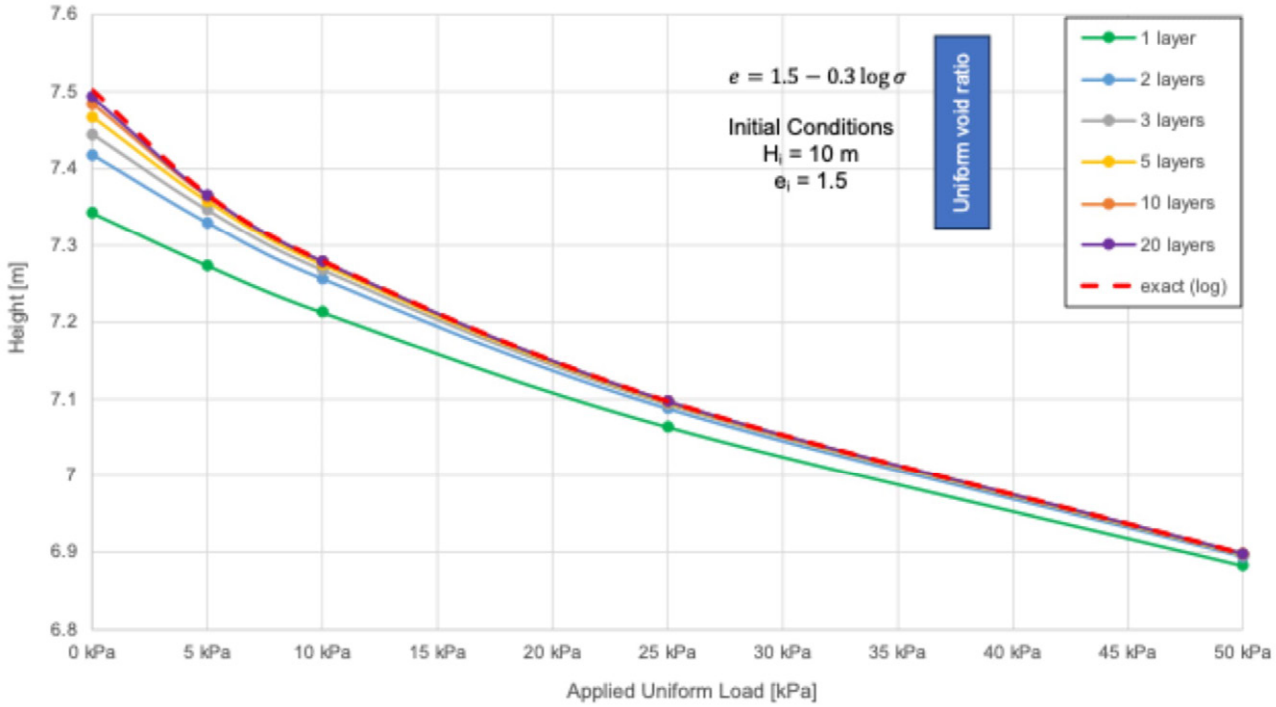

Figure 6: Comparison of the approximate solution based on a number of layers and applied surcharge load and the closed-form solution in Eqn (12)

3.2 VERIFICATION USING NUMERICAL ANALYSIS

Equations 13 and 14 have been checked against the commercial software package FSConsol developed by GWP Geo Software (GWP (2021). FSConsol provides approximate solutions to 1D large strain consolidation programs using numerical integration. Solutions are approximate due to the solution of the Gibson *et al.* (1967) theory using the finite difference method which assumes void ratio and pore pressure is constant within each segmental volume.

Equations 15 and 16 and FSConsol have been used to predict void ratio and density profiles for an example consolidation relationship as shown in Figure 7. Equations 15 and 16 can be used to derive void ratio and density profiles using the following approach:

1. Calculate the height of solids in the profile, H_s, from the initial height, H_i, and the initial void ratio, e_i, (assumed to be uniform) and Equation 3.
2. Divide the profile into a number of layers based on increments of H_s up to and including the total H_s.
3. Calculate the final height from the height of solid using either Equation 12 or 13 (depending on available compressibility parameters) modified for the drainage condition (drained or undrained),
4. Calculate the effective stress under fully consolidated conditions using the relevant undrained or drained relationship given in Equations 7 or Equation 8 respectively,
5. Calculate the corresponding void ratio from the effective stress (and thus dry density or any other required parameters).
6. Calculate any other required parameters, such as dry density, density, and moisture content, using the appropriate phase relationships and particle density.

In this case 12 layers have been used to derive the void ratio profile and density profiles for both one-way drainage (using Eqn 15) and two-way drainage (using Eqn 16) as shown in Figure 7. The same approach can be used to determine profiles based on the solution for log-linear compressibility (Eqn 12) with or without overburden and either one or two-way drainage.

The accuracy of the solution predicted by FSConsol is dependent upon the number of layers and therefore, a relatively large number is required to ensure an accurate prediction. The material parameters and initial sample height used for both analyses are included in Figure 7.

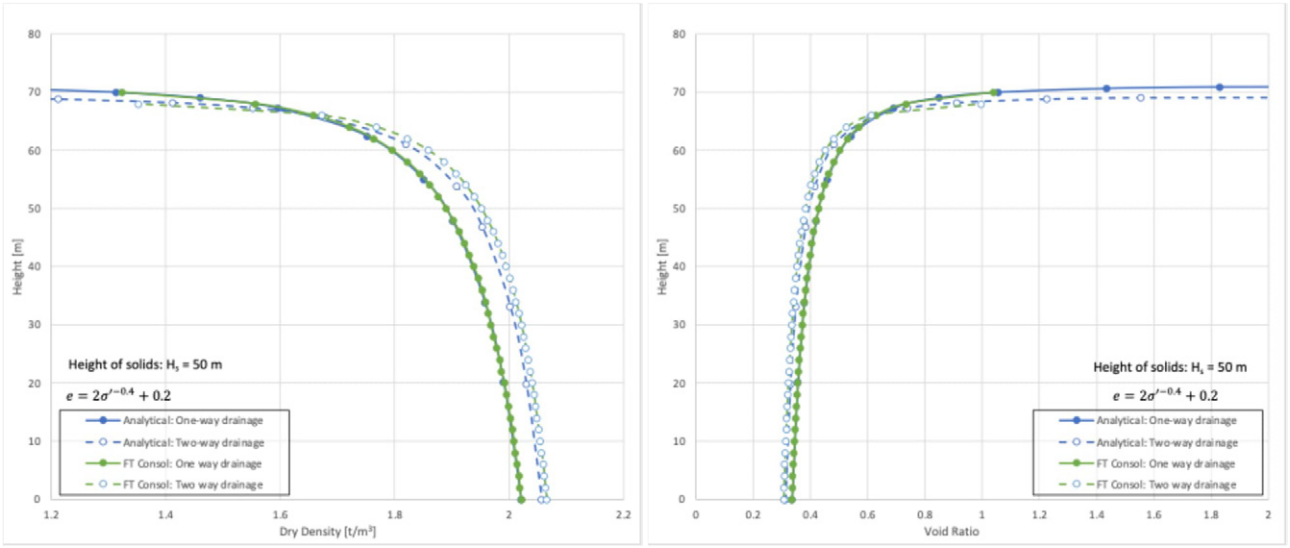

Figure 7: Comparison between Equation (13) and approximate (FSConsol) density and void ratio profiles

Figure 7 shows close agreement between analytical and numerical solutions, particularly one-way drainage cases, which plot exactly over one another, indicating the validity of Equation 13 against a well-accepted numerical solution. A paired t-test found there was no significant difference between the analytical (Equation 13) and numerical (FSConsol data sets.

4 APPLICATION

4.1 ALTERNATE APPLICATIONS

The derived solutions are analytical solutions, which can be solved quickly. The solutions are useful for reliability assessments because they allow the application of, for example, Monte Carlo techniques. In addition, analytical solutions lend themselves to being inverted or rearranged such that they can be used to solve other unknowns, such as the underlying material properties (e.g. compressibility).

Examples of how equations 12 and 13 may be used are provided below:

1. A closed form solution to the consolidated height under self-weight and surcharge loading.
2. Back-calculation of compressibility parameters from column settling tests, assuming either a logarithmic or power compressibility relationship.
3. To determine the void ratio and effective stress profiles within a tailings mass after consolidation.
4. Estimate the final settled density from the knowledge of the deposited mass of tailings and compressibility parameters.
5. Facilitate compressibility parameter determination by the best fit of compression (Rowe cell and/or oedometer) and column test data combined into one set of data.
6. Back-calculation of compressibility parameters from a soil density profile.

Application 1 has already been demonstrated in Section 2. Examples of applications 2, 3, 4, 5 and 6 are provided below.

4.2 APPLICATION 2 – ANALYSIS OF COLUMN SETTLING DATA

Figure 8**Error! Reference source not found.** shows an example of predictions for column setting data. All samples were tailings from the same gold mine, tested using drained and undrained cylindrical columns. The initial heights were similar; however, the initial solids content varied from 25 to 60% by mass, such that the final height varied significantly. As suggested by Equations 12 and 13, it is the height of solids that dictates the final settled height, and this can be varied between tests by either varying the initial solids content, initial column height, or both. Usually, off-the-shelf equipment comes in standard heights, such that changing the solids content is easier than trying to run tests on shorter samples.

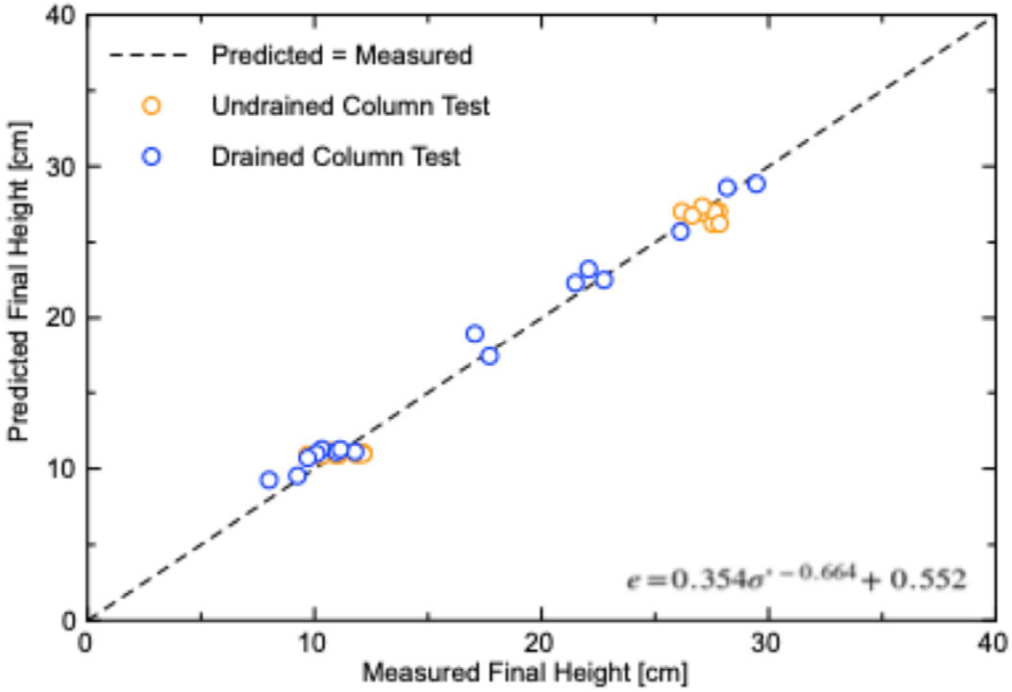

Figure 8: Estimated settled height of column tests

Figure 8 was prepared by the following steps:

1. The particle density, γ_s, final height, H_f, and height of solids, H_s, were determined for each column test while the height of solids was derived from the initial height and initial void ratio following Equation 3.
2. Initial estimates of compressibility parameters were set assuming a power relationship (Equation 2), i.e. initial estimates for A, b and e_{min}.
3. The predicted final height was calculated for each column test based on these initial estimates of compressibility parameters and Equation 13, noting that there was no surcharge in any tests (p = 0 Equation 15) and γ_s = 0 (Equation 16) for column tests that were allowed to drain from the base (two-way drainage).
4. The difference between the measured and predicted final heights was calculated and summed to determine the overall error. Optimising software (in this case, Solver in Excel) was used to adjust the compressibility parameters to determine the best fit by iteration and error minimisation.
5. Predicted final heights were then plotted against measured final heights to create Figure 8.

The line of best fit for the data in this example is included in Figure 8. The fit for the power relationship (Equation 13) was found to be slightly better than a logarithmic relationship (Equation 12). From Figure 8 it is evident that:

- Predicted heights are a reasonable match to measured heights across a range of final heights (100 to 400 mm); and
- Both undrained and drained tests show acceptable predictions, with different relationships to capture different drainage conditions (i.e., Equations 15 and 16, respectively).

The parameters A, b, and e_{min} derived from this fitting process describe the tailings compressibility and can be used for any tailings thickness.. However, care should be taken not to extrapolate too far beyond the range used in laboratory testing. This approach can be used to supplement testing under higher stress, such as Rowe cell testing, as described in Section 4.5..

4.3 APPLICATION 3 – DENSITY PROFILES

The analytical solutions provided here can be used to derive a fully consolidated profile, such as void ratio, density or water content. The steps to derive such a profile are outlined in Section 3.2.

Figure 9 and Figure 10 depict density and void ratio profiles under fully consolidated conditions respectively (primary consolidation) using this approach.

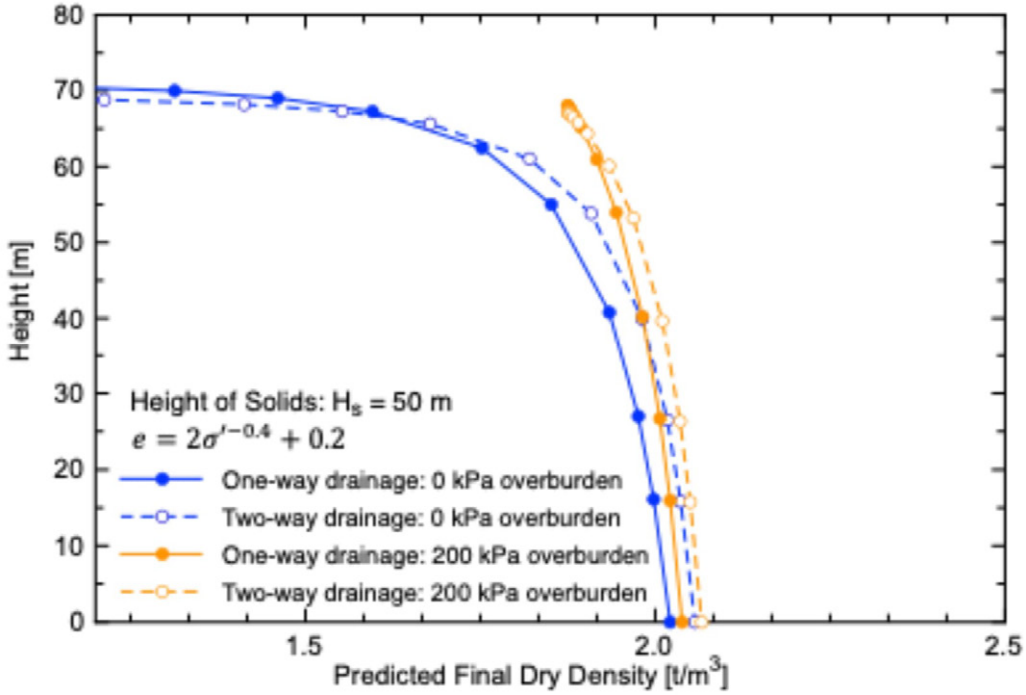

Figure 9: Estimated density profiles using Equation 15

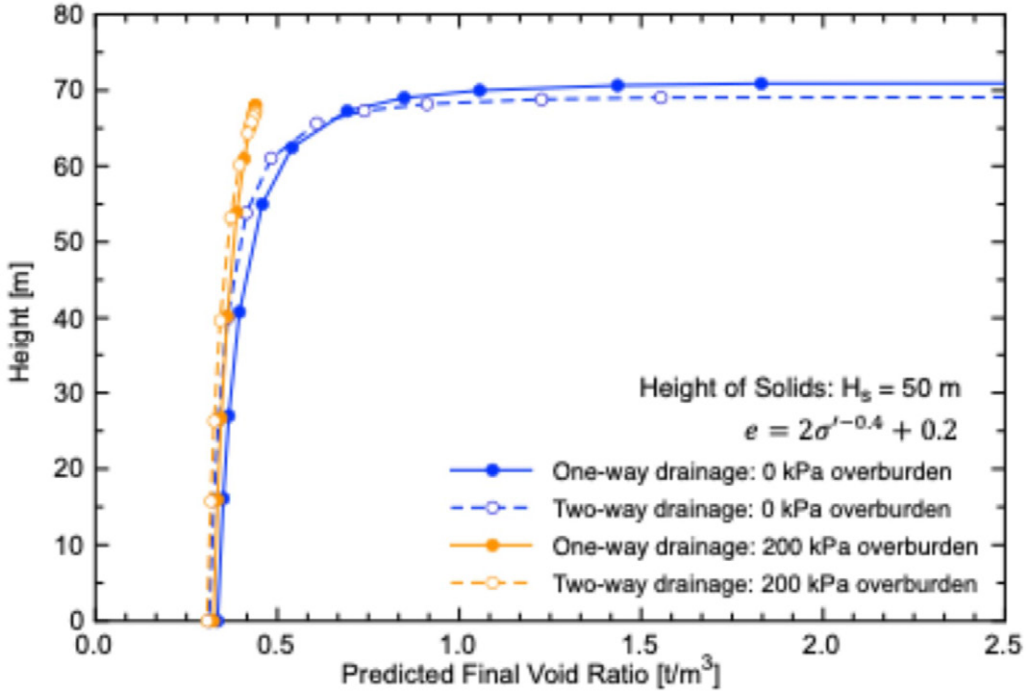

Figure 10: Estimated void ratio using Equation 15

Knowledge of the consolidated profiles allow the derivation or estimation of other parameters such as strength and permeability through correlations or established relationships.

4.4 APPLICATION 4 – ESTIMATE OF FINAL DENSITY FROM STORED MASS

Another example is the derivation of final density based on the stored mass of tailings in combination with compressibility parameters. Examination of Equations 12 and 13 show that the final height of a depth of tailings is related to the compressibility parameters, soil particle density and height of solids. The particle density is often known or can be

estimated. This means that if the compressibility is known in terms of Equations 1 or 2, and the mass of solids is known or can be estimated, then the average density can be estimated from the settled height using equations 12 and 13.

Examples of this application are shown in Table 1 whereby total stored dry mass, material parameters being particle density and compressibility (as defined by Eqn 2) and geometric parameters such as average area and height of solids (derived from stored mass, particle density and area) were derived for six sites from public literature or technical reports. Particle density, compressibility and height of solids were then used to derive the final height using Eqn 13, including any overburden pressure. The final dry density was derived from the final height and compared to the actual measured dry densities provided in the same public publications and reports.

The six examples provided in Table 1 demonstrate that it is possible to get an accurate estimate of final dry density without the need for any detailed numerical analysis. This approach may also be helpful in demonstrating the benefits of accurately recording the mass of solids deposited into a storage facility.

Table 1: Predicted and measured final dry density based on storage mass and compressibility

Parameter	Uranium[1]	Zinc[2]	Gold[3]	Gold[4]	Gold[5]	Rare Earth[6]
Particle density [t/m^3]	2.7	3.16	2.81	2.74	2.74	3.08
Dry mass of tails [Mt]	41.7	10.5	0.83	121.2	121.2	1.4
Storage area [Ha]	35.2	20.6	2.1	42.6	42.6	36.2
Overburden pressure [kPa]	400	0	0	0	0	0
Height of solids	43.9	16.1	14.1	103.8	103.8	1.29
A [1/kPa] (Eqn 2)	1.482	1.5	0.718	1.26	0.94	0.64
b (Eqn 2)	-0.1171	-0.12	-0.35	-0.076	-0.0813	-0.76
e_{min} (Eqn 2)	0	0	0.58	0	0.25	0.4
Final height [m]	73.9	29.8	24.6	183.9	187.4	2.1
Predicted final dry density [t/m^3]	1.60	1.71	1.61	1.55	1.52	1.89
Measured final dry density [t/m^3]	1.62	1.70	1.62	1.51	1.51	1.71[7]

1 Uranium mine – source of information not publicly available
2 McArthur River Mine – parameters extracted from GHD (2016) and GHD (2017)
3 Gold mine in Australia – source of information not publicly available
4 Gold mine in Canada – parameters extracted from Tripathi *et al.* (2020)
5 Gold mine in Canada – parameters extracted from Tripathi *et al.* (2020) with refitting
6 Yangibana Rare Earth Project – parameters extracted from column testing data provided in GHD (2020)
7 Estimate based on linear shrinkage testing given in GHD (2020)

4.5 APPLICATION 5 – COMBINING DIFFERENT COMPRESSIBILITY TESTING

The analytical equations presented here can be used to facilitate a combined fit of compressibility parameters under both low stress (such as column tests) and elevated stress (such as oedometer and Rowe cell testing). This allows derivation of a single set of parameters over an extended stress range thus better capturing overall tailings consolidation behaviour.

The combined fit can be undertaken simply by using the fitting techniques described in Section 4.2 in unison with fitting of the same parameters to Rowe cell, oedometer and/or any other relevant data (e.g. slurryometers). Figure 11 shows an example whereby compressibility relationships have been fitted to data from column settling tests and Rowe Cell testing, both separately and combined.

Note that it is not possible to plot column settling data on as compressibility as column settling data measures average and not provide single point values of void ratio and effective stress. Column test data in Figure 11 has been plotted as the average effective stress in the column against the average void ratio attained after consolidation for illustrative purposes only. Although the plot does not accurately reflect column test data, the compressibility parameters upon which the fitted curve is based are accurate as they are fitted to the analytical solution through the use of equations 12 or 13.

Figure 11 includes three fitted relationships:

- column settling test data fitted to Equation 15,
- Rowe Cell test data fitted to Equation 2,
- both datasets fitted to equations 15 and 2 in unison.

Figure 11 demonstrates the following:

- no single test method (for those methods used for this particularly set of tests) covered the full range of stress expected in a column of tailings; and
- the combination of data sets provided the ability to develop a single relationship that works reasonably well across a large stress range.

The void ratios derived from column testing are significantly less than for the Rowe cells tests. This difference is due to the low stress conditions simulated in column tests, which rely entirely on self-weight. This is opposed to Rowe cells where the initial void ratio is dictated by the lowest applied stress. Columns tests that are around 0.5 m tall, will have average effective stress due to self-weight of around 0.5 to 2 kPa after settling, whereas the minimum applied stress for Rowe cells is around 25 kPa. This difference in stress results in differences in the void ratio attained during the test.

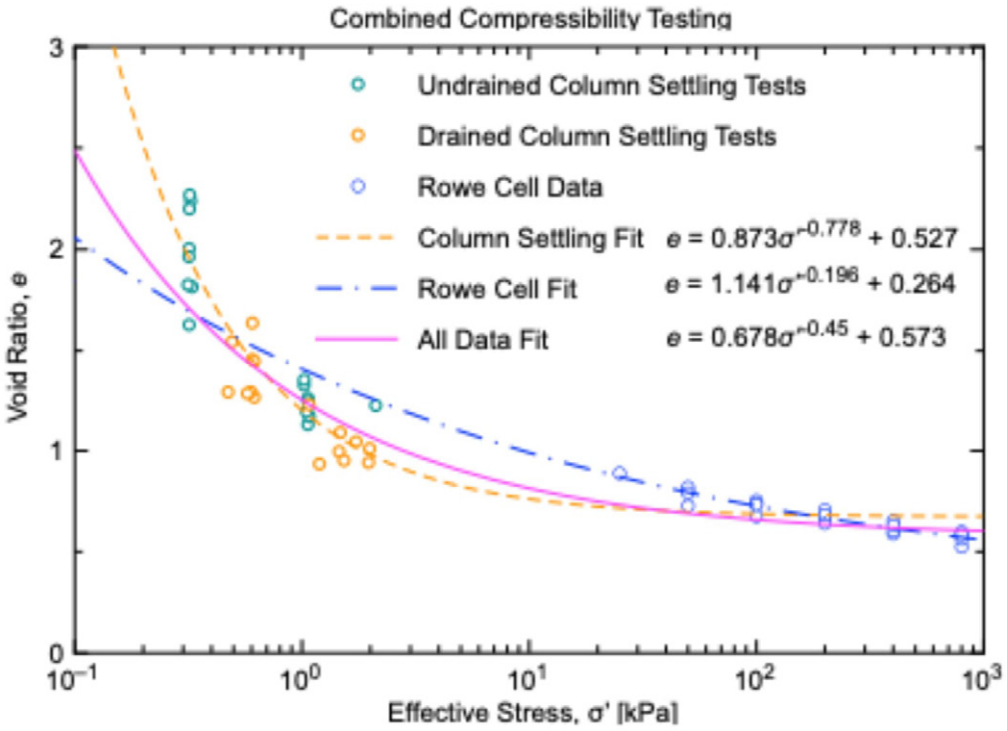

Figure 11: Combined compressibility data from settling columns and Rowe Cell testing

Although the data sets are based on a combination of average and point measurements, the combined data sets demonstrate that they are governed by a common compressibility relationship, notwithstanding the variation observed in column testing results and the discussion on the potential effects of high initial solids content as discussed in Section 1.2. Column test variation is usually attributed to adhesion of the tailings to the internal walls of the column test apparatus, causing 'hang up' and overestimation of the void ratio in some cases. This effect worsens as the diameter and height of test samples decrease.

5 CONCLUSIONS

The equations provided here (i.e. Equation 12 and 13 in particular) provide analytical solutions to the height of tailings (or other slurry) material at the end of primary consolidation. Key assumptions in the derivation of these solutions are:

- tailings can be represented as homogenous with reasonable accuracy for the problem being assessed or analysed,
- compressibility of the tailings can be represented as a single, smooth continuous relationship, with reasonable accuracy for the problem being assessed or analysed

It is noted that the second assumption must be valid to attain a solution to large strain theory generally.

The relationships derived here, by virtual of their analytical nature, provide several capabilities in the area of tailings consolidation, including:

- determination of the consolidated height under self-weight and surcharge loading based on two well-known compressibility relationships,
- determination of void ratio and effective stress profiles after consolidation from the compressibility relationship,
- back-calculation of compressibility parameters from column settling tests or from soil profiles; and
- estimation of consolidated height from the height of solids and compressibility parameters.

The author has used these relationships over many years to estimate compressibility parameters and undertake predictions under a number of different conditions. It is hoped that these relationships prove useful to others.

CRediT authorship contribution statement

Gareth Swarbrick: Methodology, Writing - original draft.

6 REFERENCES

Ahmed M., Beier N.A. and Kaminsky H. (2023), *A Comprehensive Review of Large Strain Consolidation Testing for Application in Oil Sands Mine Tailings*, Mining, ISSN:2673-6489, 3(1):121-150, https://www.mdpi.com/2673-6489/3/1/8.

Carrier W.D. and Beckman J.F. (1984), *Correlations between index tests and the properties of remoulded clays*, Géotechnique, 34(2):211-228.

Carrier W.D., Bromwell L.G. and Somogyi F. (1983), *Design capacity of slurried mineral waste ponds*, Journal of Geotechnical Engineering, ASCE, 109(5):699-716.

Fourie A., Verdugo R., Bjelkevik A., Torres-Cruz L.A. and Znidarcic D. (2022), *20ICSMGE State of the Art - Tailings*.

GHD (2016), *Tailings Deposition into Open Pit Consolidation Modelling*, McArthur River Mine Overburden Management Project - Draft Environmental Impact Statement, 32/17476/05 65221, 3 November, pp 22, https://ntepa.nt.gov.au/__data/assets/pdf_file/0010/407566/mrm_overburden_draft_eis_appendixAC_tailings_deposition_open_pit_consolidation_modelling.pdf.

GHD (2017), *Appendix P – Revised Tailings Consolidation Report*, McArthur River Mine Overburden Management Project - Supplement to Environmental Impact Statement, G:\32\1747605\WP\65221, 5 December, pp 18, https://ntepa.nt.gov.au/__data/assets/pdf_file/0020/554024/mrm_overburden_supplement_AppendixP_Updated_Tailings_Consolidation_Report.PDF.

GHD (2020), *TSF Design Development – Pre-Construction Report*, Yangibana Rare Earths Project, YGB-31-100-ENG-CIV-REP-0001, 2 September, pp 218, https://www.epa.wa.gov.au/sites/default/files/Referral_Documentation/Hastings%20APPENDIX%204-7.pdf.

Gibson R.E., England G.L. and Hussey M.J.L. (1967), *The theory of one-dimensional consolidation of saturated clays, I. Finite non-linear consolidation of thin homogeneous layers.*, Géotechnique, 17:261-273.

Gibson R.E., Schiffman R.L. and Cargill K.W. (1981), *The theory of one-dimensional consolidation of saturated clays, II. Finite nonlinear consolidation of thick homogeneous layers*, Canadian Geotechnical Journal, 18(2):280-293.

GWP (2021), *FSConsol: Program*, Edmonton, Canada, GWP Geo Software

Holtz R.D. and Kovacs W.D. (1981), *An Introduction to Geotechnical Engineering*, Newmark N.M. and Hall W.J. eds, New Jersey, Prentice-Hall.

Imai G. (1981), *Experimental Studies on Sedimentation Mechanism and Sediment Formation of Clay Materials*, Soils and Foundations, ISSN:0038-0806, 21(1 March:7-20 https://www.sciencedirect.com/science/article/pii/S0038080620324847.

Islam S., Williams D.J. and Bhuyan M.H. (2021), *Consolidation testing of tailings in a slurry consolidometer using constant rate and accelerated loading*, Proceedings of the Institution of Civil Engineers-Geotechnical Engineering, ISSN:1751-8563, 176(3):295-305.

Ito M. and Azam S. (2013), *Large-strain consolidation modeling of mine waste tailings*, Environmental Systems Research, ISSN:2193-2697, 2(1) 2013/07/24:7, https://doi.org/10.1186/2193-2697-2-7.

Krizek R.J., Casteleiro M. and Edil T.B. (1977), *Desiccation and consolidation of dredged materials*, Journal of Geotechnical Engineering, ASCE, 103:1399-1418.

Li A.L., Been K., Ritchie D. and Welch D. (2009), *Stability of Large Thickened, Non-Segregated Tailings Slopes*, Paste 2009: Proceedings of the Twelfth International Seminar on Paste and Thickened Tailings, R. Jewell A.B.F.S.B. and Wiertz J. eds., Viña del Mar, 21-24 April, Australian Centre for Geomechanics, https://papers.acg.uwa.edu.au/p/963_34_Li/.

Li Y. and van Zyl D. (2024), *Analysing the segregation of coarse tailings particles with a zone-formation differential settling model*, Paste 2024: Proceedings of the 26th International Conference on Paste, Thickened and Filtered Tailings, Fourie A.B. and Reid D. eds., Perth, 16-18 April 2024, Australian Centre for Geomechanics, https://papers.acg.uwa.edu.au/p/2455_22_Li/.

McBride R. and Baumgartner N. (1992), *A simple slurry consolidometer designed for the estimation of the consistency limits of soils*, Journal of terramechanics, ISSN:0022-4898, 29(2):223-238.

Murphy S.D. (1997), *Consolidation modelling of deep tailings deposition - A Case Study*, Geoenvironment 97 - 1st Australia-New Zealand Conference on Environmental Geotechnics, Bouzza A., Kodikara J. and Parker R. eds., Melbourne, Australia, 26-28 November, A.A. Balkema, 401-406.

Pane V. and Schiffman R.L. (1981), *FSCON4-I, Version 1, level A, one-dimensional finite strain consolidation of a thick, normally consolidated homogeneous layer*, Department of Civil Engineering, University of Colorado.

Pane V. and Schiffman R.L. (1997), *The permeability of clay suspensions*, Géotechnique, ISSN:0016-8505, 47(2):273-288.

Priestley D. (2011), *Modeling multidimensional large strain consolidation of tailings*, The Faculty of Graduate Studies (Mining Engineering), December, The University of British Columbia, https://open.library.ubc.ca/collections/24/items/1.0053478.

Rowe P.W. and Barden L. (1966), *A new consolidation cell*, Géotechnique, 4(2):162-170.

Schiffman R.L. and Carrier W.D. (1990), *Large strain consolidation used in the design of tailings empoundments*, International Symposium on Safety and Rehabilitation of Tailings Dams, Sydney, Australia, Australian National Committee on Large Dams, Vol 1, 156-174.

Schiffman R.L., Vick S.G. and Gibson R.E. (1988), *Behaviour and properties of hydraulic fills*, in Hydraulic Fill Structures, van Zyl D.J.A. and Vick S.G. eds, Colorado State University, American Society of Civil Engineers, pp. 166-202.

Seddon K.D. (2021), *The geomechanics of thickened and paste tailings*, Paste 2021: Proceedings of the 24th International Conference on Paste, Thickened and Filtered Tailings, Fourie A.B. and Reid D. eds., Online and Perth, Australia, 21-23 September, Australian Centre for Geomechanics, https://papers.acg.uwa.edu.au/p/2115_18_Seddon/.

Somogyi F. (1980), *Large strain consolidation of fine-grained slurries*, Canadian Society for Civil Engineering Annual Conference, Winnipeg, Manitoba, Canada, Canadian Society for Civil Engineering.

Suthaker N.N. (1995), *Geotechnics of Oil Sand Fine Tailings*, Department of Civil Engineering, Faculty of Graduate Studies and Research, Fall, University of Alberta, https://era.library.ualberta.ca/items/e3747c37-c2d9-4da8-bf46-508004b16b6d.

Swarbrick G.E. (1992), *Transient unsaturated consolidation in desiccating mine tailings*, School of Civil Engineering, Sydney, April, University of NSW.

Swarbrick G.E. (1995), *Large strain consolidation in unsaturated porous media*, First International Conference on Unsaturated Soils, Alonso E.E. and Delage P. eds., Paris, 6-8 September, ENDPC, ISBN:2-85978-241-9, Vol 2, 583-590.

Swarbrick G.E. and Fell R. (1992), *Modelling the desiccating behaviour of mine tailings*, Journal of Geotechnical Engineering, ASCE, ISSN:0733-9410, 118(4):540-557.

Terzaghi K. (1943), *Theoretical soil mechanics*, John Wiley and Sons.

Tito L. (2015), *Numerical evaluation of one-dimensional large-strain consolidation of mine tailings*, Department of Civil & Environmental Engineering, Department of Civil and Environmental Engineering, Colorado State University, 110.

Tripathi S., Scheremeta J., Coffin J. and Reiva J. (2020), *Consolidation Modeling for Design of Complex In-pit Tailings Storage Facility*, proceedings of the 24th international conference on tailings and mine waste, Virtual Event, November 15–18, UBC Studios, https://tailingsandminewaste.com/2020/TMW2020_V3.pdf.

Yang J.W., Yin X.T., Liao Y.F. and Ou X.D. (2011), *Experimental Study on Mechanism for Self-Weight Consolidation of the Red Mud Tailings Placed in the Karsts*, Applied Mechanics and Materials, ISSN:1660-9336, 90-93:3102-3107.

Zhou H., Amodio A. and Boylan N. (2019), *Informed mine closure by multi-dimensional modelling of tailings deposition and consolidation*, Mine Closure 2019: Proceedings of the 13th International Conference on Mine Closure, Fourie A.B. and Tibbett M. eds., Perth, 3-5 September 2019, Australian Centre for Geomechanics, https://papers.acg.uwa.edu.au/p/1915_23_Zhou/.

Znidarcic R., Schiffman R.L., Pane V., Croce P., Ko H.-Y. and Olsen H.W. (1986), *The theory of one-dimensional consolidation of saturated clays, V. Constant rate of deformation testing and analysis*, Géotechnique, 36(2):227-237.

Douglas PARTNERS

INFORMED GROUND DECISIONS.

STRONGER PROJECT OUTCOMES.

- GEOTECHNICAL
- ENVIRONMENTAL
- GROUNDWATER
- ROCK MECHANICS
- GEOPHYSICS
- MATERIALS TESTING

WWW.DOUGLASPARTNERS.COM.AU

AUSTRALIA'S CHOICE FOR GROUND EXPERTISE

Douglas Partners is an Australian employee-owned engineering consulting firm, trusted for over 60 years to deliver practical, cost-effective solutions. With 19 offices and 14 labs nationwide, we provide grounded solutions in various fields.

- **24 Client Choice Awards awards won since 2008.**
- **Data driven insights.**
- **60 years of retained industry knowledge.**

NATURAL HAZARD PROTECTION? SURE!

Tested to the world's toughest standards and beyond, our systems provide the level of protection you need. Whether from rockfall, landslides, debris flows, or coastal erosion. Whether standard or special solutions. Learn more: **www.geobrugg.com**

MANUFACTURED IN AUSTRALIA

Geobrugg Australia Pty Ltd
300 Victoria Road | Malaga WA 6090
T +61 8 9249 9939
www.geobrugg.com.au

Regional offices
Sydney NSW, T +61 400 845 289
South Melbourne VIC, T +61 488 044 708
Brisbane QLD, T +61 488 044 003
Perth, WA +61 477 470 064

BRUGG
Geobrugg

Safety is our nature

CHARACTERISATION OF INTERMEDIATE MINE TAILINGS USING THE MEDUSA FLAT PLATE DILATOMETER

Mahdi Naeini[1], Mark Chapman[2], Arun Muhunthan[1], Marty Viney[3] and Pamela Soto[4]

[1] ATC Williams, Melbourne, Australia; [2] Insitu Geotech Services, Brisbane, Australia; [3] Oceanside Consulting, Sulphur Creek, Australia; [4] MMG Limited, Australia

https://doi.org/10.56295/AGJ6049

ABSTRACT

Recently, a new fully automated flat plate dilatometer, Medusa DMT, has been introduced to field investigation works. Along with the capability to conduct high-quality and repeatable DMT tests, this device provided an opportunity for a new series of in situ tests designed to estimate in situ horizontal stress. These extensions to the capability of the DMT are particularly valuable in materials with intermediate behaviour, such as mine tailings, where partial drainage effects can significantly impact test outcomes. This paper introduces the new methods available with the Medusa DMT, namely DMT-Whilst Penetrating (DMT-WP) and DMT-Repeated A (DMT-RA), describes a method for screening for intermediate material behaviour and discusses the process used to reduce the partial drainage effects by testing to measure drained or undrained behaviours. The results from the DMT-WP and DMT-RA tests are analysed alongside adjacent CPTu and Vane Shear Tests (VSTs). The findings demonstrate the value of the new Medusa DMT tests in characterising intermediate mine tailings materials, assessing the drainage effects and providing insight in estimation of coefficient of earth pressure at rest, K_0.

1 INTRODUCTION

Investigating tailing materials typically involves using the Cone Penetration Test with Pore Pressure measurements (CPTu), in situ Vane Shear Testing (VST) and collecting disturbed and undisturbed samples for laboratory testing. The Flat Plate Dilatometer (DMT) test, whilst common in traditional civil and building site investigations, is not as commonly used for tailings investigations. The DMT test provides information about important material characteristics such as strength, stiffness and state. The importance of the Coefficient of Earth Pressure at Rest, K_0, in tailings has been discussed in recent studies by Jefferies and Been (2006), Wang and Ismail (2022), and Reid et al. (2021) where the static liquefaction assessments are heavily relying on the initial state of the tailings.

Unfortunately, there is some reluctance to use the DMT, which stems from partial drainage effects observed in tailing and intermediate materials (niche silts). Schnaid et al. (2015) discussed these impacts extensively in a study using DMT with a pore pressure sensor to monitor the decay of pore pressure during the test.

Advances in DMT tooling in the last five years have led to greater testing capability, understanding of the test and the soil response to the test, particularly in partially drained materials (Marchetti et al., 2019; Schnaid et al., 2021; Marchetti Danziger et al., 2024). The new Medusa DMT allows for drainage to be readily assessed, and new test methods have been developed to overcome these effects.

This paper discusses these new DMT test methods conducted with the Medusa DMT and reviews the impact on material characteristics derived from the tests.

2 DMT TESTING

2.1 FLAT PLATE DILATOMETER TESTING

The flat plate dilatometer is comprised of a 0.2 to 0.3mm thick circular aluminium diaphragm mounted on a flat stainless-steel blade. It has a sensing disk beneath it to detect electrical contact during insertion and target inflation of 1.1mm. The dilatometer is typically pushed into the ground using equipment like a CPT rig or SPT hammer, with measurements taken at 0.2 to 0.5-meter vertical intervals (Marchetti, 1980).

Once at the target depth, pneumatic pressure is immediately applied to the diaphragm via a surface control box and nitrogen gas bottle, causing the diaphragm to inflate to the A position in 15 seconds and the B position in another 15 seconds. Additionally, a C reading can be collected during the deflation process. (Marchetti, S. 2001).

The definitions of the three reading parameters are as follows (Marchetti, 2001):

- A reading: lift-off pressure, required to start the membrane expansion against the soil
- B reading: pressure for 1.1 mm membrane expansion at the centre

- C reading: membrane closing pressure, measured immediately after the B reading by slowly deflating the membrane

A schematic figure of the DMT blade is presented in Figure 1.

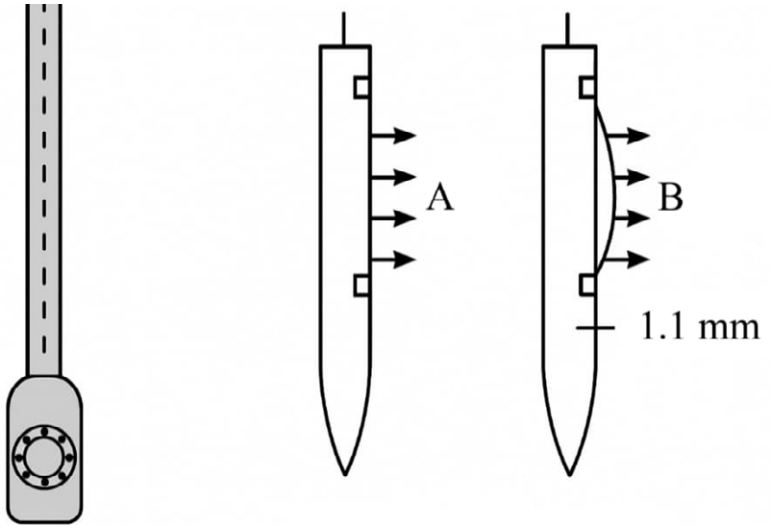

Figure 1: Schematic of DMT blade and pressure readings

2.2 IMPACT OF PARTIAL DRAINAGE

The standard DMT test is typically performed under drained conditions for sands and undrained conditions for clays. However, partial drainage can occur in intermediate soils, like natural silts and mine tailings, making distinguishing between drained and undrained conditions difficult, leading to unreliable data (Monaco et al., 2020). The DMT measures total horizontal stress in the soil but does not differentiate between pore water pressure and effective stress. In intermediate soils, excess pore pressure generated during penetration can dissipate over time, causing parameters like constrained modulus, over consolidation ratio, undrained shear strength, and K_o to be underestimated.

In gold tailings, Schnaid & Obebrecht (2015) observed that A readings decayed along with excess pore pressure dissipation, resulting in readings that did not fully align with drained or undrained conditions. They recommended taking initial readings within 1-3 seconds of penetration, but this is difficult to achieve with standard DMT equipment, requiring expert operation.

The challenge of the partial drainage effect in tailings has been observed through various field testing methods other than DMT, such as CPTu and VST. Various research studies consistently emphasise the importance of conducting tests at rates that maintain truly undrained conditions to ensure accurate interpretation of soil behaviour. (DeJong et al., 2012; Reid et al., 2023).

2.3 MEDUSA DMT

The Medusa DMT is an advanced version of the traditional mechanical DMT, incorporating hydraulic automation and a pressure measuring system for autonomous testing. It includes a motorised syringe, electronic board, pressure transducer, and a hydraulically operated flat dilatometer blade. The Medusa DMT applies hydraulic pressure to the diaphragm, unlike the original compressed gas system. A pressure transducer monitors the pressure during inflation to A, B and C readings. The device connects to a laptop on the surface, allowing technicians to control parameters like inflation rate, test duration, and penetration rate.

The Medusa DMT's high level of inflation control enables two new test procedures, which are discussed in more detail below.

2.4 DMT-WHILST PENETRATING

The Medusa DMT diaphragm is inflated to and ‘held’ in the A position by small adjustments to the diaphragm position. The DMT blade is then advanced into the soil at the nominated penetration rate by the CPT Pusher with a 1m stroke. The DMT pressure and positions measurements are collected at a high frequency whilst the blade is advanced, subject to soil consistency, creating a near continuous vertical profile of DMT A readings. A, B and C readings are also collected at 1m

vertical intervals as additional rods are added and the pusher reset. Initial tests conducted using this approach have shown remarkable repeatability in young clay-type materials discussed in Marchetti et al. (2021).

This research conducted the DMT-Whilst Penetrating (DMT-WP) tests using the DMT Repeated A (DMT-RA) module within the acquisition software. The tests were conducted over a fixed penetration distance of 1.0m at a fixed velocity. The data collected is then adjusted from pressure versus time readings to pressure versus depth readings.

2.5 DMT-REPEATED A

In the DMT RA test, the blade is advanced into the soil and at the target depth, the membrane is inflated to the A position. The Medusa system makes minor adjustments to the plunger position and pressure to maintain the membrane at the A position, compensating for the decay in the excess pressure. The test measures the decay in total horizontal stress. If no change in horizontal stress occurs during the A reading, it indicates either drained or undrained conditions over the period of the test. A stress drop suggests partial drainage, meaning the conditions are neither fully drained nor undrained. An example of this behaviour is conceptually shown in Figure 2(a), for A readings measured over 15 seconds. Figure 2(b) also presents example data measured in the current study on tailings under drained and partially drained conditions. Empirical correlations used to estimate undrained shear strength and K_0 from DMT results are derived for undrained conditions. To maintain consistency with these assumptions, materials exhibiting partial drainage behaviour should be tested over shorter time periods to minimise excess pore pressure dissipation during the test.

DMT-RA with Medusa DMT provides an opportunity to improve on the standard DMT test with A readings taken continuously for 15 seconds followed by a 15-second inflation to B, allowing for monitoring of excess pore pressure dissipation and screening for partial drainage (Marchetti and Totani, 1986 and Totani et al., 1998).

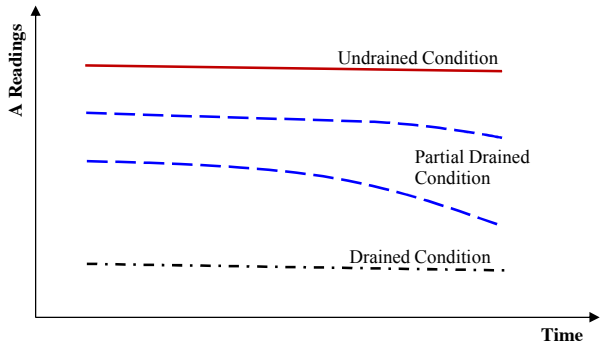

(a) Conceptual A reading response in different drainage conditions

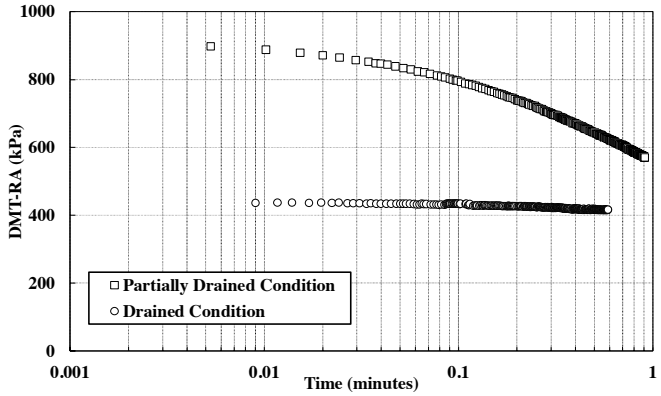

(b) Sample data demonstrating drainage influence on A-Reading

Figure 2: Variation in A-Reading response under different drainage conditions

3 SITE CONDITION AND TESTING PROGRAM

The DMT tests were performed on the tailings of an operational upstream Tailings Storage Facility (TSF) in Australia. The tailings in the TSF typically consist of varying thicknesses of coarse (sandy silt and silty sand) and fine tailings (silts). The fines contents of tailings vary from 10% to 100%. Due to the deposition methodology through the years, interbedded layers of coarse and fine tailings are encountered in the TSF. The fine portion of tailings is predominantly made of low to medium plasticity, with a plasticity limit ranging from 7 to 40%. The tailings have an average bulk density of 20 kN/m^3,

with a specific gravity of 3 to 3.3. The fine portion of tailings is predominantly contractive, while the coarser layers are mainly dense with a dilative response during penetration.

The testing was conducted in a TSF constructed using an upstream method. The dam geometry comprised a starter embankment followed by a series of upstream raises. Testing was carried out along a single cross-section at two different clusters. Cluster 1 was positioned on the upstream side, situated on the tailings beach and away from the starter embankment, with a maximum penetration depth of 40 m. In contrast, Cluster 2 was located closer to the starter embankment and reached a total penetration depth of approximately 25 m. The phreatic level was inferred to be at 5.3 m in Cluster 1 and at 3.15 m in Cluster 2.

Two CPTu tests were performed in each cluster at penetration rates of 20 mm/sec and 100 mm/sec. A total of 19 dissipation tests were conducted across both clusters to assess drainage conditions. Thirty-eight VSTs were conducted in Cluster 1 and four in Cluster 2 using a down-the-hole vane shear device to calibrate the CPTu-derived shear strength results. Both DMT-RA and DMT-WP tests were also performed in each cluster. The DMT tests were carried out at a penetration rate of 20 mm/sec.

4 RESULTS AND DISCUSSIONS

4.1 DISSIPATION TESTS

Pore water pressure dissipation testing was conducted during the CPTu to assess the site's drainage condition. The horizontal coefficient of consolidation, c_h, was derived using the procedure outlined by DeJong and Randolph (2012). The rigidity index was estimated using the shear wave velocity data and Method B proposed by Krage et al. (2014).

The estimated c_h values in Figure 3 suggest the tailings are prone to partial drainage conditions with the t_{50} (time to 50% pore pressure dissipation) of less than 30 seconds in all cases (Robertson et al., 1992). Although attempts were made to assess the drainage condition further using the normalised velocity concept developed by DeJong et al. (2012), the limitations were mainly related to the estimation of the anisotropic consolidation ratio for tailings with different properties and layer thicknesses.

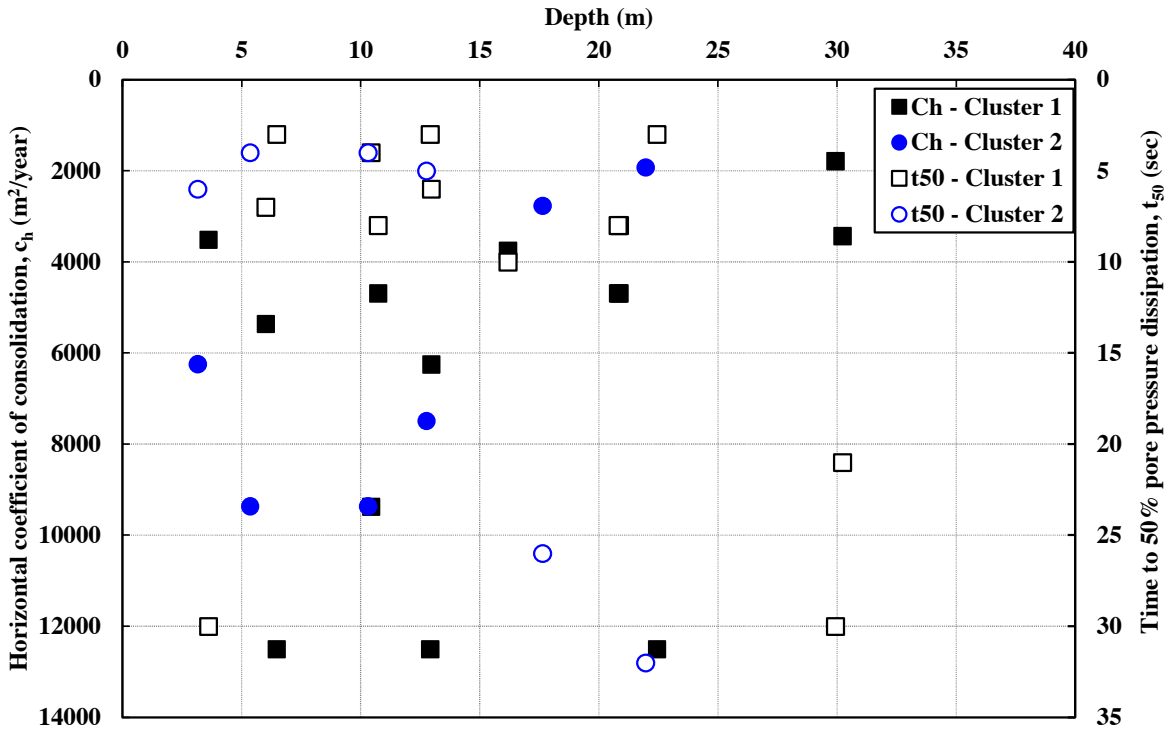

Figure 3: Dissipation test results: C_h and t_{50} versus depth

4.2 CPTU RESULTS

The results of the CPTu investigation profiles are presented in Figures 4 to 6 with both penetration rates of 20 and 100 mm/sec. In both clusters, the Normalized CPT Soil Behaviour Type (I_c) indicates interbedded coarse and fine tailings

layers in the upper section, as shown in Figure 4. However, the tailings exhibit a uniformly clay-like behaviour at depths of more than 25m in Cluster 1. In Cluster 2, a clay-like response is also observed beyond 15 m depth, although some layers of coarser tailings are present within this interval. For the purposes of this study, these deeper, clay-like zones are classified as the lower tailings unit, while the overlying materials are referred to as the upper tailings unit. Although, in theory, a faster penetration rate should affect the I_c estimation due to changes in cone resistance and sleeve friction in partially drained material, the difference in estimated I_c between the two penetration rates is not significant enough to indicate a different material type behaviour at any given depth.

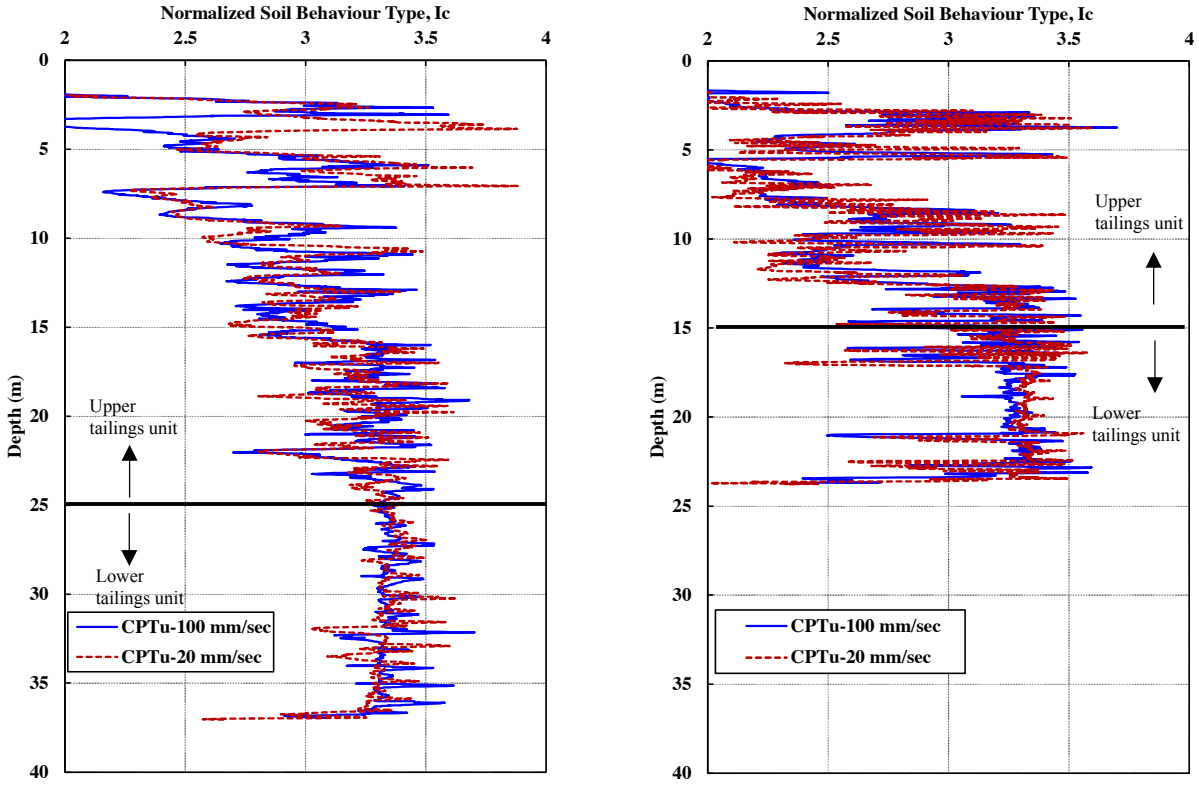

(a) Cluster 1 **(b) Cluster 2**

Figure 4: Normalized CPT Soil Behaviour Type, I_c versus depth

The normalised pore pressure parameter, B_q, was calculated for both clusters and shown in Figure 5 to assess the drainage condition. Generally, the faster the penetration, the higher the pore pressure induced in fine tailings, especially the fine tailings in the upper tailings unit. An example of this is highlighted in the Cluster 1 data (Figure 5a), within the depth range of 8 to 15 m, where the 100 mm/sec penetration rate results in significantly higher B_q values compared to the other dataset. This emphasises the possibility of partial drainage at lower penetration rates. For the lower tailings units, the difference in B_q of two penetration rates is marginal, potentially indicating "undrained" penetration condition. These layers have a uniform I_c of more than 2.95.

To assess the shear strength response, the following equation was used:

$$S_u = \frac{q_t - \sigma_v}{N_{kt}} \quad (1)$$

where q_t is corrected tip cone penetration, σ_v is total vertical stress, and N_{kt} is an empirical parameter.

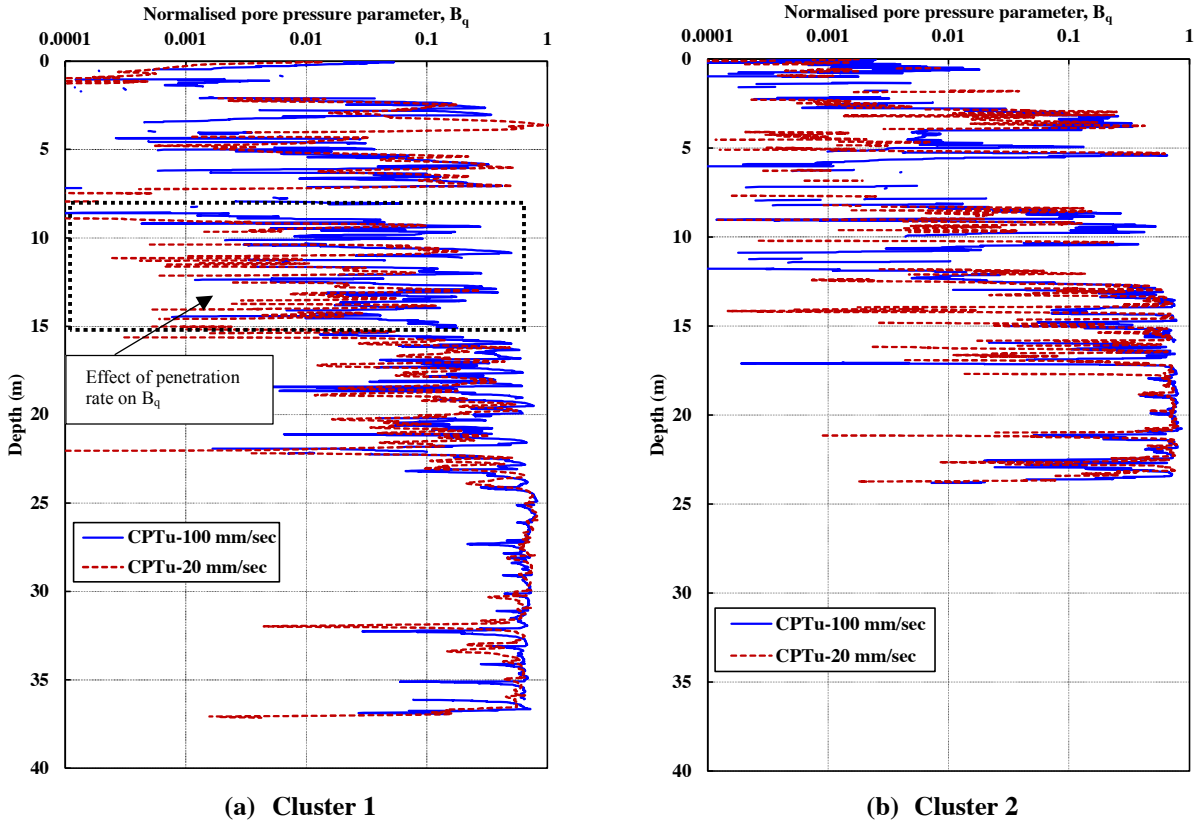

Figure 5: Normalised pore pressure parameter, B_q versus depth

Mayne and Peuchen, (2018) proposed the following correlation for estimation of N_{kt}:

$$N_{kt} = 10.5 - 4.6\ln(B_q + 0.1) \quad (2)$$

Equation (2) was used as a preliminary estimate of N_{kt}. Two important limitations of this equation in the context of the current investigation are: (a) it was primarily developed for natural clay materials, and (b) B_q, as shown in Figure 5, can be influenced by the penetration rate. Therefore, the estimated S_u was compared against field VST data, with the results shown in Figure 6. The S_u was only estimated for layers with B_q greater than 0.02 and I_c greater than 2.95. Although this is not an entirely robust criterion for distinguishing undrained from drained penetration, it provides a reasonable level of data filtering.

The VSTs were conducted at two rotation rates: 120 and 360 degrees per minute in Cluster 1, while all four tests in Cluster 2 were performed at 360 degrees per minute. According to the criteria proposed by Chandler (1988), none of the tests conducted at 120 degrees per minute could be classified as undrained. In contrast, the tests performed at 360 degrees per minute in both clusters either satisfied the undrained condition or are close to the dimensionless time factor T of 0.05, as defined by Chandler (1988).

For Cluster 1, a broad range of VST data is available at various depths to validate Equation (2). As the CPTu data matches reasonably well with the measured VST data, the same methodology was applied to Cluster 2. The results show that the two CPTu penetration rates yield relatively similar S_u estimates in the lower tailings unit, particularly in Cluster 1 supporting the trends observed in the B_q data. It should be noted that using Equation (2), an approximate N_{kt} of 12 was derived for the lower tailings unit. The estimated undrained shear strength ratio (S_u/σ'_{v0}) is shown in Figure 7. Between the two clusters, and within the lower tailings unit, a marginal difference in S_u/σ'_{v0} is observed, with higher values determined in Cluster 2.

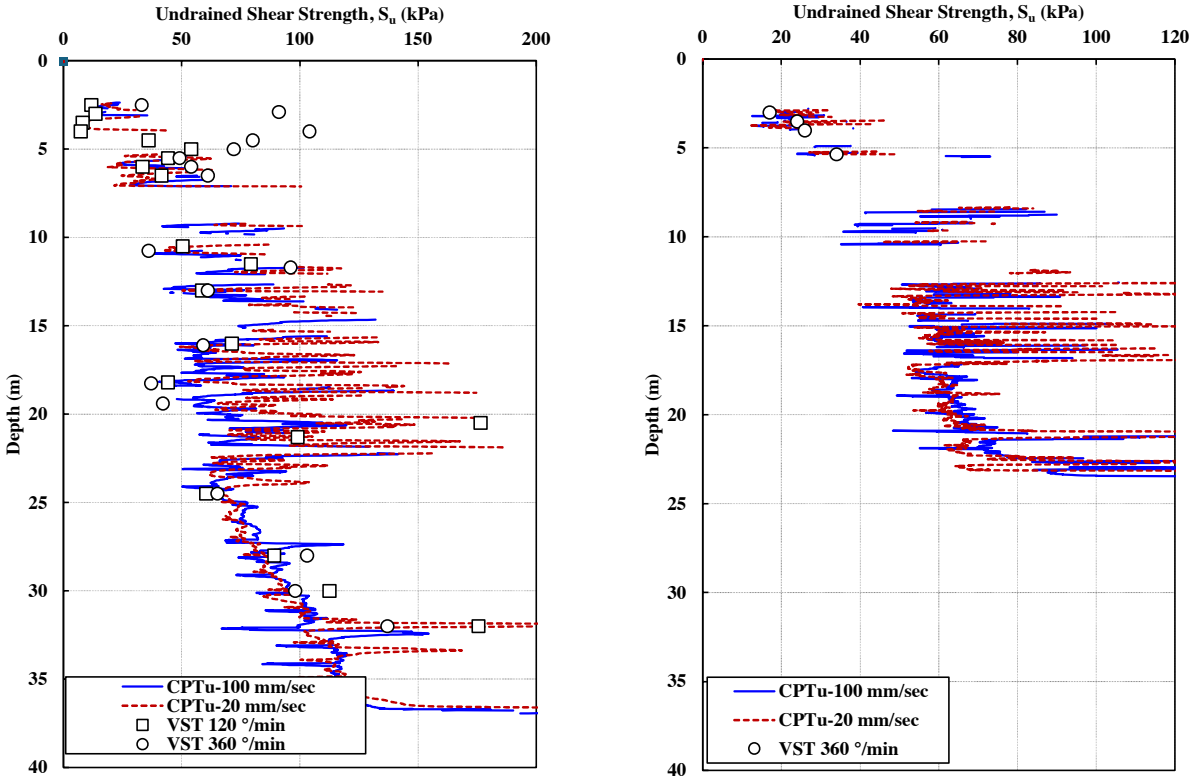

(a) Cluster 1 (b) Cluster 2

Figure 6: CPTu estimated S_u

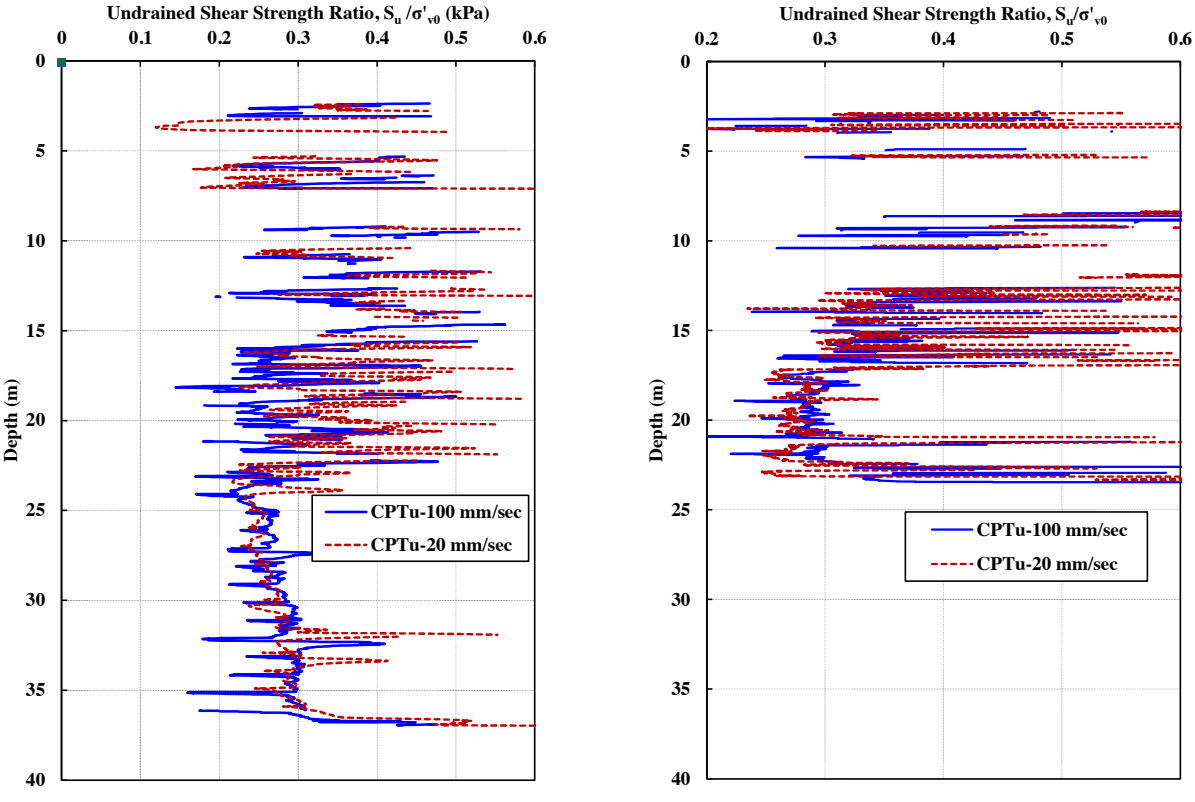

(a) Cluster 1 (b) Cluster 2

Figure 7: CPTu estimated S_u/σ'_{v0}

4.3 DMT RESULTS

Figure 8 provides the DMT-WP initial Readings. The A readings were collected at a depth interval ranging between 5-30 mm, while the B readings are only performed after every 1m penetration interval. Therefore, parameter B was linearly interpolated between each two points. Given the interbedded nature of the tailings in this investigation, the one metre interval of B readings may have missed important responses in both coarse and fine tailings. However, the continuous and accurate A readings carry significantly more weight in the estimation of parameters such as K_o, particularly through the application of Equations (3–8) presented below.

The initial readings in Figure 8 can be used to estimate the following corrected readings (Marchetti, S. 2001):

$$P_0 = 1.05(\mathrm{A} + \Delta A) - 0.05(\mathrm{B} + \Delta B) \tag{3}$$

$$P_1 = (\mathrm{B} + \Delta B) \tag{4}$$

where ΔA and ΔB are membrane calibration values, P_0 is the corrected lift-off pressure, and P_1 is the corrected second reading. The parameter P_o, which is predominantly derived from A readings with minimal influence from B readings, can be used to estimate several intermediate parameters, as outlined below (Marchetti, S., 2001):

$$I_D = (P_1 - P_0)/(P_0 - U_0) \tag{5}$$

$$K_D = (P_0 - U_0)/\sigma'_{v0} \tag{6}$$

where I_D is a material index, K_D is the Horizontal Stress Index, U_0 is the equilibrium water pressure and σ'_{v0} is the effective vertical stress. The parameter I_D provides an indication of material type and penetration condition (drained or undrained), while parameter K_D is used to estimate the interpretation parameters such as K_0 and undrained shear strength (Marchetti, S. 2001):

$$K_0 = (K_D/1.5)^{0.47} - 0.6 \tag{7}$$

$$S_u = \alpha\, \sigma'_{v0}(0.5K_D)^{1.25} \tag{8}$$

where parameter α is an empirical factor to estimate undrained shear strength. The α of 0.22 was suggested based on the discussions of Mesri (1975) for normally consolidated soft clays (Marchetti 1980) and it is mainly used in DMT test results evaluations (Marchetti, 2001). For the lower tailings unit in this study, the 50th percentile undrained shear strength ratio is approximately 0.27 (Figure 7), and this value was adopted in Equation (8). The median was selected for this unit because the data shows relatively low variability compared to the upper tailings unit. In contrast, a lower-bound value corresponding to the 20th percentile ($S_u/\sigma'_{v0} = 0.3$) was used for the upper tailings unit, due to the greater variability in the data caused by the presence of interbedded coarse and fine tailings.

Equations (6) and (7) were proposed for I_D less than 1.2, classifying as clay and silt materials (Marchetti, S. 2001). However, partially drained materials such as tailings can also yield an I_D less than 1.2, while undrained penetration remains in question.

Equations (7) and (8) were originally derived from studies on natural clays and silty materials (Marchetti, 1980), primarily under undrained conditions. While the tailings in this study contain low to medium plasticity fines, their behaviour may deviate from the assumptions underlying these empirical correlations, particularly given the potential for partially drained condition. In the absence of site-specific calibration data, these equations are applied for initial estimates of S_u and K_0, with recognition of the associated uncertainty. Future work incorporating laboratory testing or direct in-situ stress measurements K_0 would help validate and refine the applicability of these correlations to tailings materials.

The resulting undrained shear strength from DMT-WP is shown in Figure 9. The comparison is made using CPTu data with a 100 mm/s penetration rate, as the effects of partial drainage are less pronounced at higher penetration rates. The results are presented for lower and upper tailings units in different colours. Good agreement is observed between DMT-WP and CPTu/VST data for the lower tailings units in Cluster 1. In Cluster 2, VST data are not available for the lower tailings unit; however, given the similarity of the material to Cluster 1, comparison between DMT and CPTu data is considered appropriate. This suggests that a potential undrained condition could be met at a lower depth where uniform layers of fine tailings are present. Spikes in the DMT results are mainly linked to the start of penetration at each 1 m interval, where undrained conditions were not properly achieved. The primary cause is the pore pressure decay that happens when penetration is stopped to perform the B reading. For the upper tailings unit, the undrained shear strength cannot be estimated accurately due to partial drainage

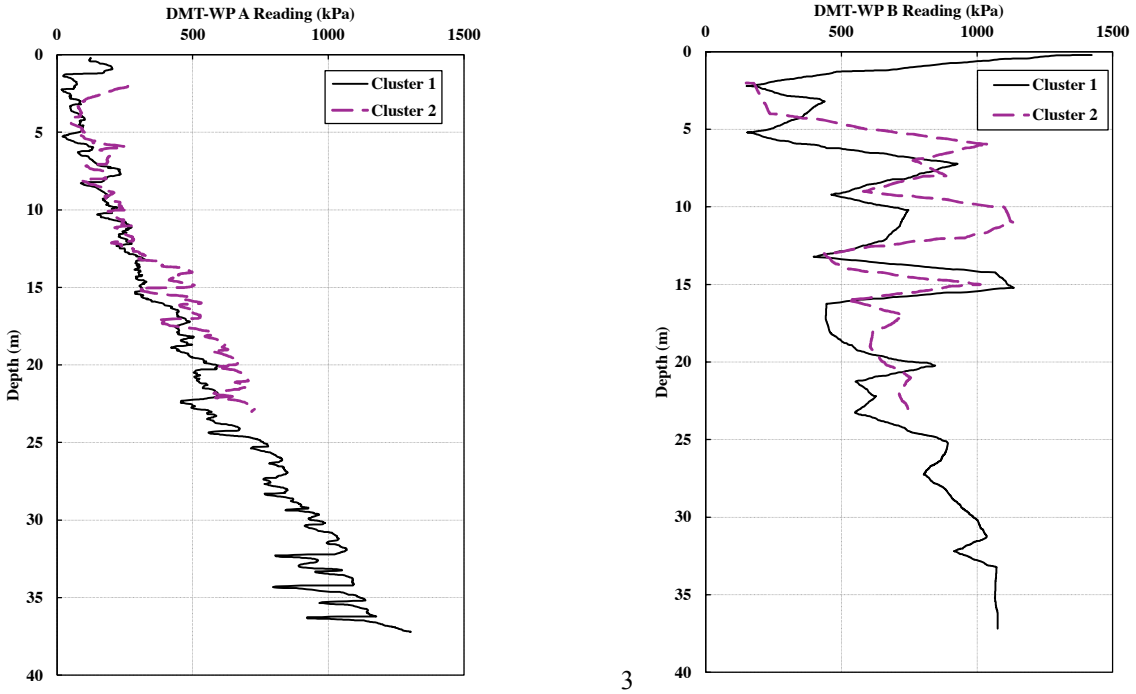

(a) Cluster 1 (b) Cluster 2

Figure 8: DMT-WP A and B readings

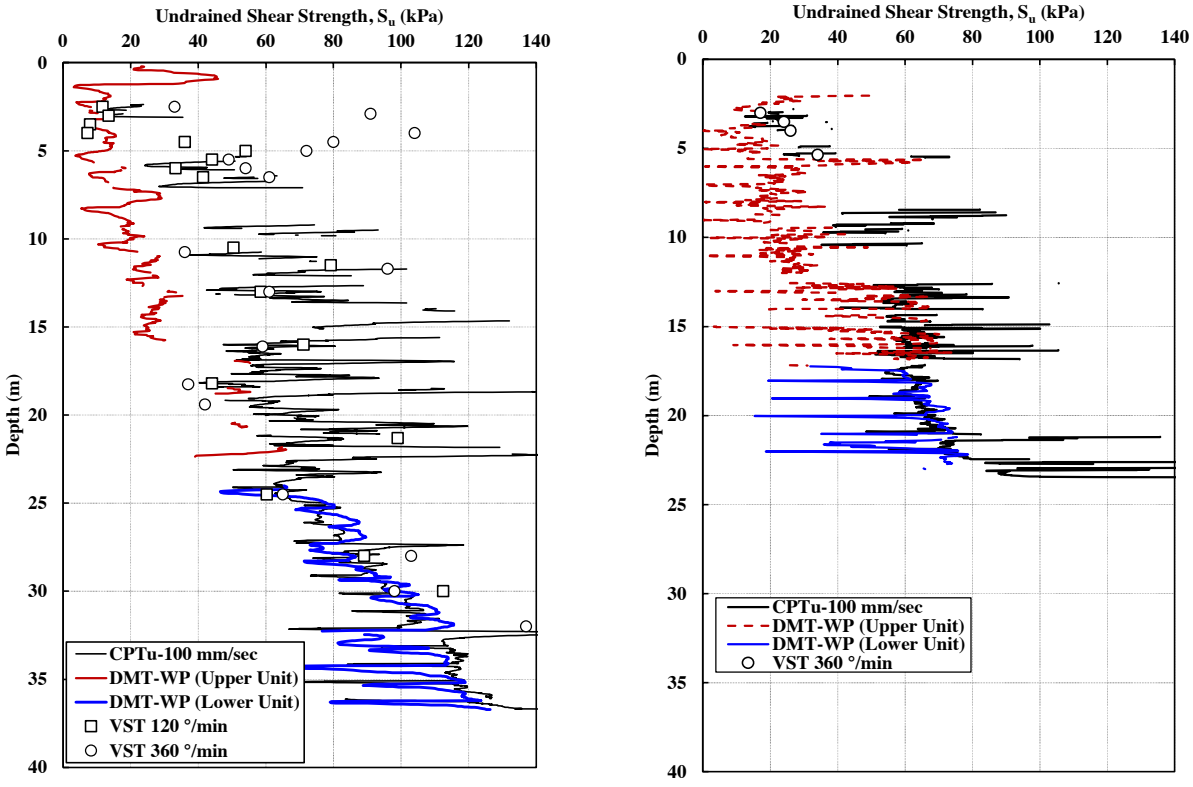

(a) Cluster 1 (b) Cluster 2

Figure 9: DMT-WP estimated Su against the CPTu data.

The parameters K_0 and S_u are derived directly from P_0 readings, with no influence of P_1 readings. Since the DMT-WP provided reasonable shear strength results for the lower tailings unit, the parameter K_0 was only determined for the same depth and is presented in Figure 10(a). The data predominantly ranged between 0.5 and 0.6 in Cluster 1 and 0.5 to 0.65 in Cluster 2. This is appropriate given that Cluster 2 data are closer to the starter embankment and early stages of upstream raises, tolerating some level of bias, which results in higher K_0 than Cluster 1.

As shown in Figure 10(a), the onset of rod penetration consistently corresponds to the lowest estimated K_0 value within each penetration interval. This is likely due to the B reading being taken prior to rod advancement, allowing some pore pressure dissipation and resulting lower A (and consequently P_0) readings. Upon resuming rod penetration, the A reading increased until stabilising at a relatively constant value within each interval. This stabilisation is evident in the final 10 cm of rod penetration for each interval in Cluster 1 data, as illustrated in Figure 10(b). In Cluster 1, most of the data points in the last 10 cm penetration are confined to a narrow K_0 range (less than 0.3), except for one data set around the 33 m depth. In contrast, Cluster 2 exhibits more scatter, likely due to the presence of interbedded coarse tailings observed beyond 15 m depth, as shown in Figure 4(b).

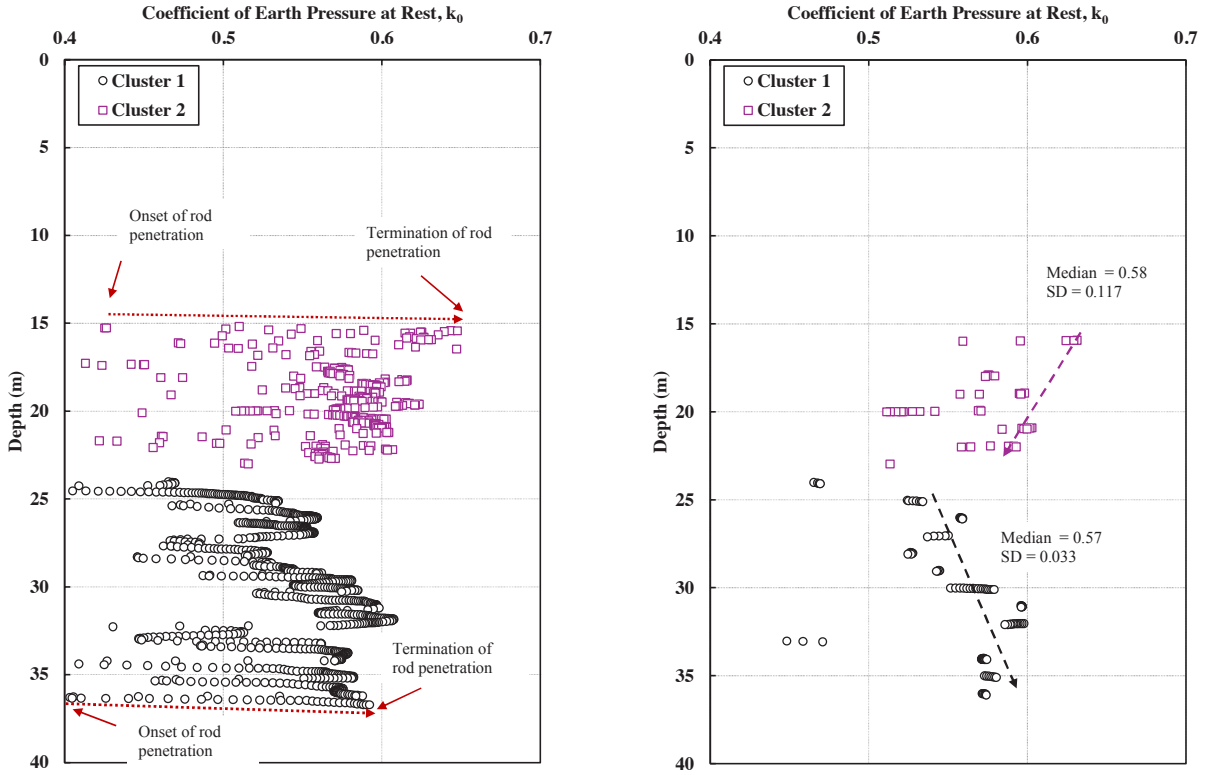

(a) All data in lower tailings unit **(b) Last 20cm penetration of each rod interval**

Figure 10: DMT-WP estimated K_0 versus depth

The significant drop in A readings over a short time span and its impact on K_0 can be further assessed with DMT-RA testing. DMT-RA tests were performed, not in the same clusters but in proximity with similar tailings profiles. The resulting A decay with time is shown in Figure 11 for the upper and lower tailings units. For the lower tailings unit, the decay in A readings occur immediately after the penetration is stopped to collect reading, while for the upper units, the penetration is either in a drained condition or the decay in excess pore pressure has occurred before the start of A readings.

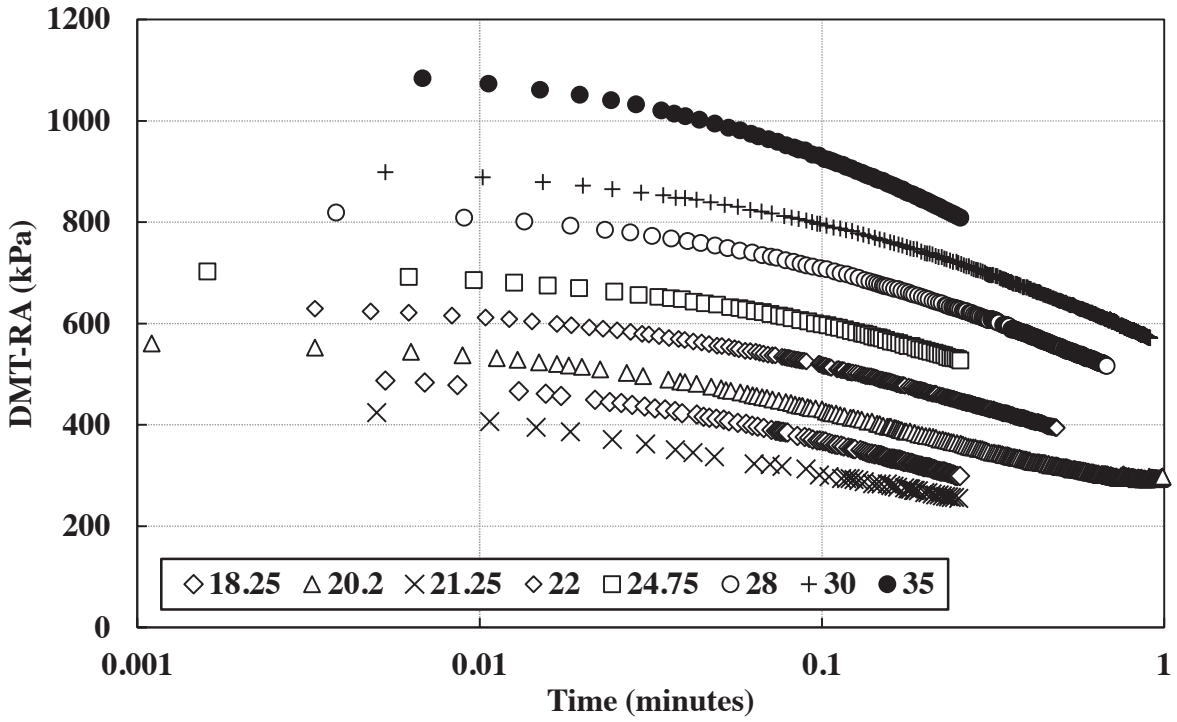

(a) Lower tailings unit

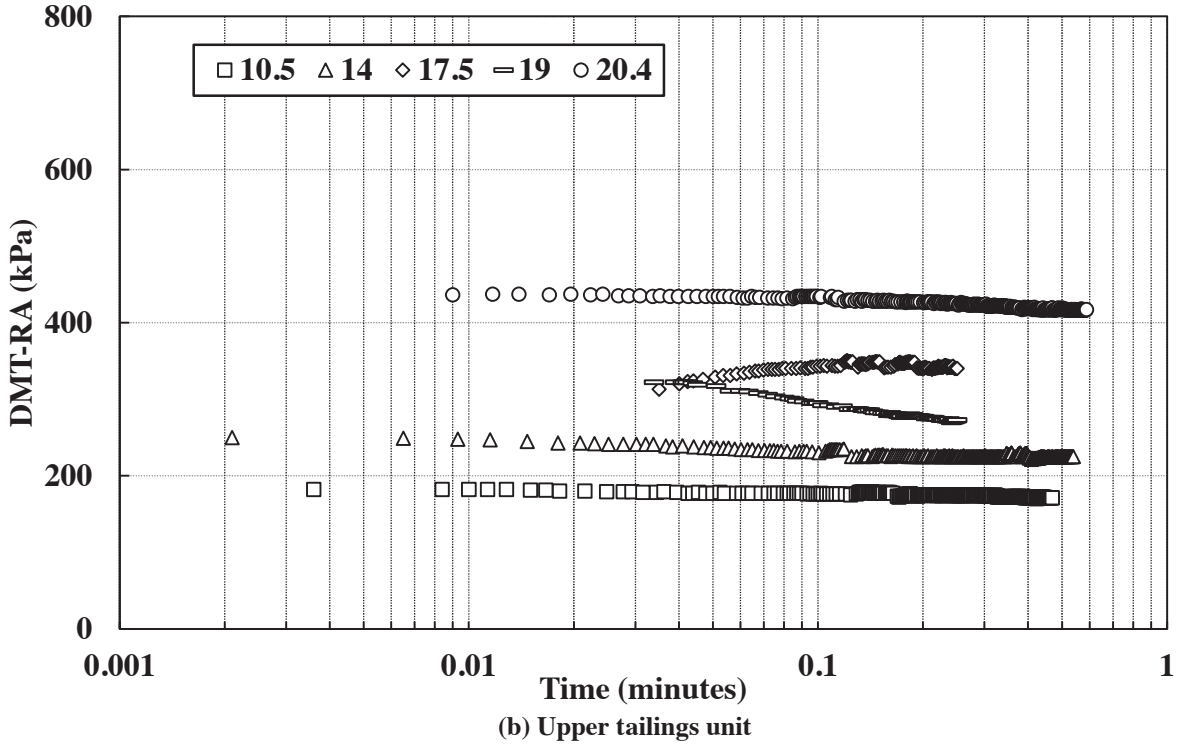

(b) Upper tailings unit

Figure 11: Variation of DMT-RA readings with time

To emphasise the rate effect on DMT test results in intermediate materials, a comparison in estimated P_0 is shown between the standard DMT, Corrected DMT-RA and DMT-WP in Figure 12 for Cluster 1 data. It can be observed that the standard DMT significantly underestimates the P_0 using the A readings at 15 seconds. The normal DMT results can be corrected by using the A readings at the time ~ 0-1 seconds, and the results of calculated P_0 are closer to the DMT-WP, although still on the lower bound. These results indicate that the A readings should occur as quickly as possible in intermediate materials, prior to drainage occurring which directly results in an underestimate of P_0.

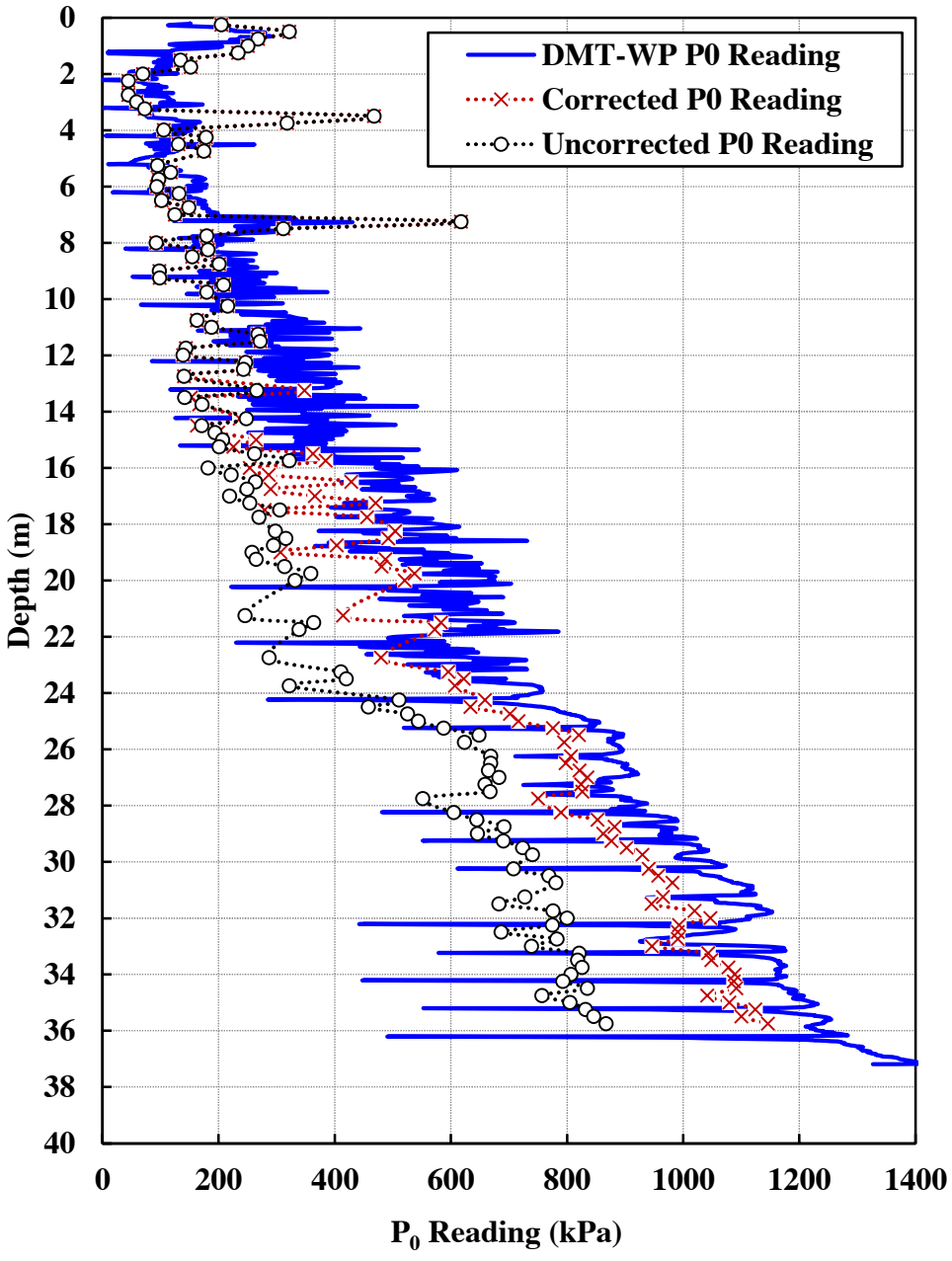

Figure 12: P_0 readings in DMT-WP and corrected and uncorrected Normal DMT

5 LIMITATIONS

The following limitations are highlighted as part of the current study:

- The DMT tests are generally performed at a penetration rate of 20 mm/sec. Given the significant A decay with time observed in this study, employing higher penetration rates could enhance the accuracy of parameter estimations by reducing pore pressure dissipation during testing.
- The empirical correlations used to derive parameters such as S_u and K_0 from DMT data were primarily developed for natural clays. Their direct application to tailings and low-plasticity silts may introduce uncertainties, highlighting the need for further calibration specific to these materials.

6 CONCLUSIONS

A series of in-situ test were performed on tailings, including CPTu, VST and DMT testing. The tailings range from coarse to fine, with varied plasticity and fines content. The dissipation test results suggested that the materials are prone to partial drainage, where penetration rate and testing speed can influence the results. The CPTu data illustrated that the upper tailing units consist of a combination of interlayered coarse and fine tailings, while the lower unit were predominantly uniform clay-like behaving material.

The CPTu test results suggested differences in upper unit under different penetration rates, the lower units were less affected, showing similar results. There was a noticeable difference in the P_0 readings in the lower unit between the three different DMT test methodologies, with the DMT-WP results less or unaffected.

The values from the DMT-WP test were used to estimate the undrained shear strength for lower units, which matched well with CPTu and VST results. This alignment supported the assessment of the other P_0 derived parameters, K_0 and S_u in lower tailings units. The field-testing procedure adopted in this work provides valuable information in the interpretation of the DMT test results.

DMT-RA tests were conducted at regular intervals as part of a standard DMT profile to access the drainage during the test. This test method provides helpful information regarding the drainage condition of the material and assessment of A reading decay with time. It is envisaged that this test procedure will become standard practice with every DMT test, particularly in tailings.

These new DMT test methodologies are only possible with the new Medusa DMT which enables high-quality operator-independent tests. The high-speed readings and adjustments to the diaphragm position enable new tests that can assess and manage partial drainage effects. In intermediate materials the DMT test should be performed in the fastest practical way to estimate the parameters related to the undrained condition, such as undrained shear strength and K_0.

CRediT authorship contribution statement

Mahdi Naeini: Data curation, Formal analysis, Writing - original draft. **Mark Chapman:** Methodology, Data curation, Writing – review & editing. **Arun Muhunthan:** Conceptualisation, Supervision, Writing – review & editing. **Marty Viney:** Project administration. **Pamela Soto:** Funding acquisition.

7 REFERENCES

Chandler, R.J. (1988) “The in-situ measurement of the undrained shear strength of clays using the field vane”, Vane shear strength testing in soils: field and laboratory studies, 1014, pp.13-44.

DeJong, J. T., Jaeger, R. A., Boulanger, R. W., Randolph, M. F. and Wahl, D. A. J. (2012) ‘Variable penetration rate cone testing for characterization of intermediate soils’, Geotechnical and Geophysical Site Characterization, 4(1), pp. 25–42.

Jefferies, M. and Been, K. (2006) ‘Initiation of static liquefaction and the role of K_o consolidation’, Canadian Geotechnical Journal, 43(6), pp. 746–758. https://doi.org/10.1139/t06-048.

Krage, C. P., Broussard, N. S. and DeJong, J. T. (2014) ‘Estimating rigidity index (IR) based on CPT measurements’, in Proceedings of the 3rd International Symposium on Cone Penetration Testing, Las Vegas, NV, pp. 727–735.

Marchetti, D., Danziger, F. A. B. and Jannuzzi, G. M. F. (2021) 'Comparison of DMT results using traditional pneumatic equipment and the Medusa DMT in the Sarapuí II soft clay deposit in Brazil', Proceedings of the 6th International Conference on Geotechnical and Geophysical Site Characterization (ISC'6), Budapest, Hungary.

Marchetti, D., Monaco, P., Amoroso, S. and Minarelli, L. (2019) 'In situ tests by Medusa DMT', Proceedings of the XVII European Conference on Soil Mechanics and Geotechnical Engineering (ECSMGE-2019), Reykjavik, Iceland.

Marchetti, S. (1980) 'In situ tests by flat dilatometer', Journal of the Geotechnical Engineering Division, 106(3), pp. 1529–1540. Available at: https://ascelibrary.org/doi/10.1061/AJGEB6.0000934.

Marchetti, S. (2001) The flat dilatometer test (DMT) in soil investigations: TC16 report, International Society for Soil Mechanics and Geotechnical Engineering, Technical Committee TC16.

Marchetti, S. and Totani, G. (1986) 'The DMT-A test method for evaluating permeability in soft soils', Proceedings of the International Conference on In-Situ Testing in Geotechnical Engineering, pp. 1–10.

Mayne, P.W. and Peuchen, J. (2018) 'Evaluation of CPTU Nkt cone factor for undrained strength of clays', In Cone Penetration Testing 2018 (pp. 423-429). CRC Press.

Monaco, P., Amoroso, S., Chiaradonna, A., Marchetti, D., Le, T. M. H. and L'Heureux, J. S. (2024) 'Characterization of intermediate soils by innovative in-situ testing procedures using Medusa DMT', in Geotechnical Engineering Challenges to Meet Current and Emerging Needs of Society, pp. 679–682. CRC Press.

Robertson, P. K., Sully, J. P., Woeller, D. J., Lunne, T., Powell, J. J. M. and Gillespie, D. G. (1992) 'Estimating coefficient of consolidation from piezocone tests', Canadian Geotechnical Journal, 29(4), pp. 539–550.

Schnaid, F., Marchetti, S., Odebrecht, E. and Belloli, V. A. (2015) 'Effects of test procedures on DMT results in intermediate soils', Canadian Geotechnical Journal, 52(10), pp. 1550–1562. https://doi.org/10.1139/cgj-2015-0463.

Schnaid, F., Marchetti, S., Odebrecht, E. and Belloli, M. V. A. (2018) 'Interpretation of the DMT in silts', Geotechnical Testing Journal, 41(5), pp. 868–876.

Totani, G., Calabrese, M. and Monaco, P. (1998) 'In situ determination of ch by flat plate dilatometer', in Proceedings of ISC-1, Atlanta, Georgia, pp. 883–888.

Wang, T. and Ismail, M. (2022) 'Static liquefaction triggering and post-liquefaction strengths of oil sands tailings', Journal of Geotechnical and Geoenvironmental Engineering, 148(5), p. 04022017.

Reid, D., Dickinson, S., Mital, U., Fanni, R. and Fourie, A. (2021) 'On some uncertainties related to static liquefaction triggering assessments', Proceedings of the Institution of Civil Engineers – Geotechnical Engineering, 175(2), pp. 181–199.

Reid, D., Rodriguez, C., Fourie, A. and Tiwari, B. (2023) 'Partial Drainage Effects during Vane Shear Tests, with an Emphasis on the Measurement of Remoulded Strengths', Proceedings of Tailings and Mine Waste, Vancouver, Canada.

WAGSTAFF PILING

BUILDING WORLD-CLASS FOUNDATIONS WITH YOU

Wagstaff Piling is Australasia's Leading Foundations Contractor since 1981.

From design to installation, we're ready to build foundations for all your geotechnical needs.

- Ground Improvement
- Retention Systems
- Driven Piles
- Bored Piling
- CFA Piles
- Foundation Design & Techniques
- Micro/Mini Piles Specialists
- Grouting
- Ground Anchors
- Down the Hole Hammer

PILING AND FOUNDATION SPECIALISTS FEDERATION
DEEP FOUNDATIONS INSTITUTE DFI
CONCRETE INSTITUTE of AUSTRALIA
SIMSG ISSMGE
bsi ISO 45001 Occupational Health and Safety Management CERTIFIED ISO 9001 Quality Management Systems CERTIFIED ISO 14001 Environmental Management CERTIFIED

WAGSTAFF PILING

WAGSTAFFPILING.COM.AU

PROBABILITY OF DAM SLOPE FAILURE AND DECISION-MAKING

Jiri Herza[1] and Hugo Fellows-Smith[2]

[1] HATS Consulting, [2] University of Western Australia

https://doi.org/10.56295/AGJ60410

ABSTRACT

Contemporary approaches to estimating slope failure probabilities of dams combine two main frameworks. One employs numerical models that represent input variability with statistical distributions. The other relies on empirical relationships and expert judgement to account for unquantifiable factors and limited knowledge. Whatever the analytical sophistication, any probability assigned to the one-off event of slope failure eventually incorporates a subjective degree of belief.

Despite its subjectivity, any framework used for safety-critical decisions should be internally consistent and logically coherent, so resulting decisions remain ethically and legally defensible. With this principle in mind, this paper examines the method introduced by Silva et al. (2008), a framework designed to inform dam-safety decisions and widely adopted in Australia and overseas. Using formal logic as the primary lens, the paper evaluates the coherence of the Annual Probability of Failure – Factor of Safety – Project Category approach without assessing data availability or judging practical convenience.

Our analysis reveals three key points. First, the anchor points that define the curves are not supported by a probabilistic model or empirical observations. Second, the fixed ordering of Project-Category curves does not fully reflect the key premise that more rigorous engineering reduces uncertainty. Third, the progressive flattening of the curves could discourage practitioners from adopting proven risk-control measures.

To strengthen its logical footing, this paper restates the framework as a formal theorem that makes every assumption explicit and outlines adjustments that resolve the inconsistencies. Well-documented cases where failures occurred despite apparently adequate Factors of Safety motivate an alternative probability estimate based on the likelihood of a critical engineering error. The paper concludes with a streamlined procedure for addressing foreseeable slope-instability risks within the Australian context.

1. MOTIVATION

The greatest tragedies are often labelled as "black swan" events, a term that allows individuals to evade admitting that earlier action could have been taken.

While some adverse events have been extensively studied, modelled, and assessed, others appear entirely unprecedented, shocking observers when they occur. This perception stems from the vast number of possible adverse scenarios, our incomplete understanding of underlying processes, and the limited resources available for their study.

The Swiss National Bank's decision on 15 January 2015 to scrap its CHF 1.20 per EUR cap caused the largest one-day move in a major currency since the 1970s. Foreign-exchange broker FXCM lost USD 225 million in fifteen seconds and called the event a "40-sigma" shock (Euromoney, 2015), implying a probability below 10^{-800}. Yet the scenario was never impossible: the SNB retained unilateral control over the cap and had publicly hinted at its removal months earlier (WSJ, 2014), while similar policy reversals by other central banks were well documented (Askari & Mirakhor, 2015). FXCM's loss arose because its risk models ignored a policy-driven discontinuity of that scale. The episode shows how omitting a plausible mechanism can render probabilistic estimates meaningless, a failure mode that becomes critical where the consequences are severe, as with dam failures.

Every dam failure is unique because the exact combination of structural conditions and triggers cannot be replicated. Although sabotage, warfare, and deliberate removal can cause failure, dams are designed and operated for stability and longevity, so unintended failures arise only under unforeseen or unaccounted-for conditions.

The 2019 Brumadinho tailings-dam disaster in Brazil exemplifies this problem. The owner, Vale S.A., reported that the dam contained 94 piezometers and 41 water-level indicators, with data collected and analysed regularly (Vale, 2019). Routine inspections revealed no deterioration, and Vale stated that "*the dam had a Safety Factor in accordance with world best practices and was above the Brazilian Standard reference point*." Two "Stability Condition Statements" issued by TÜV SÜD do Brasil in 2018 (TÜV SÜD, 2018) likewise attested to the dam's physical and hydraulic safety; the lowest pre-failure factor of safety reported was 1.09.

The case highlights a critical question: what does a pre-failure factor of safety actually signify when failure still occurs despite apparent compliance with accepted standards?

Faced with incomplete knowledge, engineers turn to risk assessment to evaluate possible outcomes, represent uncertainty, and judge the plausibility of extreme events such as dam failures. Yet the FXCM and Brumadinho examples show that a highly regulated environment, complete with multiple checks and balances, can fail abruptly when a governing failure mechanism is missing from the risk catalogue.

Acknowledging that dams can fail in many ways, this paper concentrates on embankment failures driven by slope instability. Specifically, it examines how the pre-failure factor of safety (*FoS*) is interpreted, how relevant it remains after failure, and how it informs decision-making.

Maintaining an adequate *FoS* is a cornerstone of engineering practice and is embedded in guidelines, standards, and legislation. The ANCOLD Guidelines on Tailings Dams (ANCOLD, 2019) provide an Australian example, recommending minimum *FoS* values that accommodate modelling limitations, material variability, and other uncertainties.

FoS is often converted to a probability of failure for slope instability. Silva et al. (2008) extended Lambe's (1985) ideas by creating an empirical relationship that links slope stability *FoS* and project category (*PC*) to annual probability of slope failure (P_f). Their framework, based on expert elicitation, blends calculated *FoS* with engineering diligence. Recognising that higher *FoS* values do not always imply lower P_f, the method has gained wide acceptance and is cited in the ANCOLD Guidelines on Risk Assessment (ANCOLD, 2020).

Other probability-estimation approaches derive from reliability theory, which models component interactions within a formal probabilistic framework (e.g. Whitman, 1984). Although reliability methods are well developed in many fields and have been studied for geotechnical structures (Christian et al., 1992; Dunken, 2000; Hartford & Baecher, 2004 and Xiao et al., 2020), uptake for embankment dams remains modest. Key obstacles include limited high-quality failure data, difficulties in producing robust phenomenological models, and lingering gaps in fundamental soil-mechanics knowledge (Mitchell & Soga, 2005). Consequently, reliability-based estimates for slope instability still rely, at least in part, on expert judgement (Hicks & Li, 2021).

Given its broad use in Australia, this paper focuses on the Silva et al. (2008) framework that the authors offered for "*risk-based decision making for situations involving slope failures.*" Under Australian law, safety decisions must be defensible, reasonable, and based on sound rationale. We therefore test the P_f-*PC*-*FoS* relationship proposed by Silva et al. (2008) for logical consistency, without judging the quality of its data, its predictive power or practical utility. In this paper we:

- Construct an explicit regression function that represents the relationship inferred by Silva et al. and test it for internal coherence
- Examine the method presented by Silva et al. (2008) through the lens of formal logic
- Outline modifications that resolve identified consistency issues
- Propose an alternative probability model based on the likelihood of critical engineering error
- Present a practical method that addresses slope-instability concerns within the Australian legal framework without requiring a quantitative failure-probability estimate

2. PHILOSOPHICAL BASIS OF SUBJECTIVE PROBABILITY

Though we can construct a formal logical system to quantify a subject's degree of belief, which we may call probability, such probability has no physical meaning.

Recognising the limitation of our knowledge, data and tools for dam risk assessment, ANCOLD (2022) defines probability as: "*A measure of the degree of confidence in a prediction, as dictated by the evidence, concerning the nature of an uncertain quantity or the occurrence of an uncertain future event. It is an estimate of the likelihood of the magnitude of the uncertain quantity, or the likelihood of the occurrence of the uncertain future event*."

Furthermore, ANCOLD (2022) clarifies: "*This type of probability is not a property of the dam, but a reflection of the best understanding of the analysis team, given the available knowledge and data concerning the question at issue*."

This view echoes Laplace (1774), who described probability as a measure of our ignorance, implying that with complete knowledge, probability statements would collapse into tautology. Chapter 6 will revisit this idea when we propose an alternative estimate of slope-failure probability based on the chance of critical engineering error.

When assessing the probability of dam slope failure through *FoS* estimation, we must recognise that the estimated *FoS* is not a physical feature of the dam. Instead, it is a computed (expected) ratio of resisting and driving forces calculated using methods and models that significantly simplify the very complex processes (e.g. Mitchell and Soga, 2005). Despite its

name, the *FoS* values alone do not explicitly define safety, as explained in Silva et al. (2008). The same applies to the *PCs*, which are judgement-based indicators of uncertainty in input data and their analysis, not inherent properties of the project.

At this point, it is worth clarifying a common misconception that the method presented in Silva et al. (2008) was based on best fitting of observed annual failure frequencies of real-like projects separated into four categories. While the projects analysed by Silva's team were real, the P_f values presented Silva's team degree of belief in the notion of slope failures informed by their own calculations of *PC* and *FoS* variables. In Silva et al.'s (2008) own words "*the failure probabilities reflect their judgement of the relative degree of safety of the various earth structures."*

Due to their subjective nature, the P_f-*PC*-*FoS* relation is meaningful only within the context established by Silva's team. Nonetheless, if it is to guide rational decisions, the underlying reasoning must be logically sound. For this paper we adopt the general conception of logic as the discipline of rational thought that ensures that the beliefs and their analytical products are not self-contradictory (Ramsey, 1926).

3. THE SILVA METHOD

Risk assessment holds no greater value than the utility of its outcomes, for its worth is measured not in the precision of probabilities and consequences, but in the insight, it affords to action.

Silva et al. (2008) adopted, refined and generalised the relationship between *PC, FoS* and P_f previously used to assess risks of slope failure of the coastal Amuay cliffside in Venezuela (Lambe, 1985). Lambe (1985) presented this relationship only in a graphical form and explained that "*We prepared Figure 21* [reproduced in Figure 1 – left] *as a numerical expression of our judgement – we had little data to prepare these plots*."

Silva et al. (2008) explained that his team, including Dr. Lambe and Dr. Marr together with their associates also developed their plot (Figure 1: - right) through quantification of the team's expert judgement.

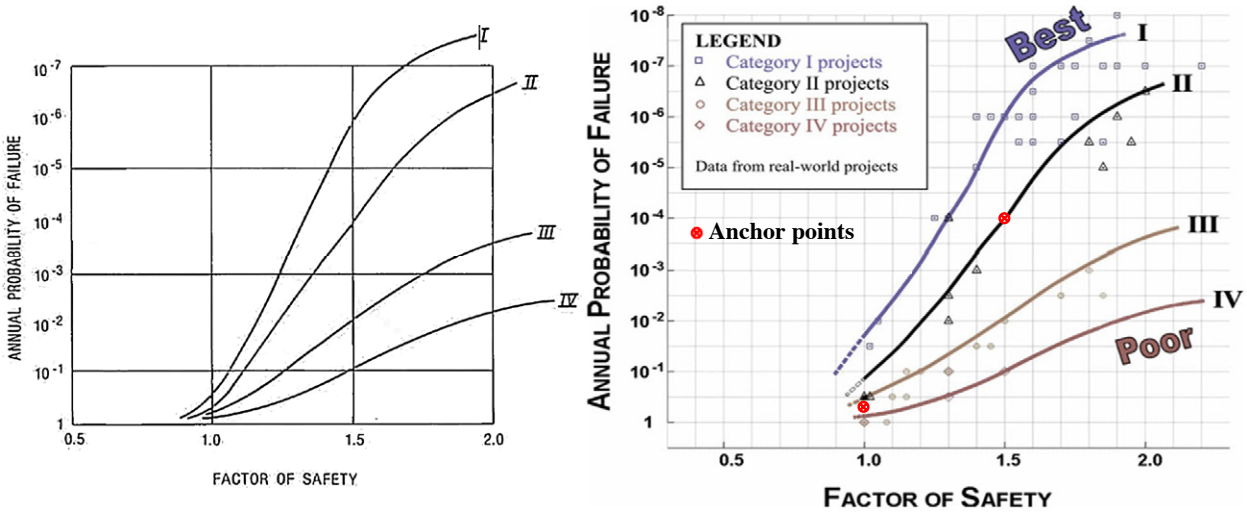

Figure 1: Annual Probability of Failure vs Factors of Safety, Figure 21 from Lambe (1985) – left, Figure 1 from Silva et al. (2008) - right

Silva's team analysed previously completed projects that included zoned and homogeneous earth dams, natural and cut slopes, and earth retaining structures. Based on their judgement of the level of engineering applied in the facilities design, construction and operation, the projects were assigned *PCs* from I to IV. Facilities designed, built, and operated with state-of-the-practice engineering were assigned Project Category I (PC_1); projects using standard engineering practice were assigned Category II (PC_2); projects with no site-specific design and substandard construction or operation were referred to as Category III (PC_3) Projects; and Category IV Projects (PC_4) were constructed with little to no engineering. Silva et al. (2008) provided a tabulated framework, similar to the one presented in Lambe (1985), for deriving the *PC* value and a weighted average of five partial factors.

Silva's team then performed stability analyses to determine the *FoS* values for the previously completed projects. Through an elicitation process, they then estimated P_f for each project by comparing the project with other projects and with two pre-defined anchor points (shown in Figure 1:, right).

The first anchor point was based on the work by Vick (1994) who estimated that the *FoS* = 1.0 yielded a probability of slope failure of 0.5, assuming a log-normal distribution of the FoS uncertainty. Silva et al. (2008) stated that this anchor

point was assigned to PC_3 assets. The other anchor point (FoS = 1.5, $P_f = 1\times10^{-4}$) was assigned to PC_2 assets based on historical probabilities.

After agreeing on the position of the discrete projects in the FoS-P_f space, Silva et al. (2008) drew lines to fit the data points for each PC. These curves group projects with similar uncertainty and reflect the view that a larger FoS does not necessarily imply a smaller P_f, because its effect can be negated by the presence of larger uncertainties.

Silva et al. (2008) stated that the general shape of their four curves agrees with theoretical probability distributions without providing formal definitions, explicit assumptions or the probability distribution type. For practical use, Silva et al. (2008) encouraged the reader to interpolate between the regression lines to estimate the annual probability of slope failure for specific earth structure based on the estimated FoS and the PC value.

As the definitions and the key assumptions are important for finding a suitable probability framework and our later discussion, we have deduced these from Silva et al. (2008) and present them in Table 1.

Table 1 Summary of key assumptions inferred from Silva et al. (2008)

#	Definition/Assumption	Logical notation
1.	$P_f(FoS, PC)$ maps reported FoS and PC to the probability of failure in frequentist sense.	$P_f(FoS, PC) \coloneqq \mathbb{P}[\text{fail} \mid FoS, PC]$
2.	PC is a proxy for the uncertainty in FoS estimates.	FoS is a random variable with standard deviation $\sigma_{FoS}(PC)$
3.	Improved engineering reduces uncertainty. Using Silva et al. (2008)'s convention, high PC represent higher uncertainty in FoS estimate.	$PC_2 > PC_1 \Rightarrow \sigma_{FoS}(PC_2) > \sigma_{FoS}(PC_1)$
4.	There is a PC-specific relationship between P_f, and FoS such that P_f for any given $FoS > 0$ is always greater for higher PC.	$PC_2 > PC_1 \Rightarrow P_f(FoS, PC_2) > P_f(FoS, PC_1)$
5.	Increasing FoS for a given slope reduces its probability of failure.	$FoS_2 > FoS_1 \Rightarrow P_f(FoS_2, PC) < P_f(FoS_1, PC)$
6.	P_f asymptotically approaches 1 when FoS approaches 0 for all PCs.	$\forall PC, \lim_{FoS\to 0} P_f(FoS, PC) = 1$

4. MATCHING REGRESSION MODEL

A dam failure caused by slope instability is a binary outcome—a singular moment in which the complexity of countless interactions resolves into either collapse or stability, with no in-betweens.

4.1. LOGISTIC MODEL

In this chapter, we address the missing formula for the theoretical probability distributions by examining the characteristic S-like shape of the regression lines and constructing a regression function that explicitly captures the essence of the P_f-PC-FoS relationship. As a dam slope failure is a binary event, a logistic regression, being a statistical model designed to predict binary outcomes based on one or more predictor variables, initially appeared to be a reasonable candidate for formalising the P_f-PC-FoS relationship.

At the core of the logistic model is the logistic function that models the probability of an outcome, in this case a dam slope failure, of the binary process:

$$P(y = 1|\boldsymbol{X}) = \frac{1}{1 + e^{-(a_0 + a_1X_1 + a_2X_2 + \cdots a_pX_p)}} \quad (1)$$

Where P(y=1|x) is probability that the outcome y is 1 (e.g., slope failure), x_1 , x_2 , …., x_p are predictor variables, a_o is the intercept term and a_1 , a_2 , …., a_p are coefficients that measure the effect of predictor variables on the outcome

This logistic function ensures that the predicted probability remains between 0 and 1 regardless of the values of the predictors and the typical S-shape logistic regression function plot is provided in Figure 2:.

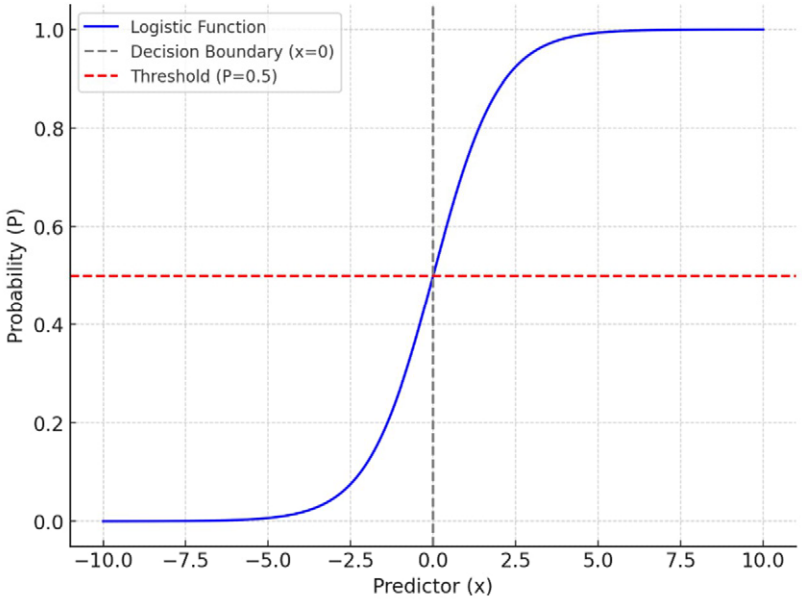

Figure 2: Typical logistic regression function

Logistic regression models perform optimally when the number of occurrences and non-occurrences of the binary outcome are similar (e.g. Chang, Dalpatadu, & Phanord, 2018). In the dataset and the symmetry around the decision boundary is apparent in Figure 2:. Given the extreme rarity of dam failure caused by slope instability, the logistic regression model in its natural form would not be suitable.

4.2. SUPER EXPONENTIAL FORM OF LOGISTIC MODEL

For modeling exceedingly rare events with binary outcomes, the logistic regression needs to be modified to respect the uneven nature of the outcomes and the expected form (shape) of the distribution curve in the corresponding scales.

As we attempt to formalise the approach presented by Silva et al. (2008) and achieve similar P_f-FoS relationship, our theorem is based on the assumptions listed in Table 1, except for assumption no. 3. We have to omit this assumption for the time being because it contradicts the shape of the regression lines in Silva et al. (2008), and we will revisit this problem later on.

In modifying the logistic function to correspond with the observed disproportionality of the outcomes (very rare events of dam slope failures), we first express the logistic probability as a logarithm of odds that the dam fails due to slope instability (P_f) as follows:

$$\text{logit}(P_f) = \ln\left(\frac{P_f}{1-P_f}\right) = a_0 + a_1X_1 + a_2X_2 + \cdots a_pX_p \tag{2}$$

We then formalise the decay of the P_f with increasing FoS, acting as a predictor variable, as follows:

$$\text{logit}(P_f) = \ln\left(\frac{P_f}{1-P_f}\right) = a_0 + a_1 \cdot FoS \tag{3}$$

The relationship between P_f and logit(P_f) is then expressed in terms of the logistic probability as follows:

$$P_f = \frac{e^{(a_0+a_1\cdot FoS)}}{1+e^{(a_0+a_1\cdot FoS)}} \tag{4}$$

To formally capture the assumed non-linearity of the relationship between FoS and P_f we can denote the logistic term as logistic (FoS):

$$\text{logistic}(FoS) = \frac{e^{(b\cdot FoS-c)}}{1+e^{(b\cdot FoS-c)}} \tag{5}$$

where "b" is a steepness coefficient similar to "a_1", and "c" is the threshold coefficient similar to "a_0" and this term presents the assumed sigmoid probability in logistic regression.

Because Silva's curves flatten at high *FoS*, we embed the logistic term inside an exponential decay so that P_f can approach a non-zero residual, with "*a*" being a scaling factor for "stretching" the probability values along the vertical axis as per the Silva et al. (2008) regression lines:

$$P_f = e^{-a \cdot logistic(FoS)} \tag{6}$$

By substituting the logistic probability back into equation (6), we obtain the following super exponential form of the logistic regression (SELR) function:

$$P_f = e^{-a\frac{e^{(b \cdot FoS - c)}}{1+e^{(b \cdot FoS - c)}}} \tag{7}$$

The parameter a governs the scaling of the probability decay, b determines the steepness of the transition, and c defines the threshold for the sigmoid-like progression along the *FoS* axis.

If *a, b* and *c* are non-zero real numbers, we can derive the limits of P_f when *FoS* approaches zero and infinity as follows:

$$\lim_{FoS \to \infty} e^{-a\frac{e^{(b \cdot FoS - c)}}{1+e^{(b \cdot FoS - c)}}} = e^{-a} \tag{8}$$

$$\lim_{FoS \to 0} e^{-a\frac{e^{(b \cdot FoS - c)}}{1+e^{(b \cdot FoS - c)}}} = e^{-a\frac{e^{-c}}{1+e^{-c}}} \tag{9}$$

The expression e^{-a} represents the residual risk of failure that resist all our efforts to prevent dam failures, while the second expression represents the remnant uncertainty on the other side of the spectrum where *FoS* is approaching zero and the probability is expected to approach one. While the characteristics of the SELR are consistent with regression lines presented in Silva et al. (2008), the parameters *a*, *b* and *c* lack empirical justification, and the model remains firmly within the realm of subjective probabilities and valid only for the key assumptions provided earlier.

4.3. MODEL PARAMETRISATION

The presented SELR form has a single predictor variable (*FoS*), which limits its generalisation and ability to represent the complex interplay of factors influencing slope stability. We can address this issue by adding predictors other than the *FoS*, such as embankment and foundation types, to better capture the multidimensional nature of slope stability. Introducing additional predictors may, however, overcomplicate the model without achieving more useful outcomes because the importance of potentially infinite candidates for additional predictors is not known, and the end calibration remains limited by the inherently small failure sample. Alternatively, we can define parameters *a, b* and *c* as functions of other parameters and factors.

We follow the latter approach and incorporate the *PC* variable to obtain regression curves similar to the regression lines presented in Figure 1: (right).

First, we express the variables *a, b* and *c* as linear functions of *PC* as follows:

$$a = m_a + k_a\, PC,\ b = m_b + k_b\, PC,\ c = m_c + k_c\, P\, C \tag{10}$$

where m_i and k_i are independent parameters.

By substituting the independent parameters, *a, b* and *c* in equation (7) with the above linear equations, we obtain the SELR function in this extended form:

$$P_f = e^{-(m_a + k_a\, PC)\frac{e^{[(m_b + k_b\, PC) \cdot FoS - m_c + k_c\, PC]}}{1+e^{[(m_b + k_b\, PC) \cdot FoS - m_c + k_c\, PC]}}} \tag{11}$$

The resulting SELR curves with the following set of m_i and k_i, superimposed by the regression lines drawn in Silva et al. (2008) are provided in Figure 3:.

$$m_a = 22.0, k_a = -4.0, m_b = 5.1, k_b = -0.3, m_c = 6.2, k_c = 0.0 \tag{12}$$

While the parameters *a*, *b* and *c* could be further optimised using more complex relations with the project category variable to "better" match the hand-drawn lines presented in Silva et al. (2008), we leave this to the reader. Our aim is to demonstrate that a mathematically consistent formulation can reproduce the qualitative features presented in Silva et al. (2008).

We will, however, revisit the consistency of the assumptions in Table 1 and logic behind the shape of the regression lines from Silva et al. (2008) in the next chapter.

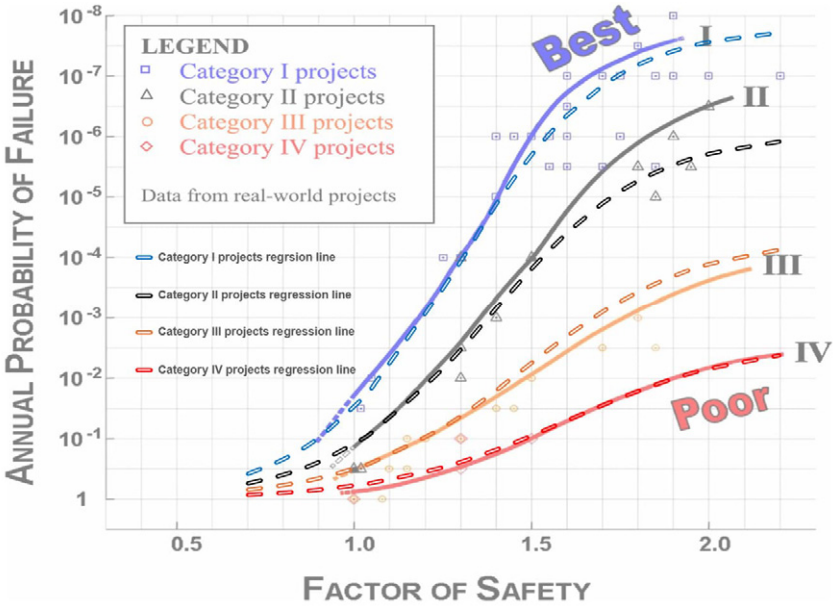

Figure 3: Comparison of regression lines from Silva et al. (2008) with super exponential form of the logistic regression

5. REVIEW OF CONSISTENCY AND COHERENCE

While the laws of logic and mathematics that describe the real world apply to our degrees of belief, they do not guarantee that our conclusions reflect reality—only the coherence of our thought.

5.1. OVERVIEW

We acknowledge that humans operate and thrive within internally inconsistent concepts such as love or art, where contradictions are expected, tolerated and even cherished. However, internal consistency and coherence are essential in probability frameworks used to inform safety-critical decisions.

The following examination of the method presented in Silva et al. (2008) focuses on its internal consistency and logical coherence without discussing the validity of the underlying data, the accuracy of the probability predictions, or the practical use of the method.

Silva et al. (2008) stated that their team used data from 75 projects to develop the relationships shown in Figure 1: – right without disclosing the underlying dataset or clarifying whether any of the analysed projects had actually experienced slope failure. Therefore, the *PC, FoS* and P_f values they assigned to the analysed projects can only be read from Fig.1 included in Silva et al. (2008).

5.2. ASSIGNMENT OF PROJECT CATEGORIES

Silva et al. (2008) stated that the *PC* should be calculated as a weighted average of five partial values taken from their Table 1. Yet, Silva's team assigned integer *PC* values to all their projects. As it is extremely unlikely ($\sim 3.4 \times 10^{-53}$) that weighted averages of five partial values for 75 different projects all happened to be integers, we consider that Silva's team likely rounded the *PC* values to the nearest whole number or directly assigned an integer *PC* value for each project. This could explain the broad spread of P_f values within the same category and the partial overlap of data points with different *PCs*. For example, a $P_f = 1\times10^{-7}$ was assigned to at least seven PC_1 projects with *FoS* values ranging from 1.6 to 2.2, while $P_f(FoS = 1.3) = 1\times10^{-4}$ appears in both PC_1 and PC_2 projects.

5.3. LINEAR VS. GEOMETRIC MEAN

Another notable pattern in Figure 1: – right is the plotting of P_f values at either major or minor gridlines denoting whole orders of magnitude, and geometric means of the closest orders, respectively. Silva et al. (2008) stated that a point ($P_f(FoS = 1 | PC_3) = 0.5$) was used as one of the two anchor points for assigning subjective probabilities and fitting the regression lines. However, Figure 1: – right shows the regression line for PC_3 projects clearly intersecting $FoS = 1$ and the horizontal gridline presenting the geometric mean of $P_f = 0.1$ and 1.0. Because the geometric mean of 0.1 and 1.0 is not 0.5, the

regression line for Category III Projects does not pass through the anchor point that Silva et al. (2008) stated was adopted. The pattern indicates the authors might have applied geometric rather than arithmetic averaging when plotting P_f values. In such case, it is possible that projects were assigned failure probabilities in whole or half orders of magnitude, with the latter appearing as geometric means in their Fig.1.

5.4. SHAPE OF REGRESSION LINES

When comparing Silva et al. (2008) to Lambe (1985) both provided in Figure 1, we find that their regression lines match almost perfectly for $FoS \geq 1.4$. Silva et al. (2008) declared this similarity when noting that their *Pf-PC-FoS* relationship differs from Lambe (1985) only for low *FoS* values, which the authors explained by stating that their analysis of structures "*on the verge of failure*" allowed them to refine curves near $FoS = 1$. Therefore, the resulting regression lines appear to match a pre-selected shape more closely than they match the distribution of P_f values assigned in the study, which would then explain the following observations:

- PC1: The regression line was drawn with 16 out of 25 data points falling below it
- PC2 and PC3: The regressions were drawn consistently above the data points, with each line having one data point above it
- PC4: The regression line is based on just four data points with $FoS \leq 1.5$

5.5. SELECTION OF ANCHOR POINTS

Silva et al. (2008) pre-selected an anchor point for Category II projects ($P_f(FoS = 1.5 | PC_2) = 1\times10^{-4}$) "*based on historic probabilities*" while referring to Baecher et al. (1980), Whitman (1984), and Christian et al. (1992). An attentive reader would note that:

- Baecher (1980) proposed the annual probability of a dam failure as 1×10^{-4} as a reasonable default value based on a limited data set of dams constructed in the US between 1940 and 1984, and as he stated, his provisional estimate was pending the results of further research.
- Whitman (1984) stated that *"...it was suggested that a default value for annual risk of 10^{-4} be used in the absence of other information about the safety of a particular project*." Whitman further noted that "*This value of 10^{-4} was simply the average annual rate of failure for actual dams, as reported by several investigators*".
- Christian et al. (1992) did not provide an independent estimate and referred to Baecher et al. (1980) when stating that *"....the historical rate of failure of dams is about 1×10^{-4} per dam-year*".

Based on the above, it appears that $P_f(FoS=1.5, PC_2)=1\times10^{-4}$ used by Silva et al. (2008) as an anchor point was based on Silva's team agreement with prior judgement of others rather than empirical historical data. This is understandable given that estimating the frequency of dam failures is extremely difficult due to limited data regarding both the total numbers of dams and the name and nature of their failures as shown by Rana et al. (2022). Furthermore, as discussed in Herza et al. (2023), the reference class issue severely erodes the relevance of observed frequency of dam failures, even if such frequency is known, to specific assets.

5.6. COMPARISON WITH LOG-NORMAL DISTRIBUTION

Silva et al. (2008) claimed that the general shape of their regression lines agreed with the probability distributions proposed by Whitman (1984). However, a closer examination of the superimposed *Pf-PC-FoS* plots, presented in Figure 4, reveals significant differences. While the log-normal probability distribution function used by Whitman (1984) dictates the convex shape of the curves, Silva et al. (2008) presented arguments for sigmoid-like distribution shapes resulting in each *PC* pairs that consistently diverge from each other beyond the points of their intersection. For illustration, the P_f values for PC_1 projects at $FoS = 1.5$ provided by Silva et al. (2008) and inferred from Whitman (1984) differ 100 times.

The probability distribution functions inferred from Whitman (1984) intersect in a single point ($FoS = 1.0$, $P_f = 0.5$), and their order would invert for $FoS < 1$, because Whitman assumed an impartial distribution of FoS values. In contrast Silva et al. (2008) maintain relative order of project categories on both sides of $FoS = 1.0$. This feature implies either a reversal in uncertainty or a significant bias in *FoS* estimates that the Silva's team incorporated in their analyses.

We acknowledge that Silva et al. (2008) presented their P_f values as annual probabilities of slope failure while Whitman (1984) discussed atemporal probabilities of slope failure based on the principles of reliability theory. Although these two approaches may not be directly comparable, to our knowledge there is no published transformation method that would explain the vast differences between the P_f-*PC-FoS* shown in Figure 4.

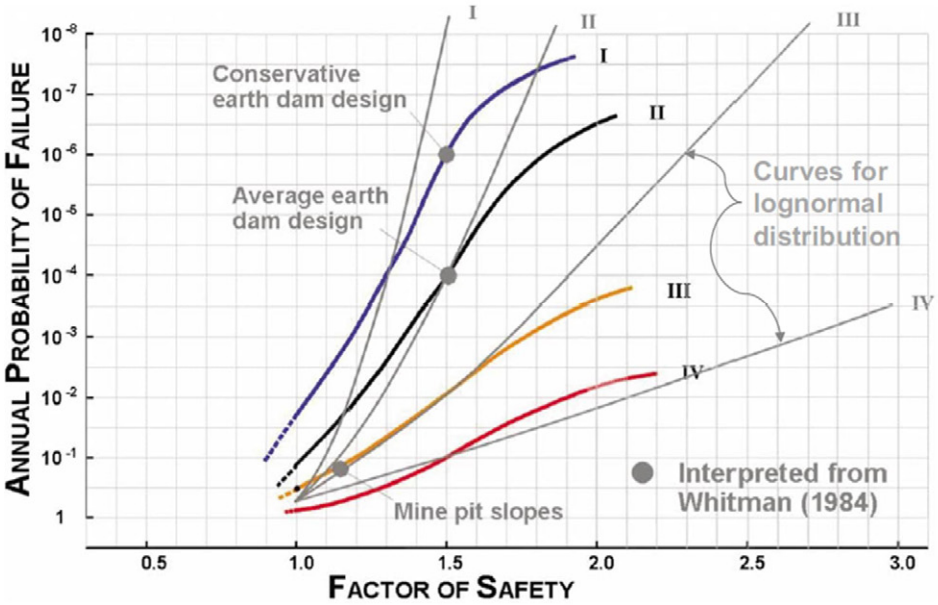

Figure 4: FoS versus Pf, with lognormal distribution and data from Whitman 1984 (adopted from Silva et al., 2008)

5.7. FIXED ORDER OF REGRESSION LINES

By maintaining the relative order of the regression lines irrespective of *FoS* (Assumption no. 4 in Table 1), Silva's team expressed their lower confidence in the slope instability predictions made for Category I Projects compared to Category IV projects for $FoS \leq 1.0$. This, however, contradicts the key principle used by Silva et al. (2008) that lower *PC* values represent comparatively smaller *FoS* uncertainty (Assumption no. 3 in Table 1). Using the key assumptions presented earlier we can formally show this contradiction as follows:

$$PC_i > PC_j \Rightarrow \sigma_{FoS}(PC_i) > \sigma_{FoS}\left(PC_j\right) \Rightarrow P_f(FoS < 1|PC_i) > P_f\left(FoS < 1|PC_j\right) \quad (13)$$

Equation (13) expresses the reversal in the order of the regression lines when $FoS < 1$, as a mathematical consequence of *PCs* being taken an impartial measure of uncertainty. However, this reversal is contradicted by the monotonic ordering of the regression lines observed in Silva et al. (2008), and mathematically reproduced as:

$$P_f(FoS < 1|PC_i) < P_f\left(FoS < 1|PC_j\right) \quad (14)$$

Silva et al. (2008) clarified that the shape of the regression lines near FoS = 1: "*come from the consideration that engineers inherently apply more conservatism in their choice of assumptions and selection of parameters as the importance of the structure and the consequences of failure increase. This produces a bias in their analyses such that their computed safety factors at low values does not represent the actual expected safety factor value, but something higher.*"

However, Silva et al. (2008) also advised the reader to determine *FoS* objectively, when using their method, stating that: *"The strength determination corresponds to the best estimate of the strength acting in the field and not necessarily the average strength or a "conservative" value of strength."*

This contradiction is not limited to the regression lines; it also extends to the individual project points established by Silva's team. Let us take the following points from Figure 1 – right as an example: $P_f(FoS = 1.02|\ PC_1) = 3.2\times10^{-2}$ and $P_f(FoS = 1.05|\ PC_1) = 1.0\times10^{-2}$. If Silva's team followed their own procedure and used their best engineering judgement to estimate the *FoS* and computed the *PC* values as weighted averages of the five defined factors, then assigning P_f values significantly less than 0.5 to these projects cannot be logically justified on the basis of conservatism in their own *FoS* estimates. Conversely, departing from the stated procedure would undermine the internal logic of the method.

Although Silva et al. (2008) discussed the influence of engineering conservatism in relation to PC_1 projects, the shape of all regression lines and the placement of individual points near $FoS = 1$ shown in Figure 1 (right), indicates a wider bias. For example, at least one PC_3 and one PC_4 project with $FoS = 1.0$, estimated by Silva's team, were assigned $P_f = 1.0$. Silva's team also assigned $P_f = 1.0$ to one PC_3 project with $FoS = 1.08$. These assignments suggest that the team treated *FoS* values for PC_3 and PC_4 projects as somewhat optimistic outliers, yet viewed some *FoS* values for PC_1 and PC_2 projects as deliberately conservative, which indicates methodological inconsistency.

5.8. FLATTENING OF REGRESSION LINES

Silva et al. (2008) clarified that the flattening of the curves near FoS of two reflected the team's belief "*that increasing the safety factor well beyond the typical values used for earth structures provides little benefit with respect to the corresponding probability of failure.*" Silva et al. (2008) then explained that "*discontinuities, weak zones, wet zones, high or low permeability zones, and other features that can elude a geotechnical investigation control the level of safety for grossly overdesigned facilities.*"

Through the flattening of the regression curves, Silva's team appears to be accounting for uncertainties beyond those captured by "*the standard deviation of FoS calculated with four distinct levels of engineering*". While it is admissible to assume that adverse conditions can evade a geotechnical investigation, the flattening of the regression lines at different levels suggests that increasing *FoS* through physical modifications, would not materially reduce the subjective probability of failure. For example, it implies that $P_f(PC_4) > 1\times10^{-3}$, irrespective of the geometrical arrangement of the PC_4 slopes.

This implication is inconsistent with principles of slope stability. A flatter slope of an embankment results in a higher ratio of resisting to driving forces and should therefore be perceived of having a lower P_f compared to a steeper slope given that all conditions other than the geometry stays the same. Further discussion on the practical implication of regression lines' flattening at different levels is provided in Chapter 7.

5.9. POTENTIAL METHODOLOGICAL IMPROVEMENTS

To address the formal inconsistencies discussed above, the work by Silva et al. (2008) could be further enhanced by following methodological adjustments:

- Objectivity in Slope Stability Calculations: Slope stability calculations should be conducted objectively and consistently, independent of the assigned *PC*, to prevent bias in *FoS* estimation.
- Transparent *PC* Assignment: *PC* should be assigned using a clear, consistent, and transparent methodology that allows for non-integer values, ensuring that uncertainty is accurately represented, and without considering the *FoS* values or consequences of the slope failure.
- Independent Expert Elicitation Process: The expert elicitation process to derive slope failure probabilities should be internally consistent, incorporate stability assessment results, and remain independent of *PC* assignment to eliminate potential bias.
- Three-Dimensional Representation of Results: The results of the expert elicitation process should be combined with the *PC* assignment and stability assessment results in a 3D matrix or plot, with *PC*, *FoS*, and P_f plotted along perpendicular axes.
- Formal Regression Analysis: A formal regression method should be applied to quantify the relationship between *PC*, *FoS*, and P_f (if any exists), ensuring that the obtained data are interpreted logically and consistently.
- The process should be clearly documented including defining the key terms, disclosing data, listing the key assumptions and outlining the methods used in every step.

In Chapter 6, we develop a formal theorem that resolves these inconsistencies.

6. FORMAL IMPROVEMENTS AND ALTERNATIVE APPROACH

Improving what exists and creating afresh are both essential pathways to meaningful advancement.

6.1. RESOLVING FORMAL INCONSISTENCIES

Obtaining SELR curves that resemble the regression lines in Silva et al. (2008) required omitting Assumption No. 3 (uncertainty increases with increasing *PC*) while maintaining Assumption No. 4 (constant order of regression lines), which would otherwise lead to contradictions, proven earlier.

Because engineering quality is widely accepted to reduce epistemic uncertainty, formalised in Assumption No. 3, we have to address the contradiction by removing Assumption No. 4 and formulating the following condition:

$$P_f(FoS = 1.0) = 0.5, \forall PCi \tag{15}$$

By removing the constant ordering (Assumption 4) and enforcing $P_f(1) = 0.5$ for all PCs, we eliminate the contradiction established in (13)–(14) while retaining Assumption 3. To satisfy the above condition within the context of the SELR (equation 7), we need to solve the following:

$$e^{-a\frac{e^{(b-c)}}{1+e^{(b-c)}}} = \frac{1}{2} \tag{16}$$

which is equivalent to

$$-a\frac{e^{(b-c)}}{1+e^{(b-c)}} = \ln\frac{1}{2} \tag{17}$$

Since $e^{(b-c)} = \frac{e^b}{e^c}$, we can reorganise equation (17) for the scaling factor a to:

$$a = \ln(2)\frac{e^b + e^c}{e^b} \tag{18}$$

The removal of the constant ordering of the regression lines (Assumption No. 4), also allows us to address the issue of asymptotic flattening of the regression at different P_f values, discussed in Section 5.8. To address the possibility that adverse conditions, evading our attempts to detect them, may present a residual risk even for state-of-art facilities, we can incorporate the residual risk level in the SELR. For illustration, we may assign an arbitrary number (P_r), greater than 0, as the residual P_f irrespective of PC and impose this condition by defining the scaling factor a as:

$$a = -\ln(P_r) \tag{19}$$

We then express the logistic value required at $FoS = 1$ as:

$$r = \frac{\ln 0.5}{\ln P_r}, (0 < r < 0.5) , \tag{20}$$

and solve the sigmoid threshold c for any positive slope parameter $b > 0$

$$c = b - \ln\left(\frac{r}{1-r}\right) \tag{21}$$

The exponential term $\frac{e^{(b\cdot FoS-c)}}{1+e^{(b\cdot FoS-c)}}$ is now equal to r when $FoS = 1$ and the resulting SELR gains the following form:

$$P_f = e^{\ln P_r \frac{e^{[b\cdot FoS - b + \ln\left(\frac{r}{1-r}\right)]}}{1+e^{[b\cdot FoS - b + \ln\left(\frac{r}{1-r}\right)]}}} \tag{22}$$

Like we did before, we can now relate the slope parameter b to PC as a proxy of FoS uncertainty, inspired by Silva et al. (2008). If desired, the sigmoid asymmetry in the lin-log scale shown in Figure 1 – right, can then be achieved by relating the slope parameter b to both the PC and FoS variables.

Figure 5 presents an example of two SELR curves derived from equation (22) with slope parameter b expressed as a polynomial function of PC. For comparison we superimposed the curves by a semitransparent segment of Figure 1 (right).

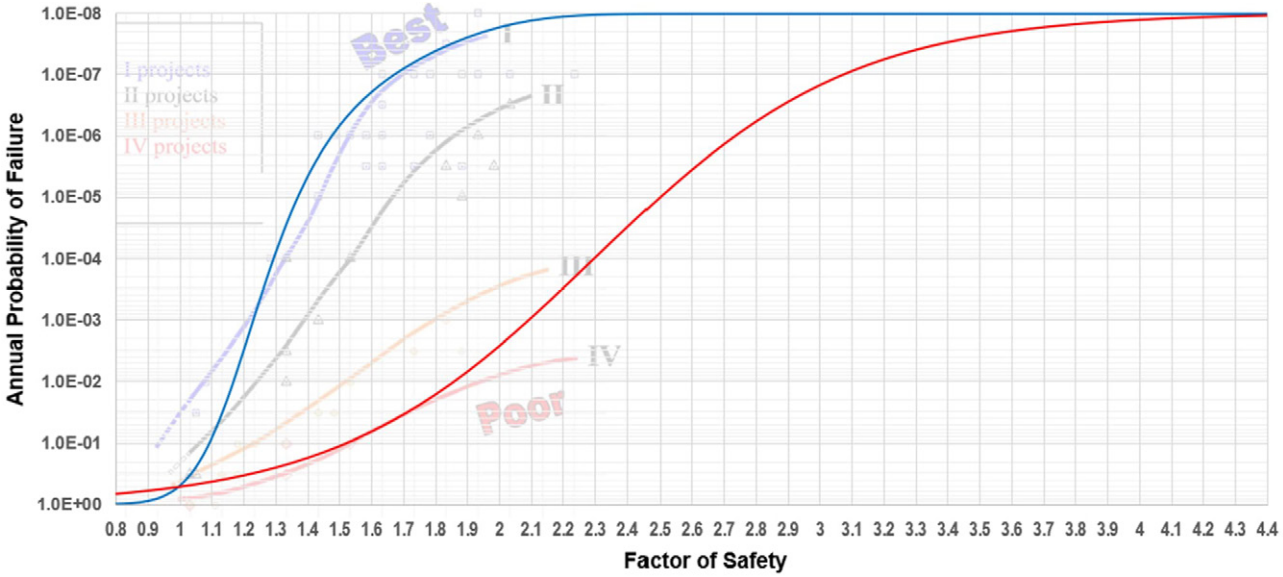

Figure 5: Examples of adjusted super exponential form of the logistic regression

Figure 5 now conforms to the assumptions that an impartial calculation of $FoS = 1$ should always return P_f value of 0.5 and that the probabilities of failure would asymptotically approach a common residual risk of failure, which we set at 1×10^{-8} to be directly comparable with Silva et al. (2008). The residual probability of failure can, however, be set arbitrary close to zero, to respect the perception of the risk analyst. Figure 5 also supports the notion that structures with limited

data but with very conservative *FoS* may be assigned similar subjective P_f values that are assigned to well-engineered structures with comparatively much smaller *FoS*.

Although the slope parameter *b* in equation (22) can be related to both *FoS* and the *PC* to achieve different sigmoid shape, there are more suitable methods of direct parameterisation to fit the desired probability shapes, such as the Metalog Distribution (MD), introduced by Thomas W. Keelin (2016) (Keelin, 2016). The generic MD form for estimating P_f as a function of *FoS* is as follows:

$$P_f(FoS) = \frac{1}{1 + e^{-M(FoS)}} \tag{23}$$

where M(*FoS*) is a Metalog function with a generic form of:

$$M(FoS) = a_1 + a_2 \ln(FoS) + a_3 FoS + a_4 FoS \ln(FoS) + a_5 (FoS)^2 + \cdots \tag{24}$$

Parameters a_i control the position and shape of the distribution function and can be related to *PC*. Additionally, the MD could be used as the argument of an external exponential function to achieve a desirable function shape in the lin-log scale, similar to the transformations applied to the logistic function earlier.

Given the subjective character of the P_f-*PC*-*FoS* relationship, the regression function can be parameterised by directly selecting coefficients that express this relationship, without resorting to anchor points, and thus sidesteps the inconsistencies that can accompany purely heuristic curve fitting.

6.2. ALTERNATIVE APPROACH

Irrespective of the method used to express the P_f-*PC*-*FoS* relationships, the probability of failure would be related to some form of statistical distribution of uncertainty associated with the *FoS* estimate. However, we observed that past slope failures of dams occurred under conditions that were not accounted for prior to the failure and hence could not be captured by the statistical distribution of uncertainty associated with the pre-failure *FoS* estimate.

To address this observation, we propose an alternative theorem for estimating slope failure probability that as the probability that the pre-failure assessment was significantly incorrect. Rather than directly relating the probability of failure to the pre-failure *FoS*, we instead link it to the error in the *FoS* estimate, emphasising the limitation of predictive analytical models we touched upon in the introduction section of this paper.

Using Silva et al. (2008) *PC*, the idealistic, "Category 0 Project" represents a fictional dam which is designed, built, operated and monitored such that the entirety of its composition and its surrounding environment is known, with no uncertainty regarding the dam's performance. For such a dam, the probability of failure is

$$P_f(FoS, 0) = \begin{matrix} 0 & FoS \geq 1 \\ 1 & \text{otherwise} \end{matrix} \tag{25}$$

Where, because $PC = 0$, the modeller's calculation FoS equals the actual (not modelled) ratio between the true stabilising and destabilising forces, true Factor of Safety ($tFoS$).

The calculated *FoS* reported by an analyst is, in practice, an estimation of this value derived from information that can only give inferences about the $tFoS$. For example, sampling the dam's material in several locations to calculate friction coefficients will give a probabilistic understanding of the true friction coefficients, and the way in which these values are mathematically combined assumes a degree of understanding about the mechanisms of failure. This means that the calculated *FoS* is wrong with respect to *tFoS* according to some distribution $Error_{PC}$, which we may represent as:

$$\frac{FoS}{tFoS} = Error_{PC} \tag{26}$$

Error is measured proportionally rather than additively. If the distribution of $Error_{PC}$ depends only on *PC*, the model never supposes $tFoS$ could be negative and $\frac{FoS}{tFoS}$ is independent of FoS.

$$\frac{FoS}{Error_{PC}} = tFoS \tag{27}$$

$$tFoS \leq 1 \Rightarrow Error_{PC} \geq FoS \tag{28}$$

If $f_{PC}(x)$ is the probability density function of $Error_{PC}$, then

$$P_f(FoS, PC) = \int_{FoS}^{\infty} f_{PC}(t)dt \tag{29}$$

This framework can be directly applied to decision-making processes, as the marginal improvement in failure probability given a marginal improvement in *FoS* is:

$$\frac{d}{dx}P_f(x, PC) = -f_{PC}(x) \tag{30}$$

In selecting an appropriate distribution for the error, a strong starting point is to use the centralised lognormal distribution with median = 1, as this is the canonical distribution for proportional error of a measurement. In this case,

$$P_f(FoS, PC) = \int_x^{\infty} \frac{1}{t\sqrt{2\pi}\,\sigma} \exp\left(-\frac{(\ln t)^2}{2\sigma^2}\right) dt = \Phi\left(\frac{-\ln x}{\sigma}\right) \tag{31}$$

where Φ is the cumulative density function (equation 32) of the standard normal distribution, and anchor points or regressions may be used to fix the degree of freedom to a function of *PC*.

$$\Phi(x) = \frac{1}{\sqrt{\pi}} \int_{-\infty}^{x/\sqrt{2}} \exp(-t^2)\, dt \tag{32}$$

By expressing the error function (*erf*) as:

$$erf\left(\frac{-\ln x}{\sigma}\right) = \frac{2}{\sqrt{\pi}} \int_0^{z} \exp(-t^2)\, dt \tag{33}$$

and using symmetry and the Gaussian integral $\int_0^{\infty} e^{-t^2}\, dt = \sqrt{\pi}/2$, equation (31) becomes:

$$P_f(FoS, PC) = \frac{1}{2} + \frac{1}{\sqrt{\pi}} \int_0^{x/\sqrt{2}} \exp(-t^2)\, dt = \frac{1}{2}\left[1 + erf\left(\frac{x}{\sqrt{2}}\right)\right] \tag{34}$$

As a result, any set of error distributions with median $= 1$ and variance determined monotonically by *PC* tending to 0 as $PC \to 0$ will have the desirable properties that:

$$P_f(FoS = 1, PC) = 0.5 \; \forall PC \tag{35}$$

and

$$\lim_{PC \to 0} P_f(FoS, PC) = P_f(FoS, 0) = \begin{matrix} 0 & FoS \geq 1 \\ 1 & \text{otherwise} \end{matrix} \tag{36}$$

Figure 6 shows the failure probability curves from the lognormal error model for σ values of 0.25 (blue), 0.1 (red), and 0.02 (green), illustrating that reduced epistemic dispersion (lower σ = lower *PC*) steepens the transition and lowers P_f for $FoS > 1$.

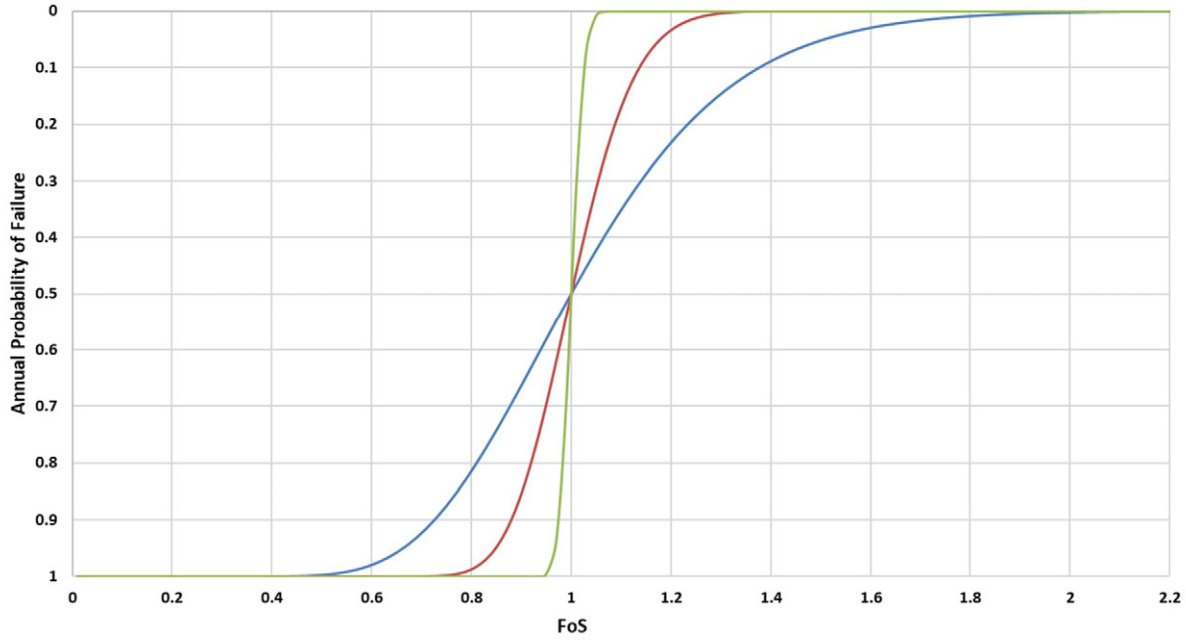

Figure 6: A plot of failure probability generated from a lognormal error distribution

If the method was to apply historical data to the risk assessment process, the notion of known unknowns versus unknown unknowns, and the fact that modes of failure in historical cases have been unexpected (e.g. Vale, 2019) may remind the analyst to consider the impact of higher *PC* on f_{PC}.

For example, consider partitioning $f_{PC} = \sum_i \chi_i f^i$ such that $\sum_i \chi_i = 1$, where each f^i is the probability density function for failure given the dam fails through a particular failure mechanism, or set of mechanisms, i; and χ_i is the observed historical proportion, within failed dams of similar *PC*, of failure through that mechanism or set of mechanisms. If these are grouped by the degree to which they have been considered and mitigated, then the impact of an increasing PC can be seen to continuously migrate modes of failure from less considered to more considered.

Even a simple model of two categories, "completely unconsidered" and "completely prevented", can represent the phenomenon where dam failure is often a black swan event, and hence acknowledges the limited ability to reduce failure probability beyond a certain residual level through improving *PC*.

The method offers potential for practical application, but the current dearth of data on modellers' sentiments about failed dams prior to their failure, and the degree to which the realised mode of failure was previously considered by modellers, is a major obstacle to implementation. Further development of this novel approach will require establishing credible ways of linking *PC* to a suitable error distribution and demonstrating the method's robustness through synthetic case studies.

7. SLOPE STABILITY CONCERNS IN AUSTRALIAN CONTEXT

The words 'reasonably practicable' are ordinary words bearing their ordinary meaning……And the question whether a [risk] measure is or is not reasonably practicable is one which requires no more than the making of a value judgement in the light of all the facts. Slivak v Lurgi [2001] HCA 6, [55].

7.1. AUSTRALIAN CONTEXT

The Australian legal context requires duty holders to make decisions affecting safety of workers and others based on rational, defensible and reasonable methods and through rational, defensible and reasonable systems. Because Silva et al. (2008) proposed a "*method of risk-based decision making for situations involving slope failures",* and their method is widely used across Australia, this chapter discusses the context of risk-related decision making in Australia.

Before estimating probabilities to support a dam risk assessment, we must understand the purpose of the assessment and how the outcomes will be used by the duty holder. Answering these questions often reveals that estimating the probability of slope failure is not always the most appropriate approach, nor is it necessary to achieve the intended outcomes.

This is illustrated by the probability and risk assessment example included in Silva et al. (2008), which concluded that installing relief wells to decrease pore pressures near the toe of the assessed dam "*made a lot of sense*". While we may disagree with the cost benefit rationale for this decision, we concur with Silva et al. (2008) that addressing the foundation conditions at the dam's toe, where personnel reportedly *"sank into the ground up to their knees"* made a lot of sense. However, we question whether the quantitative risk assessment was needed to arrive at this conclusion; a question that applies to all other conclusions from the example in Silva et al. (2008).

If probability-based assessments of dam slope failure are used to inform risk mitigation decisions in Australia, all involved parties must carefully consider the Australian legal context and the owners' obligations under the WHS Acts supported by case law, which are consistent with the obligations under other mining, water and dams acts. Greg Smith, a lawyer specializing in Work Health and Safety, clarified this legal context in a presentation and Q&A session organized by Engineers Australia in August 2024 (Smith, 2024).

We recognise that simplified quantitative risk assessments, cost-benefit analyses and comparison of risk position against risk tolerability thresholds, such as those discussed in Silva et al. (2008), are valuable in many situations. However, we must be mindful of the extent to which focusing on these assessments might distract the duty holder from fulfilling their fundamental duty to identify and implement all reasonably practicable measures to eliminate or reduce risks to health and safety, as is often the case in tailings dam failures.

Without straying too far from the technical nature of this paper, we stress that Australian WHS law (e.g., the Work Health and Safety Act 2020 (WA), Section 18, paragraph e) demands that when determining what is reasonably practicable in ensuring health and safety, the cost of risk control measures, and whether the cost is grossly disproportionate to the risk, may only be considered after assessing the available ways to eliminate or minimise the risk. Furthermore, to our knowledge, there is no legal precedent in Australia where a risk tolerability threshold has been accepted as a defence in a legal case concerning the safety of workers or others. Therefore, dam owners in Australia should exercise extreme caution before choosing not to look for risk reduction measures based on a risk assessment concluding that the risks fall below a specific tolerability or acceptability threshold, or that the dam is "*Adequately Safe*" as suggested in Fig. 3 of Silva et al. (2008).

7.2. CHALLENGES IN APPLYING PROBABILISTIC ESTIMATES IN AUSTRALIAN CONTEXT

It is worth noting that one of the primary reasons for introducing risk assessment into dam safety was to address areas where deterministic, standards-based methods were not available, such as piping phenomena or the reliability of spillway gates (ANCOLD, 2003). Standards-based, deterministic methods and their associated threshold values (e.g., minimum recommended FoS) can be considered implicit forms of risk assessment. ANCOLD (2022) acknowledges this link between standards-based FoS estimates and probability-based assessments in the following statement: "*For most dams, if the FoS for the steady state seepage condition is ≥ 1.5 using reasonable but conservative assumptions, and the monitoring of settlement (and lateral movements if available) indicates there are no unusual movements, the likelihood of failure by slope instability can be taken as negligible*."

The implicit conservatism in these methods must be acknowledged and appropriately addressed when using deterministic, standards-based slope stability outcomes to estimate dam failure probabilities. This is challenging because the various levels and types of implied conservatism are never explicitly stated. For example, slope stability analyses for embankment tailings dams are typically performed for specific, discrete sets of conditions (e.g., phreatic pressures, tailings levels, material characteristics), without the analyst explicitly defining their conditional probabilities that would be required for estimates of annual probabilities of slope failure. Beyond the fundamental challenge of incorporating deterministic, standards-based outcomes into probabilistic estimates, ANCOLD (2022) highlights additional difficulties, including unknown or unrecognized features and behaviours (unknown unknowns) that are not captured in the analysis. Given the historically low frequency of slope instability-triggered dam failures, ANCOLD (2022) concludes that in relation to slope failure "*the use of formal probabilistic methods is typically not warranted, even in the most detailed risk analyses*."

Available evidence suggests that many slope-instability failures might have been avoided had current ANCOLD-aligned practices been followed and we emphasize that compliance with current industry practices is a fundamental duty of dam owners in Australia. This duty extends well beyond slope stability considerations. In this context, we view the *PC* classification as equivalent to a gap assessment against current industry practices, with a Category I Project meeting current industry practice, while a Category IV Project has substantial deficiencies.

These deficiencies can be resolved by addressing gaps in current practice related to the understanding of materials, geometry, and loading conditions that control slope stability. Alternatively, the uncertainties can be managed by adopting a solution that ensures stability, so far as is reasonably practicable, under all foreseeable conditions. In practice, this may involve flattening the slope in high PC projects. Such a solution may be appropriate at mines where legacy embankments and other structures have a seemingly sufficient FoS though supported by limited engineering knowledge (e.g., PC_3 and PC_4 structures), and where construction materials, equipment, and workforce are readily available.

In such circumstances, physically flattening the downstream slope, without having a substantially improved engineering knowledge, may still be a reasonably practicable risk reduction measure, provided the construction activities are appropriately planned and managed. For example, conventional slope flattening by pushing material from the upper portion of the slope downward reduces the overall slope angle without adding new surcharge, and thus lowers the risk of failure once construction is complete. Buttressing slopes is another conventional method of reducing the risk of slope instability, particularly where deep foundations do not govern slope stability, as is often the case with in-pit structures.

The regression lines from Silva et al. (2008) suggest that such works would have virtually no effect on the subjective annual probability of slope failure, which could discourage the dam owner from implementing effective and well-understood risk reduction measures. Instead, the owner may opt to conduct additional investigations and analyses aimed at improving the PC, which, according to Silva et al. (2008), could result in a significant reduction in P_f.

7.3. RATIONAL METHOD FOR ADDRESSING SLOPE STABILITY CONCERNS IN AUSTRALIA

If, after meeting current industry practices, an owner seeks to further strengthen their embankment slope safety, perhaps as part of compiling a safety case demonstrating that all reasonably practicable risk controls are in place (Herza et al., 2022), we propose the following process. This process is inspired by the method outlined in Appendix B of ICOLD Bulletin 194 (ICOLD, 2023), which advocates for a rational approach to uncertainty and provides guidance for decision-making when existing tailings facilities do not meet the recommended FoS values. Since we believe this fundamental approach is applicable regardless of specific FoS values, we propose the following steps:

- Determine the worst foreseeable conditions, objectively informed by evidence, which could lead to slope failure resulting in an uncontrolled release of the dam content.
- Determine physically possible measures that would increase the FoS for any condition or combination thereof.
- Assess, from the owner's perspective, which of the identified measures are not reasonably practicable to implement. This assessment may include a probability analysis of specific phenomena (flood, seismic event etc.)
- Implement all reasonably practicable measures to reduce the risk of slope failure.

We acknowledge that owners have limited resources, which may prevent them from implementing all reasonably practicable risk controls across their entire portfolio simultaneously. In this context, risk assessment, including probability estimation, plays an important role in enabling comparative analysis (e.g., portfolio risk assessments) and informing prioritisation of risk control measures.

If a quantitative risk assessment is conducted for comparison or compliance purposes, an owner may choose a method that prioritises internal consistency and logical coherence over purely heuristic methods based on subjective interpretation of probability estimates subjectively made by the interpreters. For such circumstances, this paper offers improvements to the Silva et al. (2008) method together with an alternative methods for estimating probabilities of slope failure.

In Australia, however, these methods must not be the sole basis for decisions over risk-control measures for a particular dam under specific conditions, because relying on them alone may fail to meet ethical expectations or regulatory and legal scrutiny.

8. CONCLUSIONS

Progress comes from adding to what serves us well, subtracting what doesn't, and advancing with ever clearer reasoning.

While we acknowledge the widespread occurrence and benefits of inconsistent frameworks in our society, we consider that internal consistency and coherence are essential in probability frameworks used to inform safety-critical decisions in Australia.

Silva and his team successfully achieved their objective of making quantitative risk assessment more accessible to geotechnical engineers. Their methodology is now widely recognised and successfully applied as a contemporary approach to evaluating the probability of slope instability, both in Australia and internationally.

Analysing the extensive work by Silva et al. (2008) we have shown that applying a formal regression function to express subjective probabilities is not only possible but also desirable. It avoids inconsistencies that may otherwise be introduced when probability relationships are heuristically established from data that were previously approximated by the same authors.

Through further analysis of the method presented in Silva et al. (2008), we highlighted the importance of logical coherence and proposed steps that could resolve the formal contradictions associated with the heuristic approach. The parametrisation of the introduced regression functions can also directly express the subjective P_f–PC–FoS relationship directly, thereby sidestepping the inconsistencies that often accompany purely heuristic curve fitting.

We have also proposed a novel approach to estimating slope failure probability that focuses on the unknown unknowns to address our observations that previous dam failures were unexpected, and we expressed the subjective probability of failure as the probability that the pre-failure assessment was grossly incorrect in predicting stable conditions. We offer this path for other researchers to explore.

Quantified probabilities offer significant potential, particularly in areas where standards-based approaches are unavailable and for comparison and prioritisation purposes. However, owners making decisions over dam safety should recognise the inherent challenge of quantifying probabilities of one-off events, such as slope instability, magnified by incorporating outcomes from incomparable standards-based methods and by the inherently abstract nature of the subjectively estimated probabilities.

This is even more important in Australia where the legislative requirements are based on a different rationale, and the contemporary probability-based methods may neither be required nor sufficient to fulfill their legal obligations. As an alternative, we have proposed a simple, rational framework for addressing foreseeable risks associated with potential slope instability, inspired by the methods outlined in ICOLD Bulletin no. 194 (ICOLD, 2024).

9. ACKNOWLEDGEMENT

The authors would like to express their gratitude to Ryan Singh for his patience and insightful discussions throughout the development of this paper. We also extend our appreciation to Ryan Singh and James Thorp for their thoughtful review, valuable feedback, and inspiring comments.

CRediT authorship contribution statement

Jiri Herza: Conceptualization; Methodology; Visualisation; Writing – original draft; Writing – review & editing. **Hugo Fellows-Smith:** Formal analysis; Writing – original draft.

10. REFERENCES

Australian National Committee on Large Dams (ANCOLD) (2003). *Guidelines on Risk Assessment,* ANCOLD, Melbourne.

Australian National Committee on Large Dams (ANCOLD) (2022). *Guidelines on Risk Assessment*, ANCOLD, Melbourne.

Australian National Committee on Large Dams (ANCOLD) (2019). *Guidelines on Tailings Dams: Planning, Design, Construction, Operation and Closure*, ANCOLD, Melbourne.

Askari, H. & Mirakhor, A. (2015). Recurring financial crises—the causes, in *The next financial crisis and how to save capitalism, Palgrave Macmillan*, New York, pp. 16–34.

Baecher, G.B., Paté, M.-E. & de Neufville, R. (1980). Dam failure in benefit–cost analysis, *Journal of the Geotechnical Engineering Division*, vol. 106, no. 1, pp. 101–105.

Baecher, G. B., & Christian, J. T. (2003). *Reliability and statistics in geotechnical engineering*, John Wiley & Sons, Chichester.

Chang, M., Dalpatadu, R.J., Phanord, D. & Singh, A.K. (2018). A bootstrap approach for improving logistic regression performance in imbalanced data sets, *Matter: International Journal of Science and Technology*, vol. 4, no. 3, pp. 11–24.

Christian, J.T., Ladd, C.C. & Baecher, G.B. (1992). Reliability and probability in stability analysis, in *Stability and Performance of Slopes and Embankments II: Proceedings of the ASCE Specialty Conference*, vol. 2, American Society of Civil Engineers, New York, pp. 1071–1111.

Duncan, J. M. (2000). Factors of safety and reliability in geotechnical engineering. *Journal of Geotechnical and Geoenvironmental Engineering*, 126(4), vol. 126, no. 4, pp. 307–316.

Euromoney 2015. SNB's shock move on the franc: lessons from Black Thursday, *Euromoney*, January, viewed 12 March 2025, https://www.euromoney.com/.

Government of Western Australia 2020, *Work Health and Safety Act 2020*, Government of Western Australia, Perth, viewed 12 March 2025,

Hartford, D. N. D., & Baecher, G. B. (2004). *Risk and uncertainty in dam safety*. Routledge, London.

Hicks, M., & Li, Y. (2018). Influence of length effect on embankment slope reliability in 3D. *International Journal for Numerical and Analytical Methods in Geomechanics*, 42(7), 891-915.

Herza, J., Coffey, J., & Singh, R. (2022). Key elements of tailings dam safety case. Proceedings of the 2022 ANCOLD Conference, Australian National Committee on Large Dams, Hobart.

Herza, J. & Singh, R. (2023). The risk of quantifying risk for tailings dams, in Management for Safe Dams*, Proceedings of the Symposium, 91st Annual Meeting of the International Commission on Large Dams*, Gothenburg, Sweden, 13–14 June 2023, International Commission on Large Dams, Paris.

Keelin, T. W. (2016). The metalog distributions, *Decision Analysis*, 13(4), 243–277, doi:10.1287/deca.2016.0338.

Lambe, T. W. (1985). Amuay landslides, Proc., *11th Int. Conf. on Soil Mechanics and Foundation Engineering*, Golden Jubilee Volume, San Francisco, Balkema, Boston, 137–158.

Laplace, P. S. (1774). Memoire sur les suites recurro-recurrentes et sur leurs usages dans la theorie des asards, *Memoire de l'Academie Royale des Sciences de Paris (savants etrangers)*, Tome VI, 353–371.

Mitchell, J. K., & Soga, K. (2005). Fundamentals of soil behavior (3rd ed.), Hoboken, NJ: Wiley.

Rana, N.M., Ghahramani, N., Evans, S.G., Small, A., Skermer, N., McDougall, S. & Take, W.A. (2022). Global magnitude–frequency statistics of the failures and impacts of large water-retention dams and mine tailings impoundments, *Earth-Science Reviews*, vol. 232, article 104144, doi:10.1016/j.earscirev.2022.104144.

Robertson, P. K., Rowe, R. K., & Olsen, K. B. (2019). Brumadinho dam failure: Lessons for tailings dam risk assessment and management, *Geotechnical News*, 37(3), 22–27.

Silva, F., Lambe, T. W., & Marr, W. A. (2008). Probability and risk of slope failure. *Journal of Geotechnical and Geoenvironmental Engineering*, 134(12), 1691–1699.

Slivak v Lurgi (Australia) Pty Ltd [2001] HCA 6; 205 CLR 304, [53] (Gaudron J).

Smith, G. (2024, August 8). What is reasonably practicable – A work health and safety perspective [Webinar]. Engineers Australia.

The Economist (2015). The day the Swiss franc ceased to be boring, *The Economist*, 17 January, viewed 2 Jan 2025, https://www.economist.com/.

TÜV SÜD do Brasil (2018). Stability condition statement: Dam I, Córrego do Feijão Mine, *technical report prepared for Vale S.A*., Belo Horizonte, Brazil, September 2018.

Vale S.A. (2019). Vale's statement on the Brumadinho dam collapse, *media release*, 29 January. Vale S.A., Rio de Janeiro, viewed 12 February 2025. https://vale.com/fi/w/clarifications-on-the-dam-i-of-the-corrego-do-feijao-mine.

Whitman, R. V. (1984). Evaluating calculated risk in geotechnical engineering. *Journal of Geotechnical Engineering,* 110(2), 143–188.

The Wall Street Journal (2014). Swiss National Bank faces pressure on franc cap, *The Wall Street Journal*, 5 December, viewed 10 December 2024, https://www.wsj.com/.

Xiao, Z., Lü, Q., Zheng, J., Liu, J., & Ji, J. (2020). Conditional probability-based system reliability analysis for geotechnical problems, *Computers and Geotechnics*, vol. 126, article 103751, doi:10.1016/j.compgeo.2020.103751

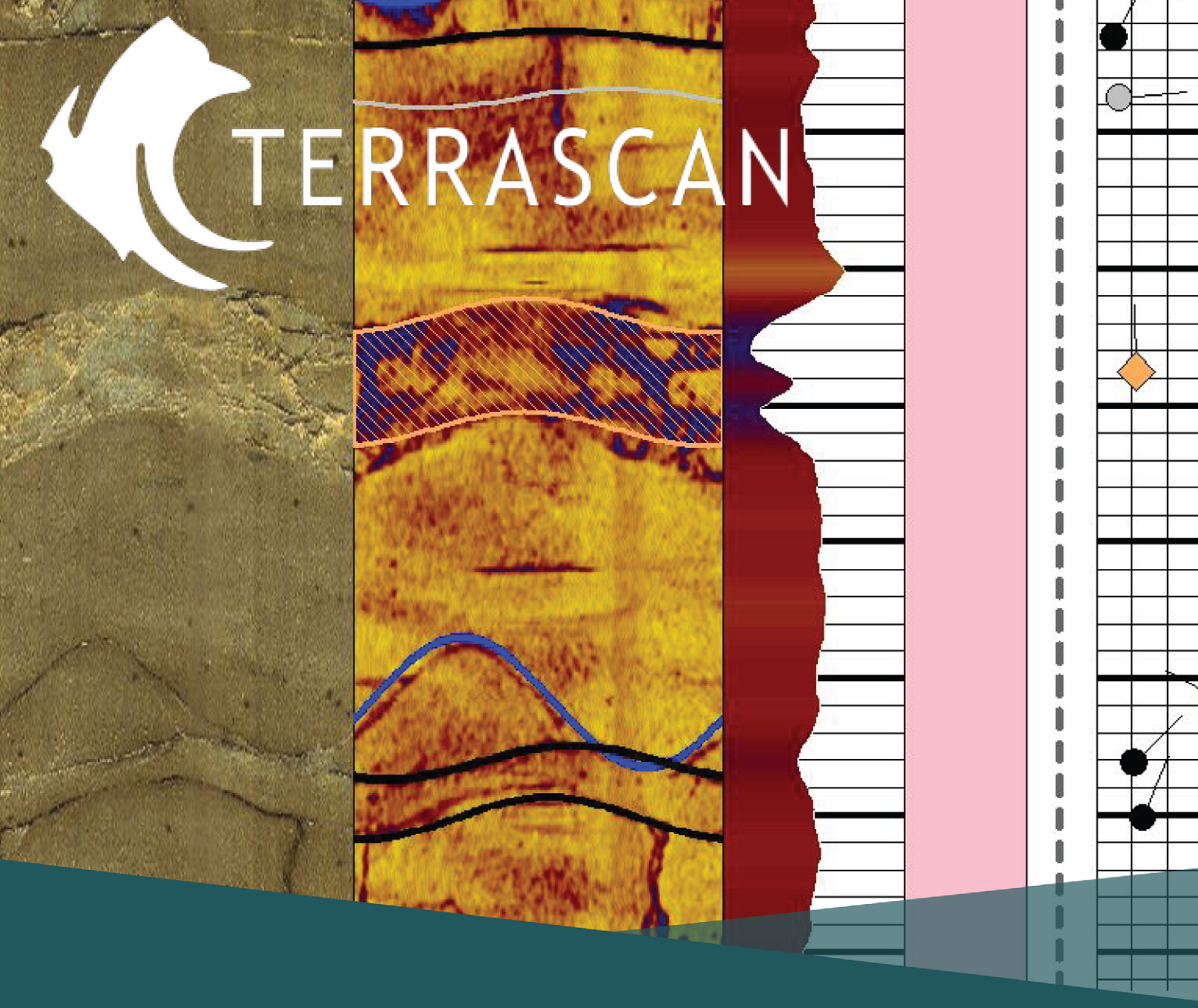

Providing Wireline & Geological services across Australia for the geotechnical and resource industries.

Contact us now to talk about your next project
wade@terrascangroup.com.au

TERRASCAN OFFERS

Downhole Wireline Geophysics

- Optical & Acoustic Televiewer
- Full Waveform Sonic (FWS)
- Resistivity
- Natural Gamma

Geological Services

- Core & Soil Logging
- Rig supervision
- Field Assistant

1300 884 198 | www.terrascangroup.com.au | 0408 723 340

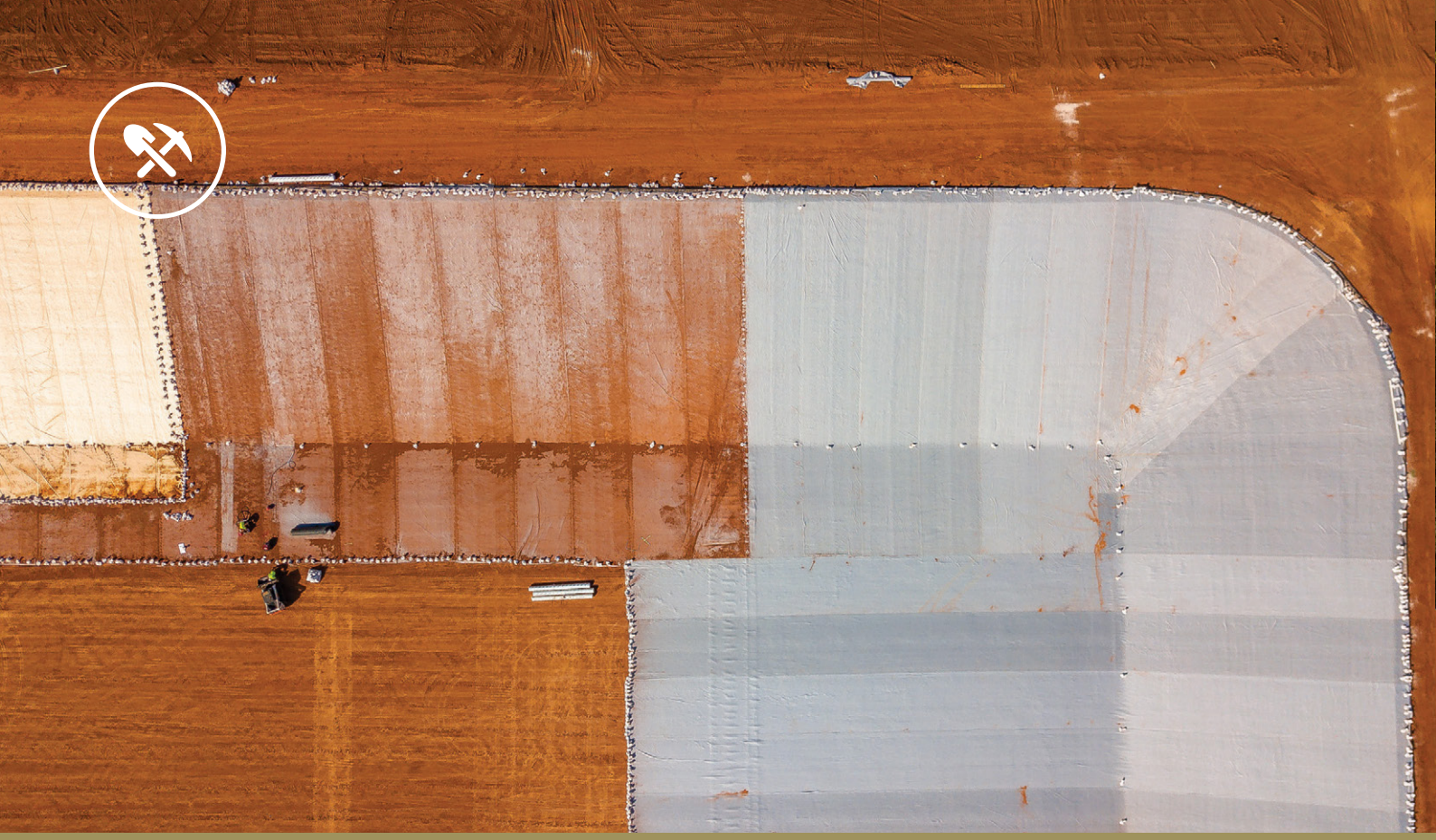

PROVEN PROTECTION FOR WASTE CONTAINMENT
ELCOSEAL GEOSYNTHETIC CLAY LINER

Engineered for high-performance barrier systems, Elcoseal® geosynthetic clay liner is designed to meet the demanding requirements of tailings dams, landfills, and other critical containment structures.

Proudly manufactured in Australia, it features a layer of premium sodium bentonite clay bonded between durable polypropylene geotextile. When hydrated, the bentonite swells to form a low-permeability seal that self-seals around punctures, reducing the risk of leakage.

By effectively isolating contaminants, Elcoseal not only protects soil and groundwater but also supports your project's sustainability objectives, helping preserve natural ecosystems and meet environmental compliance.

Choose Elcoseal for reliable, Australian-made containment performance.

To find out more, visit **geofabrics.co**
or call **1300 60 60 20**

GEOFABRICS®
Sustainable solutions

PhD Thesis abstracts for publication in *Australian Geomechanics*

AUSTRALIAN GEOMECHANICS SOCIETY

The Australian Geomechanics Society invites PhD students to submit an abstract of their thesis completed in 2025 to *Australian Geomechanics*.

This invitation is restricted to PhD theses submitted to Australian universities and accepted as partial fulfilment of the requirements for the degree of Doctor of Philosophy and to PhD theses by Australian students submitted at overseas institutions.

The thesis should have been completed and accepted within one year of the abstract being published in *Australian Geomechanics*.

The invitation is open to all theses related to geomechanics topics. AGS requests promotion of this initiative among PhD students and academic networks.

The abstracts will be published in the March 2026 issue of *Australian Geomechanics*.

The following information is required for publication:

- Author's name (with current affiliation and contact information)
- Thesis title
- Date submitted/approved
- Sponsoring Professor / Academic Supervisor and University (contact address, telephone and e-mail address)
- A brief abstract (strictly max 250 words)
- Scanned page of Title Page of thesis.
- Information should be submitted to the *Australian Geomechanics* Editor, via email: editor@geomechanics.org.au Please attach as a MS Word document.

Deadline: Friday 6th February 2026

AUSTRALIAN GEOMECHANICS SOCIETY

We need YOU!

Australian Geomechanics was established to meet the needs of the practicing geotechnical professional. As such we are keen on publishing practical papers that are of use to local consultants and researchers.

We are always pleased to receive content in the form of review articles, technical papers, letters to the Editor, original research papers, case studies, and methodologies or methods.

Submissions are required at least 4 months prior to publication and can vary in length from 1-page to 20-pages.

More details on our Editorial Policy can be found at the AGS website (australiangeomechanics.org/journal/editorial-policy/)

Technical papers may be submitted via the AGS Scholastica website: (https://ags.scholasticahq.com/for-authors)